Acta Morphologica et Anthropologica 32 (3–4)

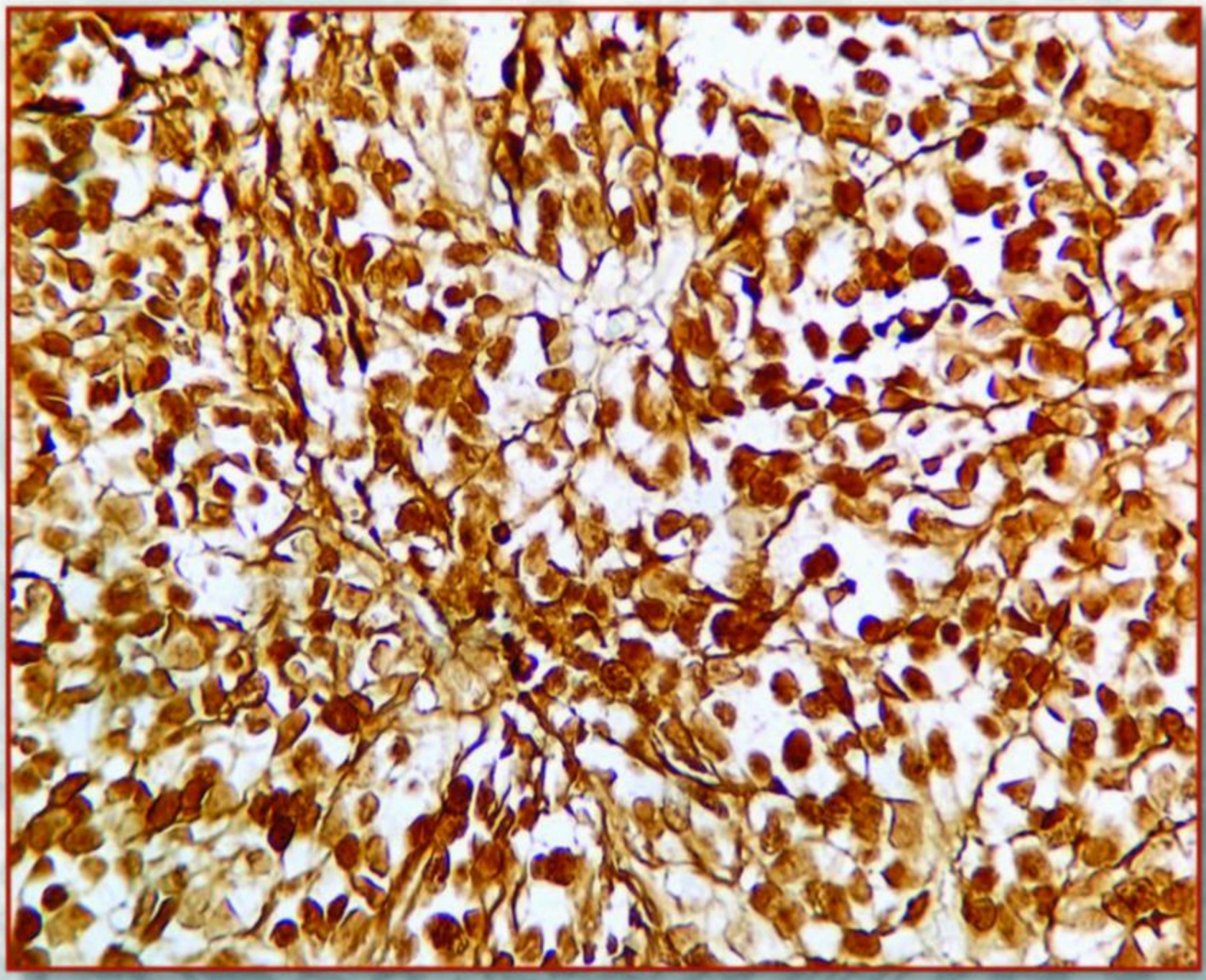

Acta Morphologica et Anthropologica
is the continuation of Acta cytobiologica et morphologica

Indexed in:

BIOSIS databases
Life sciences and biomedical literature on Web of Science

WEB OF SCIENCE

WorldCat®

NCBI
NLM Catalog

INTERNATIONAL STANDARD SERIAL NUMBER INTERNATIONAL CENTRE

ZDB ZEITSCHRIFTEN DATENBANK

Editorial Correspondence
Institute of Experimental Morphology, Pathology and Anthropology with Museum
Bulgarian Academy of Sciences
Acta Morphologica et Anthropologica
Acad. Georgi Bonchev Str., Bl. 25
1113 Sofia, Bulgaria

E-mail: ama.journal@iempam.bas.bg; yordanka.gluhcheva@iempam.bas.bg; ygluhcheva@hotmail.com

Tel.: +359 2 979 2344

Издаването на настоящия том 32, книжки 3 и 4 е осъществено с финансовата подкрепа на Фонд „Научни изследвания“ по Договор КП-06-НП6/16 от 02.12.2024 г. Фонд „Научни изследвания“ не носи отговорност за съдържанието на материалите

The publication of this volume 32, issues 3 and 4, was made possible with the financial support of the Scientific Research Fund under Contract KP-06-NP6/16 of 02.12.2024. The Scientific Research Fund is not responsible for the content of the materials.

Graphic designer: Veronika Tomcheva.
Format 70×100/16 Printed sheets 11,00

Printing Office of Prof. Marin Drinov Publishing House of Bulgarian Academy of Sciences
Bulgaria, 1113 Sofia, Acad. Georgi Bonchev Str., Bl. 5

Acta Morphologica et Anthropologica

ISSN 1311-8773 (print)
ISSN 2535-0811 (online)

Acta Morphologica et Anthropologica 32 (3-4)

32 (3-4) ● Sofia ● 2025
Institute of Experimental Morphology, Pathology and Anthropology with Museum
Bulgarian Anatomical Society

Contents

MORPHOLOGY 32 (3)

Original Articles

Review Articles

Original Articles

Review Articles

Institute of Experimental Morphology, Pathology and Anthropology with Museum
Bulgarian Anatomical Society

Acta Morphologica et Anthropologica, 32 (3-4)
Sofia ● 2025

Accelerated Aging Model Effects in the Colorectal Region

Nikolay Genov[1], Nikolay Dimitrov[1], Lubomir Petrov[2,3], Elina Tsvetanova[3], Albena Alexandrova[2,3], Dimitrinka Atanasova[1,3*]*

[1] Department of Anatomy, Faculty of Medicine, Trakia University, Stara Zagora, Bulgaria
[2] National Sports Academy "Vassil Levski", Sofia, Bulgaria
[3] Institute of Neurobiology, Bulgarian Academy of Sciences, Sofia, Bulgaria

* Corresponding authors e-mails: nikolay.genov@trakia-uni.bg
dimitrinka.atanasova-dimitrova@trakia-uni.bg

D-galactose is widely used to induce accelerated aging, oxidative stress, neurodegeneration, and inflammation, but its effects on the large intestine remain poorly understood. We studied male ICR mice divided into two groups: a control group and a group treated with D-galactose (500 mg/kg/day, orally, for 6 weeks). Histological slides were obtained from all levels of the large intestine and were stained with Azan, van Gieson and Toluidine blue. Azan staining demonstrated an increase in collagen fibers in the proximal colon by over 30% and in the rectum by 73% in D-galactose-treated mice compared to the control group. Van Gieson staining showed 83% increase in the periganglionic space in the proximal colon compared to the control group. Toluidine blue staining for mast cells demonstrated an increase of over 30% in the proximal colon, a 48% increase in the rectum, and a nine-fold higher density of mast cells in the distal colon.

Key words: D-galactose–induced aging, ICR mice, large intestine, myenteric plexus, periganglionic space, collagen deposition

Introduction

The gastrointestinal tract possesses an intrinsic neural network—comprising neurons, glial cells, and ganglia organised into the myenteric (Auerbach's) and submucosal (Meissner's) plexuses – collectively referred to as the enteric nervous system (ENS) [5, 6]. The ganglia of the Auerbach plexus are encapsulated by a structure composed of extracellular matrix (ECM) molecules such as agrin and collagen type 4 (Col4), playing a role as a blood-myenteric barrier (BMB) [4]. It is reported that the amount of collagen deposition (predominantly collagen type I) around the ganglia increases with age [10, 7]. Enteric neuroinflammation induced by various reasons could cause neurodegeneration and disruption of the capsule providing BMB [6, 4]. Neuronal loss

in the myenteric plexus is commonly reported as a change occurring with advanced aging [15]. The use of D-galactose is known as the safest method to induce accelerated aging-related changes in vivo by increasing reactive oxygen species (ROS) as well as inflammatory cytokine levels [1]. At the colonic level, it causes a significant reduction in neuron cell bodies [8]. D-galactose has been shown to disrupt the structure of the intestinal mucosa, thereby compromising the intestinal barrier [17].

No studies have focused on the changes that this accelerated ageing model has on the BMB and the components of the ECM around the myenteric plexus. The present research aimed to demonstrate the shifts induced by our model around the ganglia of the Auerbach plexus and the inflammatory response it triggers at different levels of the *intestinum crassum*.

Material and Methods

For this experiment, twelve (n=12) sexually mature male ICR mice (body mass 25–30g) were brought in from the Breeding facility for Laboratory Animals, Slivnitsa, Bulgaria. The animals were acclimated for 7 days before the experiment and then randomly allocated to a control group (K1, n = 6) or a D-galactose-treated group (D-gal, n = 6). The mice were kept under standard laboratory conditions, which consisted of a 12:12 h light–dark cycle, and they were given free access to food and water. Their housing conditions were: temperature (21–23°C), relative humidity (45–65%) and cage type (Type II polysulfone).

D-galactose was administered ad libitum in the drinking water for 6 weeks at an average daily dose of 500 mg/kg. All procedures were approved by the Bulgarian Food Safety Agency and complied with Directive 2010/63/EU on the protection of animals used for scientific purposes (approval No. 424/24.02.2025).

To perform the morphometric analysis, all animals were anaesthetised with 87 mg ketamine/kg body weight combined with 13 mg xylazine/kg, administered by simultaneous intraperitoneal injections. The intestinum crassum of the examined animals was dissected, cleared under running water, and submerged in 4% paraformaldehyde overnight at a temperature of 4°C. Samples were then divided into proximal colon (PC), distal colon (DC) and rectum (REC). The standard protocol for embedding tissue samples in paraffin was applied. 6 µm sections were taken from the paraffin blocks and mounted onto chrome gelatinised glass slides. Standard protocols for Azan, van Gieson and Toluidine blue staining were applied.

The following morphological characteristics were evaluated: percentage of collagen fibers in the preganglionic space as part of the area of the entire ganglion (C%), as well as mast cell density in the samples (MCd). MCd was presented as a mast cell count per mm^2 (mc/mm^2).

Each of the glass slides was carefully examined under the research microscope, Leica DM1000, equipped with a digital camera, Leica DFC 290. Adobe Photoshop 24.1.0 was used to enhance the contrast and provide a more precise representation of the studied structures.

For the morphometric analysis, the graphic software ImageJ (National Institutes of Health, Bethesda, MD, USA) was employed. The plug-in ColourDeconvolution2

helped us measure the percentage of the connective tissue surrounding the ganglia of the ENS by separating the different colors of the used stain.

The statistical data were analysed using GraphPad Prism 8 software (San Diego, CA, USA). We used: Shapiro-Wilk test for normal distribution of the studied values, as well as Dunn's multiple comparisons test, or Ordinary one-way ANOVA (depending on the distribution of the values) to determine the significance of the collected data. Statistical significance was determined if p-values were <0.05.

Results

Collagen fibers surrounding the myenteric ganglia were visualised with classical histochemical stains – Azan trichrome (**Fig. 1C-D**) and van Gieson (**Fig. 1A-B**). Azan delineated collagen as a well-defined blue–green meshwork adjacent to the *plexus myentericus*. Tangential and transverse sections, 6 µm thick, were examined. The proportion of collagenous connective tissue relative to total ganglionic area (C%) was quantified across n = 69 ganglia. Because the data were non-normally distributed, results are reported as medians and group differences were assessed using a Kruskal –

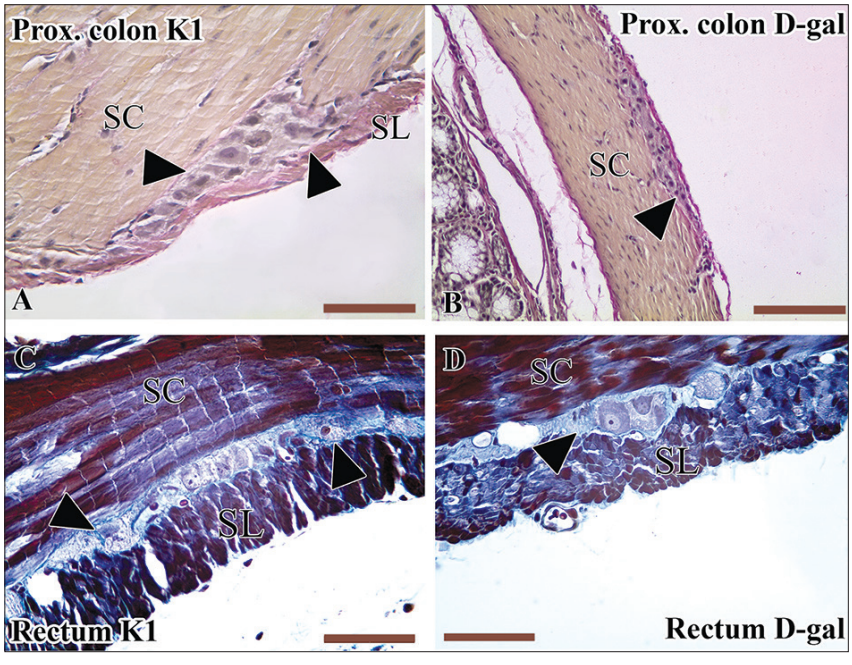

Fig. 1. Van Gieson (A-B) and Azan (C-D) staining of transverse cut of proximal colon (A) and sagittal cut of proximal colon (B) and rectum (C-D) of the control group K1 (A, C) and D-Galactose treated one (B, D) in ICR mice. Arrowheads indicate the collagen fibres around the preganglionic space. SL-stratum longitudinale, SC – stratum circulare. Scale bars = 50 µm (A, C, D), 100 µm (B).

Wallis test followed by Dunn's multiple comparisons. Overall differences in C% were observed ($H(5) = 23.07$, $p = 0.0003$). Median (Mdn) values were: PC–K1 = 12.22, D-Gal = 16.84; DC–K1 = 18.53, D-Gal = 11.67; REC–K1 = 9.344, D-Gal = 16.18 (**Fig. 3B**). Relative to controls, D-galactose exposure produced a marked reduction in C% at the DC level (by almost 60% decrease; $p = 0.0063$) and a significant increase at the REC level (73% increase; $p = 0.0075$) (**Fig. 3A**).

Using van Gieson staining (**Fig. 1A-B**), collagen surrounding myenteric ganglia appeared with the characteristic red coloration. A total of 79 ganglia were analyzed across control (K1) and D-galactose–treated (D-Gal) groups. Because C% (collagen area as a percentage of total ganglionic area) was not normally distributed, group differences were evaluated with the Kruskal – Wallis test, which indicated a significant overall effect ($H(5) = 22.52$, $p = 0.0004$) (**Fig. 3B**). Dunn's post hoc analysis showed a significant increase in C% in the proximal colon, with medians rising from 8.056 (K1) to 14.78 (D-Gal; $p < 0.05$). In the distal colon, C% likewise increased by 47% relative to controls (control median = 6.3; $p < 0.05$) (**Fig. 3B**).

Mast cells were visualized using toluidine blue staining (**Fig. 2A-B**). Mast cell (MC) density was expressed as cells per mm². Mast cell (MC) density was expressed as cells per mm² (**Fig. 3C-D**). In total, 36 histological slides were examined (K1, n = 18; D-Gal, n = 18), with 183 MCs identified. Normality was assessed with the Shapiro–Wilk test; data are reported as mean ± SD. One-way ANOVA across the six groups showed a significant overall effect, $F(5,30) = 12.69$, $p < 0.0001$. In controls (K1), MC density was highest in the rectum (REC: 1.041 ± 0.6584 cells/mm²) and proximal colon (PC: 0.7528 ± 0.2320 cells/mm²), and lowest in the distal colon (DC: 0.3259 ± 0.2035 cells/mm²) (**Fig. 3D**). Following D-galactose exposure, MC density increased and redistributed across segments, peaking in the DC (2.907 ± 1.172 cells/mm²), followed by the REC (1.541 ± 0.3905 cells/mm²) and PC (0.9948 ± 0.4704 cells/mm²) (**Fig. 3C**).

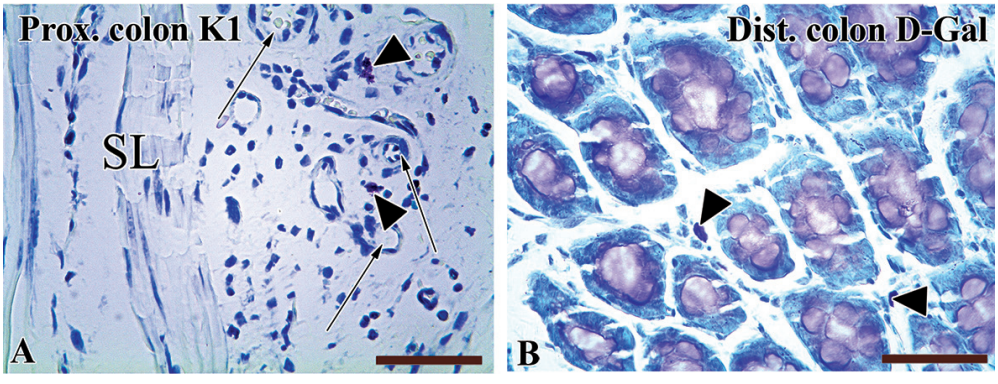

Fig. 2. Microphotographs stained with Toluidine blue of the proximal colon in the control group (A) and the distal colon in D-galactose-treated mice (B). Arrowheads are pointing at mast cells situated between the stratum longitudinale (A) and the mucosa (B). Arrows indicate small blood vessels; SL-stratum longitudinale. Scale bars = 50 μm.

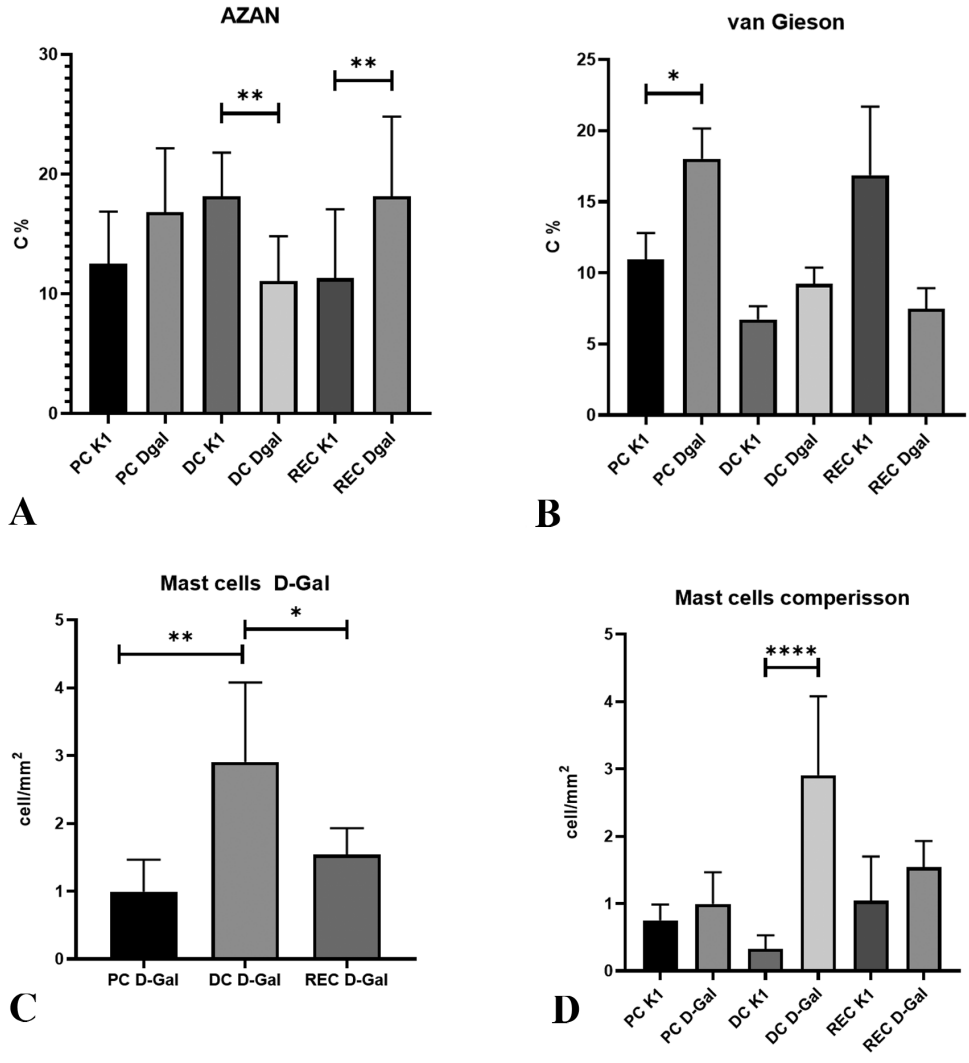

Fig. 3. Histograms showing (A–B) the percentage area of collagen fibers relative to the area of myenteric ganglia in Azan (A) and Van Gieson (B)–stained sections, and (C–D) the distribution of mast cells across different segments of the large intestine in K1 (control) and D-galactose–treated mice. Error bars indicate SD. Data were compared using the Kruskal–Wallis test followed by Sidak's multiple comparisons test; *$p < 0.05$, **$p < 0.01$, ****$p < 0.0001$.

Discussion

Our study extends previous work on the D-galactose–accelerated aging model by shifting the focus from the well-described neurodegeneration of the myenteric plexus [8] to remodeling of the myenteric ganglionic capsule and associated inflammatory responses across levels of the large intestine in ICR mice. Consistent with prior reports,

gastrointestinal aging is accompanied by an increase in collagen deposition [2]. The collagen family includes more than 20 subtypes, commonly grouped into fibril-forming (types I–III) and network-forming (type IV) categories [16], with type IV as the predominant collagen of the ganglionic basement membrane in the myenteric plexus [4].

Our approach integrates complementary histological stains with attention to their interpretive limits. Van Gieson staining, widely used to visualise type I collagen [11] and in our previous work [7], serves as a practical indicator of fibrillar collagen within and around myenteric ganglia. In contrast, Azan staining is a non-specific method for demonstrating collagen [9]; its findings require follow-up immunohistochemical analyses to resolve collagen subtype composition and provide detailed characterisation. Our analysis centres on capsule remodeling and inflammation as key features of D-galactose–induced aging in the enteric environment, while acknowledging the need for immunohistochemical confirmation to refine collagen profiling.

Mast cells play a key role in inflammatory processes [3]. While normally present throughout the gastrointestinal tract, increased mucosal counts indicate inflammation and are associated with conditions such as irritable bowel syndrome (IBS) [12]. In this study, we used toluidine blue staining to identify and quantify mast cells as a measure of inflammation in the large intestine. This established metachromatic dye has been used to visualize mast cells by targeting their heparin-rich granules since the late 19th century [14,13].

We observed increased mast cell concentrations at all three levels of the large intestine. Within the D-galactose model, these results align with oxidative stress and suggest that this approach can induce mast cell changes similar to those seen in IBS.

Our data indicate that D-galactose provokes remodeling of the myenteric (Auerbach's) plexus, manifested as an overall thickening of the collagenous capsule that envelops the ganglia. These findings accord with our previous observations of connective-tissue alterations around the myenteric plexus in naturally aged specimens and are consistent with reports of collagen remodeling in the ageing gut.

A region-specific divergence was observed in the distal colon. Although type I collagen increased by 47%, overall collagen fibres decreased according to the Azan stain. This suggests qualitative matrix remodeling, with a shift toward fibrillar type I collagen and a reduction in other Azan-positive components. These findings underscore the limitations of relying on single-stain assessments to infer collagen composition.

At the same intestinal level, this matrix profile was accompanied by a ninefold increase in mast cells in D-galactose–treated animals, suggesting that inflammation promotes collagen turnover and capsule restructuring. D-galactose-induced inflammation may involve mechanisms of myenteric barrier disruption similar to those seen in dextran sulfate sodium–induced colitis [4]. At the same level of the large intestine, this matrix profile coincided with a ninefold increase in mast cells in D-galactose–treated animals, suggesting that inflammation drives collagen turnover and capsule restructuring. The D-galactose-triggered inflammation may converge on mechanisms of myenteric barrier disruption similar to those described in dextran sulfate sodium–induced colitis [4].

To resolve these patterns mechanistically, additional immunolabeling for collagen subtypes and related extracellular-matrix markers, along with ultrastructural imaging, will be needed. These analyses should clarify how D-galactose–induced changes

inform the trajectory of myenteric ageing and the shifts that inflammatory diseases impose on the enteric nervous system.

Conclusions

This study is among the few to examine how an accelerated-ageing paradigm, specifically D-galactose, affects the myenteric plexus. D-galactose induced remodelling of the collagenous capsule surrounding myenteric ganglia – changes consistent with ageing – while simultaneously eliciting inflammatory responses, including marked mast cell accumulation, reminiscent of colitis and irritable bowel syndrome. The pattern was segment-specific, indicating that the colorectal region does not respond uniformly to the treatment. These findings support the use of D-galactose as a practical model for investigating the interplay between ageing, extracellular matrix organisation, and inflammation in the enteric nervous system, warranting confirmation through collagen subtyping, immunophenotyping, and functional readouts.

Acknowledgements: This research is supported by the Bulgarian Ministry of Education and Science under the "National Program Young Scientists and Postdoctoral Students – 2"; by the Bulgarian National Science Fund (contract No. КП-06-Н81/2); by the National Recovery and Resilience Plan (Project BG-RRP-2.004-0006-C02); and by the Faculty of Medicine, Trakia University – Stara Zagora (Grant No. 8/2023).

References

1. Azman, K. F., R. Zakaria. D-Galactose-induced accelerated aging model: an overview. – *Biogerontology*, **20**(6), 2019, 763-782. https://doi.org/10.1007/s10522-019-09837-y.

2. Baidoo, N., E. Crawley, C. H. Knowles, G. J. Sanger, A. Belai. Total collagen content and distribution is increased in human colon during advancing age. – *PloS One*, **17**(6), 2022, e0269689. https://doi.org/10.1371/journal.pone.0269689.

3. Collington, S. J., T. J. Williams, C. L. Weller. Mechanisms underlying the localisation of mast cells in tissues. – *Trends Immunol.,* **32**(10), 2011, 478-485. https://doi.org/10.1016/j.it.2011.08.002.

4. Dora, D., S. Ferenczi, R. Stavely, V. E. Toth, Z. V. Varga, et al. Evidence of a myenteric plexus barrier and its macrophage-dependent degradation during murine colitis: Implications in enteric neuroinflammation. – *Cell. Mol. Gastroenterol. Hepatol.*, **12**(5), 2021, 1617–1641. https://doi.org/10.1016/j.jcmgh.2021.07.003.

5. Furness, J. B. The enteric nervous system and neurogastroenterology. – *Nat. Rev. Gastroenterol. Hepatol.,* **9**(5), 2012, 286-294.

6. Furness, J. B., T. V. Nguyen, K. Nurgali, Y. Shimizu. The enteric nervous system and its extrinsic connections. – *Textbook of Gastroenterology*, 2008, 15-39. https://doi.org/10.1002/9781444303254.ch2.

7. Genov, N., N. Dimitrov, D. Atanasova. Aging of the myenteric plexus in the rat colorectal region. – *Acta Morphol. Anthropol.*, **32**(1–2), 2025, 31-36. https://doi.org/10.7546/ama.32.1-2.2025.04

8. Genov, N., N. Tomov, N. Dimitrov, T. Kirov, L. Petrov, et al. Morphometric changes of the myenteric plexus in the colon of the mice-D-galactose ageing model. – *C. R. Acad. Bulg. Sci.*, **77**(4), 2024, 576–583. https://doi.org/10.7546/CRABS.2024.04.13

9. Golberg, M., J. Kobos, E. Clarke, A. Bajaka, A. Smędra, et al. Application of histochemical stains in anatomical research: A brief overview of the methods. – *Transl. Res. Anat.*, **35**, 2024, 100294. https://doi.org/10.1016/j.tria.2024.100294.

10. Gomes, O. A., R. R. de Souza, E. A. Liberti. A preliminary investigation of the effects of aging on the nerve cell number in the myenteric ganglia of the human colon. – *Gerontology*, **43**(4), 1997, 210-217. https://doi.org/10.1159/000213852.

11. Guo, S. B., Z. J. Duan, Q. M. Wang, Q. Zhou, Q. Li, X. Y. Sun. Endogenous carbon monoxide downregulates hepatic cystathionine-γ-lyase in rats with liver cirrhosis. – *Exp. Ther. Med.*, **10**(6), 2015, 2039-2046. https://doi.org/10.3892/etm.2015.2823.

12. Panarelli, N. C., J. L. Hornick, R. K. Yantiss. What is the value of counting mast cells in gastrointestinal mucosal biopsies? – *Mod. Pathol*., **36**(2), 2023, 100005. https://doi.org/10.1016/j.modpat.2022.100005.

13. Puebla-Osorio, N., S. N. E. Sarchio, S. E. Ullrich, S. N. Byrne. Detection of Infiltrating Mast Cells Using a Modified Toluidine Blue Staining. – *Methods Mol. Biol.*, **1627**, 2017, 213-222. https://doi.org/10.1007/978-1-4939-7113-8_14

14. Ribatti, D. The staining of mast cells: A historical overview. – *Int. Arch. Allergy Immunol*., **176**(1), 2018, 55-60. https://doi.org/10.1159/000487538

15. Sri Paran, T., U. Rolle, P. Puri. Age-related changes in the myenteric plexus of the porcine bowel. – *J. Pediatr. Surg.*, **44**(9), 2009, 1771-1777. https://doi.org/10.1016/j.jpedsurg.2008.12.018

16. Tvaroška, I. Glycosylation Modulates the Structure and Functions of Collagen: A Review. – *Molecules*, **29**(7), 2024, 1417. https://doi.org/10.3390/molecules29071417

17. Zhao, Y., Z. Zeng, W. Zheng, Zhang, Z., Zhang, H. et al. Cow placenta peptides ameliorate D-Galactose-induced Intestinal Barrier Damage by Regulating TLR/NF-κB Pathway. – Vet. Sciences, **12**(3), 2025, 229. https://doi.org/10.3390/vetsci12030229

Institute of Experimental Morphology, Pathology and Anthropology with Museum
Bulgarian Anatomical Society

Acta Morphologica et Anthropologica, 32 (3-4)
Sofia ● 2025

Primary Invasive Intraoral Malignant Melanoma of the Mandibular Mucosa

Alexander Ivanov[1,2,3], Iliya Bivolarski[1], Mariya Popivanova[1,2,3]*

[1] Department of General and Clinical Pathology, Medical University, Plovdiv, Bulgaria
[2] Department of Clinical Pathology, UMHAT "St. George", Plovdiv, Bulgaria
[3] Regular PhD students in Medical University, Plovdiv, Bulgaria

*Corresponding author e-mail: aleksandar.ivanov@mu-plovdiv.bg

Primary oral malignant melanoma is an exceptionally rare neoplasm, comprising approximately 0.2-8% of all melanomas, with even fewer cases originating from mandibular mucosa. It is characterised by an aggressive clinical progression, rapid local invasion, early metastases and poor prognosis. Unlike cutaneous melanomas, oral melanomas often present asymptomatically, which significantly delays diagnosis and limits treatment options. This report presents a case of a 78-year-old female patient with an asymptomatic, pigmented lesion located in the left mandibular region. Radiological imaging revealed an infiltrative heterodense mass with underlying bone destruction. The histopathological analysis showed solid tumour nests with marked atypia and brown pigmentation. Immunohistochemical staining demonstrated strong positivity for S-100 and Melan-A, confirming the diagnosis of primary invasive mucosal melanoma. This case underscores the diagnostic challenges posed by mucosal melanomas, particularly in atypical locations such as the mandible, and emphasizes the critical role of early biopsy and immunohistochemistry in establishing a definitive diagnosis.

Key words: melanoma, oral, mucosa, mandible, primary

Introduction

Melanomas are malignant neoplasms arising from melanocytes, which are neural crest-derived cells [3, 5, 7, 8]. The first description of oral mucosal melanoma was provided by Weber in 1859, and in 1869, Lucke coined the term "melanotic sarcoma" [2, 4 ,8]. Most melanomas develop on the skin, originating from melanocytes in the basal layer of the epidermis.

Mucosal melanomas constitute approximately 1.4% of all melanomas across all races, and 0.8-3.7% among Caucasians. Some sources report a higher incidence in Asians (particularly Japanese), Indians, Hispanics and individuals of African descent [5, 9] – possibly due to the greater prevalence of oral mucosal pigmentation – whereas

others suggest a higher incidence in Caucasians. Mucosal melanomas have been documented in various anatomical sites, including the rectum, anal canal, vagina, cervix, larynx, esophagus, and head and neck regions. Within the head and neck, the oral cavity is the least frequently affected site [4, 9].

Primary intraoral malignant melanoma is a rare and aggressive subtype with a greater propensity for rapid metastasis and often presents asymptomatically. Consequently, it is frequently diagnosed at an advanced stage, contributing to its poor prognosis and low survival rate [2, 9]. An important fact to note is that tumour thickness, ulceration and level of invasion are not of any prognostic value [9].

Case Report

We report the case of a 78-year-old female patient who presented with an asymptomatic lesion located in the upper ridge of the left mandibular region. The lesion exhibited infiltrative behavior and destruction of the surrounding bone. A CT scan revealed a heterodense mass measuring 31 × 48 mm, involving adjacent tissues. Clinically, the lesion appeared darker in colour. No relevant clinical history was provided. A biopsy sample was submitted to our department for histopathological evaluation.

Materials and Methods

Tissue specimens were fixed in 10% neutral buffered formalin and embedded in paraffin. Sections of 4 μm thickness were obtained for histological analysis. Further immunohistochemical testing was performed to confirm the diagnosis using the following antibodies – **S-100, Melan-A, p63, CK AE1/AE3, CK34βE12**. All the antibodies are supplied by Dako and are ready-to-use (pre-diluted). The staining protocols are validated by Dako.

Results

Hematoxylin and eosin (H&E) staining revealed fragmented material covered with multilayered squamous epithelium. Underlying infiltration of solid tumour nests exhibiting marked cellular atypia and the presence of brown pigment, with focal ulceration of the overlying mucosa. The most likely diagnosis is primary invasive melanoma of the oral mucosa (**Fig. 1).**

Immunohistochemical analysis supported this diagnosis: S-100 and Melan-A **- strong positive (+++) in tumour cells;** p63**,** CK AE1/AE3**,** CK34βE12 - negative in tumour cells and positive in squamous epithelium (internal control); CD79a - negative in tumour cells (**Fig. 2, Fig. 3).**

The comprehensive immunohistochemical panel confirmed the final diagnosis of primary invasive malignant melanoma of the mandibular mucosa, as supported by the images below:

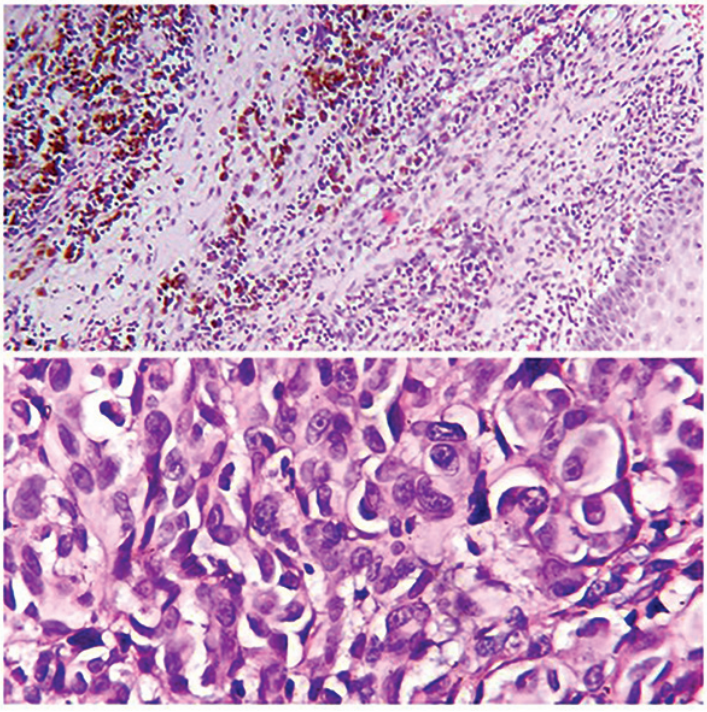

Fig. 1. Solid nests of polygonal atypical cells filled with intracytoplasmic brown pigment H-E (Upper picture x 200) and an achromatic area with scarse pigment granules H-E (lower picture ×400).

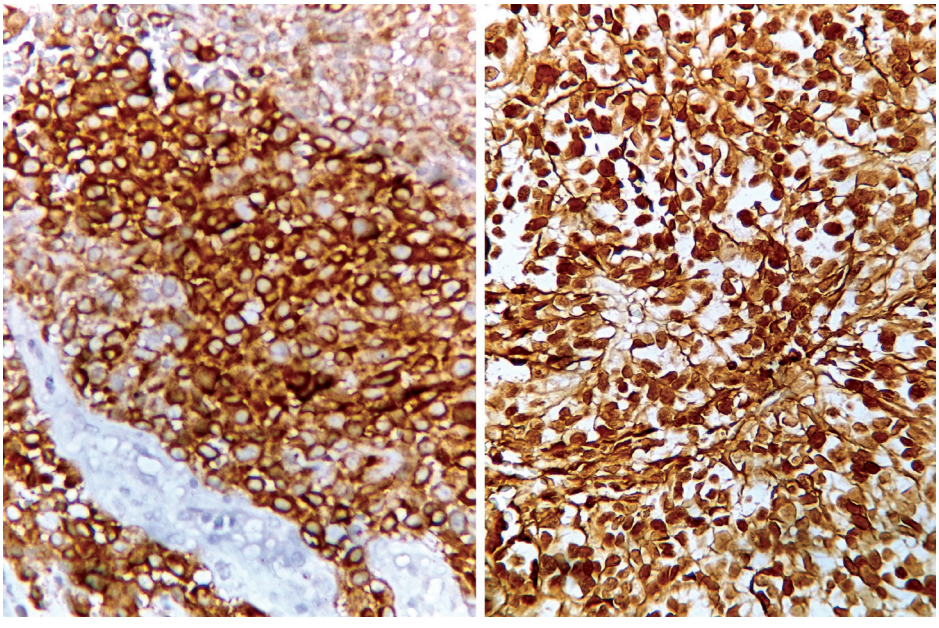

Fig. 2. Strong positive reaction in the tumour cells with Melan-A (left x400) and S-100 (right ×400)

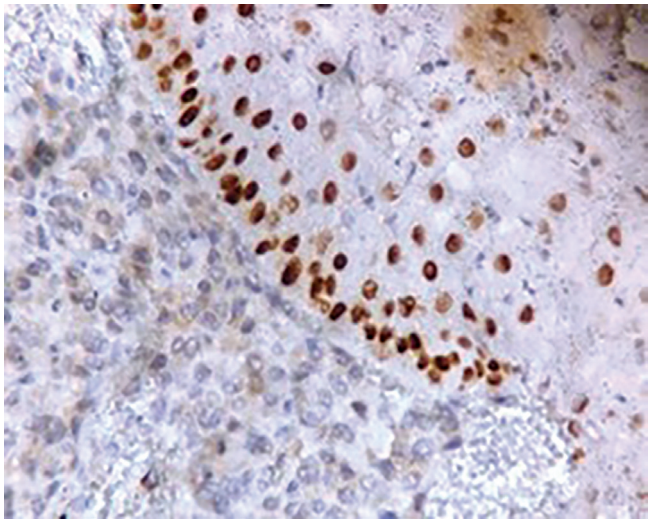

Fig. 3. Negative reaction in the tumour cells, with a positive internal control in the epithelial cells with p63 (×400)

Discussion

Primary mucosal malignant melanoma of the mandible is an exceptionally rare tumour, with mandibular localization being particularly uncommon. While the etiology remains unclear, some reported contributing factors may include smoking, denture use, and exposure to carcinogens such as tobacco and formaldehyde [3, 4]. Genetic mutations such as NRAS**,** BRAF**, and c-**KIT **have been implicated [7, 8]. Although the lesion can occur at any age, the average age of diagnosis is around 56 years [4]. The condition is reported to be two to three times more common in males than females [2, 3, 4, 8].**

Within the head and neck region, the most frequent sites of mucosal melanoma include the nasal cavity/septum and maxillary sinus, followed by the paranasal sinuses and, less commonly, the oral cavity. When present in the oral cavity, lesions most frequently involve the palate and maxillary gingiva (in 80–90% of cases) [1, 2, 3, 4, 6, 7, 8].

The differential diagnosis of oral melanoma includes [4, 6, 7]:

- Amalgam tattoo
- Melanotic macule
- Melanotic nevus
- Melanoacanthoma
- Post-traumatic or racial pigmentation
- Systemic conditions (e.g., Peutz–Jeghers syndrome, Addison‘s disease)
- Drug-induced pigmentation
- Vascular malformations
- Epulis, pyogenic granuloma, irritation fibroma
- Peripheral giant cell granuloma, peripheral ossifying fibroma
- Kaposi sarcoma
- Metastatic non-pigmented lesions

The reported five-year survival rate is approximately 7% [7], underscoring the aggressive nature and diagnostic challenges of this malignancy.

Conclusion

This case underlines the importance of considering primary mucosal melanoma in the differential diagnosis of pigmented oral lesions, especially in older patients – even in the absence of symptoms. Early biopsy and histopathological evaluation, supported by immunohistochemistry, remain critical tools for accurate diagnosis. Given the aggressive behaviour and poor prognosis associated with oral melanomas, raising clinical awareness and promoting routine oral examinations may aid in earlier detection and potentially improve patient outcomes.

Patient consent

The authors certify to obtaining the patient's consent for using of the information, age and gender, as well as pictures of the microscopic slides.

References

1. Akhil, S., V. K. Rb, S. M. Mustafa, J. Mathew. A rare case of primary oral malignant melanoma of mandibular gingiva with an update on clinical staging. – *Indian J. Dermatol*., **66**, 2021, 427-430.

2. Fauzdar, S., D. D. Rao, K. K. Arthanari, G. Krishnan, V. G. Naikmasur, M. M. Revanappa. Malignant melanoma of the mandibular gingiva. – *Rare Tumors,* **2**, 2010, e25.

3. Gayathri, M., G. S. Gnanadeepam, C. P. Raghu, P. Selvajothi, M. W. Sumathy, S. Kuzhali, J. S. Jebapriya. Primary malignant melanoma of mandibular gingiva with cerebral metastasis – a case report with review of literature. – *Saudi Journal of Pathology and Microbiology*, **5** (1), 2020, 13-18.

4. Jun, K. B., H. S. Kim, Y. J. Chang, K. H. Kwon, S. J. Cho. Primary amelanotic melanoma of the mandibular gingiva. – *Archives of Craniofacial Surgery*, **21**(2), 2020, 132-136.

5. Pathologyoutlines.com

6. Patil, P. B., S. Venkatraman, A. Goe. Primary intraoral malignant melanoma involving multiple sites – a case report and review of literature. – *Int. J. Oral-Med. Sci.*, **10**(2), 2011, 103-108.

7. Pradhan, P., A. K. Adhya. Extensive malignant melanoma of the oral cavity: a rare occurrence. – Autops Case Rep. 2020, 11:e2021299.

8. Tamgadge, S., T. Pereira, A. Date, P. Kalimuthu, A. Tamgadge. Oral malignant melanoma of the lower jaw – a case report with immunohistochemical investigations –*ecancr,* **17**, 2023, 1561.

9. Verma, N., A. Srivastava. Primary malignant melanoma of mandibular gingiva: A rare case report. – *Journal of Cancer Research and Therapeutics,* **17**(6), 2021, 1565-1568.

Institute of Experimental Morphology, Pathology and Anthropology with Museum
Bulgarian Anatomical Society

Acta Morphologica et Anthropologica, 32 (3-4)
Sofia ● 2025

Cleansing efficiency of the new endodontic tip of Lite Touch Er:YAG laser – a SEM study

Georgi Tomov[1], Kostadin Georgiev[2], Stela Atanasova-Vladimirova[3]*

[1] Dept. of Healthcare and Social Work, New Bulgarian University, Sofia, Bulgaria
[2] Dept. of Operative Dentistry and Endodontics, Faculty of Dental Medicine, Medical University of Plovdiv, Bulgaria
[3] Institute of Physical Chemistry, Bulgarian Academy of Sciences, Sofia, Bulgaria

*Corresponding author e-mail: dr.g.tomov@gmail.com

The Er:YAG laser-assisted endodontics has a long-standing history since the late 1990s. The materials for the endodontic tips manufacturing, their design and the parameters used however varied significantly in time. The current article is addressing the new flexible tip developed by Light Instruments Ltd. for endodontic use and is focused on evaluation of its cleansing efficiency and morphological changes in the root canal. In this pilot study 11 extracted single-rooted teeth were used. After shaping with ProTaper™ F3 Ni-Ti files an Er:YAG laser-activated irrigation was performed with 17% EDTA irrigation for 60 second with flexible endodontic tip inserted in the root canal 4 mm coronally from apical foramen. The SEM study demonstrates that the new endodontic tip is effective in smear layer elimination of all root canal segments, and can be adjusted successfully in the endodontic therapy.

Key words: Er:YAG, laser tip, cleansing, SEM

Introduction

The Er:YAG laser's use in endodontics emerged after its 1997 FDA approval for hard tissue procedures, with the first clinical applications and development of endodontic-specific devices occurring in the late 1990s [10]. Following FDA approval and further researches, specialized flexible fibers and specific endodontic tips were developed for the Er:YAG laser, making it feasible for clinical use in endodontics [3, 5, 10]. Clinical studies and commercialization of Er:YAG lasers increased after 2000, demonstrating its advantages in endodontic procedures, such as improving cleaning and disinfection of root canals using different techniques all based on same phenomenon - photoacoustic activation including cavitation, shock waves and fluid streaming [10]. Techniques like

PIPS (Photon-Induced Photoacoustic Streaming), SWEEPS (Shock Wave-Enhanced Emission Photoacoustic Streaming) and LT-IPI (Lite Touch-Induced Photomechanical Irrigation) use low-energy laser pulses to agitate the irrigants and to detach debris, biofilm and vital pulpal remnants from the main root canal, dentinal tubules, cul-de-sac and lateral canals, leading to superior debridement, disinfection and a better healing environment [2, 3, 4, 5, 6, 10]. Despite the existence of sound evidences for the benefits of laser-activated endodontic irrigation, the manufacturers continue to launch on the market new endodontic tips with improved design. The clinical implementation of any new tip requires a complete and thorough study of its characteristics, and in the context of endodontic irrigation - its cleansing efficiency, which is crucial for the endodontic therapy success.

The current article addressees the new flexible quartz tip developed by Light Instruments Ltd. for endodontic use and is focused on the morphological effects in the root canal after its use evaluated by scanning electron microscopy.

Materials and Methods

Tooth Samples

Eleven single-rooted human teeth extracted for periodontal reasons were used in this in vitro study. Root canal preparation was carried out using ProTaper™ (Dentsply Maillefer, Baillaigues, Switzerland) F3 Ni-Ti files accomplished with 2.5% NaOCl irrigation. At the end of the mechanical shaping, each root canal was finally irrigated with 17% EDTA using Er:YAG laser (LiteTouch™, Light Instruments, Israel) equipped with a cylindrical quartz fiber tip (25mm, 440 μm). Energy was set to 0.4 W (40 mJ, 10 Hz) for 60 seconds (**Fig. 1A**). The water/air spray of the laser was turned off and the irrigation solution (17% EDTA) was injected constantly during irradiation (**Fig. 1B**). The laser tip was inserted 4 mm coronally from apical foramen and moved up and down during the procedure. After this final irrigation, two longitudinal cuts were made with a high-speed bur and the teeth were split in half for further evaluation by SEM.

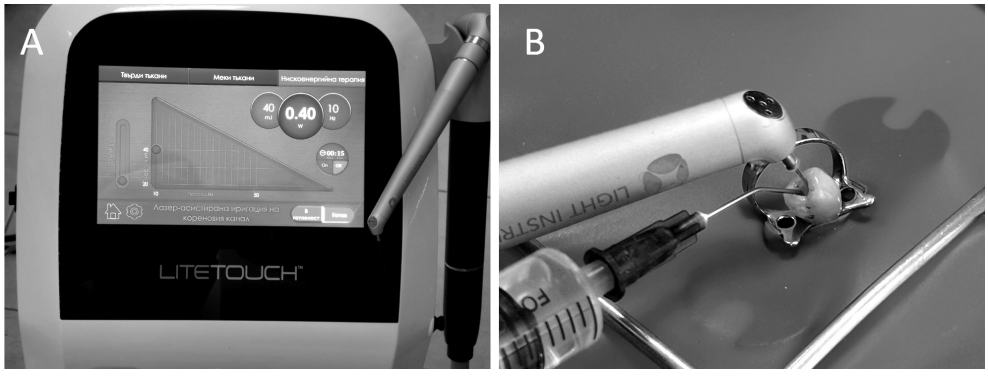

Fig. 1. *The laser settings used for irrigant activation are 0.4 W (40 mJ/10 Hz) without water/air spray (**A**). The irrigant (17% EDTA) is constantly delivered during the irradiation (**B**).*

Scanning Electron Microscopy (SEM)

All samples were desiccated and fixed on stubs and then coated with gold using an JEOL JFC 1200fine coater (Tokio, Japan). Images were collected on an JEOL JSM 6390 (Tokio, Japan) with acceleration voltage of 20 kV. The morphological effects of the laser-assisted irrigation were examined at a magnification of 600X for all three portions of each root canal. The scoring of the smear layer was done according to the modified criteria given by Tomov et al. [1]:

Score 1 – Complete absence of a smear layer and open dentinal tubuli free of debris.

Score 2 – Presence of a smear layer only in dentinal tubules orifices (>50% are visible).

Score 3 – Presence of a thin homogeneous smear layer covering the canal wall with a few dentinal tubules open (<50% are visible).

Score 4 – A thick smear layer covering completely the canal wall. The dentinal tubules are filled with debris and their contours are not clear.

Score 5 – The entire canal wall is covered by a heavy smear layer with no visible dentinal tubules.

A single-blind evaluation of the SEM micrographs was carried out by two examiners (G.T. and K.G.) according to this scoring system. Data was analyzed using SPSS software, version 16. Friedman and Wilcoxon tests were applied for the comparison of smear layer removal between the three regions. Additional pictures of other artefacts were done at different magnifications.

Results

The results obtained from this study are summarized in **Table 1**. The smear layer removal was greater in the coronal and middle regions than the apical region of the root canal (P=0.003 and P=0.02, respectively) with no differences between the coronal and middle regions (P=0.09).

Table 1. *Mean amounts of smear layer by regions*

Regions	**Mean±SD**
Coronal portion	1.62±1.94
Middle portion	2.37±1.70
Apical portion	3.43±1.38

The morphological analysis of the microphotographs revealed that the coronal and the middle portion of the root canal are almost completely free of smear layer and the majority of the dentinal tubules are visible and clean – scores 1 and 2 (**Fig. 2A, B**). In the apical portion some areas are partially covered with thin smear layer and not all dentinal tubules are clean – scores 2 and 3 (**Fig. 2C**).

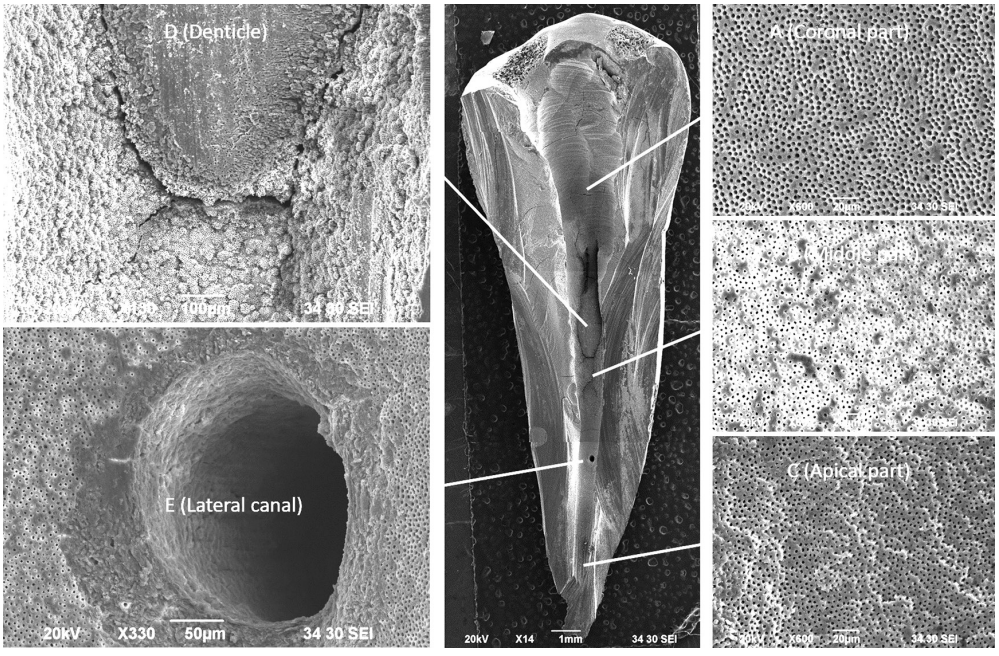

Fig. 2. *SEM evaluation at magnification X 600 revealed lack of smear layer after Er:YAG laser-assisted irrigation with 17% EDTA for 60 seconds. The coronal (**A**) and the middle (**B**) are clean with open dentinal tubules. In the apical portion (**C**) some dentinal tubules are covered with thin smear layer. Additional observations showed specific root canal artifacts like impacted denticle (D) and lateral canal(E), both clean and free of debris.*

The additional observations revealed different structures and root canal artifacts like impacted denticle (**Fig. 2D**) and lateral canal (**Fig. 2E**), both clean and free of debris.

Discussion

The laser-assisted irrigation is based on delivering the laser beam through a tip into the root canal filled with liquid. The energy of the Er:YAG laser is highly absorptive in water at between 1–3 μm penetration depth [10], resulting in formation of cavitation bubbles that create shock waves in proximity to canal walls during their collapses and generating shear flows capable of removing debris from the dentinal surface [10]. Additionally, due to the emitted shock waves in proximity to the canal walls, they encounter the root canal wall at supersonic speed with energy efficient enough for optimal cleaning and disinfecting the root canal system.

However, the application of these physical principles depends on many factors including the design of the "delivery system" i.e. the endodontic tip. The endodontic portfolio of Light Instruments has been enriched in the past ten years with 3 available modalities at the moment – conical sapphire tip (17±0.1mm, 400±0.2μm), conical metal side-firing spiral tip (25mm, 300μm) and the newly developed cylindrical quartz fiber tip (25mm, 440-μm) (**Fig. 3A, B, C**). The first two endodontic tips are studied both

experimentally and clinically [2, 6, 7, 8, 9]. Their advantages and limitations are also well known. The conical sapphire tip is usually inserted into the coronal third or even into the pulp chamber in completely straight canals, with the beam activating the irrigant in all its volume. [2] In curved canals however, the generated shock waves encounter resistance at the canal curvature and the residual photoacoustic effects apically are insufficient for good cleaning [9]. The reported clinical effectiveness in the literature is referred only to straight root canal cases [2, 7]. The limitations of the sapphire tip were overcome with the introduction of so-called side-firing tip by A. Stabholz. It demonstrates good cleansing effectiveness but requires significant enlargement of the root canal [8, 9] (**Fig. 3D**). The use in a very curved canals is also problematic.

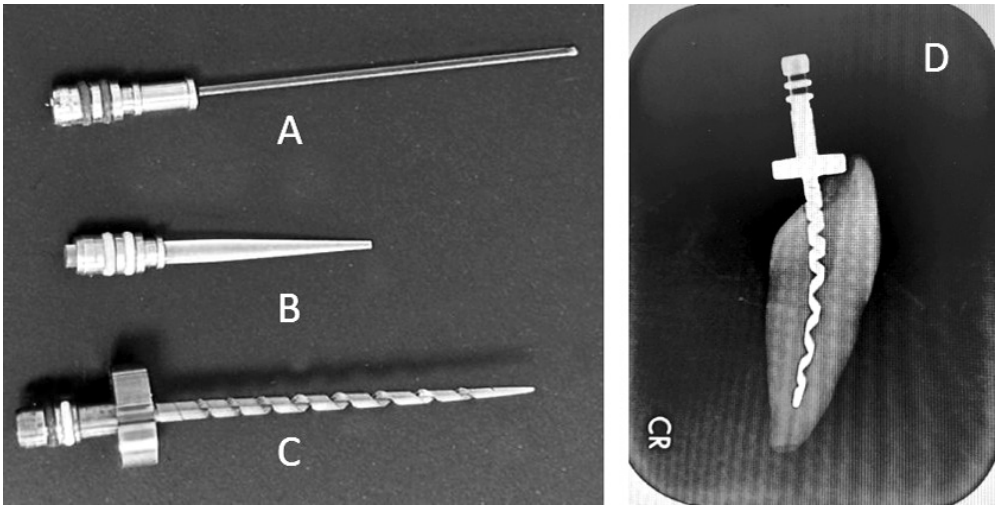

Fig. 3. *The available endodontic tips - cylindrical quartz fiber tip (**A**), Endo tip LIFG4001A (**B**) and Sapphire tip AS7075X (**C**) revealed different designs that interfere with their effectiveness. X-ray of the Endo tip LIFG4001A inserted into root canal (**D**).*

To address all these limitations Light Instruments designed new plastic quartz fiber tip which was subject of the current study where both the cleansing abilities and the morphological effects of 17% EDTA together with laser irradiation were evaluated in vitro on a root dentin. Intact teeth were used to simulate the clinical reality as closely as possible. Our previous study revealed that prolonged exposition on EDTA might provoke severe demineralization of the root dentin [11] and that is why the irrigation time and irrigant volume were limited to 1 minute and 10 ml respectively, to minimize potential changes in the dentin's microhardness, permeability, and solubility characteristics.

The energy used was also different from the previously reported studies. In contrast to Bibova N. (0.5 W:50 mJ/10 Hz) and Sahar-Helft S. (1.5 W:150 mJ/10 Hz) in this experiment a lower energy (0.4 W:40 mJ/10 Hz) was used for the same time of activation achieving comparable cleansing effectiveness [2, 7]. The position of the laser tip inside of the root canal is also important. When using fiber tip along the root canal, the clinicians have to consider the possibility for occurring apical extrusion of the irrigant during laser activation [2, 11]. Therefore, in this in vitro study the laser tip was inserted 4 mm coronally from apical foramen and moved up and down during the procedure.

The results obtained are in essence close to the effectiveness reported by other authors [2, 3, 7]. The main differences are the lower energy used and the ability of this flexible tip to be used in narrow and curved root canals.

Conclusion

Since the physical principles behind Er:YAG laser-activated irrigation are essentially the same, the aspiration of manufacturers and clinicians is to have an endodontic tip that is both effective and safe. This in vitro SEM study demonstrates that the new flexible quartz fiber tip met these requirements and can be adjusted successfully for endodontic therapy. However, additional clinical research with multiple patients is required to verify this modality as a routine.

Acknowledgements: The original contributions presented in the study are included in the article. Further inquiries can be directed to the corresponding author.

R e f e r e n c e s

1. Belcheva, A., **G. Tomov**. Hard dental tissues in norm and pathology. SEM atlas. *Medical University of Plovdiv*, 2018. (in Bulgarian)

2. Bibova, N. Er:YAG laser-activated irrigation in endodontic treatment (experimental, laboratory and clinical studies). – *PhD thesis*, 2016, Plovdiv, Bulgaria.

3. DiVito, E., O. A. Peters, G. Olivi. Effectiveness of the erbium:YAG laser and new design radial and stripped tips in removing the smear layer after root canal instrumentation. – *Lasers Med. Sci*., **27**(2), 2012, 273-280.

4. DiVito, E., A. Lloyd. ER:YAG laser for 3-dimensional debridement of canal systems: use of photon-induced photoacoustic streaming. – *Dent Today*, **31**(11), 2012, 122, 124-127.

5. Guidotti, R., E. Merigo, C. Fornaini, J. P. Rocca, E. Medioni, P. Vescovi. Er:YAG 2,940nm laser fiber in endodontic treatment: a help in removing smear layer. – *Lasers Med. Sci.*, **29**(1), 2014, 69-75.

6. Kurtzman, G. M. Laser-enhanced endodontic treatment. – *LASER: international magazine of laser dentistry*, **4**, 2017, 26-28.

7. Sahar-Helft, S., A. Stabholz. Rermoving smear layer during endodontic treatment by different techniques – an invitro study. A clinical case – Endodontic treatment with Er:YAG Laser. – *Stoma Edu J.*, **3**(2), 2016, 162-167.

8. Sahar-Helft, S., A. Farber, N. Sebbane, C. Helft, R. Dakar, V. Gutkin, R.V. Sionov, D. Steinberg. Effect of Er:YAG Laser-Activated Irrigation with Side-Firing Spiral Endo Tip on Dentin Mineral Composition of Tooth Root Canals. – *Photonics*, 2024, 11, 978. https://doi.org/10.3390/photonics11100978

9. Sebbane, N., D. Steinberg, D. Keinan, R.V. Sionov, A. Farber, S. Sahar-Helft. Antibacterial Effect of Er:YAG Laser Irradiation Applied by a New Side-Firing Spiral Tip on Enterococcus faecalis Biofilm in the Tooth Root Canal – *An Ex Vivo Study. – Applied Sciences*, **12**(24), 2022, 12656.

10. Stabholz, A., S. Sahar-Helft, J. Moshonov. Lasers in endodontics. – *Dent. Clin. N. Am*., **48**, 2004, 809-832.

11. Tomov, G. Irrigation of infected root canals (laboratory and clinical research). – *Folia Medica (Plovdiv)*, **53**(1), 2011, 82-85.

Institute of Experimental Morphology, Pathology and Anthropology with Museum
Bulgarian Anatomical Society

Acta Morphologica et Anthropologica, 32 (3-4)
Sofia ● 2025

Forensic analysis of morphological changes in death due to drowning

Deyana Velkova

Department of General and Clinic Pathology, Forensic Medicine and Deontology Medical University – Varna

*Corresponding author e-mail: Deyana.Velkova@mu-varna.bg

The present study aims to track the frequency of detection and characteristics of some of the main morphological changes observed during the autopsy of corpses that died as a result of drowning. A total of 151 forensic medical examinations reports of non-decomposed corpses diagnosed with drowning, were reviewed and for each case, the type of water body, the sex and age of the corpse, and some of the main autopsy findings related to the diagnosis of drowning were recorded – cyanosis, subconjunctival hemorrhages, foam, lung overinflation, subpleural hemorrhages, Sveshnikov's sign with presence or absence of diatoms and other foreign bodies. Analysis of the obtained results and data from reviewed literature clearly shows that there is no single morphological sign that is diagnostically specific only for drowning. The results of the study contribute to expanding knowledge about the main morphological changes observed in drowning, which significantly aids daily forensic medical practice.

Key words: drowning, mechanical asphyxia, autopsy findings, forensic examination

Introduction

Drowning is a type of mechanical asphyxia that results from aspiration of liquid into the airways and lungs with the subsequent development of cerebral hypoxia. Death by drowning is an unnatural (violent) death, most commonly accidental, but it can also be a suicide, and in some rare cases, a homicide [14, 22, 31]. According to the World Health Organization, about 300,000 people die each year worldwide as a result of drowning [34]. Literature sources distinguish several predisposing factors as having a significant role in the occurrence of this type of accident (swimming in rough seas, alcohol use, presence of acute and chronic diseases, etc.) [24, 35].

It should be noted that not every cadaver found in a water environment died as a result of drowning. In the forensic literature, a general term is found – immersion death, which refers to bodies found in water. Some authors propose classifying these cases into several groups in relation to the cause of death, for example: death from

natural causes during or before entering the water; death due to trauma during or before entering the water; death due to drowning, where several variants are also possible – when drowning occurred after trauma or pathological conditions that have left the victim in a helpless state (secondary drowning) and when it is not accompanied by any other event (primary drowning) [7, 29, 33].

In many cases, it is difficult to diagnose mechanical asphyxia due to drowning because there are no specific autopsy findings. It should be emphasised that there is no sign specific to drowning, so all findings related to drowning must be interpreted in the context of the circumstances in which death occurred. Some authors believe that drowning is actually a diagnosis of exclusion [3, 12, 14, 19, 22, 36].

When a corpse is discovered in a water environment with suspicion of drowning, two main groups of findings should be clearly distinguished – classic signs of asphyxiation death and signs indicating that the body has been in water for a certain period of time (signs of immersion). The main morphological changes observed in cases of various types of asphyxia (including drowning) are cyanosis, petechial hemorrhages on the conjunctivas, sometimes on the skin of the face and torso, on the serous membranes of the internal organs, incontinence of the sphincters of the pelvic organs, the presence of liquid blood, venous stasis in the internal organs, anemic spleen, edema of the brain and lungs, and others. It should be noted that the presence of these morphological changes must be analyzed with special attention, since they can also be observed in other causes of death than asphyxia, respectively, drowning. The group of signs that indicate the body was in an aquatic environment, such as piloerection, maceration changes on the skin, saponification, etc., are not conclusive evidence that death occurred due to drowning. On the other hand, those signs provide important information about the post-mortem submersion period [3, 7, 8, 12, 14, 22].

It is particularly difficult to establish the diagnosis of drowning in decomposing corpses. The process of decay is usually slower in an aquatic environment, especially in cold water, but it also depends on many other factors [3, 35]. It has been established that a body removed from the aquatic environment develops significantly faster decay processes. Therefore, according to the literature and forensic practice, it is important that after removal from the water, the body should be cooled as quickly as possible and an autopsy be performed within a short period of time [3, 8, 22, 35]. Saponification, as a specific preservation process of corpse decomposition occurring in an aquatic environment, can preserve both the anatomical integrity of the corpse and the possibilities for conducting additional examinations [3, 22].

Typically, external examination of the body of an individual who has died from drowning may reveal certain signs that are not strictly specific to this diagnosis - froth (foam) in front the nose and mouth orifices and along the airways, petechial hemorrhages on the conjunctivas (subconjunctival hemorrhages), cyanosis, and others. The foam, found around the nose and mouth and along the respiratory tract, is considered by some authors to be a specific sign of drowning and represents an important diagnostic indicator [14, 17, 19, 22, 31, 35, 37]. Facial cyanosis (sometimes also of the neck and chest), as well as subconjunctival hemorrhages, are not present in all cases of drowning and can also be a sign of other types of mechanical asphyxia or a pathological process leading to death [3, 22, 35].

Internal examination of the corpse may reveal certain morphological changes that aid in a more accurate diagnosis of drowning: overinflation of the lungs, subpleural

hemorrhages, presence of fluid in the sphenoidal sinus (Sveshnikov‘s sign), presence of watery fluid in the stomach and duodenum, presence of free fluid in the pleural and peritoneal cavities (Moro‘s sign), and others [8, 22, 31, 35]. A number of authors believe that morphological changes, especially in the lungs, differ between drownings in fresh and salt water. This is related to the pathophysiological processes that are observed when aspirating a hypotonic solution (fresh water), and those when aspirating a hypertonic solution (salt water) [9, 14, 17].

The overinflation of the lungs is one of the main morphological signs observed in drowning. When drowning occurs in fresh water, it passes in large quantities through the alveolar-capillary membrane into the bloodstream. With this mechanism, the lungs appear very inflated (similar to a soaked sponge), at the same time their cut surface appears relatively dry, but when pressed, a foamy liquid is released. This is the morphological type of the lung’s inflation that some authors defined as a hyperaerated form and corresponds to the concept of “emphysema aquosum” or the more accurate term “emphysema spumosum” (spongy emphysema). It is important to note that this type of emphysema differs from disease-related emphysema, in which typical bullae are usually found, and the cut surface shows prominence of the cut bronchi and blood vessels [7, 8, 14, 19, 22, 29, 35, 36].

When drowning occurs in salt water, due to the fact that it is a hypertonic solution, the water component of the bloodstream passes through the alveolar-capillary membrane and is retained in the alveoli themselves. These processes lead to a different morphological appearance of the lungs - they are markedly swollen, heavy, and a large amount of fluid leaks from their cut surface. Some authors call this form of overinflation hyperhydremic, while others use the term edema aquosum [8, 19, 22, 35, 36].

The term “dry drowning” is often encountered in literature, which is associated with the corresponding morphological finding of “dry lungs.” In these cases, the lungs show no pronounced signs of acute distension, no significant increase in their weight, and their cut surface appears dry. As reasons for this finding, some authors highlight mechanisms such as laryngospasm, vago-vagal inhibition due to water contact with the upper respiratory tract, cardiac arrest, and others [9, 17, 19]. Other authors believe that the terms „dry drowning“ and „dry lungs“ should not be used in connection with drowning, as they do not correspond to the definitions of this type of mechanical asphyxia, suggesting instead that such autopsy findings likely indicate a cause of death other than drowning [16, 27, 30].

Typically, two main types of subpleural hemorrhages can be found on the lungs: pinpoint, petechial (small) hemorrhages, known as Tardieu‘s spots (hemorrhages), and larger, diffuse hemorrhages with indistinct borders, known as Paltauf’s spots. According to some authors, Tardieu‘s spots predominate in cases of saltwater drowning, while Paltauf‘s spots are more commonly observed in freshwater drowning [3, 8, 22, 31, 35, 36].

The presence of fluid in the sphenoid bone sinus (Sveshnikov‘s sign) is a common occurrence in drowning cases [1, 8, 15, 22, 35, 36]. Some authors believe that the sign is positive even when the body has been in water without drowning being the cause of death [3, 37]. The amount of accumulated fluid in the sphenoidal sinus varies and depends primarily on the volume of the sinusoidal cavity itself. The fluid can be aspirated with a syringe and examined for the presence of diatoms and other foreign bodies [3, 15, 22, 35]. Diatom analysis can also be performed on other biological samples taken from the corpse during autopsy, such as lung tissue, bone marrow, liver, and others. The diatom test should be analyzed with particular attention, as there are a number of possibilities for false results. These can be due to many factors, such as contamination during collection

and subsequent processing of the samples, passive penetration of diatoms into the body, the degree of postmortem changes in the corpse, respectively, postmortem interval, what materials (body liquids and tissue) from the corpse are subjected to examination, etc. The diatom test can be significantly useful in the process of diagnosing drowning, however, it should not be used alone, but in combination with other established evidence, such as the circumstances of death and discovery of the corpse, morphological findings during autopsy, etc. [12, 22, 28, 35].

Among the literature, there are also some additional autopsy findings in cases of drowning: Wydler‘s sign (separation of stomach contents into three components), Sehrt‘s Sign (micro-ruptures of the gastric mucosa), Neil‘s sign (hemorrhages in the middle ear cavity), and others [1, 9, 14, 28, 36].

Given the difficulties in diagnosing death due to drowning, the present study aims to track the frequency of detection and characteristics of some of the main morphological changes observed during the autopsy of corpses that died as a result of drowning.

Materials and Methods

A total of 151 forensic medical expertise for autopsies of non-decomposed corpses diagnosed with drowning, conducted at the Clinic of Forensic Medicine at St. Marina University Hospital in Varna, Bulgaria, during the period 2008-2024, were examined.

In all forensic case, including drowning cases, the preliminary part of the expert examination indicates the circumstances of the death or discovery of the corpse, as well as available data regarding the victim, such as health status, chronic alcohol or drug use, etc. The external examination of each corpse usually includes an examination of the clothes, identification of postmortem changes (including maceration changes) and the degree of their development, detailed description of all traumatic injuries and their characteristics. The internal examination of the corpse is carried out by applying classical section techniques with a description of the macroscopic findings, and in the cases of bodies found in an aquatic environment, often the sphenoidal sinus is also opened. In some cases, additional examinations are carried out - histological and toxicological analysis, as well as a diatom testing.

With a focus on the purpose of the present study, only the following data were extracted and analyzed from forensic medical examination reports for each of the cases, diagnosed as drowning:

- ***The type of water*** the body was found in (saltwater or freshwater), the ***sex and age*** of the corpse.
- ***Cyanosis and subconjunctival hemorrhages***: these signs were recorded as present or absent.
- ***Foam (froth)***: this sign was considered present not only when found around the nose and mouth but also when discovered along the upper respiratory tract.
- ***Overinflation of the lungs***: cases were divided into three categories based primarily on the condition of the cut surface: cases where the lungs were heavy, markedly distended, and copious frothy (edematous) fluid spontaneously flowed out or with pressure from their cut surface were classified as the hyperhydremic form; cases where the lungs were enlarged, with a dry cut surface and released foamy fluid upon compression, were classified as the hyperaerated form; cases

where the morphological finding of the lungs could not be definitively assigned to either form were classified as a mixed (intermediate) form.

● ***Subpleural hemorrhages***: cases were divided into four groups based on this sign: absence of hemorrhages; presence of only petechial hemorrhages (Tardieu's spots); presence of large, diffuse hemorrhages (Paltauf's spots); presence of both petechial and larger hemorrhages.

● ***Sveshnikov's sign***: cases were divided into three groups based on this indicator: cases where the sign was not examined, presence of fluid, and absence of fluid in the sphenoidal sinus. In the practice of the our clinic, fluid from the cavity is aspirated with a sterile syringe for subsequent microscopic examination to detect ***diatoms and other foreign particles***, which was also recorded in the present study. For this purpose, the usual practice of our clinic is to perform direct microscopy of the sphenoidal fluid. In rare cases, we use other kind of fluid (for example, blood) or tissue samples (lungs, liver, kidney, bone marrow), which makes it necessary to perform chemical destruction to remove the organic component and prepare permanent microscope slides. The results of the test were limited to recording the "presence" or "absence" of diatom forms, sand grains, parts of plant origin, and other particles. Regarding diatom forms, in some rare cases, to determine the genus of the found diatoms, we use ADIAC - Diatom Image Database [4]. This step was usually applied only in cases where it is necessary to compare the diatom forms found in the corpse with those found in the water where drowning may have occurred.

Statistical analysis of the obtained data and results, as well as the creation of corresponding tables and graphs, was performed using Microsoft Excel®.

Results

During the period 2008-2024, a total of 3364 autopsies were performed at the Clinic of Forensic Medicine at St. Marina University Hospital, with 14.12% of them being cases of mechanical asphyxia. Drowning cases constituted 4.49% of all autopsied cases and 31.79% of all cases of death due to mechanical asphyxia (**Fig. 1**).

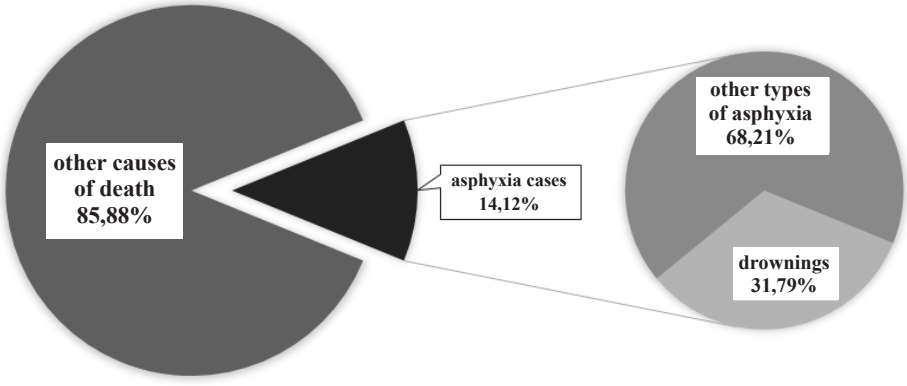

Fig. 1. The percentage distribution of asphyxia cases (as drownings and other types of asphyxia) relative to all cases for the period 2008-2024

Regarding the water in which the incident occurred, 72.85% of cases involved drowning in saltwater (Black Sea and associated Varna Lake and Beloslav Lake), and 27.15% involved drowning in freshwater (reservoirs, rivers, irrigation and drainage canals, springs, and others). The distribution of drowning cases by sex and age of the deceased is presented in **Table1**.

Table 1. *Distribution of drowning cases by sex and age groups.*

	n (%)	
	Male	**Female**
	122 (80,79%)	29 (19,21%)
n = 151	**age group (years)**	**n (%)**
	1-20	18 (11,92%)
	21-40	43 (28,48%)
	41-60	38 (25,17%)
	61-80	41 (27,15%)
	81-89	11 (7,28%)

Upon examining the external signs associated with the diagnosis of drowning, it was found that cyanosis and subconjunctival hemorrhages were observed in 27.15% and 29.80% of all drowning cases, respectively. Foam (including along the airways), which is one of the main signs of mechanical asphyxia due to drowning, was found in 80.13% of cases.

The different forms of overinflation of the lungs were observed in the following percentages: hyperaerated form in 11.26% of cases, hyperhydremic form in 35.10%, and mixed form in 53.64%. Subpleural hemorrhages, on the other hand, were not found in 21 drowning cases (13.91%), while Tardieu‘s spots were observed in 39.74%, Paltauf‘s spots in 17.22%, and both types of hemorrhages in 29.14% of cases.

Given the connection between a particular form of overinflation of the lungs and the type of subpleural hemorrhages with the water in which drowning occurred (freshwater or saltwater), **Table 2** presents the percentage distribution of these macroscopic findings.

Table 2. *Percentage distribution of the variations of overinflation of the lungs and subpleural hemorrhages in drowning cases in freshwater and saltwater.*

		salt water (n=110)	**fresh water** (n=41)
Lung overinflation	**hyperaerated form**	n=11 (10,00%)	n=6 (14,63%)
	hyperhydremic form	n=43 (39,09%)	n=10 (24,39%)
	mixed (intermediate) form	n=56 (50,91%)	n=25 (60,98%)

Subpleural hemorrhages	**Tardieu's spots**	n=56 (50,91%)	n=4 (9,76%)
	Paltauf's spots	n=10 (9,09%)	n=16 (39,02%)
	Presence of both Tardieu's and Paltauf's spots	n=29 (26,36%)	n=15 (36,59%)
	absence of hemorrhages	n=15 (13,64%)	n=6 (14,63%)

Of all 151 drowning cases, the sphenoid bone sinus was examined for free fluid in 143 of them, with such fluid being found in 96.50% of the examined cases. Regarding the presence of diatoms and other particles, 98 drowning cases were tested by direct microscopy of the sphenoidal fluid, and diatom forms and other foreign bodies were found in 87.76% of them.

Discussion

From the 1960s to the present day, the Clinic of Forensic Medicine at the St. Marina University Hospital in Varna and the corresponding department at the Medical University – Varna, have been actively involved in the forensic medical aspects of drownings in the Varna region. Two studies on this topic have been published: one by Yovchev I, covering drowning cases from 1963-1972 [35], and another by Radoynova D. et al., focusing on the period 1998-2007 [23].

Analysis of the data from the present study and comparison with the results of the aforementioned two studies showed that for the period 1963-1972, drowning cases autopsied at the forensic medicine clinic represented 9.23% of all autopsies, decreasing significantly to 5.41% for the period 1998-2007, and representing 4.49% of all autopsies for the period of the present study. This indicates a clear trend of decreasing incidents of this type in recent years [23, 35]. These data are also confirmed by the general statistics on drowning mortality in Bulgaria for the period 2010-2023, where after a peak in 2014, when cases were 2.2 per 100,000 people, in 2023 they were 1.3 per 100,000 [20].

Regarding gender distribution, both in the present study and in the other two conducted at the clinic for previous periods, the male to female ratio was approximately 4:1. The study for the period 1963-1972 found that 68.90% of the reviewed drowning cases were under 35 years of age, with 8.64% being children under 10 years. In the study during 1998-2007, the average age of drowned individuals was 43.55 ± 2.5 years, and children aged up to 14 years constituted 6.12% of all deaths due to drowning [23, 35]. In the present study, the highest percentage of drownings was observed in the 21-40 age group, and deaths due to drowning under 20 years of age represented 11.92%. This indicates that there is no significant change in age distribution, and individuals in young adulthood (around 40 years) continue to be the most affected age group.

Analysis of the data from the present study regarding autopsy findings in drowning revealed that cyanosis and subconjunctival hemorrhages were observed in less than 1/3 of the cases. These data differ significantly from those obtained by Yovchev I, where

cyanosis was found in 69.17% of cases and conjunctival hemorrhages in 65.78% [35]. On the other hand, other similar studies in the literature show that subconjunctival (scleral) hemorrhages are found significantly less frequently compared to the present study. In a study of 171 autopsies of drowned bodies, conjunctival hemorrhages were observed in only 4.1% [24], while in another study of drowning cases in children aged 5 months to 17 years, this percentage was about three times higher (12.7%) [26]. Some authors believe that conjunctival hemorrhages might disappear during the body‘s stay in water due to hemolysis, especially in freshwater. Also, they may not be noticeable in cases where there is conjunctival desiccation and the appearance of Larcher‘s spots [2, 5, 22]. The significant differences in the frequency of these findings across various studies are likely due to a number of factors, such as the duration of the asphyctic process, post-mortem interval, anatomical and physiological characteristics of the individuals, and others.

In the present study, the foam (foamy content) was present in a significantly high percentage of the examined cases (80.13%). Yovchev I.‘s study observed foam in only 35.71% of drowning cases. This significant difference between the two studies may be due to the fact that in the present study, foam was observed not only at the orifices of the mouth and nose but also within the airways [35]. A study conducted at the Department of Forensic Medicine at the University of Helsinki observed foam at the respiratory orifices in 17.3% of drowning cases and in the respiratory tract in 46.5% [18]. Some authors note that for a certain period after death, the foam may no longer be detectable [3, 19]. In another similar study, foam was found in the respiratory tract in 73.3% of drowning cases, while external foam was present in only 4.0%. Complete formation of external foam was observed by the same authors only in cases where the body‘s stay in the water was less than 24 hours [25]. In summary, foam is an important sign of drowning, the presentation of which can depend on various factors (post-mortem interval, duration of body submersion in water, resuscitation efforts, etc.). When foam is found shortly after death and other causes for its formation (diseases, intoxication, etc.) are excluded, this sign represents an important criterion in the process of diagnosing death due to drowning.

The overinflation of the lungs in the present study was examined in three categories based on the morphological appearance of the lungs and their cut surface. In more than half of the reviewed cases, the form of overinflation was not clearly presented and could not be definitively classified as hyperaerated or hyperhydremic. Some authors associate the hyperaerated form with freshwater drowning and the hyperhydremic form with saltwater drowning, and the explanation is related to the pathophysiological processes associated with the aspiration of hypotonic, respectively, hypertonic solution [9, 14, 17]. The results of the present study indicate that in only 6 out of 17 cases of hyperaerated form did drowning occur in freshwater. On the other hand, the hyperhydremic form represented 35.10% of all drowning cases and was found in 39.09% of saltwater drowning cases.

In summary, the results of the study show that in the majority of the forensic autopsy reports in cases of drowning, it is not possible to definitively determine which form of overinflation of the lungs is involved. On the other hand, cases with a definitively established hyperaerated/hyperhydremic form do not always correspond to drowning, respectively, in fresh/salt water. However, the changes of the lungs are of essential importance for the diagnostic process of drowning. These data provide grounds for

making some recommendations for a more detailed description of the macroscopic characteristics of the overinflation of the lungs, as well as for conducting histological analysis to establish the details of this condition in order to more accurately determine the hyperaerated or hyperhydremic form.

Similar to the lung overinflation, the type of subpleural hemorrhages is also associated with the type of water in which drowning occurred [22, 35]. According to our results, Tardieu‘s spots were observed in approximately half of saltwater drowning cases, while in freshwater drowning cases, they occurred in only 9.76%. Paltauf‘s spots were found in 9.09% of saltwater drownings, while in freshwater cases, this percentage was 39.02%. Although both types of subpleural hemorrhages were found in 29.14% of all reviewed cases, the obtained data indicate that Tardieu‘s spots were more commonly observed in saltwater drowning, while Paltauf‘s spots were more frequently found in freshwater drowning cases. It should be noted that petechial hemorrhages on the lung surface can also be observed in other types of mechanical asphyxia, as well as in other causes of death [8, 10, 21, 22, 35]. On the other hand, a number of authors consider Paltauf‘s spots to be a major morphological sign for the diagnosis of drowning [8, 31, 32, 36]. According to a study conducted at the Institute of Forensic Medicine at the Medical University of Greifswald, Germany, Paltauf‘s spots occur in 18.0% of drowning cases. The results of the present study are significantly close to these values – Paltauf‘s spots were observed in 17.22% of all drowning cases. Some authors believe that this morphological finding has no significant diagnostic value, and the frequency of finding Paltauf‘s spots in drowning cases varies widely (from 5 to 60%) [17, 19].

In the present study, Sveshnikov‘s sign (presence of free fluid in the sphenoidal sinus) was found to be positive in a significant percentage of cases (96.50%). According to literary sources, the positivity of this sign in drowning also varies widely, from 65% to 92% [6, 22, 31, 35]. Some authors note that the presence of fluid in the paranasal cavities may not indicate drowning, as fluid can enter post-mortem during the body‘s stay in water, and the cause of death may be of another nature [3, 17, 19]. Of particular interest is a study that examined corpses divided into three groups: the first group consisted of freshwater drowning cases without signs of cadaveric decomposition; the second group included corpses with signs of decomposition that were recovered from freshwater bodies; the third group was a control group and included decomposed corpses that died outside an aquatic environment. The results of the study showed that Sveshnikov‘s sign among the three groups was positive in 79% for the first group, 78% for the second, and 41% for the third group, respectively. These data provide grounds for the authors to conclude that the presence of fluid in the sphenoidal sinus can be considered a vital reaction, but only in cases without advanced putrefaction processes [37].

Fluid from the sphenoidal sinus can be easily aspirated with a syringe and examined for the presence of diatoms and other foreign bodies [3, 22, 35]. In the practice of the Clinic of Forensic Medicine at St. Marina University Hospital, Varna, fluid from the sphenoidal sinus is usually used for diatom analysis, except in cases of advanced cadaveric decomposition, when chemical processing of internal organs, including bone marrow, is performed.

Diatoms are unicellular microorganisms with a siliceous shell that typically inhabit aquatic environments. In drowning, they enter the body along with water through the respiratory system and subsequently spread to other organs via the bloodstream. In

forensic medical practice, their detection in the corpse is of significant importance in the process of diagnosing death due to drowning. Typically, diatoms are found in about 70% of drowning cases [21, 13, 22, 28, 35]. According to Yovchev I, diatoms and other foreign bodies were found in 70.85% of cases with a positive Sveshnikov's sign, in the fluid taken from the sinus [35]. In another study that examined samples of fluid from the sphenoidal sinus and lung tissue taken from drowned corpses, diatoms were found in 86.2% of cases [15]. The results of the present study also show a significantly frequent detection of diatom forms and other foreign bodies (87.76%). Some authors believe that for diatom analysis to be considered significantly positive, the number of diatoms found in a given sample should be substantial, and their type should be the same as those found in the corresponding water body [3, 8, 22]. The diatom test can be extremely useful in cases of drowning, although there is some controversy among different authors regarding its diagnostic value. According to some authors, diatoms are usually found in high percent of all drowning cases, but their absence does not completely rule out the diagnosis of death due to drowning [9, 14, 22].

In our clinic's practice, the examination for diatoms is mainly carried out on a sample taken from the sphenoidal sinus, using direct microscopy. In addition to the presence of diatom forms, the presence of other foreign particles such as grains of sand, amorphous materials, etc. is also taken into account. The positive result of this examination is not analyzed independently, but only in combination with other findings established in the given case, such as the circumstances of death or discovery of the body, autopsy findings, etc. In individual cases, depending on the need for additional evidence, a comparative analysis is also applied between the diatom forms found in the body and those found in the water where the incident likely occurred.

Conclusion

Although there is a trend towards a decrease of drowning cases, this type of incident continues to be one of the leading causes of death worldwide and therefore a significant problem for public health and forensic medicine. The analysis of the results obtained and the data from the reviewed literature clearly show that there is no single morphological sign that is diagnostically specific only for cases of death resulting from drowning. The frequent detection of foam in the nasal and mouth orifices, as well as along the airways, in cases of drowning, both in the present study and according to the data of a number of studies, emphasizes the significant diagnostic value of this autopsy finding. On the other hand, cyanosis and subconjunctival hemorrhages are not specific for drowning, but their detection together with other findings can also be of significant importance in the diagnostic process. The changes in the lungs analyzed in the present study indicate the need for a more precise description of the morphological findings and the application of additional histological examination in order to determine in detail the form of lung overinflation in cases of drowning and the possible relationship with the type of water in which it occurred (fresh or salt water). Regarding the high percentage of the studied drowning cases in which fluid is found in the sphenoidal sinus, it is advisable to refine some additional details, such as the volume of fluid that is detected. This feature is also of interest for future studies, such as the inclusion of control groups with corpses in different stages of decomposition, who died outside

the aquatic environment. Refining the diatom analysis would also help to improve the quality of the diagnostic process in cases of bodies being discovered in the water, but again the results should be commented on in combination with the other findings from the examination of the corpse and the circumstances of the scene.

The results of the present study highlight the need for a comprehensive and detailed assessment of autopsy findings, examinations performed, and all investigation data in cases of body discovery in water with suspected drowning. The data from the present study contribute to expanding knowledge about the frequency and diagnostic value of some of the main morphological changes observed in drowning, which in turn significantly supports daily forensic practice.

References

1. **Aflanie, I., G. Suharto, P. Nurikhwan.** Postmortem characteristics of drowning death in freshwater: a systematic review. – *Russian Journal of Forensic Medicine*, **10** (2), 2024, 220-228.
2. **Alexander, R., J. Jentzen.** Neck and Scleral Hemorrhage in Drowning. – *Journal of Forensic Sciences*, **56** (2), 2011, 522-525.
3. **Armstrong, E., K. Erskine.** Investigation of Drowning Deaths: A Practical Review. – *Academic Forensic Pathology*, **8** (1), 2018, 8-43.
4. Automatic Diatom Identification and Classificatoin (ADIAC) – Diatom Image Database. Available at: https://websites.rbge.org.uk/ADIAC/db/adiacdb.htm
5. **Betz, P., R. Penning, W. Keil.** The detection of petechial haemorrhages of the conjunctivae in dependency on the postmortem interval. – *Forensic Science International*, **64** (1), 1994, 61-67.
6. **Bohnert, M., D. Ropohl, S. Pollak.** Forensic medicine significance of the fluid content of the sphenoid sinuses. – *Archiv fur Kriminologie*, **209** (5-6), 2002, 158-164. [In German]
7. **Davceva, N., A. Duma.** Differential diagnostic elements in the determination of drowning. – *Romanian Journal of Legal Medicine*, **13** (1), 2005, 22-30.
8. **Dettmeyer, R. B., M. A. Verhoff, H. F. Schütz.** Forensic Medicine: Fundamentals and Perspectives, Berlin, Heidelberg: Springer Berlin Heidelberg, 2014, 243-260.
9. **Di Maio, V., K. Molina.** DiMaio's forensic pathology. Third edition. Boca Raton, FL: CRC Press, 2022, 373-384.
10. **Fn, J., J. Liando, J. Gotama, K. Masreni, K. Christina.** The Challenges of Diagnosing Drowning Death Case. – *IIMJ*, **3** (2), 2022, 108-118.
11. **Girela-Lopez, E., C. M. Beltran-Aroca, H. García-Mozo H.** Diatoms in Forensic Analysis – In: *Modern Trends in Diatom Identification* (Eds. Cristóbal G., Blanco S., Bueno G.). Springer International Publishing, 2020, 239-256.
12. **Hansen, I., A. Thomsen.** Circumstances and autopsy findings in drownings, Department of Forensic Medicine, Aarhus University, 2006-2015. – *Scandinavian Journal of Forensic Science*, **24** (1), 2018, 1-6.
13. **Klevno, V., Y. Chumakova, M. Kislov, O. Popova, S. Dubrova.** New diagnostic signs of drowning based on virtual autopsy results. – *Russian Journal of Forensic Medicine*, **6** (3), 2020, 53–57.
14. **Knight, B., P. J. Saukko.** Knight's Forensic pathology. 3rd ed. London : New York: Arnold, Distributed in the United States of America by Oxford University Press, 2004, 395-411.

15. Lin, C., W. Yen, H. Hsieh, L. Tsai, T. Huang, C. Huang, Y. Yu, C. Shun, J. Wu, C. Chou, A. Linacre, J. Lee. Diatomological investigation in sphenoid sinus fluid and lung tissue from cases of suspected drowning. – *Forensic Science International*, **244**, 2014, 111-115.

16. Lunetta, P., J. H. Modell, A. Sajantila. What Is the Incidence and Significance of "Dry-Lungs" in Bodies Found in Water? – *American Journal of Forensic Medicine & Pathology*, **25** (4), 2004, 291-301.

17. Lunetta, P., J. H. Modell. Macroscopical, Microscopical, and Laboratory Findings in Drowning Victims. – In: *Forensic Pathology Reviews* (Eds. Tsokos M). Totowa, NJ: Humana Press, 2005, 3-77.

18. Lunetta P., A. Penttilüa, A. Sajantila. Circumstances and Macropathologic Findings in 1590 Consecutive Cases of Bodies Found in Water. – *The American Journal of Forensic Medicine and Pathology*, **23** (4), 2002, 371–376.

19. Madea, B. Asphyxiation, suffocation, and neck pressure deaths. Boca Raton: CRC Press, 2020, 260-284.

20. National Statistical Institute – Mortality by causes, sex and age. Available at https://www.nsi.bg/en/statistical-data/236/765

21. Nečas, P., P. Hejna. Eponyms in forensic pathology. – *Forensic Sci. Med. Pathol.*, **8** (4), 2012, 395-401.

22. Radanov, St. Forensic medicine and deontology. Sofia: *Siela*, 2006; 192-216. [In Bulgarian]

23. Radoinova, D., Y. Kolev, E. Kaisheva, M. Baltov. Forensic medical examination of drownings in the districts of Varna, Gabrovo and Smolyan. – *Society of Water Rescue Specialists* – Varna. 2008, 63-68. [In Bulgarian]

24. Rao, V., C. Wetli. The Forensic Significance of Conjunctival Petechiae. – *The American Journal of Forensic Medicine and Pathology*, **9** (1), 1988, 32-34.

25. Schneppe, S., M. Dokter, B. Bockholdt. Macromorphological findings in cases of death in water: a critical view on "drowning signs". – *Int. J. Legal Med.*, **135** (1), 2021, 281-291.

26. Somers, G., D. Chiasson, G. Taylor. Presence of periorbital and conjunctival petechial hemorrhages in accidental pediatric drowning. – *Forensic Science International*, **175** (2–3), 2008, 198-201.

27. Szpilman, D., J. Sempsrott, J. Webber, S. C. Hawkins, R. Barcala-Furelos, A. Schmidt, A. Queiroga. "Dry drowning" and other myths. – *CCJM*, **85** (7), 2018, 529-535.

28. Tambuzzi, S., G. Gentile, R. Zoia. Forensic Diatom Analysis: Where Do We Stand and What Are the Latest Diagnostic Advances? – *Diagnostics*, **14** (20), 2024, 2302.

29. Tasis, M., B. Budakov, D. Draskovic, M. Durendic-Brenesel, A. Oros, V. Pilija, M. Simic, G. Stojiljkovic, B. Susnjar, S. Takac, I. Veselinovic, R. Vukovic, D. Zgonjanin, P. Budakov. Forensic medicine. Novi Sad: *ZMAS*, 2007, 88-94. [In Serbian]

30. Van Beeck, E., C. Branche, D. Szpilman, J. Modell. A new definition of drowning: towards documentation and prevention of a global public health problem. – *Bulletin of the World Health Organization*, **83** (11), 2005, 853-856.

31. Viter, V., A. Vavilov, V. Kungurova. Forensic examination of mechanical asphyxia. – *Izhevsk Press*, 2008, 20-29. [In Russian]

32. Voloshynovych, V., N. Kozan, V. Voloshynovych, J. Kotsyubynska, M. Voloshynovych, G. Zelenchuk, V. Chadiuk. Current state and prospects of forensic-medical diagnosis of drowning: A review of the literature. – *Problems of Forensic Sciences*, **129**, 2022, 49-73.

33. Whitwell, H., P. Harvey, A. Kolar, K. Thorne. Mason's Forensic Medicine and the Law. London: *Bloomsbury Professional*, 2023, 131-144.

34. World Health Organization. Drowning, 2024 Available at https://www.who.int/news-room/fact-sheets/detail/drowning
35. Yovchev, I. Morphological changes and laboratory diagnostics in drowning in seawater: on expert cadaveric material and on experimental animals. *Varna, Medical University – Varna*, 1974. [In Bulgarian]
36. Zhulzhik, E. Diagnostics of drowning in modern forensic medicine. – *Scientific-methodological electronic journal "Koncept"*, **4**, 2015, 191–195. [In Russian]
37. Zivkovic, V., D. Babic, S. Nikolic. Svechnikov's sign as an indicator of drowning in immersed bodies changed by decomposition: an autopsy study. – *Forensic Sci. Med. Pathol.,* **9** (2), 2013, 177-183.

Institute of Experimental Morphology, Pathology and Anthropology with Museum
Bulgarian Anatomical Society

Acta Morphologica et Anthropologica, 32 (3-4)
Sofia ● 2025

Ex vivo histological study on the effects of non-fractional ER:YAG laser for wrinkle therapy

Georgi Tomov[1], Parvan Voynov[2], Svitlana Bachurska[3,4]*

[1] Dept. of Healthcare and Social Work, New Bulgarian University, Sofia, Bulgaria
[2] Unit of Plastic Surgery, Medical Center Uni Hospital, Sofia, Bulgaria
[3] Dept. of Clinical Pathology, University Hospital Tokuda, Sofia, Bulgaria
[4] Dept. of Health Care, National Sport Academy "Vasil Levski", Sofia, Bulgaria

*Corresponding author e-mail: dr.g.tomov@gmail.com

The Er:YAG laser-assisted wrinkle therapy is based on both superficial tissue ablation and tissue remodeling via stimulation of the collagen synthesis. Non-fractional or fractional laser handpieces perform this treatment modality, and there is no consensus in the literature about their effectiveness. This pilot ex vivo study aimed to evaluate the histological changes after wrinkle treatment with non-fractional Er:YAG laser with air/water cooling. Prior to planned facial skin excision, the pilot patient received laser irradiation in intervals (0-14-30 days) on a linear wrinkle divided into three equal sections. The parameters used were 40mJ/10Hz with air/water spray. The treated skin zone was removed and evaluated histologically. The observed histological changes for all studied intervals of treatment revealed satisfactory healing processes without side effects. This pilot ex vivo study demonstrates that the conventional non-fractional Er:YAG laser is effective and safe, and can be adjusted successfully in wrinkle therapy.

Key words: Er:YAG laser, non-fractional, wrinkle, histology

Introduction

Er:YAG laser skin therapy (including treatment for wrinkles) involves controlled tissue ablation and subsequent tissue remodeling. Histologically, this translates to the removal of damaged skin layers, collagen stimulation, and new collagen formation, leading to wrinkle reduction and skin rejuvenation [8]. The extent of ablation and thermal damage can vary depending on laser parameters like fluence and pulse duration, influencing the healing process and clinical outcomes [2, 9]. Er:YAG laser penetrates to an average depth of 2-5 μm per J/cm^2 and the residual necrotic layer does not exceed 10-15 μm [1]. The fractional Er:YAG laser is reported to be effective in resurfacing skin, yielding similar results to non-fractional Er:YAG lasers, which involve a more continuous ablation pattern, which may

require longer healing times and have a higher risk of side effects [4]. However, the different outcomes after procedures with fractional and non-fractional Er:YAG have been discussed in various publications, and not only in favor of the fractional lasers [1]. The specific goal of the procedure – skin rejuvenation versus wrinkle reduction - is decisive when choosing a laser. The rejuvenation therapy usually covers a broad skin area, in contrast to the wrinkle "elimination", which is focused on a minor linear defect. The controversies in the literature and the fact that only a few articles include human subjects have stimulated our team to conduct this pilot ex vivo study, evaluating the histological effects of non-fractional Er:YAG laser on wrinkle therapy [11, 14].

Materials and Methods

This pilot study included one healthy female volunteer aged 64 years with Fitzpatrick skin type II. The study was performed according to principles of good clinical practice and the Declaration of Helsinki. The enrolled patient was referred for a facial lift procedure to the Clinic of Plastic Surgery (Uni Hospital, Sofia, Bulgaria), and the area for laser treatment was carefully selected to be within the borders of the planned skin excision. The patient was informed about the goal of the study, and informed consent was signed. In order to evaluate histologically the wound healing process in vivo, a facial area of human skin with presented wrinkles was selected and treated with an Er:YAG laser system (LiteTouch™, Light instruments Ltd., Israel) using a non-fractional esthetic handpiece with air/water cooling. The parameters were as follows: 40mJ/10Hz, air/water spray (level 2). The selected linear wrinkle was divided into three equal sections, and each one was irradiated in a homogeneous pattern within three consecutive laser passes. No anesthesia was used during the treatment. Three laser sessions without overlap were performed consecutively before the skin excision – the first section was irradiated 30 days before, the second section was irradiated 14 days before, and the last section was irradiated immediately before the skin excision. The patient was instructed to avoid sun exposure, use of products containing acids, make-up, and any abrasive processes for the skincare routine for the first few days before and after the laser irradiation. Protective ointment was prescribed (Eucerin Aquaphor Protective Ointment).

Histological evaluation

Immediately following excision, each sample was fixed in 10% buffered neutral formalin overnight and then embedded in paraffin. The samples were sectioned, stained with Hematoxylin and Eosin, and examined under a light microscope using 4X and 10X magnifications.

Results

The histological sample representing the skin area immediately after laser irradiation revealed a well-controlled ablation penetrating approximately 120 μm deep through the epidermis and near the underlying papillary dermis. A thin area of coagulation with a more basophilic appearance surrounding the ablation area was observed (**Fig. 1a**).

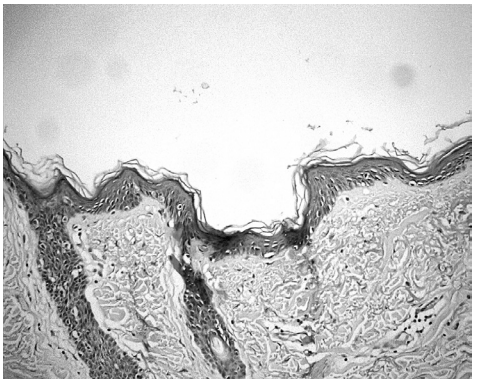

Fig. 1. A

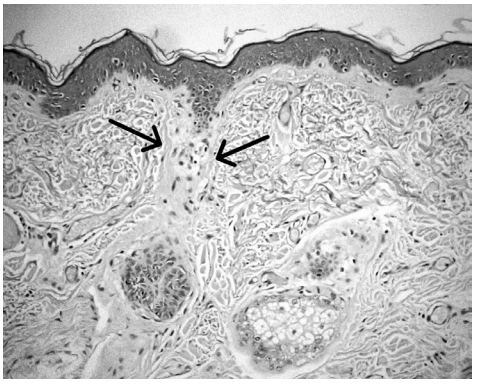

Fig. 1. B

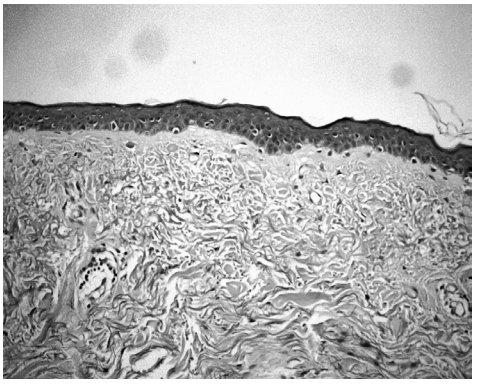

Fig. 1. C

Fig. 1. *Histological findings in human skin after non-fractional Er:YAG laser irradiation immediately after the treatment (**a**), 14 days after the treatment (**b**), and 30 days after the treatment (**c**). Hematoxylin/eosin, 10× magnification.*

Fourteen days after the laser treatment, re-epithelialization with a hyperproliferative epithelium and normal maturation, manifested with the presence of stratum corneum and orthokeratosis, was observed (**Fig. 1b**). Under the area of re-epithelialization, the smaller area of subepidermal fibrin and a few neutrophil infiltrations could be observed (**indicated with arrows**). Thirty days after the treatment, complete re-epithelialization with normal maturation of the epidermis was observed, manifested by normal-width orthokeratosis, the presence of stratum corneum, and stratum granulosum. Below the epidermis, the presence of multiple fibroblasts and evidence of glomeruloid angiogenesis (**Fig. 1c**).

Discussion

The Er:YAG lasers, with a wavelength of 2940 nm, are highly absorbed by water in the skin. This absorption leads to rapid vaporization and removal of the epidermis and superficial dermis. The depth of ablation is controllable by adjusting laser parameters, allowing precise targeting of wrinkles. Ablative techniques are still considered the most effective methods for improving photodamaged skin, but are associated with

a prolonged recovery time and high risk of side effects [10]. Thus, the minimally invasive or even non-ablative (the ablation is microscopically presented but its volume is clinically insignificant) methods are gaining popularity in modern rejuvenation therapy. The mechanisms behind this dermal remodeling are the minimal trauma (micro ablation) combined with mild heating of the dermis caused by the laser, affecting both the microcirculatory complex and the fibroblasts' activity [6]. The Er:YAG laser used in the current study demonstrated an ablation depth of approximately 120 μm through the epidermis and near the underlying papillary dermis, which corresponds with the micro ablation techniques. In such a situation, only the epidermis is affected, while deep dermal structures are heated. The expected thermal effects, however, leading to both beneficial collagen denaturation and potentially undesirable thermal damage, must be controlled adequately. Residual thermal damage, characterized by vacuole formation and severe inflammation, was not observed in the current study. Proper laser settings and cooling techniques can minimize the thermal damage and promote more effective collagen remodeling. The Er:YAG laser used in the current study delivers controlled thermal energy to the skin without significantly ablating its outer layer. In combination with air/water spray, this controlled heating stimulates the production of new collagen, leading to a tightening effect and wrinkle reduction. This noninvasive methodology is a basis of many different therapies such as laser vaginal tightening, stress urinary incontinence therapy, treatment of snoring [5, 7, 12].

The other point of controversy in the literature is the effects of non-fractional versus fractional Er:YAG lasers used for skin therapies. The non-fractional lasers are considered much more invasive in contrast with the fractional Er:YAG lasers which create microscopic "columns" of tissue ablation, leaving surrounding tissue almost intact for faster healing and potentially reduced side effects [13]. The non-fractional Er:YAG lasers involve a more continuous ablation pattern, which may require longer healing times and have a higher risk of side effects [3]. The main misinterpretation however is the primary goal of the therapy. The skin resurfacing and rejuvenation therapies cover a significantly larger treatment area than the wrinkle "elimination", which is focused on a tiny linear defect(s) requiring a precise and controlled approach. In this context, the non-fractional Er:YAG lasers are the only reasonable choice, but they must be used carefully, operating in subablative mode and with proper cooling.

Conclusion

This ex vivo histological study demonstrates that the conventional non-fractional Er:YAG laser is effective and safe, and can be adjusted successfully for wrinkle therapy. However, additional clinical research with multiple patients is required to verify this modality as a routine. Additionally, the histological findings are correlated with clinical improvements in skin texture, wrinkle depth, and overall appearance, but the duration of these improvements can vary, and multiple treatment sessions may be necessary for optimal and sustained results. In this context, the long-term clinical effects also must be studied.

Acknowledgements: The original contributions presented in the study are included in the article. Further inquiries can be directed to the corresponding author. This study was

performed under the permission of the heads of the *Department of Healthcare and Social Work, New Bulgarian University, Sofia* and the *Unit of Plastic Surgery, Medical Center Uni Hospital, Sofia*. The authors want to express their special gratitude to all above-mentioned personnel.

References

1. **Asfour, A. R., H. A. Shokeir, T. F. Alwakil, F. M. Ghareeb, M. Elbasiouny.** Evaluation of the Efficacy of Ablative vs. Fractional Er:YAG Laser Modes as a Treatment of Post-Burn Scars. – *Biol. Med. (Aligarh),* **9**(6), 2017, 1-9.
2. **Bass, L. S.** Erbium:YAG laser skin resurfacing: preliminary clinical evaluation. – *Ann. Plast. Surg.*, **40**(4), 1998, 328-334.
3. **Chen, K. H., K. W. Tam, I. F. Chen, S. K. Huang, P. C. Tzeng, H. J. Wang, C. C. Chen.** A systematic review of comparative studies of CO2 and erbium:YAG lasers in resurfacing facial rhytides (wrinkles*). – J. Cosmet. Laser Ther.* **19**(4), 2017, 199-204.
4. **El-Domyati, M., T. Abd-El-Raheem, H. Abdel-Wahab, W. Medhat, W. Hosam, H. El-Fakahany, M. Al Anwer**. Fractional versus ablative erbium:yttrium-aluminum-garnet laser resurfacing for facial rejuvenation: an objective evaluation. – *J. Am. Acad. Dermatol*., **68**(1), 2013, 103-112.
5. **Fistonic, I., S. Findri-Gustek, N. Fistonic.** Minimally invasive laser procedure for early stages of stress urinary incontinence (SUI). – *J. Laser Heal. Acad*., **1**, 2012, 67-74.
6. **Gaspar, A., G. A. Gasti.** Tightening of facial skin using intraoral 2940nm Er:YAG SMOOTH mode. – *J. Laser Health Acad*., **2**, 2013, 1-5.
7. **Gaviria, J. E.** Laser Vaginal Tightening (LVT) – evaluation of a novel noninvasive laser treatment for vaginal relaxation syndrome. – *J. Laser Heal. Acad*., **1**, 2012, 59–66.
8. **Lanigan, S. W.** Lasers in dermatology. (Ed. Springer-Verlag), London, 2000, Available at: https://doi.org/10.1007/978-1-4471-0437-7
9. **Lee, S. J., J. M. Kang, W. S. Chung, Y. K. Kim, H. S. Kim**. Ablative non-fractional lasers for atrophic facial acne scars: a new modality of erbium:YAG laser resurfacing in Asians. – *Lasers Med. Sci*., **29**(2), 2014, 615-619.
10. **Sadick, N. S., A. Cardona**. Laser treatment for facial acne scars: a re-view. – *J. Cosmet. Laser Ther*., **20**(7-8), 2018, 424- 435.
11. **Shanina, N. A., A. V. Patrushev, A. Zorman**. Histological and immunohistochemical changes infacial skin treated with combined ablative and non-ablativelaser therapy. – *J. Cosmet. Dermatol*., **20**, 2021, 3509–3516.
12. **Unver, T., E. Aytugar, O. Ozturan, T. Kıran, E. Ademci, A. Usumez.** Histological Efects of Er:YAG Laser Irradiation with Snoring Handpiece in the Rat Soft Palate. – *Photomed. Laser Surg.,* **34**(8), 2016, 321–325.
13. **Verma, N., S. Yumeen, B. S. Raggio**. Ablative Laser Resurfacing. (Ed. StatPearls Publishing), 2025, PMID: 32491406.
14. **Zgavec, B., N. Stopajnik**. Clinical and Histological Evaluation of Er:YAG Ablative Fractional Skin Resurfacing. – *J. Laser Heal. Acad*., **1**, 2014, 1-6.

Institute of Experimental Morphology, Pathology and Anthropology with Museum
Bulgarian Anatomical Society

Acta Morphologica et Anthropologica, 32 (3-4)
Sofia ● 2025

Morphological and Morphometric Analysis of the Radius Bone in South Indian Adults: Implications for Surgical Applications and Prosthesis Design

Chaitra D[1], Divya N Pai[2], Ashwija Shetty[3]*

[1] Nitte (Deemed to be University), KS Hegde Medical Academy (KSHEMA), Department of Anatomy, Mangalore, Karnataka, India.
[2] Nitte (Deemed to be University), KS Hegde Medical Academy (KSHEMA), Department of Anatomy, Mangalore, Karnataka, India.
[3] Department of Anatomy; Kasturba Medical College Manipal, Manipal Academy of Higher Education, Manipal, Karnataka, India.

*Corresponding author e-mail: Chaitrad@nitte.edu.in

The radius bone plays a key role in forearm stability, mobility, and load transmission, making its morphometry crucial for surgical and prosthetic applications. This study analysed 61 adult radius bones (33 right, 28 left) from South Indian individuals using SPSS v22.0, revealing minor but significant side differences. The transverse diameter of the radial head and the distal shaft were significantly larger on the right side ($p=0.003$ and $p=0.019$, respectively), likely due to limb dominance. Other parameters showed no notable variation. These findings underscore the importance of population-specific data for improving fracture fixation, implant design, and surgical outcome.

Key words: radius, elbow joint, south Indian adults, orthopaedic anatomy, implant design

Introduction

The radius is a bone situated on the lateral side of the forearm. The name “radius” is derived from the Latin word for ray, reflecting its rotational function around its axis, which extends diagonally from the center of the capitulum to the center of the distal ulna. The radius generally ossifies from three centers: one primary center for the shaft and two secondary centers for the proximal and distal ends [9]. When the forearm is in a supine position, the radius, a long bone, lies on the lateral side. Together with the ulna and carpal bones, the radius plays a key role in enabling extensive dynamic motion at both the elbow and wrist joints. The radius is composed of three main parts:

the proximal end, the shaft, and the distal end. The circular proximal end articulates with the radial notch of the ulna at the radioulnar joint and features a concave articular facet that connects with the capitulum of the distal humerus at the elbow joint. Below the radial head is the radial neck, followed by the radial tuberosity, which is positioned medially and serves as an attachment site for arm muscles [7].

The radius, along with the radioulnar joint, is critical for maintaining the physiological and physical stability of the elbow. Fractures of the hand and wrist account for about 1.5% of all emergency room visits, with radial and ulnar fractures representing 44% of these cases. Fragility fractures of the distal radius are especially common, with a lifetime risk of 15% in women, and are the most frequent initial fracture occurring during the postmenopausal period. In children, distal radius fractures are the most common, accounting for 22.4% of all fractures [10].

The radius and ulna are integral to the pronation and supination of the forearm, which is why the radioulnar joint is considered a "functional joint." A malunited fracture can impair the joint's function and restrict its range of motion. Therefore, it is crucial to restore the correct length, alignment, and rotation of both bones to ensure the forearm's dynamic function remains intact [11]. Considering these factors, understanding the morphological characteristics of the radius bone, particularly in South Indian adults, is essential for improving clinical outcomes and ensuring the optimal function of the forearm and its associated joints.

Materials and Methods

Sixty-three intact adult radius bones (33 right and 28 left) were included, excluding those with incomplete ossification, fractures, or deformities. Morphometric parameters of the proximal and distal ends were measured in supinated and semi-pronated positions and categorized into three regions: proximal radius, radial shaft, and distal radius. For the radial head, circumference, anteroposterior (AP) diameter, transverse diameter, medial height, and lateral height were recorded. Proximal and distal lengths, radial neck diameter, and the head–neck angle in the coronal plane were also noted. The length of the shaft was measured using an osteometric board, while the maximum

Fig. 1. Measurement of radius bone using osteometric board.

and minimum diameters at the proximal and distal thirds, along with the width, length, circumference, and maximum diameter of the bicipital tuberosity, were measured using a digital vernier caliper (accuracy 0.01 mm) and a non-elastic tape.

Statistical Analysis

The statistical analysis was performed using IBM SPSS software, version 22.0. Continuous variables are expressed as mean ± standard deviation (range), while categorical variables are presented as frequencies and percentages. An independent, two-tailed Student's T-test was utilized to assess differences between sides, with a p-value of <0.05 considered statistically significant.

Results

Table 1. Difference between the sides on various parameters of radius:

Variables	Right Side (33)	Left side (28)	p-Value
Length of radius	24.12±1.64	23.96±1.91	0.88
AP measurement of radial head	19.39±1.71	19.02±1.89	0.33
Transverse measurement of radial head	16.13±1.61	15.37±2.24	0.003*
Width of radial tuberosity	11.60±1.28	11.42±1.48	0.494
Length of radial tuberosity	21.44±2.46	21.95±2.98	0.520
Transverse diameter of distal end	26.13±2.07	25.73±2.35	0.138
Articular surface of lunate	9.58±1.04	9.38±0.95	0.208
Articular surface of scaphoid	14.82±1.46	14.90±1.50	0.719
Medial head height	8.30±0.99	8.56±0.91	0.416
Lateral head height	4.55±0.76	4.35±0.64	
Neck length	11.10±2.09	11.19±2.16	0.653
Neck Width P	14.63±1.92	14.74±1.91	0.929
Neck Width D	13.43±1.53	13.24±1.28	0.457
Radial shaft diameter proximal	12.32±1.24	12.11±1.31	0.317
Radial shaft diameter distal	15.43±1.61	14.36±1.37	0.019

The morphometric comparison between the right and left adult radius bones (**Table 1**) revealed that most parameters did not show statistically significant differences, indicating general bilateral symmetry. The length of the radius, anteroposterior (AP) and transverse measurements of the radial head, dimensions of the radial tuberosity, distal end diameters, and articular surface measurements were largely comparable between the sides. However, two parameters demonstrated statistically significant differences.

The transverse diameter of the radial head was significantly greater on the right side (16.13 ± 1.61 mm) compared to the left (15.37 ± 2.24 mm), with a p-value of 0.003, indicating a notable side difference possibly due to functional dominance. Similarly, the distal radial shaft diameter was significantly larger on the right (15.43 ± 1.61 mm) than the left (14.36 ± 1.37 mm), with a p-value of 0.019. These findings suggest subtle morphological asymmetry, likely attributable to habitual use and biomechanical stress on the dominant limb. Other parameters, such as the neck dimensions, proximal radial shaft diameter, and articular surface measurements of the lunate and scaphoid, did not vary significantly, supporting a general morphological consistency across sides in the South Indian adult population.

Discussion

The treatment of displaced and comminuted radial bone fractures often involves internal fixation using plates and screws or reconstructing the radial head. To assess the anatomical features of the radius bone, techniques such as computed tomography, radiography, and cadaveric studies are commonly utilized [10]. Approximately one-third of all elbow fractures are attributed to radial head fractures [2]. Accurate morphometric measurements are essential for the proper reduction of distal radius fractures. Orthopedic surgeons commonly rely on the reference values established by Gartland and Werley [5]. Nevertheless, it is important to note that morphometric parameters can vary due to factors like geographic location, ethnicity, racial differences, and individual physical characteristics [1].

Knowledge of the radial head's size and shape is critical for developing effective radial head prostheses, as these factors play a pivotal role in ensuring successful replacements. Similarly, understanding the parameters of the distal radius is necessary for creating prostheses for cases like Colles' fractures, while the size and shape of the radial tuberosity are particularly important in procedures like bicipital tendon reconstruction [9].

Distal radial fractures are commonly caused by trauma to the forearm. These fractures can include Smith's, Colles', Torus/Buckle, Greenstick, Die-punch, and isolated radial shaft fractures [3]. The incidence of radial fractures is increasing with the rise in life expectancy, resulting in a growing population of patients at risk for these injuries. Such fractures are predominantly observed in children, adolescents, and the elderly [4].

The current study shows that the AP measurement of the radial head (19.39 ± 1.71 mm on the right and 19.02 ± 1.89 mm on the left) is consistently larger than the transverse measurement (16.13 ± 1.61 mm on the right and 15.37 ± 2.24 mm on the left), indicating an elongated anteroposterior profile and a natural asymmetry favoring the AP diameter. These findings align with those of Kuhn et al., who also reported a greater AP diameter compared to the transverse diameter, emphasizing its functional significance in maintaining joint stability and load distribution during forearm movements [6]. Similarly, Reddy et al. observed a larger AP diameter relative to the transverse diameter, though their study highlighted variability based on population and handedness, with their measurements indicating slightly larger overall dimensions than those found in the current study [10].

In this study, the width of the radial tuberosity was measured as 11.60 ± 1.28 mm on the right and 11.42 ± 1.48 mm on the left, while the length was 21.44 ± 2.46 mm on the right and 21.95 ± 2.98 mm on the left, showing minimal differences between the sides. Comparatively, Rajashree et al. reported slightly larger dimensions for the radial tuberosity in their study, with the width and length both exceeding the values observed in this study [8].

The study underscores the importance of morphometric analysis of the radius for surgical applications, particularly in prosthesis and fixation device design. Variations in radial head and tuberosity measurements suggest the need for personalized approaches in orthopedic care. These findings can enhance surgical precision and patient outcomes. However, the study is limited by the small sample size and the failure to account for soft tissue variations, which may influence the results.

Conclusion

In conclusion, the findings of this study underscore the importance of detailed morphometric analysis of the radius bone, particularly the radial head and tuberosity, for clinical and surgical applications. The observed variations in anteroposterior and transverse dimensions, as well as side-specific differences in radial tuberosity measurements, highlight the need for individualized approaches in the design and selection of prostheses and fixation devices. These measurements also emphasize the functional significance of the radial head's elongated anteroposterior profile in ensuring joint stability and effective load distribution. Furthermore, the variability reported across different populations and studies underscores the necessity of accounting for geographic, ethnic, and individual factors in orthopedic practice. Such comprehensive morphometric data can aid in the refinement of surgical techniques, enhance the accuracy of fracture reduction, and improve the outcomes of reconstructive procedures, ultimately contributing to better patient care.

Limitations and Future Scope:

The study is limited by sample size and absence of gender-specific data. Future research with larger cohorts and advanced imaging may provide more accurate measurements and broader population comparisons.

Acknowledgement: We express our sincere gratitude to the Department of Anatomy KS Hegde Medical Academy Karnataka India for providing the necessary facilities and support essential for conducting this study.

References

1. Anasuya, D. G., A. Kumar, S. Arasu, J. Shanmugam, M. Vijaianand, D. Praveen, S. Arasan. Radiographic morphometric analysis of the distal radius in the Tamil Nadu population: a retrospective study. – *Cureus*, **16**, 2024, 6.

2. Avnioğlu, S., S. Yılmaz, D. Ünalmış. Morphometric examination of radius. – *J. US-China Med. Sci.*, **17**, 2020, 172-176.

3. Caldwell, R. A., P. L. Shorten, N. T. Morrell. Common upper-extremity fracture eponyms: a look into what they really mean. – *J. Hand Surg. Am.*, **44**, 2019, 4, 331-334.
4. Corsino, C. B., R. A. Reeves, R. N. Sieg. Distal radius fractures. Updated August 8, 2023. – In: *StatPearls [Internet]. Treasure Island (FL): StatPearls Publishing*; January 2025.
5. Gartland, J. J. JR., C. W. Werley. Evaluation of healed Colles' fractures. – J. *Bone Joint Surg. Am*., **33**, 1951, 4, 895-907.
6. Kuhn, S., K. J. Burkhart, J. Schneider, B. K. Muelbert, F. Hartmann, L. P. Mueller, P. M. Rommens. The anatomy of the proximal radius: implications on fracture implant design. – *J. Shoulder Elbow Surg.*, **21**, 2012, 9, 1247-1254.
7. Ngidi, N. L., S. O. Olojede, S. K. Lawal, O. S. Aladeyelu, C. O. Rennie. Morphometric study of the radius bone in a KwaZulu-Natal population: laterality and sexual dimorphism. – *Forensic Sci. Int. Rep.*, **7**, 2023, 100316.
8. Rajashree, G., T. Sucharitha, D. S. Karuppiah, L. Hema. Morphology and morphometry of proximal dry radii in south coastal population. – *IJRDO*, **1**, 2016, 69-91.
9. Rayna, A. B., Y. M. Francis, S. B. Baskaran, P. Gouthaman, Z. Begum, K. Guruswami, P. Sankaran, G. Raghunath. Morphometric study of proximal and distal end of radius and its clinical significance. – *J. Clin. Diagn. Res*., **12**, 2018, 9, AC09-AC12.
10. Reddy, S., D. Jain, K. Pradyumna, R. Prajwal, R. Sandeep. The morphology and morphometric analysis of the radius bone: a study on freshly frozen cadavers in the Indian population. – *Cureus*, **15**, 2023, 6, 1-13.
11. Schneppendahl, J., J. Windolf, R. A. Kaufmann. Distal radius fractures: current concepts. – *J. Hand Surg. Am.*, **37**, 2012, 8, 1718-1725.

Institute of Experimental Morphology, Pathology and Anthropology with Museum
Bulgarian Anatomical Society

Acta Morphologica et Anthropologica, 32 (3-4)
Sofia ● 2025

Review Articles

Comparing Cadaveric Dissection and Advanced Imaging Techniques in Coronary Artery Visualization: Implications for Surgical Planning and Patient Outcomes

Divia Paul Aricatt[1], Subramanyam Kodangala[2], Ashraf Safiya Manzil[3]*

[1] Department of Anatomy, MVJ Medical College and Rescarch Hospital, Hoskote, Bangalore, Karnataka, India
[2] Department of Cardiology, Srinivas Medical College and Research Center, Mukka- Suratkal, Mangalore, India
[3] Department of Cardio Vascular Sciences, Sahakarana Hrudayalaya, Govt. Medical College, Pariyaram, Kannur, Kerala, India

* Corresponding author e-mail: diviaaricatt@gmail.com

Accurate coronary artery visualization is critical for successful angiography and surgery. This study compares cadaveric dissection and in-situ surgical views in aiding surgical planning and patient outcomes.A comparative analysis reviewed cadaveric dissection and angiographic imaging, focusing on advancements like 3D coronary angiography. Strengths, limitations, and clinical applications were assessed.Cadaveric dissection provides detailed anatomical insights, while 3D angiography offers dynamic, real-time imaging that improves surgical precision. Recent intraoperative imaging advancements enhance visualization, reduce complications, and improve outcomes.Dissection remains essential for detailed anatomy understanding, but modern imaging technologies offer a less invasive, complementary approach for surgical planning. Combining these methods enhances clinical decision-making and outcomes.Advanced imaging technologies play a vital role in coronary artery visualization, complementing dissection-based learning to improve surgical accuracy and patient care.

Key words: coronary artery, cadaveric dissection, advanced imaging, surgical planning, patient outcomes

Introduction

The coronary arteries, essential for supplying oxygen-rich blood to the myocardium, are fundamental to the heart's functioning. A precise understanding and visualization of their anatomy are crucial for diagnosing coronary artery diseases (CAD) and planning interventions such as coronary artery bypass grafting (CABG), angioplasty, and stent placement. CAD, often caused by atherosclerosis, is a leading cause of morbidity and mortality globally. Accurate coronary artery visualization is vital for effective surgical planning and improving patient outcomes. Thus, both clinical and research efforts have focused on methods to achieve detailed coronary artery imaging.

Historically, coronary angiography has been the gold standard for diagnosing CAD, providing clear images of the coronary lumen to detect blockages and assess their severity. However, it is a two-dimensional (2D) technique with limitations in visualizing complex coronary anatomy, particularly in patients with tortuous or branching vessels. Over the past few decades, advancements in imaging technologies have significantly enhanced coronary artery visualization. Innovations such as three-dimensional (3D) coronary angiography, optical coherence tomography (OCT), and intravascular ultrasound (IVUS) have greatly improved the understanding of coronary anatomy, refined surgical planning, and optimized interventional procedures [5, 8, 12].

Recent developments in 3D coronary angiography allow more accurate vessel reconstructions, enabling better visualization of vessel orientation, branching patterns, and stenoses. Technologies like OCT and IVUS provide high-resolution images of the coronary lumen, assessing plaque composition and coronary flow, thereby improving diagnostic accuracy and procedural guidance. Various studies demonstrated the superiority of 3D angiography and OCT in improving procedural outcomes, particularly in patients with complex coronary anatomy [16, 28].

Despite the technological advances in imaging, cadaveric dissection remains a cornerstone for understanding coronary anatomy. Dissections provide detailed insights into coronary artery variations that may be missed or misinterpreted by in vivo imaging techniques. However, cadaveric dissection is limited by the static nature of the body and post-mortem tissue changes. Still, studies continue to underscore the value of cadaveric dissection in understanding coronary anomalies relevant to surgical procedures [9, 14]. This study explores the evolving landscape of coronary artery imaging, aiming to compare the accuracy and limitations of angiographic, cadaveric, and in-situ surgical views of coronary anatomy. By evaluating the strengths and weaknesses of each method, the study will assess their contributions to surgical planning and clinical outcomes. The integration of modern imaging techniques alongside traditional dissection methods presents an opportunity to improve coronary artery assessment, offering real-time, non-invasive visualization that overcomes the limitations of previous approaches. The study will also consider the impact of fusion imaging, hybrid techniques, and advancements in artificial intelligence on the future of coronary artery imaging and surgical practices.

The aim of this study is to conduct a comparative analysis of coronary artery anatomy visualization through two primary methods – cadaveric dissection and angiographic imaging techniques emphasizing their contributions to surgical planning, accuracy, and patient outcomes. The objectives are:

● To compare the effectiveness of cadaveric dissection and angiographic imaging in visualizing coronary artery anatomy.

● To assess the advantages and limitations of each method in terms of anatomical precision and clinical applicability.

● To evaluate the impact of recent advancements in 3D coronary angiography and intraoperative imaging technologies on surgical planning and patient outcomes.

● To explore how cadaveric dissection and modern imaging techniques complement each other in enhancing surgical decision-making.

● To identify the role of advanced imaging methods in improving surgical precision, reducing complications, and enhancing overall patient care.

Coronary artery anatomy and its significance in surgery

Anatomical overview

The coronary arteries are essential for supplying oxygenated blood to the heart muscle, ensuring its proper function. These arteries originate from the aorta just above the aortic valve and branch out into a complex network that supplies different regions of the heart. The coronary arterial system is generally divided into the left and right coronary arteries, each with major branches supplying specific territories of the myocardium.

Left Coronary Artery (LCA): The LCA is a short vessel that divides into two main branches:

Left Anterior Descending Artery (LAD): This artery runs along the anterior surface of the heart, supplying the anterior wall of the left ventricle, the interventricular septum, and the apex of the heart. It is considered critical due to the high mortality risk if obstructed [10, 11].

Left Circumflex Artery (LCx): The LCx supplies the lateral and posterior walls of the left ventricle, and in some cases, the inferior wall, depending on coronary variations [21].

Right Coronary Artery (RCA): The RCA supplies the right atrium, right ventricle, and inferior wall of the left ventricle. It also typically supplies the sinoatrial (SA) and atrioventricular (AV) nodes, along with several branches, including the acute marginal artery, which feeds the right ventricular free wall [25, 6].

Variations in coronary anatomy

Although most individuals have a standard coronary anatomy, variations are common, either congenital or acquired, and have clinical significance, especially during surgical procedures such as coronary artery bypass grafting (CABG) and angioplasty.

Dominance: Coronary artery dominance refers to which artery supplies the posterior descending artery (PDA) and posterior left ventricular branches. Most people have right dominance, where the RCA supplies the PDA, but about 10% exhibit left dominance, where the LCx supplies the PDA [25]. Rarely, both arteries may supply the PDA, a condition called codominance [15].

Dual LAD: In some individuals, the LAD is duplicated, and two branches supply the anterior wall of the heart. This variation, called dual LAD, is clinically significant, especially when CAD affects both branches. Surgeons must address both arteries in procedures like CABG or percutaneous coronary intervention (PCI) [21].

Anomalous Coronary Arteries: Anomalous coronary arteries, such as those originating from unusual sinus positions or having abnormal courses, are rare but carry significant clinical implications, particularly in cases where compression of the anomalous artery occurs during physical activity [6].

Role in surgical procedures

An accurate understanding of coronary anatomy is essential for successful cardiac surgeries, including CABG, angioplasty, and stent placement. Knowledge of coronary anatomy enables surgeons to plan procedures that restore heart blood flow while minimizing complications.

Coronary Artery Bypass Grafting (CABG): In CABG, blocked or narrowed coronary arteries are bypassed using grafts to restore blood flow. Surgeons must understand coronary anatomy, including variations and blockage locations, to avoid ischemia. For instance, in a patient with a dominant RCA, grafts must bypass the RCA and its branches effectively [21]. In dual LAD cases, both arteries must be re-vascularized.

Percutaneous Coronary Intervention (PCI): PCI, including angioplasty and stenting, uses a catheter to open blocked arteries. Precise knowledge of coronary anatomy guides stent placement. Variations such as dual LAD or left dominance complicate PCI and may require special attention [17, 6].

Other Interventional Strategies: Other surgical strategies like left ventricular assist device (LVAD) implantation, heart transplantation, and valve surgeries also rely on understanding coronary anatomy. Each patient's unique vascular structures may require modifications in approach [25].

Coronary artery disease (CAD) and its impact on coronary anatomy

CAD, caused by the accumulation of atherosclerotic plaques, significantly affects coronary anatomy. It reduces blood flow to the myocardium, leading to symptoms such as angina, myocardial infarction (MI), and heart failure. Over time, CAD can alter coronary artery structures, complicating diagnosis and treatment.

Impact on Coronary Anatomy: The progression of CAD leads to vessel remodeling and collateral circulation, where new vessels form to supply blood to affected areas. These collateral vessels can mislead surgeons, making it challenging to differentiate well-perfused vessels from those with underlying disease [6]. Severe stenosis in areas like the LAD or RCA requires careful planning to ensure revascularization.

Role of Imaging in Diagnosing CAD: Imaging techniques like coronary angiography, CT angiography, and MRI are essential for diagnosing CAD and planning treatment. These methods help assess blockages, vessel anomalies, and variations, which are critical for tailoring interventions such as PCI or CABG [25].

Interventional Planning in CAD: CAD treatment options like PCI or CABG depend on disease severity and coronary anatomy. Variations in coronary arteries require a personalized approach to ensure complete revascularization. For example, special care is needed to bypass the RCA in right-dominant patients, while dual LAD cases require both arteries to be treated [21]. Accurate imaging remains a cornerstone for diagnosing coronary disease, identifying anomalies, and planning treatment strategies effectively.

Coronary angiography: techniques and advances

Coronary artery disease (CAD) is a leading cause of morbidity and mortality worldwide, making accurate and timely diagnosis crucial. Coronary angiography (CA) remains the gold standard for diagnosing CAD, enabling clinicians to visualize coronary arteries and identify obstructions, stenoses, or plaques that impair blood flow to the heart muscle. Over time, coronary angiography has advanced significantly, with technological innovations enhancing its accuracy and clinical utility. This article explores the methodology of coronary angiography, recent advancements, and their impact on diagnostic precision and patient outcomes.

Standard coronary angiography

Coronary angiography emerged in the 1960s, with the first successful selective coronary arteriography performed in 1962 [23]. The procedure became the gold standard for evaluating coronary artery anatomy and diagnosing CAD. It involves injecting a contrast medium into the coronary arteries via a catheter, typically through the femoral or radial approach, the latter of which is becoming more popular due to lower complication rates and shorter recovery times.

Coronary angiography helps identify the location, severity, and number of stenoses or blockages in the coronary vessels, which is crucial for determining treatment strategies such as medical therapy, percutaneous coronary intervention (PCI), or coronary artery bypass grafting (CABG). Results are usually classified using the coronary artery disease severity index, which helps estimate the need for interventional procedures. Although widely used, conventional coronary angiography has limitations. It provides a two-dimensional (2D) view, which can distort the assessment of complex lesions, tortuous vessels, or small arteries. Moreover, it does not provide detailed information on plaque composition or vessel wall injury, both important for assessing the risk of cardiovascular events.

Technological advancements in coronary angiography

Recent advancements in imaging technologies have significantly improved coronary angiography. Innovations such as three-dimensional (3D) angiography, intravascular ultrasound (IVUS), optical coherence tomography (OCT), and fusion imaging have been integrated into clinical practice to overcome the limitations of traditional 2D angiography.

3D coronary angiography

The development of 3D coronary angiography has greatly enhanced cardiovascular imaging. By combining multiple 2D images obtained during traditional angiography, 3D angiography creates detailed, three-dimensional reconstructions of the coronary arteries. This allows for more accurate visualization, especially in complex cases involving bifurcation lesions or coronary artery stenting. Advances in software and image processing have improved visualization in challenging anatomical features like tortuosity or calcification, improving treatment planning precision and increasing the success of coronary interventions. Additionally, 3D angiography reduces procedural time and radiation exposure compared to conventional 2D angiography [17,22].

Intravascular ultrasound (IVUS)

IVUS has substantially improved coronary angiography's diagnostic capabilities. This technique involves inserting an ultrasound probe into the coronary artery to

provide real-time imaging of the vessel wall and surrounding structures. Unlike angiography, IVUS offers detailed images of the vessel's internal structure, helping assess the true severity of coronary lesions. IVUS can detect lipid-rich plaques or thin-cap fibroatheromas that may be missed by conventional angiography, which are associated with increased rupture risk and myocardial infarction. It also guides stent placement during PCI, ensuring optimal stent size and positioning [9].

Optical coherence tomography (OCT)

OCT offers high-resolution imaging of coronary lesions, using near-infrared light to capture detailed cross-sectional images with a resolution of up to 10 micrometers, surpassing that of IVUS. This superior resolution helps visualize finer features of coronary arteries, such as plaque microstructure and intimal hyperplasia. OCT is particularly useful in guiding stent implantation in complex coronary anatomies, enabling clinicians to assess stent expansion and apposition, thus reducing restenosis or post-procedural complications [20].

Fusion imaging

Fusion imaging combines data from multiple imaging modalities, such as coronary angiography, computed tomography (CT), and magnetic resonance imaging (MRI), to create a comprehensive representation of the coronary vasculature. This technique provides a more holistic assessment of coronary lesions, considering factors like plaque composition, vessel elasticity, and blood flow, which single imaging methods may miss. Fusion imaging aids in better risk stratification and guides treatment decisions, improving patient outcomes by integrating functional and anatomical data[2].

Comparison with other imaging methods

While advances in coronary angiography have improved diagnostic precision, the technique still has limitations. Traditional 2D angiography sometimes provides incomplete or distorted images due to the complexity of coronary anatomy. Furthermore, angiography focuses mainly on structural assessment without evaluating the functional significance of coronary lesions. This has led to complementary imaging techniques like fractional flow reserve (FFR) [1] and computed tomography angiography (CTA), which assesses blood flow and lesion severity, providing further guidance for decision-making [24].

In conclusion, the integration of 3D coronary angiography, IVUS, OCT, and fusion imaging into clinical practice has significantly enhanced the diagnostic and therapeutic potential of coronary angiography. These advancements not only improve the accuracy of CAD diagnosis but also contribute to better patient outcomes by enabling more personalized treatment strategies.

Cadaveric dissection and its role in understanding coronary anatomy

The study of human anatomy, particularly coronary artery anatomy, is essential in understanding cardiovascular health, guiding clinical decisions, and improving surgical outcomes. Among various educational tools and research methods, cadaveric dissection remains one of the most valuable. It provides direct insights into the complexities of the coronary arteries, revealing arterial patterns, branching, and variations that may not be fully captured through imaging techniques. This paper explores the role of cadaveric dissection in understanding coronary anatomy, its advantages, limitations, and recent contributions.

Cadaveric dissection: an overview

Cadaveric dissection offers a unique advantage by providing a detailed and direct view of coronary anatomy. Unlike imaging techniques such as CT angiography, which offer indirect representations, dissection allows for the study of actual tissue specimens. This hands-on approach enables a deep analysis of the coronary arteries' patterns, branching, and variations, which are vital for understanding coronary circulation and informing surgical planning. Cadaveric dissection is especially useful in revealing rare coronary anomalies that might be missed in living individuals. While imaging captures large-scale coronary structures, it is less effective at revealing fine details, such as variations in vessel morphology that could impact surgery or intervention. Additionally, it allows the study of arterial wall texture, which is important for procedures like coronary artery bypass grafting (CABG) or stent placement.

Advantages of cadaveric dissection

High Fidelity to Actual Anatomical Structures: One significant advantage of cadaveric dissection is its ability to provide a direct view of arteries and their variations, without reliance on imaging software interpretation. This tactile experience helps researchers and clinicians understand the coronary anatomy in depth, offering an unmediated view of structural nuances.

Study of Rare Anatomical Variations: Cadaveric dissection is invaluable for studying rare coronary variations, such as anomalous origins or abnormal branching patterns, which are difficult to detect in living individuals. These variations can be crucial for surgeries like CABG or percutaneous coronary interventions (PCI). By directly exposing the anatomy, dissection provides a unique opportunity to explore these clinically significant variations[23].

Educational Tool for Surgical Training: Cadaveric dissection has long been a cornerstone of medical education. Surgeons-in-training, particularly those in cardiothoracic and cardiovascular specialties, benefit from dissecting coronary arteries to understand the vascular system's structure. This hands-on training ensures that surgeons are well-prepared for the practical demands of heart surgery, where anatomical knowledge and precision are crucial.

Limitations of cadaveric dissection

Post-Mortem Changes: A limitation of cadaveric dissection is the alteration of anatomy due to post-mortem changes. After death, tissues undergo biochemical and physiological changes, including stiffening and the collapse or distortion of blood vessels. These changes can affect the coronary arteries' appearance, making them less representative of living conditions.

Fixed Specimens and Lack of Dynamic Conditions: Cadaveric specimens are typically fixed and preserved, which means they no longer mimic the dynamic conditions of living tissues.Coronary arteries in living bodies respond to factors like blood pressure, heart rate, and oxygen demands, which cannot be simulated in cadaveric specimens. This limits the ability to study the coronary system under in vivo conditions.

Recent studies have highlighted the critical role of cadaveric dissection in advancing our understanding of coronary artery anatomy and its clinical implications. Studies utilized cadaveric dissection to explore variations in coronary artery anatomy, identifying rare anomalies such as unusual branching of the left main coronary artery, which are important for refining surgical strategies in coronary bypass surgery [24].

Coronary artery anatomy in relation to myocardial infarction (MI) was examined and revealed subtle variations that influence outcomes of interventions like stent placement, emphasizing that cadaveric dissection is essential for understanding nuances of coronary disease [12].Variations in the right coronary artery (RCA), was focused including cases of duplicated RCA and unusual origins, which are often difficult to detect using imaging techniques [6,19]. These studies underscore the value of cadaveric dissection in both understanding rare anatomical variations and improving surgical planning for interventions such as CABG and PCI. Despite the limitations of post-mortem changes and fixed specimens, these studies highlight how dissection remains an irreplaceable tool in both research and education for clinicians.

In-situ surgical views of coronary arteries

Coronary artery disease (CAD) is a leading cause of morbidity and mortality worldwide, and its treatment often involves coronary artery bypass grafting (CABG). Successful CABG requires detailed, real-time, in-situ views of the coronary arteries, which are facilitated by advanced imaging technologies, intraoperative assessments, and refined surgical techniques. This article explores recent advancements in coronary artery visualization, focusing on imaging technologies, artery visualization techniques, and their impact on surgical outcomes.

Imaging technologies for in-situ coronary artery visualization

The role of imaging in CABG has evolved significantly. Traditional methods like angiography provide useful preoperative views but have limitations during surgery due to the heart's complex anatomy. Recent intraoperative imaging advancements, including intravascular ultrasound (IVUS), optical coherence tomography (OCT), and near-infrared spectroscopy, have improved coronary artery visualization during surgery. IVUS enhances real-time, high-resolution images of coronary arteries, improving lesion identification and graft placement [4]. This allows surgeons to assess coronary artery walls in detail, improving long-term graft patency. OCT's ability to provide even higher resolution than IVUS was highlighted, offering real-time images of the intimal layer of coronary arteries [13]. OCT aids in precise graft anastomosis and minimizes graft failure post-surgery by providing detailed plaque morphology.

Role of 3D imaging and navigation systems

Three-dimensional (3D) imaging and navigation systems have revolutionized coronary artery surgery, providing surgeons with dynamic, interactive views of coronary anatomy. Authors demonstrated that 3D-printed coronary artery models, created from preoperative CT angiograms, improved surgical accuracy, reduced surgery duration, and shortened recovery times [11]. The models offered surgeons enhanced in-situ views, optimizing graft placement. Images explored augmented reality (AR), which integrates 3D coronary artery images with real-time surgical footage [18]. AR systems provided a comprehensive view of coronary anatomy while allowing surgeons to stay focused on the surgical site, improving precision and reducing complications.

Advances in intraoperative coronary artery assessment

In addition to imaging technologies, intraoperative assessments are crucial for ensuring proper graft placement and function. Intraoperative hemodynamic monitoring and coronary flow assessment help guide graft selection and confirm graft patency.

The use of fractional flow reserve (FFR) was explored during CABG to measure the pressure drop across coronary artery lesions and assess ischemia severity. The study showed that FFR measurements allow for a tailored approach to graft selection, improving graft patency and patient outcomes. Near-infrared spectroscopy (NIRS) is also gaining traction for monitoring graft patency. NIRS enables real-time, non-invasive monitoring of oxygen saturation in coronary vessels, providing immediate feedback on graft functionality [20]. This helps detect graft failure and facilitates prompt corrective measures, improving postoperative outcomes by reducing complications.

Surgical techniques and impact on outcomes

Sophisticated imaging technologies and intraoperative assessments have refined surgical techniques for coronary artery bypass. Minimally invasive techniques, such as robotic-assisted surgery, have become more prevalent due to their enhanced precision and improved visibility. These techniques reduce surgery invasiveness, shorten recovery time, and enhance patient outcomes. A study evaluated robotic-assisted coronary artery bypass surgery, enhanced by advanced imaging technologies [26]. The study found that robotic surgery with high-definition intraoperative imaging resulted in more accurate graft placements, fewer complications, and faster recovery compared to traditional open-heart surgery. Robotic systems allowed for smaller incisions, reducing hospital stays and speeding up recovery times.

Recent advancements in imaging technologies and surgical techniques have significantly improved in-situ surgical views of coronary arteries, enhancing the precision and outcomes of CABG procedures. Technologies like IVUS, OCT, 3D imaging, augmented reality, and intraoperative monitoring have improved coronary artery visualization, leading to better graft placement, reduced complications, and faster recovery. These innovations have revolutionized coronary artery surgery, promising even more refined techniques and improved outcomes as research and technology continue to advance.

Comparative analysis: cadaveric vs angiographic vs in-situ views in coronary anatomy visualization

The visualization of coronary anatomy is crucial for preoperative planning, intraoperative decision-making, and post-operative care. Among the various techniques used to study coronary arteries, cadaveric views, angiographic views, and in-situ views each provide unique insights. However, each method has its own strengths and limitations in terms of anatomical accuracy, detail, and clinical utility. This comparative analysis explores these three techniques, focusing on their accuracy, clinical implications, and advancements in coronary imaging.

Cadaveric views: accuracy and anatomical detail

Cadaveric views offer high anatomical accuracy because they are derived from human specimens. Cadaveric dissections allow for direct visualization of coronary arteries, including their branches and variations, which can provide an in-depth understanding of normal and pathological coronary anatomy. These views are often considered the gold standard for anatomical study, as they reflect true anatomical relationships.

Recent studies have emphasized the value of cadaveric dissections for teaching and understanding coronary anatomy [11]. The study highlighted that cadaveric views are

invaluable in educational settings, where detailed anatomical knowledge is critical for students and surgeons. However, while cadaveric views offer high anatomical detail, they do not reflect certain variations seen in living patients, such as the effects of plaque buildup or arterial motion. Additionally, cadaveric dissection is static, and in vivo anatomical variations such as arterial twisting, dynamic movement, and physiological change are absent, limiting the generalizability of cadaveric studies to living patients.

Angiographic views: clinical effectiveness and limitations

Angiography remains one of the most commonly used imaging techniques in clinical practice for visualizing coronary arteries. It is a real-time, dynamic procedure that uses contrast media and X-ray imaging to visualize coronary blockages, stenosis, and anomalies. Angiography is particularly effective in diagnosing coronary artery disease (CAD), allowing for the direct visualization of lumen narrowing and occlusions. Recent advancements, particularly with fractional flow reserve (FFR) and intravascular ultrasound (IVUS), have enhanced diagnostic capabilities. Combining angiography with FFR significantly improved the accuracy of identifying functionally significant coronary lesions, improving preoperative planning [5].

However, angiographic views have notable limitations. Angiograms provide a two-dimensional (2D) representation of coronary arteries, leading to issues such as foreshortening, overlapping, and distortion of vessels. This makes accurate anatomical interpretation difficult. Furthermore, angiography primarily detects blockages rather than providing a comprehensive understanding of coronary vessel anatomy, including branching patterns and anatomical variations [3]. Despite these limitations, angiography remains an essential tool for real-time decision-making, particularly in interventions like percutaneous coronary interventions (PCI), where it aids in stent placement and monitoring post-operative outcomes.

In-situ views: dynamic assessment and patient-specific factors

In-situ views are obtained directly from living patients using advanced imaging modalities, such as coronary CT angiography (CTA) and magnetic resonance imaging (MRI). These non-invasive methods provide real-time imaging, allowing dynamic assessment of the coronary arteries under physiological conditions. Coronary CTA, in particular, has gained popularity for non-invasive coronary artery disease assessment, offering detailed three-dimensional reconstructions of coronary anatomy.

The effectiveness of coronary CTA in assessing CAD was demonstrated, especially for patients with intermediate risk profiles [26]. The study emphasized that coronary CTA could visualize coronary anomalies and calcification patterns, which essential for treatment are planning. Additionally, CTA provides a dynamic view of coronary arteries, including coronary flow assessment and heart function, in one scan. However, in-situ views have limitations related to patient-specific factors, such as motion artifacts, patient movement, and anatomical variations that can affect image quality. The resolution of non-invasive imaging methods like CTA may also fall short of cadaveric dissection, making it challenging to visualize small branches and precise relationships between vessels and surrounding tissues.

Clinical implications: contributions to planning and decision-making

Each imaging technique plays a distinct role in clinical practice. Cadaveric views are particularly useful in educational settings, where understanding coronary

anatomy in detail is essential for surgeons performing coronary bypass surgery or studying coronary anomalies. Angiographic views are indispensable for intraoperative decision-making, guiding interventions such as angioplasty and stenting. Angiography is also crucial for preoperative planning, helping identify coronary lesions that require intervention.

In-situ imaging, particularly coronary CTA and MRI, is useful for both preoperative planning and post-operative follow-up. These techniques provide a comprehensive, non-invasive view of coronary anatomy, enabling clinicians to assess the impact of CAD on heart function. Furthermore, in-situ views are valuable for monitoring disease progression over time, offering a dynamic view of the patient's coronary health.

Advancements in technology: bridging the gap

Advancements in imaging technology, such as 3D reconstructions from angiographic data, are helping bridge the gap between 2D angiograms and cadaveric views. The introduction of coronary CT angiography has significantly improved the level of detail available from non-invasive imaging, providing high-resolution, 3D reconstructions that are becoming increasingly reliable in assessing coronary artery disease. The growing role of artificial intelligence (AI) and machine learning algorithms in coronary imaging demonstrated, improving precision by reducing motion artifacts and enhancing image quality [27]. These technologies are contributing to a more accurate and detailed understanding of coronary anatomy, overcoming the limitations of traditional imaging methods.

Limitations and recommendations

Each method has inherent limitations. Cadaveric views, while anatomically accurate, do not account for dynamic physiological factors. Angiography, though essential for detecting blockages, lacks detailed anatomical visualization. In-situ imaging, while offering dynamic and patient-specific data, suffers from resolution limitations and motion artifacts. A combination of these methods can provide the most comprehensive understanding of coronary anatomy. Future research should focus on integrating these imaging techniques to create hybrid models that combine the advantages of cadaveric detail, angiographic precision, and in-situ dynamics. Moreover, ongoing advancements in 3D imaging, artificial intelligence, and motion correction will continue to improve the accuracy and utility of coronary imaging.

Summary of key findings

Cadaveric dissection remains the gold standard for anatomical accuracy, offering detailed insights into the coronary arteries' structure. Studiesaffirmed the importance of cadaveric views in educational settings [11]. However, cadaveric dissections cannot replicate dynamic changes, such as arterial movement and blood flow, making them less relevant for clinical applications like preoperative planning. Angiographic views are indispensable for diagnosing coronary artery disease (CAD) and guiding interventions such as PCI. However, angiography is limited by its 2D representation, which can distort and obscure certain anatomical details, and its primary focus on detecting blockages rather than providing a complete anatomical overview.

In-situ views, particularly coronary CTA and MRI, offer dynamic, patient-specific imaging, bridging the gap between cadaveric detail and angiographic functionality. Recent advancements in coronary CTA have enhanced its accuracy, offering high-

resolution 3D reconstructions of coronary arteries [26]. However, like angiography, in-situ imaging may suffer from limitations related to resolution and motion artifacts. Despite these challenges, in-situ views remain valuable for preoperative planning and monitoring post-operative progress non-invasively.

Future directions

The future of coronary imaging lies in the integration of multiple imaging modalities, powered by emerging technologies such as AI and machine learning. Studies have shown that AI can enhance image quality by reducing motion artifacts and improving resolution. Hybrid imaging methods, combining angiography, optical coherence tomography (OCT), and cadaveric data, could further advance coronary artery visualization. These advancements hold promise for more effective diagnosis and intervention planning, improving patient outcomes.

The combination of 3D imaging and AI algorithms could allow for personalized, dynamic reconstructions of coronary arteries, taking into account patient-specific variations in vessel morphology, disease progression, and response to treatment. This could improve preoperative planning, as surgeons would be able to visualize coronary anatomy in a way that closely mimics actual patient conditions, leading to more precise and targeted interventions.

Clinical implications

The evolving landscape of coronary imaging has profound implications for clinical practice, especially in cardiology and cardiac surgery. Integrating advanced imaging technologies is expected to improve coronary disease diagnosis, reduce complications during interventional procedures, and enhance surgical planning. For example, combining angiographic data with FFR and IVUS has already improved decision-making during coronary interventions, allowing for more targeted therapies. Similarly, coronary CTA helps identify coronary anomalies, assess plaque burden, and predict complications, thus guiding surgical decisions and improving patient outcomes.

As hybrid imaging techniques and AI become more prevalent, coronary artery surgeries and interventions will benefit from improved precision, leading to better long-term outcomes. These advancements will enable more personalized treatments based on unique coronary anatomy and disease characteristics. As technology continues to evolve, future research will likely focus on optimizing the integration of these techniques into clinical workflows, ensuring they are used to their full potential in both preoperative and postoperative care.

Conclusion

The comparative analysis of cadaveric, angiographic, and in-situ views in coronary anatomy provides valuable insights into their respective roles in understanding coronary vessel structure and aiding clinical decision-making. Each of these imaging modalities has its distinct strengths and limitations, but recent advancements in technology are helping to bridge the gaps between them. This synthesis highlights the evolving role of these techniques in surgical planning, and the exciting potential of emerging technologies in enhancing coronary imaging.

References

1. **Abbasciano, R. G., G. R. Layton, S. Torre, N. Abbaker, A. Copperwheat, C. Lucarelliet, et al.** Fractional flow reserve and instantaneous wave-free ratio in coronary artery bypass grafting: a meta-analysis and practice review. – *Front. Cardiovasc. Med.,* **11**, 2024, 1348341.
2. **Abdelrahman, K. M., M. Y. Chen, A. K. Dey, R. Virmani, A. V. Finn, R. Y. Khamiset, et al.** Coronary computed tomography angiography from clinical uses to emerging technologies: JACC state-of-the-art review. – *J. Am. Coll. Cardiol.,* **76**(10), 2020, 1226-1243.
3. **Antonopoulos, A. S., A. Angelopoulos, K. Tsioufis, C. Antoniades, D. Tousoulis.** Cardiovascular risk stratification by coronary computed tomography angiography imaging: current state-of-the-art. – *Eur. J. Prev. Cardiol,* **29**(4), 2022, 608-624.
4. **Araki, M., S. J. Park, H. L. Dauerman, S. Uemura, J. S. Kim, C. Di Mario, et al.** Optical coherence tomography in coronary atherosclerosis assessment and intervention. – *Nat. Rev. Cardiol.,* **19**(10), 2022, 684-703.
5. **Barbato, E., G. G. Toth, N. P. Johnson, N. H. Pijls, W. F. Fearonet, et al.** A prospective natural history study of coronary atherosclerosis using fractional flow reserve. – *J. Am. Coll. Cardiol.,* **68**(21), 2016, 2247-2255.
6. **Beecham, R., S. Prater, J. Batlle.** Coronary artery anomalies. – *StatPearls [Internet]*, Treasure Island (FL), StatPearls Publishing, 2025. Available at: https://www.ncbi.nlm.nih.gov/books/NBK556060/.
7. **Bruschke, A. V., W. C. Sheldon, E. K. Shirey, W. L. Proudfit.** A half century of selective coronary arteriography. – *J. Am. Coll. Cardiol.,* **54**(23), 2009, 2139-2144.
8. **Choudhry, N., J. S. Duker, K. B. Freund, S. Kiss, G. Querques, R. Rosen, et al.** Classification and guidelines for widefield imaging: recommendations from the International Widefield Imaging Study Group. – *Ophthalmol. Retina*, **3**(10), 2019, 843-849.
9. **D'Souza, M. R., B. Ray, A. Saxena, P. Rastogi, A. S. D'Souza, C. Guptaet, et al.** Variations of origin of coronary artery and their importance. – *J. Morphol., Sci.,* **32**(1), 2015, 1-7.
10. **Dhole, R., D. Borse, R. Ahire, A. Sharma, P. Marathe.** Cardiovascular imaging: recent advances in atherosclerosis diagnosis. – *Int. J. Ther. Innov.,* **2**(5), 2024, 3048-4626.
11. **Fatima, N., A. Kumari, K. Sinha.** Study of branching, dominance pattern of coronary arteries in human cadaver. – *Eur. J. Mol. Clin. Med.*, **8**(4), 2021, 2201-2208.
12. **Gunderman, R. B., P. K. Wilson.** Viewpoint: exploring the human interior: the roles of cadaver dissection and radiologic imaging in teaching anatomy. – *Acad. Med.,* **80**(8), 2005, 745-749.
13. **Hasan, S. M., M. Faluk, J. D. Patel, R. Abdelmaseih, J. Patel.** Use of optical coherence tomography in coronary artery disease: review article. – *Curr. Probl. Cardiol.*, **46**(3), 2021, 100597.
14. **Kesieme, E.B., B. Omoregbee, D.L. Ngaage, M.H.D. Danton.** Comprehensive review of coronary artery anatomy relevant to cardiac surgery. – *Curr. Cardiol. Rev.,* **21**(2), 2025, e1573403X321942.
15. **Kim, Y., S. Bae, T. W. Johnson, N. H. Son, D. S. Sim, Y. J. Hong, et al.** Role of intravascular ultrasound-guided percutaneous coronary intervention in optimizing outcomes in acute myocardial infarction. – *J. Am. Heart Assoc.,* **11**(5), 2022, e023481.
16. **Kodeboina, M., K. Piayda, I. Jenniskens, P. Vyas, S. Chen, R. J. Pesigan, et al.** Challenges and burdens in the coronary artery disease care pathway for patients undergoing percutaneous coronary intervention: a contemporary narrative review. – *Int. J. Environ. Res. Public Health*, **20**(9), 2023, 5633.

17. **Leivaditis, V., E. Beltsios, A. Papatriantafyllou, K. Grapatsas, F. Mulita, N. Kontodimopouloset, et al.** Artificial intelligence in cardiac surgery: transforming outcomes and shaping the future. – *Clin. Pract.,* **15**(1), 2025, 17.
18. **Li, Q., C. Huang, S. Lv, Z. Li, Y. Chen, L. Ma.** A human-computer interactive augmented reality system for coronary artery diagnosis planning and training. – *J. Med. Syst.,* **41**(10), 2017, 159.
19. **Lichtenberg, A. B., K. A. Abouzaid, A. Y. Karim, V. Cornelio, M. Algoul, A. Imam.** A cadaveric case report of a double right coronary artery and its clinical implications. – *Cureus*, **15**(11), 2023, e48578.
20. **Masroor, M., A. Ahmad, Y. Wang, N. Dong.** Assessment of the graft quality and patency during and after coronary artery bypass grafting. – *Diagnostics*, **13**(11), 2023, 1891.
21. **McNichols, B., J. R. Spratt, J. George, S. Rizzi, E. W. Manning, K. Park.** Coronary artery bypass: review of surgical techniques and impact on long-term revascularization outcomes. – *Cardiol. Ther.,* **10**(1), 2021, 89-109.
22. **Narula, J., Y. Chandrashekhar, A. Ahmadi, S. Abbara, D. S. Berman, R. Blankstein, et al.** SCCT 2021 expert consensus document on coronary computed tomographic angiography: A report of the Society of Cardiovascular Computed Tomography. – *J. Cardiovasc. Comput. Tomogr.,* **15**(3), 2021, 192.
23. **Solanki, R., R. Gosling, V. Rammohan, G. Pederzani, P. Garg, J. Heppenstallet, et al.** The importance of three dimensional coronary artery reconstruction accuracy when computing virtual fractional flow reserve from invasive angiography. – *Sci. Rep.*, **11**(1), 2021, 19694.
24. **Sumalatha, S., V. Hari, L. S. Quadros, A. S. D'Souza.** Anatomical variations of coronary venous system and its tributaries: a cadaveric study. – *J. Cardiothorac. Surg,* **10**(Suppl 1), 2015, A255.
25. **Villa, A. D., E. Sammut, A. Nair, R. Rajani, R. Bonamini, A. Chiribiri.** Coronary artery anomalies overview: the normal and the abnormal. – *World J. Radiol.,* **8**(6), 2016, 537.
26. **Wang, C., L. Zhang, T. Qin, Z. Xi, L. Sun, H. Wu, et al.** 3D printing in adult cardiovascular surgery and interventions: a systematic review. – *J. Thorac Dis.,* **12**(6), 2020, 3227-3237.
27. **Wang, X., H. Zhu.** Artificial intelligence in image-based cardiovascular disease analysis: a comprehensive survey and future outlook. – *arXiv preprint* arXiv:2402.03394, 2024. Available at: https://doi.org/10.48550/arXiv.2402.03394.
28. **Zhang, J., X. Gao, J. Kan, Z. Ge, L. Han, S. Luet, et al.** Intravascular ultrasound versus angiography-guided drug-eluting stent implantation: the ULTIMATE trial. – *J. Am. Coll. Cardiol.,* **72**(24), 2018, 3126-3137.

Institute of Experimental Morphology, Pathology and Anthropology with Museum
Bulgarian Anatomical Society

Acta Morphologica et Anthropologica, 32 (3-4)
Sofia ● 2025

Impact of trypanosomes on infected tissues of the mammalian host (Review)

Nikola Mladenov[1], Vladislav Lazarov[1], Desislav Dinev[1], Anton Kolarov[1]*

Department of Biology, Medical Faculty, Medical University of Sofia, Sofia, Bulgaria

*Corresponding author e-mail: n.mladenov@medfac.mu-sofia.bg

The protozoan parasite *Trypanosoma* infects various warm-blooded animals, usually via an insect vector. In humans, *T. brucei* causes sleeping sickness in Africa, and *T. cruzi* causes Chagas disease mostly in South America. *Trypanosoma brucei* is traditionally observed in the blood and later in the central nervous system but new data prove additional localization in other organs including skin, lungs, liver, heart and kidneys. *Trypanosoma cruzi* is found in multiple organs and tissues during the acute form of the disease and predominantly in the skin, heart and gastrointestinal tract during the chronic form. Both species inflict specific histopathological changes in the organs depending on disease progression. *Trypanosoma equiperdum* is an equine parasite causing the sexually transmitted disease dourine. It causes inflammation of the genital tract of both sexes, and in males also degeneration of seminiferous tubules. In addition, it causes skin plaques and spinal cord lesions resulting in neurological damage.

Key words: Chagas disease, *Trypanosoma sp.*, sleeping sickness

Medical importance of *Trypanosoma*

Protozoan parasites of the kinetoplastid genus *Trypanosoma* are dangerous pathogens causing sleeping sickness and Chagas disease in the human, as well as diseases in domestic and wild animals. Comprehensive knowledge of the histopathological changes caused by their presence is needed to understand the pathogenesis of trypanosomiases and to improve the methods of diagnosis and treatment. In this respect, the most clear-cut case is the New World species *Trypanosoma cruzi* causing Chagas disease. In its mammalian hosts, including humans, T. cruzi switches to an intracellular amastigote form which causes damage by using cardiomyocytes as host cells and provoking an inflammatory response [16]. Unlike it, the African species *Trypanosoma brucei* exists in the mammalian host solely in the form of an extracellular flagellated trypomastigote which evades the antibody response by periodically changing its major surface antigen, the so-called variant surface glycoprotein [11]. However, despite the fact that *T. brucei*

does not destroy host cells directly by intracellular parasitism, it is even more virulent than its American counterpart: its invasion of the central nervous system leads to meningoencephalitis known as sleeping sickness, which is fatal if untreated [9].

Histopathological changes caused by *Trypanosoma cruzi*

Chagas disease is a sickness typically associated with Latin America, although in recent years there have been many reported cases around the world including North America and Europe [12, 21]. According CDC more than 8 million people worldwide suffer from the disease and numbers in the USA alone have reached 280 thousand [6]. *Trypanosoma cruzi* has three forms – trypomastigote, epimastigote, and amastigote (intercellular in the vertebrate host). It relies mostly on vector-borne transmission by bedbugs belonging to genus *Triatoma* (kissing bug), but other significant pathways have also been reported – blood-borne, congenital, organ-derived, salivary - mostly among reservoir hosts, and even oral transmission by food and drinks contaminated with bugs or their droppings [4]. The disease has two stages – acute and chronic. In most cases the acute form has mild or no symptoms while in other cases flu-like symptoms are reported. Chancre around the bite site, and inflammation with partial closing of one of the eyes (Romana's sign) could be observed. Eye inflammation could be attributed to either direct inoculation of the eye with the parasite or an allergic reaction to the parasite/vector. Severe symptoms as myocarditis or meningoencephalitis are rare but pose a significant risk for the patient's life. The severity of the acute form is correlated with the type of transmission. The oral pathway is more likely to cause life-threatening conditions, likely due to the low pH value in the human stomach which results in surface protein changes in the parasites [2]. The chronic stage could initially be asymptomatic (indeterminate form) but progressively leads to development of severe abnormalities in the cardiovascular system and gastrointestinal tract such as ventricular arrhythmias, bradycardia, complete heart block, an apical aneurysm, thromboembolic phenomena, dysphagia, odynophagia, bowel ischemia, etc. [4].

During the acute stage T. cruzi is believed to invade a diversity of nucleated cells in the spleen, gut, adipose tissue, heart endothelium, striated muscles, immune cells etc. The same results were demonstrated using animal models, mostly rodents. Interestingly, no parasites were found in the brain or liver during the initial stages, and no parasites were observed in the spleen and striated muscles during the chronic form [20]. This is a direct result of the *T. cruzi* tissue tropism. The way the parasite recognizes the target tissue is still debatable but galectins are presumed to play a major role in the process, especially Galectin-1 for cardyomiocyte recognition. After recognizing the host cell, the parasite penetrates it in a Ca^{2+} dependent manner, using its tc85, gp35/50, gp 82, gp 80, and other surface proteins [19]. During the acute form of the disease inflammatory and immune response changes can be observed in heart tissue (**Fig. 1**). In the amplification stage multiple parasites could be seen in the cytoplasm of the cells. Activated phagocytes and lymphocytes infiltrate the area, which leads to an increased production of proinflamatory proteins, and a histological picture similar to many forms of myocarditis. After the acute stage ends there are fewer infected cells and usually no significant damage to the organ. During the chronic form cardiomyocytes start to die out mostly due to local inflammation and are replaced by connective or fat tissue. The heart becomes enlarged, but the miocard becomes thinner with hypertrophic muscle cells [5]. The arrhythmia observed in such

patients is believed to be caused by either direct or indirect neural damage caused by the presence of *Trypanosoma cruzi* [14].

Damage to the gastrointestinal tract caused by *T. cruzi* is not observed as frequently as other symptoms, and could be attributed to the destruction of neural cells and damage caused by inflammation in regions in the lower or upper part of the gastrointestinal tract. The symptoms may vary from constipation to dysphagia and megacolon. Many factors are considered to play a role in the manifestation and severity of the symptoms including the genetic variant of *T. cruzi*, the microbiome, and the presence of mutations affecting epithelial receptors such as NOD2 [13].

Histopathological changes caused by *Trypanosoma brucei*

Sleeping sickness, or human african trypanosomiasis, develops in two stages: 1) early or hemolymphatic stage, characterized by non-specific symptoms and presence of trypanosomes in the blood plasma, and 2) late or meningoencephalitic stage, when the parasite spreads to the central nervous system and causes neurological impairment [15]. In other mammals, the disease follows a similar course though the predominant symptom is weight loss [7].

Trypanosomes in the blood and central nervous system have understandably attracted most attention due to their importance for diagnosis and pathogenesis, respectively, and also because of a key treatment criterion: after the disease has progressed to the late stage, treatment options are narrowed down to drugs able to pass the blood-brain barrier, which are few, not very efficient, and highly toxic [9]. However, *T. brucei* is by no means limited to the blood and the central nervous system. Recent studies have revealed presence of the parasite in extravascular spaces of other organs such as the skin, adipose tissue, eyes, and testis; a cathepsin-like protease secreted by it, called brucipain, is presumed to help its extravasation [7]. There are data that these tissue-resident trypanosomes are the main reproducing pool and a proportion of their daughter cells, carrying new versions of the variant surface glycoprotein, are "seeded" to the bloodstream where they are accessible to the vector – the tse-tse fly *Glossina* [11]. In studies on experimentally infected animals, trypanosomes have been found also in the lungs, liver, heart and kidneys [15]. They tend to adhere to collagen fibers in the skin and other tissues [7]. This behavior of the parasite may be related to the fact that the vector bite injects it into the collagen-rich dermis, which is thus the first tissue of the mammalian host contacted by the trypanosome. Moreover, extravascular trypanosomes may persist in the skin of infected hosts that present no symptoms and no detectable blood forms. Such latent infections, usually omitted from textbook descriptions of African trypanosomiasis, can be transmitted to tsetse flies and therefore will hinder any effort to eradicate the parasite [1].

For obvious reasons, tissue pathology has been more extensively studied in animal models than in human patients. Both in the central nervous system and in other organs, it includes blood vessel congestion and infiltration by lymphocytes and mononuclear phagocytes. There are also organ-specific changes such as pulmonary fibrosis and renal tubular necrosis [15]. In the skin, a common finding during the early stage is the so-called trypanosomal chancre. It forms around the inoculating tse-tse fly bite and is an inflamed nodule full of proliferating parasites. Host fibroblasts and endothelial cells also proliferate. In addition to this localized lesion, there are often rashes, pruritus, and dermatitis during both the early and the late stage. Testicular infection has been studied in experimentally

infected animal models, and seems limited to connective tissue. So far, *T. brucei* has not been observed beyond the blood-testis barrier; and while experimentally infected male mice can infect their partners, sexual transmission is extremely rare in natural hosts [7].

Trypanosoma brucei is thought to invade the brain through the choroid plexus and circumventricular organs, which contain relatively permeable capillaries devoid of a blood-brain barrier [3]. Microglial cells, as resident mononuclear phagocytes of the brain, are the cell population most prominently engaged with controlling the infection. In an experiment with experimentally infected mice, activation and proliferation of microglia surprisingly started during the early, hemolymphatic stage of trypanosomiasis. In addition to increasing their number and activity, microglial cells, as in other pathological processes in the brain, decreased their structural complexity, i.e. reduced the number and length of their processes (**Fig. 2**). The microglia is involved also in the natural infection, since brain samples of patients who died of sleeping sickness reveal hyperplasia and formation of nodules by the microglia [22].

In the final stage of the above described experimental infection, peripheral immune cells massively infiltrated the brain, but this last-resort attempt to eliminate the pathogen did not seem to mitigate the pathological process [22]. One of the reasons may be the maladaptive nature of the immune response against the parasite. In another experiment on mice, *T. brucei* infection caused formation of extopic lymphoid aggregates in the meninges, making the meninges behave as a secondary lymphoid organ. Many of the B cells differentiated there, however, were autoreactive and produced antibodies against myelin basic protein and other brain components [18]. *Trypanosoma brucei* and other kinetoplastids are known to skew the host immune response towards Th2 cells, which creates permissive conditions for their survival [1].

Histopathological changes caused by *Trypanosoma equiperdum*

Trypanosoma equiperdum is an equine parasite causing a disease called dourine. It is unique among trypanosomes by being transmitted sexually rather than by a blood-sucking insect. Despite these biological differences, *T. equiperdum* is morphologically very similar to *T. brucei*, which has made researchers speculate about their evolutionary relationship. Molecular data confirmed that *T. equiperdum* has evolved from *T. brucei* relatively recently. Concomitantly with an adaptation to sexual transmission, it lost key parts of its kinetoplast – the complex mitochondrial genome which is a hallmark of the group. This made it unable to perform oxidative phosphorylatin and, hence, to survive in the energy-poor environment inside an insect body. As a result, *T. equiperdum* was restricted to its mammalian host where it could rely on glycolysis for energy metabolism. The degenerative change paradoxically gave the parasite the opportunity to greatly expand its distribution range, while the ancestral *T. brucei* remains confined within the range of its vector, the tsetse fly [8, 10]. In the light of these data, some recent sources consider *T. equiperdum* a subspecies of *T. brucei* [17].

Little is known about pathogenesis of dourine. The gross pathology includes swelling of the genitalia, skin plaques, neurological symptoms, and emaciation often leading to death. Unlike *T. brucei*, *T. equiperdum* is present in the blood only briefly and then settles in various tissues. The testes of males and the genital tract of both sexes are infiltrated by lymphocytes, plasma cells and mononuclear phagocytes. In stallions, chronic orchitis causes degeneration of seminiferous tubules and may completely

abolish spermatogenesis (**Fig. 3**). Perineal and penile skin is affected by dermatitis leading to keratinocyte and melanocyte necrosis and, as a result, depigmentation. In addition to the reproductive system, the nervous system is also heavily infected. Degenerative lesions are observed in the distal spinal cord, especially the lumbar and sacrococcygeal regions, as well as spinal nerves and ganglia. The spinal cord damage affects white matter and is manifested as axonal degeneration and demyelination. The peripheral nerves and ganglia associated with them are inflamed and infiltrated by the same populations of immune cells as described above for the reproductive system. The spinal cord and nerve damage can explain the hindleg incoordination characteristic for dourine. Neuritis including vacuolation and demyelination has also been described in the facial nerve, though the brain seems largely undamaged [23, 24].

Conclusions

Both *T. brucei* and *T. equiperdum* invade a range of tissues and despite their strictly extracellular habitat lead to lesions, inflammation, immune cell infiltration and functional impairment. Tissue-resident forms may predominate over the blood forms even in *T. brucei*, indicating that diagnosis should be based on tissue biopsy rather than blood sample. The histopathological changes caused by the two extracellular trypanosomes are similar in many respects, which implies common features in pathogenesis. It is therefore appropriate to take advantage of the easier handling of *T. equiperdum* and use it as a model of *T. brucei* in research. An interesting finding is that both trypanosomes infect the testis but only *T. equiperdum* seems able to cross the blood-testis barrier, which presumably made possible its sexual transmission. It may be hypothesized that this ability was the first trait to evolve as *T. equiperdum* diverged from *T. brucei* and took its own independent path.

Acknowledgements: This work was supported by Grant No. D-163/04.06.2025 of the Medical University of Sofia.

References

1. Alfituri, O. A., J. F. Quintana, A. MacLeod, P. Garside, R. A. Benson, J. M. Brewer, N. A. Mabbott, L. J. Morrison, P. Capewell. To the Skin and Beyond: The Immune Response to African Trypanosomes as They Enter and Exit the Vertebrate Host. – *Front. Immunol.*, **11**, 2020, 1250.

2. Barreto-de-Albuquerque, J., D. Silva-dos-Santos, A. R. Perez, L. R. Berbert, E. de Santana-van-Vliet, D. A. Farias-de-Oliveira, O. C. Moreira, E. Roggero, C. E. de Carvalho-Pinto, J. Jurberg, V. Cotta-de-Almeida, O. Bottasso, W. Savino, J. de Meis. Trypanosoma cruzi infection through the oral route promotes a severe infection in mice: new disease form from an old infection? – PLoS Negl. Trop. Dis., **9**, 2015, e0003849.

3. Bentivoglio, M., K. Kristensson, M. E. Rottenberg. Circumventricular Organs and Parasite Neurotropism: Neglected Gates to the Brain? – *Front. Immunol.*, **9**, 2018, 2877.

4. Bern, C., L. A. Messenger, J. D. Whitman, J. H. Maguire. Chagas Disease in the United States: a Public Health Approach. – Clin. Microbiol. Rev., **33**, 2019, e00023-19.

5. Bonney, K. M., D. J. Luthringer, S. A. Kim, N. J. Garg, D. M. Engman. Pathology and Pathogenesis of Chagas Heart Disease. – *Annu Rev. Pathol.*, **14**, 2019, 421-447.

6. Centre of Disease Control, 2024 Available at https://www.cdc.gov/chagas/about/index.html
7. Crilly, N. P., M. R. Mugnier. Thinking outside the blood: Perspectives on tissue-resident *Trypanosoma brucei*. – *PLoS Pathog.*, **17**, 2021, e1009866.
8. Jensen, R. E., L. Simpson, P. T. Englund. What happens when *Trypanosoma brucei* leaves Africa. – *Trends Parasitol.*, **24**, 2008, 428-431.
9. Kennedy, P. G. Clinical features, diagnosis, and treatment of human African trypanosomiasis (sleeping sickness). – *Lancet Neurol.*, **12**, 2013, 186-194.
10. Lai, D. H., H. Hashimi, Z. R. Lun, F. J. Ayala, J. Lukes. Adaptations of *Trypanosoma brucei* to gradual loss of kinetoplast DNA: *Trypanosoma equiperdum* and *Trypanosoma evansi* are petite mutants of *T. brucei*. – *Proc. Natl. Acad. Sci. USA*, **105**, 2008, 1999-2004.
11. Larcombe, S. D., J. C. Munday, R. McCulloch. Do tissue-dwelling trypanosomes sustain transmission populations? – *Trends Parasitol.*, **41**, 2025, 13-15.
12. Manne-Goehler, J., C. A. Umeh, S. P. Montgomery, V. J. Wirtz. Estimating the burden of Chagas disease in the United States. – PLoS Negl. Trop. Dis., **10**, 2016, e0005033.
13. Medina-Rincón, G. J., S. Gallo-Bernal, P. A. Jiménez, L. Cruz-Saavedra, J. D. Ramírez, M. J. Rodríguez, R. Medina-Mur, G. Díaz-Nassif, M. D. Valderrama-Achury, H. M. Medina. Molecular and Clinical Aspects of Chronic Manifestations in Chagas Disease: A State-of-the-Art Review. – *Pathogens*, **10**, 2021, 1493.
14. Miranda, C. H., A. B. Figueiredo, B. C. Maciel, J. A. Marin-Neto, M. V. Simoes. Sustained ventricular tachycardia is associated with regional myocardial sympathetic denervation assessed with 123I-metaiodobenzylguanidine in chronic Chagas cardiomyopathy. – *J. Nucl. Med.*, **52**, 2011, 504-510.
15. Ndungu, K., J. Thuita, G. Murilla, J. Kagira, J. Auma, P. Mireji, G. Ngae, P. Okumu, P. Gitonga, S. Guya, R. Mdachi. The pathogenicity of blood stream and central nervous system forms of *Trypanosoma brucei rhodesiense* trypanosomes in laboratory mice: a comparative study. – *F1000Res.*, **11**, 2023, 260.
16. Nunes, J. P. S., V. M. P. Roda, P. Andrieux, J. Kalil, C. Chevillard, E. Cunha-Neto. Inflammation and mitochondria in the pathogenesis of chronic Chagas disease cardiomyopathy. – *Exp. Biol. Med. (Maywood)*, **248**, 2023, 2062-2071.
17. Oldrieve, G., M. Verney, K. S. Jaron, L. Hébert, K. R. Matthews. Monomorphic Trypanozoon: towards reconciling phylogeny and pathologies. – *Microb. Genom.*, **7**, 2021, 000632.
18. Quintana, J. F., M. C. Sinton, P. Chandrasegaran, L. Kumar Dubey, J. Ogunsola, M. Al Samman, M. Haley, G. McConnell, N. R. Kuispond Swar, D. M. Ngoyi, D. Bending, L. de Lecea, A. MacLeod, N. A. Mabbott. The murine meninges acquire lymphoid tissue properties and harbour autoreactive B cells during chronic *Trypanosoma brucei* infection. – *PLoS Biol.*, **21**, 2023, e3002389.
19. de Souza, W., T. M. de Carvalho, E. S. Barrias. Review on Trypanosoma cruzi: Host Cell Interaction. – Int. J. Cell Biol., 2010, 2010:295394.
20. Santi-Rocca, J., F. Fernandez-Cortes, C. Chillón-Marinas, M. L. González-Rubio, D. Martin, N. Gironès, M. Fresno. A multi-parametric analysis of Trypanosoma cruzi infection: Common pathophysiologic patterns beyond extreme heterogeneity of host responses. – *Sci. Rep.,* 2017, 7, 8893.
21. Requena-Méndez, A., E. Aldasoro, E. de Lazzari, E. Sicuri, M. Brown, D. A. J. Moore,J. Gascon, J. Muñoz. Prevalence of Chagas disease in Latin-American migrants living in Europe: a systematic review and meta-analysis. – *PLoS Negl. Trop. Dis*., 2015, 9:e0003540. doi: 10.1371/journal.pntd.0003540.
22. Uzcategui, N. L., S. Güçer, C. Richter, A. Speidel, E. Zirdum, M. Duszenko, O. Garaschuk, K. Figarella. Live imaging of microglia during sleeping sickness reveals early and heterogeneous inflammatory responses. – *Front. Immunol.*, **14**, 2023, 1253648.

23. Yasine, A., H. Ashenafi, P. Geldhof, L. Van Brantegem, G. Vercauteren, M. Bekana, A. Tola, A. Van Soom, L. Duchateau, B. Goddeeris, J. Govaere. Histopathological lesions in reproductive organs, distal spinal cord and peripheral nerves of horses naturally infected with *Trypanosoma equiperdum*. – *BMC Vet. Res.*, **15**, 2019, 175.

24. Yasine, A., M. Daba, H. Ashenafi, P. Geldhof, L. Van Brantegem, G. Vercauteren, T. Demissie, M. Bekana, A. Tola, A. Van Soom, L. Duchateau, B. Goddeeris, J. Govaere. Tissue (re)distribution of *Trypanosoma equiperdum* in venereal infected and blood transfused horses. – *Vet. Parasitol.*, **268**, 2019, 87-97.

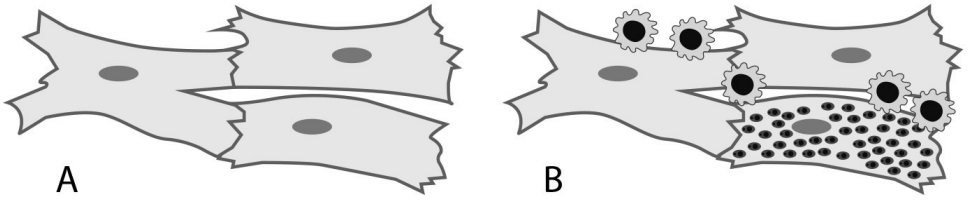

Fig. 1. A – normal muscle cells; B – muscle cells with amastigotes, and surrounded by immune cells

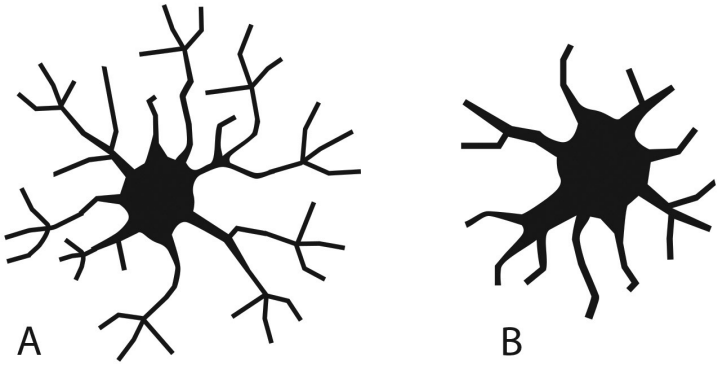

Fig. 2. A – normal glia cell; B – glia cell with changed morphology as a result of an immune reaction

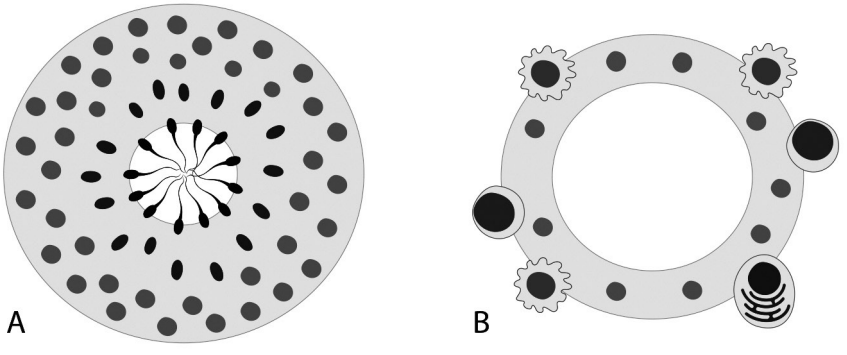

Fig. 3. A – normal seminiferous tubule; B – seminiferous tubule with abnormal morphology, and spermatogenesis due to immune cell infiltration

Institute of Experimental Morphology, Pathology and Anthropology with Museum
Bulgarian Anatomical Society

Acta Morphologica et Anthropologica, 32 (3-4)
Sofia ● 2025

Prevalence and Risk Factors of Work-Related Musculoskeletal Disorders Among Professional Vehicle Drivers in India: A Review

*P. Das, D. Chatterjee, A. R. Bandyopadhyay**

Department of Anthropology, University of Calcutta, Ballygunge, Kolkata, West Bengal, India

*Corresponding author e-mail: abanthro@caluniv.ac.in

This comprehensive review explores the high prevalence of Work-Related Musculoskeletal Disorders (WRMSDs) among professional drivers in India's rapidly expanding transportation sector. The study analyzes 43 peer-reviewed articles covering various vehicle categories, including auto-rickshaws, two-wheelers, buses, taxis, heavy vehicles, and trucks. The findings reveal that low back pain is the most common complaint across all driver types, followed by neck, shoulder, and knee discomfort. Risk factors are categorized into occupational, vehicular, and personal domains. The review underscores the urgent need for ergonomic interventions, health surveillance, and policy reforms to safeguard the musculoskeletal health and overall well-being of India's professional drivers.

Key words: Musculoskeletal disorders, low back pain, ergonomics, risk factors, professional drivers, India

Introduction

Work-related musculoskeletal disorders (WRMSDs) refer to impairments of the musculoskeletal system – including bones, tissues, tendons, joints, blood vessels, and nearby peripheral nerves – caused or aggravated by occupational activities or environments [32]. These include a wide spectrum of clinical syndromes such as tendinopathies, tenosynovitis, bursitis, neurological disorders like sciatica and carpal tunnel syndrome, osteoarthritis, and generalised pain syndromes such as low back pain [30]. WRMSDs are largely associated with poor ergonomics and constitute a major component of the global burden of occupational diseases [7].

According to the World Health Organization (WHO), musculoskeletal disorders are leading contributors to disability and limitations in daily and occupational functioning [4]. Professional drivers are particularly vulnerable to WRMSDs due to prolonged exposure to physical, environmental, and psychosocial stressors

[2,12]. Driving involves static postures, prolonged sitting, exposure to whole-body vibration, repetitive movements, and awkward positions, all of which contribute to the development of musculoskeletal pain and dysfunction [36].

Individual risk factors such as age, gender, body mass index (BMI), and overall health status also influence the susceptibility to WRMSDs [20,22]. Additionally, environmental exposures such as air and noise pollution further exacerbate the health risks faced by drivers. In India, road transport accounts for over 80% of passenger movement, and with economic growth and urbanisation, professional drivers are increasingly subjected to longer working hours, poor road conditions, and inadequate occupational support systems [23,34].

Under this background, the present review aims to synthesize existing literature to better understand the prevalence, distribution, and risk factors associated with WRMSDs among different categories of vehicle drivers in India.

Materials and Criteria

A systematic review was conducted utilizing the databases like Scopus, PubMed and Web of Science alongside the Google Scholar search engine to comprehensively assess musculoskeletal disorders among professional drivers in India, focusing on publication years spanning the last 15 years. The search strategy included a precise combination of keywords – "musculoskeletal pain," "low back pain," "professional drivers," "work-related musculoskeletal disorders (WRMSDs)," and "ergonomics"- reflecting both clinical and occupational dimensions relevant to this population. Articles were initially screened for eligibility based on study design, population, and outcomes, with priority given to research detailing prevalence rates, risk factor analysis, and specific musculoskeletal phenotypes. Out of 50 identified studies, 33 fulfilled the inclusion criteria: peer-reviewed original research focused on Indian professional drivers, quantifying the prevalence of WRMSDs and investigating associated risk factors such as prolonged sedentary driving, whole-body vibration, inadequate workplace ergonomics, and psychosocial stressors. Selected studies predominantly employed cross-sectional methodologies, standardized musculoskeletal health surveys, and subgroup analyses addressing vehicle type and driving duration. The systematic review underscores the substantial occupational health burden borne by professional drivers in India and advocates for targeted ergonomic improvements, structured health promotion initiatives, and regulatory policy interventions that address the complex interplay between occupational exposure, job design, and musculoskeletal health outcomes.

Results and Discussion

•WRMSD prevalence among professional drivers by Vehicle Type (Figure 1)

Auto-rickshaw drivers exhibit a notably high prevalence of musculoskeletal complaints, particularly in the upper extremities. Neck pain affects approximately 81% of drivers, while shoulder discomfort is reported by 70%, with carpal tunnel syndrome

also frequently observed [13,14,26,33,37]. Studies suggest that scapular alignment abnormalities are significantly correlated with neck pain within this group [11].

Two-wheeler riders – motorbike and scooter operators – regularly report musculoskeletal stress localized to the upper back, shoulders, and neck, regardless of vehicle type, rider age, or gender [9]. This stress is predominantly attributed to poor ergonomic posture and the impact of road shocks [9,31].

Bus drivers are commonly afflicted with low back pain, with prevalence rates ranging widely from 49% to 85% depending on regional and study-specific factors [3,18,19,24,25,29,35,41]. Additional affected regions include the neck, shoulders, and knees. Ergonomic risk assessments using the Rapid Entire Body Assessment (REBA) and Rapid Upper Limb Assessment (RULA) tools consistently show high-risk scores for the back and shoulder regions in bus drivers, related to prolonged postures and inadequate seat design [10].

Taxi drivers demonstrate an 87% prevalence of WRMSDs, with 49% reporting low back pain specifically [8,28,38]. In private car drivers, the overall prevalence of musculoskeletal complaints reaches 77.4%, with 66% reporting low back pain within the past year [16,27].

Heavy vehicle operators, such as dumpers, also present a significant burden, with musculoskeletal discomfort reported by 58% to 74% of drivers [15]. Common sites include the back, ankle, and shoulder regions [21,39,40]. Among the crane operators, older drivers and those with longer job tenure report higher discomfort levels, especially in the back and neck, partly due to cabin design factors such as cabin height [6].

Truck drivers frequently report lower back pain, followed by discomfort in the knees, shoulders, and cervical spine [5]. Regional and geographical differences – such as hilly versus plain terrain – further influence WRMSD prevalence in this occupational group [1,17].

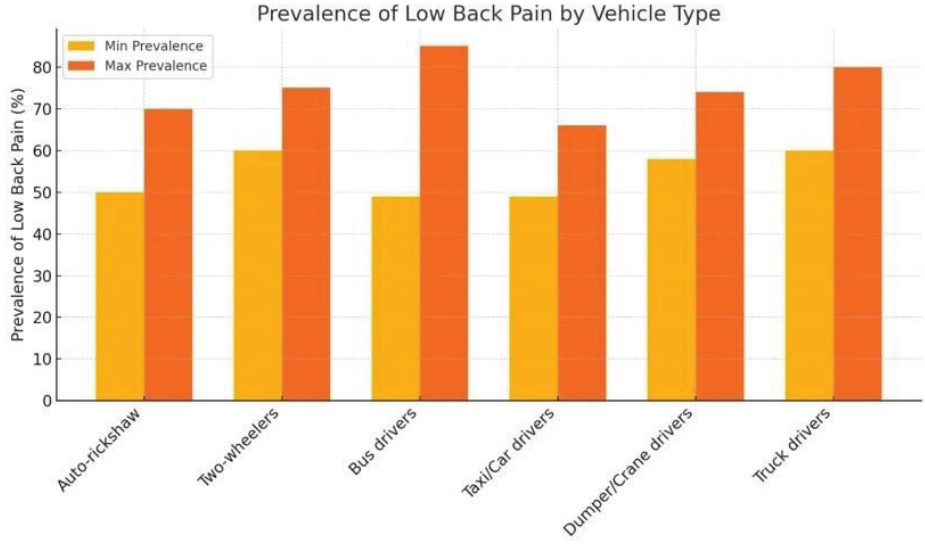

Figure 1

Figure 1(a): Prevalence of low back pain by vehicle type

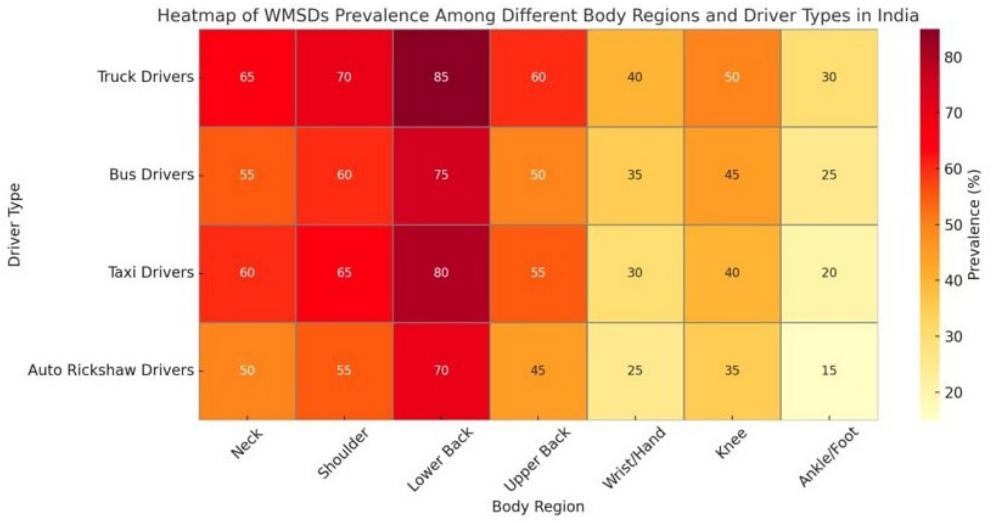

Figure 1(b): Heatmap of WRMSD prevalence among different body regions and driver types

• Risk Factors for WRMSDs (Figure 2)

Occupational factors: MSDs can affect anyone as a result of long periods of driving per shift, daily average driving exceeding 200 kilometres and total duration of service [5,17,19,24]. The risk of discomfort increases with days per week driving exceeding 48 hours per week, daily average driving seems to play a crucial role in musculoskeletal pain [3,5,17]. Repetitive work, job demand, and work design also significantly perturbs the drivers' musculoskeletal health [38]. Psychosocial work factors, such as perceptions of unfair treatment, job strain, and effort-earning imbalance creates mental stress which contribute significantly to these disorders [5,8]. Lack of enough resting duration or break in between driving hours causes susceptibility towards body pain & discomfort [5].

Vehicle related factors: Back and neck pain risks are heightened by long-term exposure to vehicle vibration and awkward seating postures [5,15,21,24,35]. Vehicle ergonomics seems to play a crucial role in the susceptibility of musculoskeletal pain [30]. Poor road condition causing exertion to the body for longer period is revealed as a confounding factor for the rapid increasing rate of musculoskeletal pain among drivers [5].

Personal factors: Age is a significant predictor reported for the development of musculoskeletal disorder with older age correlating with an elevated risk of MSD pains [18,19,21,38,41]. The prevalence of WRMSDs seemed to be influenced by sociodemographic factors like marital status, children, education reported from a study conducted among the dumper operators [38]. Excessive fat deposition & body weight in the form of abdominal obesity & higher BMI were found as the comorbid factors for musculoskeletal disorders of the drivers specially backache [19,31,39]. Reduced engagement in physical activity and unhealthy dietary habits amplify the vulnerability to WRMSDs [10,41]. Substance & alcohol consumption also encompass as predictors of body pain but not very strongly [18, 41].

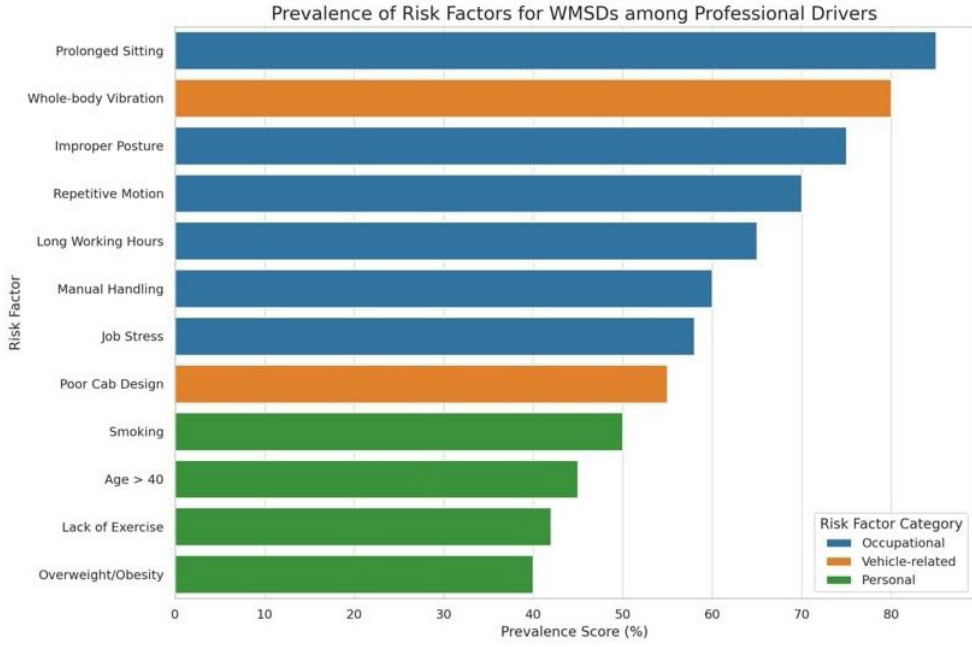

Figure 2 (a): Prevalence of risk factors for WRMSD among professional drivers

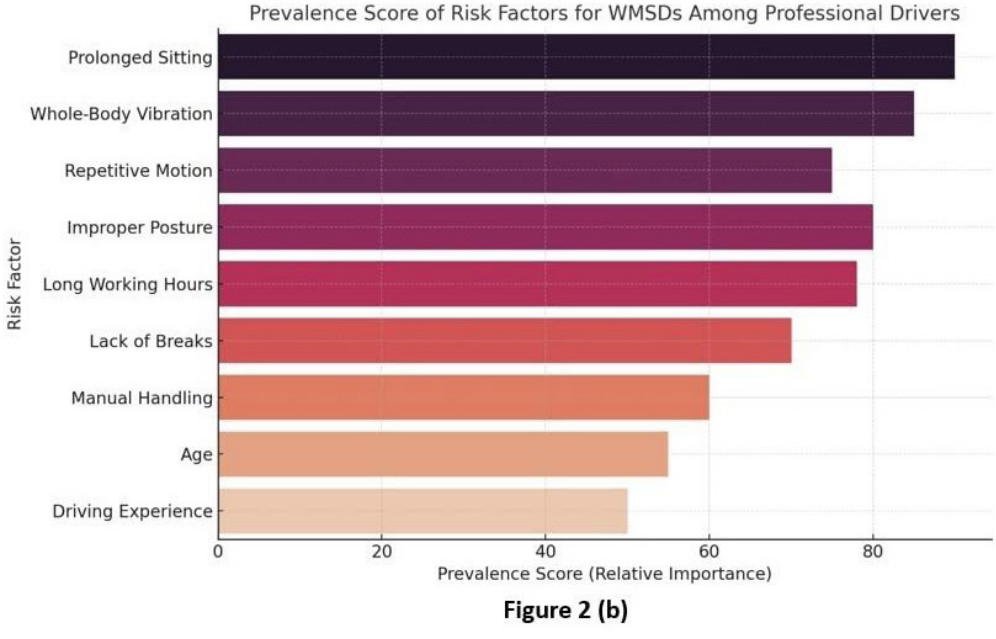

Figure 2 (b): Prevalence score of risk factors for WRMSD among professional drivers

Conclusion

This review highlights the widespread burden of WRMSDs among professional drivers in India across multiple vehicle categories. Low back pain emerged as the most frequent issue, followed by neck, shoulder, and knee discomfort. The causes are multifactorial, involving occupational, vehicular, and personal risk factors.

Recommendations:

1. Ergonomic Training: Professional drivers should be provided with regular training programs focusing on proper posture, seat adjustment, and vehicle ergonomics to reduce the risk of musculoskeletal disorders.

2. Health Monitoring: Routine medical exams, including physiotherapy evaluations and follow-up assistance, should be instituted to monitor and manage early indicators of work-related health disorders among drivers.

3. Policy Reforms: Labor regulations should be established and enforced to ensure standardized working hours, mandatory rest breaks, and occupational health protections for professional drivers.

4. Health Awareness: Awareness campaigns should be launched to highlight the need of physical activity, balanced diet, and preventative healthcare practices in sustaining musculoskeletal health.

5. Infrastructure Improvements: Road infrastructure should be regularly assessed and maintained to minimise vibration-related musculoskeletal stress by lowering vehicle vibration and enhancing driving comfort.

Collectively, these ideas underline the necessity for a multidisciplinary approach incorporating ergonomic design, occupational health surveillance, policy intervention, and infrastructure development. Implementing these approaches can significantly improve the occupational well-being, safety, and long-term productivity of professional drivers.

References

1. **Amod, B., A. Shubhangi, G. Sandeep, T. Prashant.** Study of Occupational Factors Associated with Low Back Pain in Truck Drivers of Nagpur City, India. – *Int. J. Med. Health Sci.*, **1**, 2012, 53-60.
2. **Batawi, M. A.** The Work of the World Health Organisation in Occupational Health. – *Occup. Health (Auckl).*, 1974, 228-236. Available from: http://linkinghub.elsevier.com/retrieve/pii/B9780433126805500239
3. **Borle, A., S. Gunjal, A. Jadhao, S. Ughade, A. Humne.** Musculoskeletal morbidities among bus drivers in city of Central India. – *Int. J. Recent Trends Sci. Technol.*, **3**(1), 2012, 29–32.
4. **Briggs, A. M., A. D. Woolf, K. Dreinhöfer, N. Homb, D. G. Hoy, D. Kopansky-Giles, L. March.** Reducing the global burden of musculoskeletal conditions. – *Bull. World Health Organ.*, **96**, 2018, 366.
5. **Chandrasekaran, B., M. Goon, S. Ghoshal, B. Sharma.** Prevalence of Low Back Pain in Long Distance Truck Drivers of Mountainous Terrain. – *Adv. Occup. Soc. Organ Ergonomics*, 2011, Chapter 55 CRC Press. http://dx.doi.org/10.1201/EBK1439835074-56

6. Chatterjee, A. S. Backache in Dumper Operators of a Private Iron Ore Mine in Eastern India: A Cross-sectional Study. – *J. Adv. Res. Med. Sci. Tech.*, **4**(1 & 2), 2017, 7-16. https://doi.org/10.24321/2394.6539.201702

7. European Agency for Safety and Health at Work (EU-OSHA). Work-related musculoskeletal disorders: prevalence, costs and demographics in the EU. – *EU-OSHA Report*, 2019**.** Available online: https://osha.europa.eu/en/publications/msds-facts-and-figures-overview-prevalence-costs-and-demographics-msds-europe (accessed on 4 May 2021)

8. Fatima, S., A. Fatima, U. Raj, M. Kumari, A. Anand, N. Chauhan, S. Arora. Work Related Musculoskeletal Disorders Assessment in Cab drivers. – *Indian J. Forensic Med. Toxicol.*, **14**(4), 2020, n.p. SSRN: https://ssrn.com/abstract=3760721

9. G. A. Anoop., S. A. Binoosh. A study on musculoskeletal disorders among two-wheeler riders of Kerala state in India. – *Proc 4th Ker Technol Congr – KETCON*, **6**, 2019, 411-418.

10. Geete, D., B. Mhatre, A. Mehta, M. Lokhande. Analysis of Work-Related Musculoskeletal Pain in Bus Drivers – A Cross-sectional Study. – *Indian J. PhysiotherOccup. Ther.*, **7**(2), 2013, 53-58. https://www.i-scholar.in/index.php/ijpot/article/view/41732

11. Krishna, H. S., P. K. Sreejisha, M. R. Ugale. Comparison of scapular alignment in auto rickshaw drivers with and without neck pain: A pilot study. – *Int. J. Phys. Educ. Sports Health.*, **8**(6), 2021, 14-17. https://doi.org/10.22271/kheljournal.2021.v8.i6a.2272

12. Health & Safety Executive. Work-Related Musculoskeletal Disorders (WRMSDs) statistics in Great Britain. 2015, https://www.qcs.co.uk/wp-content/uploads/2015/12/Work-related-Musculoskeletal-Disorder-WRMSDs.pdf

13. Jadhav, K., M. Shende, N. Deshmukh. Prevalence of Musculoskeletal Discomfort in Auto-Risckshaw Driver Dwelling in Pune. – *Int. J. Sci. Res. (IJSR).*, **11**(2), 2022, 320–322. https://www.ijsr.net/getabstract.php?paperid=SR22204184128

14. Kadam, A., G. Bhalekar. Prevalence of Carpal Tunnel syndrome in Auto-Rickshaw drivers. – *Int. J. Health Sci. Res.*, **11**(8), 2021, 35–44. https://doi.org/10.52403/ijhsr.20210806

15. Kar, M. B., M. Aruna, B. M., Kunar. Structural equation modelling of work related musculoskeletal disorders among dumper operators. – *Sci. Rep.*, **13**(1), 2023, 14055. https://doi.org/10.1038/s41598-023-40507-9

16. Karthikeyan, M., N. Deepak, V. P. R. Sivakumar. The prevalence of work related musculoskeletal disorders among car drivers in SRM university. – *Int. J. Multidiscip. Res. Rev.*, **1**(3), 2018, 36-43.

17. Krishna, O. B., J. Maiti, P. K. Ray, S. Mandal. Assessment of risk of musculoskeletal disorders among crane operators in a steel plant: A data mining–based Analysis. – *Hum. Factors Ergon ManufServ Ind.*, **25**(5), 2015, 559–572. https://doi.org/10.1002/hfm.20575

18. Kulkarni, A., J. Atre, R. Kaluskar. Prevalence of disability due to low back pain in MSRTC bus drivers of Pune, India. – *Int. J. Health Sci. Res.*, **12**(4), 2022, 64-69. https://doi.org/10.52403/ijhsr.20220407

19. Lalit, R. S., S. Garg. The prevalence of musculoskeletal disorders among bus drivers in Tricity. – *Int. J. Physiother.*, **2**(5), 2015, 850–854. https://doi.org/10.15621/ijphy/2015/v2i5/78244

20. Magnusson, M. L., M. H. Pope, D. G. Wilder, B. Areskoug. Are occupational drivers at an increased risk for developing musculoskeletal disorders? – *Spine (Phila Pa 1976).*, **21**(6), 1996, 710-717.

21. Mandal, B. B., A. K. Srivastava. Musculoskeletal disorders in dumper operators exposed to whole body vibration at Indian mines. – *Int. J. Min. Reclam. Environ.*, **24**(3), 2010, 233–243. https://doi.org/10.1080/17480930903526227

22. Massaccesi, M., A. Pagnotta, A. Soccetti, M. Masali, C. Masiero, F. Greco. Investigation of work-related disorders in truck drivers using RULA method. – *Appl. Ergon.*, **34**(4), 2003, 303-307.

23. Mohokar, A., A. Deoke, A. Soaji. Prevalence & risk factors of musculoskeletal impairments among auto-rickshaw drivers in a city of central India. – *IOSR J. Dent. Med. Sci.*, **17**(2), 2018, 49-54.
24. Mukherjee, S., C. K. Pradhan, S. Thakur, S. Sahu. Effects of year of work exposure on musculoskeletal problems in bus drivers of Kolkata, India. – *J. Hum. Ergol.*, **47**(2), 2018, 53–61. https://doi.org/10.11183/jhe.47.2_53
25. Pandarinath, M., T. R. Rao, S. Venkatesh. Statistical Analysis of Musculoskeletal Disorders (MSD) and Risk Factors of Public Transport Bus Drivers of India. – *Math Stat. Eng. Appl.*, **72**(1), 2023, 622–638. https://doi.org/10.17762/msea.v72i1.1953
26. Pandav, T., S. Patil. Prevalence of Upper Extremity Musculoskeletal Disorders in Auto Rickshaw Drivers. – *Int. J. Curr. Adv. Res.*, **7**(2), 2018, 9951-9953. http://dx.doi.org/10.24327/ijcar.2018.9953.1663
27. Patel, A., S. Kulkarni. Work related musculoskeletal disorders in occupational taxi drivers of Mahabaleshwar. – *VIMS J. Phys. Ther.*, **5**(1), 2023, 44-51. https://doi.org/10.46858/VIMSJPT.5110
28. Pradeepkumar, H., G. Sakthivel, S. Shankar. Prevalence of work related musculoskeletal disorders among occupational bus drivers of Karnataka, South India. – *Work (Reading, Mass.).*, **66**(1), 2020, 73–84. https://doi.org/10.3233/WOR-203152
29 Premlal, K. S., S. Nagalingam. A cross sectional study on pattern and associated risk factors of musculoskeletal morbidities among government bus drivers in Mangalore, Karnataka. – *Int. J. Community Med. Public Health.*, **5**(12), 2018, 5126–5132. https://doi.org/10.18203/2394-6040.ijcmph20184785
30. Punnett, L., D. H. Wegman. Work-related musculoskeletal disorders: The epidemiologic evidence and the debate. – *J. ElectromyogrKinesiol.*, **14**(1), 2003, 13-23. https://doi.org/10.1016/j.jelekin.2003.09.015
31. Ramasamy, S., K. Adalarasu, P. Navinchandra. Evaluation of driving-related musculoskeletal disorders in motorbike riders using Quick Exposure Check (QEC). – *Biomed. Res.*, **28**(5), 2017, 1962-1968.
32. Sekkkay, F., D. Imbeau, Y. Chinniah, P. A. Dubé, N. de Marcellis-Warin, N. Beauregard, M. Trépanier. Risk factors associated with self-reported musculoskeletal pain among short and long distance industrial gas delivery truck drivers. – *Appl. Ergon.*, **72**, 2018, 69–87. https://doi.org/10.1016/j.apergo.2018.05.005
33. Shaik, R., C. K. Gotru, C. G. Swamy, R. Sandeep. The prevalence of musculoskeletal disorders and their association with risk factors in auto-rickshaw drivers—A survey in Guntur City. – *Int. J. Physiother.*, **1**, 2014, 2-9.
34. Sharma, P. K., E. Ganguly. Morbidity profile of long distance truck drivers in Hyderabad city, India. – *J. Dr NTR Univ. Health Sci.*, **3**, 2014, 234-237.
35. Sheth, A., A. Pagdhune, A. Viramgami. Prevalence of work related musculoskeletal disorders (WRMSDs) and its association with modifiable risk factors in metropolitan bus transit drivers: A cross sectional comparison. – *J. Family Med. Primary Care.*, **12**(8), 2023, 1673–1678. https://doi.org/10.4103/jfmpc.jfmpc_532_23
36. Silverstein, B. A., D. S. Stetson, W. M. Keyserling, L. J. Fine. Work-related musculoskeletal disorders: Comparison of data sources for surveillance. – *Am. J. Ind. Med.*, **31**(5), 1997, 600-608.
37. Sontakkey, M., M. Tank, D. Suba. Prevalence of work related musculoskeletal disorders among auto-rickshaw drivers of Vadodara city. – *J. Emerg. Technol. Innov. Res.*, **6**(4), 2019, 1404–1410.
38. Srivastava, S., U. V. Kiran. Work related musculoskeletal disorder on various body segments in taxi drivers. – *Int. J. Sci. Res.*, **3**(6), 2014, 610–613. http://dx.doi.org/10.13140/2.1.1754.9443

39. Upadhyay, R., A. Bhattacherjee, A. K. Patra, N. Chau. Association between Whole-Body Vibration exposure and musculoskeletal disorders among dumper operators: A case-control study in Indian iron ore mines. – *Work (Reading, Mass.)*., **71**(1), 2022, 235–247. https://doi.org/10.3233/WOR-205140

40. Upadhyay, R., V. Jaiswal, A. Bhattacherjee, A. K. Patra. Role of whole-body vibration exposure and posture of dumper operators in musculoskeletal disorders: A case study in metalliferous mines. – *Int. J. Occup. Saf. Ergon.*, **28**(3), 2022, 1711–1721. https://doi.org/10.1080/10803548.2021.1932111

41. Yasobant, S., M. Chandran, E. M. Reddy. Are Bus Drivers at an Increased Risk for Developing Musculoskeletal Disorders? An Ergonomic Risk Assessment Study. – *J. Ergonomics.*, **S3**, 2015, 011. https://doi.org/10.4172/2165-7556.S3-011

Institute of Experimental Morphology, Pathology and Anthropology with Museum
Bulgarian Anatomical Society

Acta Morphologica et Anthropologica, 32 (3-4)
Sofia ● 2025

ANTHROPOLOGY AND ANATOMY 32 (4)

Original Articles

Correlation Between the Morphometric Characteristics of the Piriform Aperture and the Facial Skeleton: A CT-Based Study of a Bulgarian Population

Zlatizara Todorova[1], Ferihan Popova[1], Irina Angelova[2], Zdravka Harizanova[1], Iva Naydenova[3], Tsvetan Tsvetanov[4]*

[1] Department of Anatomy, Histology and Embryology, Faculty of Medicine, Medical University – Plovdiv, Plovdiv, Bulgaria
[2] Department of Imaging Diagnostics, Dental Allergology and Physiotherapy, Faculty of Dental Medicine, Medical University – Plovdiv, Plovdiv, Bulgaria
[3] Department of Mathematics, Physics, Chemistry, Technical University of Sofia, Branch Plovdiv, Plovdiv, Bulgaria
[4] Department of Dental, Oral and Maxillofacial Surgery, Dental Faculty, Medical University – Plovdiv, Plovdiv, Bulgaria

* Corresponding author e-mail: zlatizara.todorova@mu-plovdiv.bg

Advances in imaging diagnostics have enabled precise analysis of craniofacial structures. The piriform aperture, central to nasal morphology and facial aesthetics, is vital in respiration, growth, and craniofacial development. This study examines correlations between piriform aperture dimensions and facial skeletal measurements using computed tomography. A total of 120 adults of Bulgarian ethnic origin (55 males, 65 females), aged 20-60 years, were analyzed using 3D reconstructions from multi-slice CT scans. Significant positive correlations were found between piriform aperture height and nasal height, upper, and lower aperture widths. An inverse correlation was observed between aperture height and nasal bone length. Additional associations were noted between facial height and cranial width measurements. The findings underscore the relevance of piriform aperture morphology in clinical contexts and support its integration into surgical planning for reconstructive and aesthetic facial procedures.

Key words: piriform aperture, craniofacial morphology, computed tomography, 3D reconstruction

Introduction

In the early 21st century, significant progress has been made in craniofacial anthropological research, facilitated by the accumulation of large datasets derived from independent studies and the development of geometric morphometric methods [15, 17]. Traditional craniometric landmarks [3, 8, 9, 14] are gradually being complemented or replaced by 3D morphometric approaches that allow precise measurement of otherwise inaccessible skull regions [1, 4, 6, 19, 23, 24].

The nasal region plays a critical role in overall craniofacial growth. Prenatally, the nasal septum functions as a growth center, stimulating maxillary development and guiding facial elongation. Postnatally, the septum and nasal cavity continue to influence facial morphology as functional matrices [20]. The piriform aperture not only affects nasal airflow but also contributes significantly to the aesthetic perception of the human face.

This study seeks to evaluate the correlations between the linear dimensions of the piriform aperture and the facial skeleton in a representative Bulgarian population, with particular emphasis on applications in reconstructive and aesthetic facial surgery.

Material and Methods

Study sample

The study included 120 adult individuals (55 males and 65 females) aged 20–60 years, of Bulgarian ethnic origin, referred for head CT for non-craniofacial medical indications. Participants were recruited from St. Ivan Rilski Medical Complex, Plovdiv, following ethical approval from the local Ethics Committee at the St George University Hospital and written informed consent in accordance with the Helsinki Declaration.

Participants included in the study were required to be over 20 years of age and of Bulgarian ethnic origin, defined as having both parents and all grandparents of Bulgarian descent. Additionally, only individuals who were referred to a head computed tomography (CT) scan for reasons unrelated to facial trauma were considered eligible. Exclusion criteria included any non-Bulgarian ancestry, a personal history of craniofacial trauma, surgery, congenital malformations, endocrine, metabolic, or skeletal development disorders, as well as the presence of chronic obstructive pulmonary disease (COPD) and other chronic conditions leading to mouth breathing, as these influence craniofacial morphology.

All CT scans were performed using a Siemens SOMATOM Sensation Cardiac 64-slice CT scanner. The imaging protocol involved a tube voltage of 120 kV and a tube current of 250 mA. Scans were acquired with a slice thickness of 0.5 mm and reconstructed at 0.3 mm intervals. Images were processed using a 512 × 512 matrix and the H45s convolution kernel to ensure high-resolution image quality suitable for detailed anatomical assessment. Data were exported in DICOM format and processed with Radiant DICOM Viewer using 3D volume rendering (VR). Anatomical landmarks were marked, and linear measurements were taken in millimeters between standard craniometric points.

Measurements

A total of **14 cranial landmarks** (**Table 1**) were obtained and **16 linear measurements** were recorded.

Table 1. Cranial landmarks, obtained in the study.

Landmarks	Abbr.	Description:
Eurion	eu	The most lateral point on the lateral surface of the skull. / bilateral location/
Frontomalare orbitale	fmo	The point of intersection of the lateral orbital margin with the zygomaticofrontal suture. /bilateral location/
Maxillofrontale	mf	The point of intersection of the medial orbital margin with the frontomaxillary suture. /bilateral location/
Zygion	zy	The most lateral point on the zygomatic arch. /bilateral location/
Nasomaxillare	nm	The point located at the intersection of the piriform aperture with the nasomaxillary suture. /bilateral location/
Nasolaterale	nl	The most posterior point on the lateral margin of the piriform aperture. /bilateral location/
Gonion	go	Point on the mandibular angel where the outline of the mandible intersects with the line bisecting the angle formed by the line tangent to the posterior ramus border and the line tangent to the inferior border of the body. /bilateral location/
Mentale	ml	The most inferior point of the mental foramen. /bilateral location/
Ectoconchion	ec	The intersection point of the lateral orbital margin and the line originating from maxillofrontale and crossing the orbit parallel to the upper orbital margin. /bilateral location/
Nasion	n	The intersection point of the frontonasal suture and the midsagittal plane.
Rhinion	rhi	The point of intersection of the upper end of the piriform aperture and the internasal suture.
Nasospinale	ns	The point located on the intersection of the median plane with the line connecting the lower edge of the piriform aperture.
Prostion	pr	The most anterior point in the midline on the upper alveolar process.
Gnathion	gn	The most inferior point on the mandibular border in the midsagittal plane

Linear measurements calculated:

- **Piriform Aperture**: Height (rhi-ns), Upper width (nm-nm), Lower width (nl-nl);
- **Nasal Region**: Nasal height (n-ns), Nasal bone length (n-rhi);
- **Facial Skeleton**: Upper facial height (n-pr), Lower facial height (pr-gn), Morphological facial height (n-gn), Zygomatic width (zy-zy), Bigonial width (go-go), Bimental width (ml-ml), Cranial width (eu-eu), Bi-orbital width (fmo-fmo), Interorbital width (mf-mf), Orbital width (mf-ec), Orbital height (the greatest linear distance between the upper and lower orbital rims, perpendicular to the orbital width).

Statistical Analysis

Data were analyzed using SPSS 24.0 (Statistical Package for the Social Sciences 24.0). Pearson's correlation coefficient (r) was calculated to assess linear relationships between variables. The level of statistical significance was set at $P < 0.05$. Correlation strength was classified as follows: r - 0.01–0.30 – weak; r - 0.30–0.50 – moderate; r - 0.50–0.70 – strong; r - 0.70–0.90 – very strong; r - > 0.90 – near-perfect correlation.

Results

Piriform Aperture Correlations

Piriform aperture (PA) height (rhi-ns) demonstrated a positive correlation with several key nasal measurements, including nasal height (n-ns), upper PA width (nm-nm), and lower PA width (nl-nl) (**Table 2**). In contrast, PA height was negatively correlated with nasal bone length (n-rhi). Both the upper and lower PA widths were positively correlated not only with each other but also with PA height, indicating coordinated growth patterns in these regions. Notably, the lower PA width exhibited a significant inverse correlation with nasal bone length, suggesting a potential compensatory or structural relationship between these dimensions.

Table 2. Correlation relationships between the measured linear dimensions of the piriform aperture combined for both sexes in individuals from the Bulgarian population.

Total for both sexes (n=120)						
Anthropological dimensions		**rhi-ns**	**n-ns**	**n-rhi**	**nm-nm**	**nl-nl**
rhi-ns	Pearson	1	.663**	-.365**	.246**	.342**
	p		**.000**	**.000**	**.007**	**.000**
n-ns	Pearson	.663**	1	.455**	.118	.175
	p	**.000**		**.000**	.201	.056
n-rhi	Pearson	-.365**	.455**	1	-.147	-.189*
	p	**.000**	**.000**		.110	**.039**
nm-nm	Pearson	.246**	.118	-.147	1	.404**
	p	**.007**	.201	.110		**.000**
nl-nl	Pearson	.342**	.175	-.189*	.404**	1
	p	**.000**	.056	**.039**	**.000**	
**. Correlation is significant at the 0.01 level (2-tailed).						
*. Correlation is significant at the 0.05 level (2-tailed).						

Facial Skeleton Correlations

Measurements of upper, lower, and total morphological facial height were found to be strongly correlated with nearly all craniofacial width parameters (**Table 3**). Specifically, zygomatic, bigonial, and bi-orbital widths showed consistent positive correlations with various linear facial dimensions, underscoring the interconnected development of facial width and height. Orbital width was significantly correlated with most facial measurements, with the exception of interorbital width, which did

not follow the same pattern. Additionally, orbital height demonstrated significant correlations with all measured variables, excluding cranial width, bimental width, and interorbital width. These findings highlight a robust relationship among vertical and horizontal skeletal components of the face.

Table 3. Correlation relationships between the measured linear dimensions of the facial skeleton, combined for both sexes in individuals from the Bulgarian population.

Total for both sexes (n=120)													
Anthropological dimensions		**n-pr**	**pr-gn**	**n-gn**	**zy-zy**	**go-go**	**ml-ml**	**eu-eu**	**fmo-fmo**	**mf-mf**	**mf-ec**	**Orbital height**
n-pr	Pearson	1	.436**	.861**	.534**	.497**	.236**	.303**	.480**	.216*	.517**	.508**
	p		**.000**	**.000**	**.000**	**.000**	**.010**	**.001**	**.000**	**.018**	**.000**	**.000**
pr-gn	Pearson	.436**	1	.833**	.497**	.470**	.409**	.375**	.486**	.210*	.489**	.191*
	p	**.000**		**.000**	**.000**	**.000**	**.000**	**.000**	**.000**	**.022**	**.000**	**.037**
n-gn	Pearson	.861**	.833**	1	.607**	.569**	.375**	.398**	.571**	.252**	.595**	.417**
	p	**.000**	**.000**		**.000**	**.000**	**.000**	**.000**	**.000**	**.005**	**.000**	**.000**
zy-zy	Pearson	.534**	.497**	.607**	1	.703**	.476**	.477**	.766**	.440**	.619**	.267**
	p	**.000**	**.000**	**.000**		**.000**	**.000**	**.000**	**.000**	**.000**	**.000**	**.003**
go-go	Pearson	.497**	.470**	.569**	.703**	1	.570**	.263**	.617**	.357**	.490**	.325**
	p	**.000**	**.000**	**.000**	**.000**		**.000**	**.004**	**.000**	**.000**	**.000**	**.000**
ml-ml	Pearson	.236**	.409**	.375**	.476**	.570**	1	.253**	.509**	.463**	.306**	.000
	p	**.010**	**.000**	**.000**	**.000**	**.000**		**.005**	**.000**	**.000**	**.001**	.999
eu-eu	Pearson	.303**	.375**	.398**	.477**	.263**	.253**	1	.349**	.302**	.221*	.027
	p	**.001**	**.000**	**.000**	**.000**	**.004**	**.005**		**.000**	**.001**	**.015**	.767
fmo-fmo	Pearson	.480**	.486**	.571**	.766**	.617**	.509**	.349**	1	.536**	.727**	.309**
	p	**.000**	**.000**	**.000**	**.000**	**.000**	**.000**	**.000**		**.000**	**.000**	**.001**
mf-mf	Pearson	.216*	.210*	.252**	.440**	.357**	.463**	.302**	.536**	1	.050	-.049
	p	**.018**	**.022**	**.005**	**.000**	**.000**	**.000**	**.001**	**.000**		.586	.592
mf-ec	Pearson	.517**	.489**	.595**	.619**	.490**	.306**	.221*	.727**	.050	1	.370**
	p	**.000**	**.000**	**.000**	**.000**	**.000**	**.001**	**.015**	**.000**	.586		**.000**
Orbital height	Pearson	.508**	.191*	.417**	.267**	.325**	.000	.027	.309**	-.049	.370**	1
	p	**.000**	**.037**	**.000**	**.003**	**.000**	.999	.767	**.001**	.592	**.000**	

**. Correlation is significant at the 0.01 level (2-tailed).

*. Correlation is significant at the 0.05 level (2-tailed).

Table 4. Correlation relationships between the measured linear dimensions of the piriform aperture and facial skeleton, combined for both sexes in individuals from the Bulgarian population.

Total for both sexes (n=120)												
Anthropological dimensions		**n-pr**	**pr-gn**	**n-gn**	**zy-zy**	**go-go**	**ml-ml**	**eu-eu**	**fmo-fmo**	**mf-mf**	**mf-ec**	**Orbital height**
rhi-ns	Pearson	.435**	.303**	.437**	.498**	.374**	.213*	.300**	.412**	.153	.442**	.160
	p	**.000**	**.001**	**.000**	**.000**	**.000**	**.020**	**.001**	**.000**	.095	**.000**	.081
n-ns	Pearson	.794**	.318**	.667**	.588**	.446**	.195*	.315**	.457**	.185*	.500**	.378**
	p	**.000**	**.000**	**.000**	**.000**	**.000**	**.033**	**.000**	**.000**	**.043**	**.000**	**.000**
n-rhi	Pearson	.471**	.035	.309**	.139	.110	-.011	.035	.077	.048	.095	.280**
	p	**.000**	.705	**.001**	.130	.233	.909	.702	.400	.604	.302	**.002**
nm-nm	Pearson	.188*	.230*	.248**	.267**	.219*	.275**	.166	.310**	.392**	.160	-.023
	p	**.040**	**.011**	**.006**	**.003**	**.016**	**.002**	.070	**.001**	**.000**	.081	.802
nl-nl	Pearson	.100	.232*	.195*	.389**	.232*	.237**	.075	.479**	.361**	.379**	.057
	p	.275	**.011**	**.033**	**.000**	**.011**	**.009**	.415	**.000**	**.000**	**.000**	.536
**. Correlation is significant at the 0.01 level (2-tailed).												
*. Correlation is significant at the 0.05 level (2-tailed).												

Correlations between piriform aperture and facial skeleton measurements

Piriform aperture (PA) height (rhi-ns) demonstrated a strong positive correlation with most of the measured linear craniofacial parameters, except for interorbital width (mf-mf) and orbital height (**Table 4**). Nasal height (n-ns) was found to be significantly correlated with all of the facial skeleton measurements. Meanwhile the length of the nasal bones (n-rhi) exhibited a consistent positive correlation only with upper and morphological facial heights and with orbital height. Upper width of PA (nm-nm) was strongly correlated with most of the craniofacial parameters except for cranial width and orbital width and height. Lower width of PA (nl-nl) also revealed significance in correlations with most of the craniofacial parameters excluding upper facial and orbital height and cranial width.

Discussion

This study confirms that the morphometric parameters of the piriform aperture are closely linked to those of the facial skeleton. The nasal region, particularly the PA, demonstrates complex correlations indicative of integrated craniofacial growth. The inverse relationship between PA height and nasal bone length may reflect compensatory growth dynamics or developmental constraints. The results are presented for both sexes in order to assess the overall correlations between the morphometric characteristics of the piriform aperture and the facial skeleton in the general population sample. Acknowledging the potential influence of sexual dimorphism and the value of sex-specific correlation analyses further research is needed.

The growth and development of the nasal cavity have a central place in the ontogeny of the facial skull. Prenatally the nasal septum acts as a growth site and induces maxillary pull, which directs facial growth in an anteroinferior direction and leads to a sevenfold increase in facial length between the 10th and 40th weeks after fertilization [7]. Postnatally the nasal septum and cavity act as functional matrices and continue to be one of the determining factors for the development of the facial growth pattern [7, 13].

The findings align with previous studies indicating the central role of the nasal septum and nasal cavity in facial ontogeny [5, 20, 22]. The strong correlations found across multiple facial dimensions suggest that morphometric parameters can be predictive of nasal architecture — with direct applications in aesthetic and reconstructive surgical planning. Facial plastic surgery must be tailored to the close relationship between the soft tissue facial profile and the underlying bone structure, as well as the gender, age, ethnicity and geographic location of the individual [2, 10, 16, 18]. The size and shape of the nose can be determined by combined analysis of soft tissue and morphometric indices of the individual's piriform aperture and nasal bones [11]. However, this data must also be considered in accordance with the anthropological standard for the respective population. Research has shown that morphometric data of the piriform aperture and the nasal bones is a reliable source of information for determining the shape and dimensions of the nose in reconstructive and aesthetic surgical interventions in the facial area [12, 21].

Conclusion

The dimensions of the piriform aperture correlate significantly with key anthropometric parameters of the facial skeleton. These correlations should be considered in clinical practice, particularly in plastic and craniofacial surgery, where understanding individual anatomical variation is essential for optimal outcomes.

Acknowledgements: The current study is part of a research project "Doctoral and Postdoctoral Projects" at the Medical University – Plovdiv, DPDP-09/2025 "Anthropological characteristics of the facial skull and piriform aperture in the Bulgarian population – measurement on 3D reconstructions of computed tomography scans".

References

1 . Adams, D. C., F. J. Rohlf, D. E. Slice. Geometric morphometrics: ten years of progress following the 'revolution'. – *Ital. J. Zool.*, **71**(1), 2004, 5–16.

2. Alcalde, R. E., T. Jinno, M. G. Orsini, A. Sasaki, R. M. Sugiyama, T. Matsumura. Soft tissue cephalometric norms in Japanese adults. – *Am. J. Orthod. Dentofacial Orthop.*, **118**(1), 2000, 84-89.

3. Alekseev V. P., G. F. Debets. Craniometry. Methods of anthropological research. Moscow, Nauka, 1964. [in Russian]

4. Bookstein, F. L. Morphometric Tools for Landmark Data. Cambridge, UK: Cambridge University Press, June 1997, 455pp.

5. Dixon, A. D. Prenatal development of the facial skeleton. In: *Fundamentals of craniofacial growth*. CRC Press, 2017, 59-98.

6. Dryden, I. L., K. V. Mardia. Statistical Shape Analysis. J. W. Wiley: New York, 1998, 376 pp.

7. Gupta, P., T. Tripathi, N. Singh, N. Bhutiani, P. Rai, R. Gopal. A review of genetics of nasal development and morphological variation. – *J. Family Med. Prim, Care*, **9**, 2020, 1825-1833.

8. Harizanova, Z., A. Baltadjiev, F. Popova, M. Peycheva. Few dental indices in modern Bulgarian population from southern Bulgaria. – *J. Physiol. Anthropol.,* **42**(15), 2023, https://doi.org/10.1186/s40101-023-00332-5.

9. Howells, W. W. Cranial Variation in Man. A Study by Multivariate Analysis of Patterns of Difference Among Recent Populations. Peabody Museum of Archaeology and Ethnology, Cambridge, MA: Harvard University Press, 1973.

10. Hwang, H. S., W. S. Kim, J. A. McNamara Jr. Ethnic differences in the soft tissue profile of Korean and European-American adults with normal occlusions and well-balanced faces. – *Angle Orthod.*, **72**(1), 2002, 72-80.

11. Inada, E., I. Saitoh, H. Hayasaki, C. Yamada, Y. Iwase, Y. Takemoto, Y. Matsumoto, Y. Yamasaki. Cross-sectional growth changes in skeletal and soft tissue cephalometric landmarks of children. – *CRANIO*®, **26**(3), 2008, 170-181.

12. Inada, E., I. Saitoh, H. Hayasaki, Y. Iwase, N. Kubota, Y. Tokemoto, C. Yamada, Y. Yamasaki. Relationship of nasal and skeletal landmarks in lateral cephalograms of preschool children. – *Forensic Sci. Int.*, **191**(1-3), 2009, 111-e1.

13. Liang, Ce. *Characterising and predicting normal postnatal craniofacial growth and development in human*. Diss. UCL (University College London), 2024, p.56.

14. Martin, R. Textbook of Anthropology. (Ed. K. Saller), Revised third edition, *Gustav Fischer Verlag, Stuttgart,* 1957, **1**, 311-321. [in German]

15. Moreddu, E., L. Puymerail, J. Michel, M. Achache, P. Dessi, P. Adalian. Morphometric measurements and sexual dimorphism of the piriform aperture in adults. – *Surgical and Radiologic Anatomy*, **35**(10), 2013, 917-924.
16. Ominde B. S., J. E. Ikubor, J. E. Jaiyeoba-Ojigho, O. F. Omoro, P. S. Igbigbi. Morphometric assessment of the piriform aperture and its clinical and forensic applications. – *Mustansiriya Med. J.*, **23**(2), 2024, 78-83.
17. Papesch, E., M. Papesch. The nasal pyriform aperture and its importance. – *Otorhinolaryngol. Head Neck Surg*, **1**(4), 2016, 89-91.
18. Sarač-Hadžihalilović, A., Z. Ajanović, I. Hasanbegović, S. Šljuka, M. Rakanović-Todić, I. Aganović, I. Prazina, S. Maleškić Kapo, R. Hadžiselimović. Analysis of gender differences on pyriform aperture of human skulls using geometric morphometric method. – *Folia Morphologica*, **81**(3), 2022, 707-714.
19. Slice, D. E. Modern morphometrics. In: *Modern morphometrics in physical anthropology*. Boston, MA: Springer US, 2005. p.1-45.
20. Sperber, G. H. *Craniofacial Development*. B.C. Decker, 2001.
21. Stephan, C. N., M. Henneberg, W. Sampson. Predicting nose projection and pronasale position in facial approximation: a test of published methods and proposal of new guidelines. – *Am. J. Phys. Anthropol.*, **122**(3), 2003, 240-250.
22. Topal, E., T. Ormeci, A. Atasever. The Comparison of Piriform Aperture, Paranasal Sinuses, and Cranial Dimensions. – *J. Craniofac. Surg.,* **33**(1), 2022, e56-e59.
23. Yordanov, Y. Anthropology. A handbook for physicians, dentists, and biologists. Klasika i stil publishing, 2017. [in Bulgarian]
24. Zelditch, M. L., D. L. Swiderski, H. D. Sheets. *Geometric Morphometrics for Biologists: A Primer*. Elsevier, 2012.

Institute of Experimental Morphology, Pathology and Anthropology with Museum
Bulgarian Anatomical Society

Acta Morphologica et Anthropologica, 32 (3-4)
Sofia ● 2025

Comparative study of segmental and whole-body composition in male tennis players and CrossFit athletes

Albena Dimitrova[1,2], Dilyana Zaykova[1], Iveta Bonova[1], Lubomir Petrov[1]*

[1] National Sports Academy "Vassil Levski", Sofia, Bulgaria
[2] Institute of Experimental Morphology, Pathology and Anthropology with Museum, Bulgarian Academy of Sciences, Sofia, Bulgaria

*Corresponding author e-mail: albena_84@abv.bg

The present investigation includes 87 male middle-aged athletes (54 CrossFit and 33 tennis players). Body composition assessment was performed using bioelectrical impedance measurements (InBody 170 analyzer). The whole-body analysis includes body weight, body mass index, muscle mass, fat mass, fat-free mass, and total body water. The segmental distribution of muscle and fat mass (in kg and percentage) was also presented. Descriptive statistics were generated using SPSS 16 (IBM, USA), and the distribution of normality was assessed. The independent samples t-test was used to evaluate the differences in body composition. Significant differences in whole-body composition were observed for the relative values of muscle mass, with a particular emphasis on TP. A significant prevalence of fat mass values was observed among CF practitioners. Segmental analysis of body composition showed a significantly higher muscle mass of the lower limbs in the TP group and of the fat mass in all body segments of CF.

Key words: CrossFit, Tennis players, Body composition, Segmental analysis

Introduction

Body composition analysis (BC) is a method used for measurement of different components of human body, like fat mass, muscle mass, bone density, and water content. Its values are important determinants for health conditions and sports performance [3,11,20]. It is used to track changes in body composition components, and to create personalized fitness and nutrition plans. The constantly changing conditions of life (stress, sedentary lifestyle and insufficient physical activity, changes in eating habits, etc.) lead to changes in the components of body composition, with the most variability in the adipose tissue [7]. Segmental analysis of body composition provides additional information to the usual full- body analysis. Different studies have found a close association between body composition and cardio-respiratory function and strength

[6,9]. Body composition components differ among athletes participating in different sports, such as those in the same sport who occupy different playing positions [16].

In recent years, CrossFit training has been gaining increasing popularity worldwide. CrossFit (CF) is a high-intensity workout that combines both aerobic and anaerobic types of exercises, like gymnastics, jumping, running, and weightlifting. The CF athletes demonstrate a good anaerobic performance, expressed in maximum peak power that their body can generate for short-duration maximal effort. In sports BC components have a significant impact on the athlete`s performance. It is well known, that the first main component of BC – body fat, has a negative effect on sports success. Contrary to that the muscle mass and lean body mass, may positively affect the performance especially in sports with explosive power requirements [5,8,15,21,26].

Tennis is sport that requires a good explosive strength for optimal sports results. Like a CrossFit training tennis training also require aerobic and anaerobic endurance. Muscle and fat mass have a significant impact on the tennis athlete`s performance. In tennis, strength, speed and flexibility are crucial components for sports success, which correlate significantly with the muscle mass. Well-developed muscles mass particularly in the legs and upper body parts are essential for explosive movements, quick changes of direction, and overall tennis performance. On the other hand, a high percentage of body fat can negatively influence tennis players` agility and speed, and slow down overall mobility and reaction time on the court, and also can increase the risk of injuries [10,23].

The current study aimed to present a comparative analysis of segmental and whole-body composition between male tennis players and CrossFit athletes.

Materials and Methods

The present investigation includes 87 male athletes (54 CrossFit and 33 tennis players). The mean age of the tennis players (TP) and CrossFit athletes was 38.61±7.66 years and 39.56±6.39 years, respectively. All of the athletes are amateurs at the sport they practice, with a mean training experience of CF athletes 3.77±2.43 years and 5.68±3.62 years in TP. All of the participants are informed of the objective of the current study and voluntarily participate in it. The study protocol was reviewed and approved by the Ethical Committee of the National Sports Academy (Protocol №: EC-NSA-2025-001/08.04.2025) and was conducted in agreement with the principles stated in the Declaration of Helsinki for human studies and researches [24]. Body composition assessment was performed using bioelectrical impedance measurements (InBody 170 analyzer). The whole-body analysis includes body weight (BW), body mass index (BMI), muscle mass (MM), fat mass (FM), fat-free mass (FFM), and total body water (TBW). The segmental distribution of muscle and fat mass (in kg and percentage) was also presented. Descriptive statistics were generated using SPSS 16 (IBM, USA), and the distribution of normality was assessed (Shapiro-Wilk). The independent samples t-test was used to evaluate the differences in body composition.

Results

Descriptive statistics for whole-body composition in CF athletes and TP were presented in **Table 1**. Comparative analysis of the basic morphological characteristics showed that TP are taller than CF athletes, who are heavier and have higher body mass index (BMI) values. The mean values of body height are 183.62±5.35 cm in TP and 177.66±6.86 cm in CF athletes. The mean body weight is insignificantly higher in CF practitioners (83.56±10.02 kg) compared with TP (80.15±10.34 kg). The average values of BMI in CrossFit athletes were 26.47 ±2.80 kg/m^2, which were significantly higher than those of tennis players' 23.73±2.46 kg/m^2. According to the mean BMI values, we categorized TP as having a normal weight and CF athletes as having an overweight status. The higher BMI in CF practitioners is due to the higher values of muscle mass, and it would be wrong to associate them with overweight and obesity.

Significant differences in whole-body composition also were observed for the relative values of muscle mass, with a particular emphasis on tennis players ($p \leq 0.001$). The percent of muscle mass was 46.63±3.30% in CF athletes and 49.09±3.21% in TP. The average absolute values (in kilograms) of muscle mass (MM), fat-free mass (FFM) and total body water (TBW) in the two investigated groups were equal ($p \geq 0.05$). A significant prevalence of both absolute and relative fat mass values was observed among CrossFit practitioners ($p \leq 0.001$). The mean relative body fat values of TP were 13.97±5.43%, while these values for CF athletes were significantly higher by 4.21% ($p \leq 0.001$) and they were 18.17±5.43%. According to the absolute fat mass values, CF has 4.75 kg morefat mass than TP.

Table 1. Whole-body composition analysis in male CrossFit athletes and tennis players

Traits	CrossFit athletes (n=54)	Tennis players (n=33)	P-value
Age (y)	39.56±6.39	38.61±7.66	0.732
Body height (cm)	177.66±6.79	183.62±5.35	0.001
Body weight (kg)	83.56±10.02	80.15±10.34	0.132
BMI (kg/m^2)	26.47±2.80	23.73±2.46	0.001
Muscle mass (%)	46.63±3.30	49.09±3.22	0.001
Muscle mass (kg)	38.89±4.79	39.28±5.22	0.722
Fat mass (%)	18.18±5.66	13.97±5.43	0.001
Fat mass (kg)	16.10±6.89	11.35±5.22	0.001
Total body water (L)	50.28±6.19	50.41±6.45	0.930
Fat free mass (kg)	68.21±8.12	68.82±8.80	0.744

Segmental analysis of muscle mass (%, kg) and fat mass (%, kg) was presented in **Fig. 1** to **Fig. 4**. A significantly higher percentage of muscle mass of the lower limbs ($p \leq 0.004$; $p \leq 0.001$) in the TP group was obtained. Opposite to these results the absolute and relative values of fat mass have a great prevalence for all body segments in CF athletes ($p \leq 0.005$; $p \leq 0.001$).

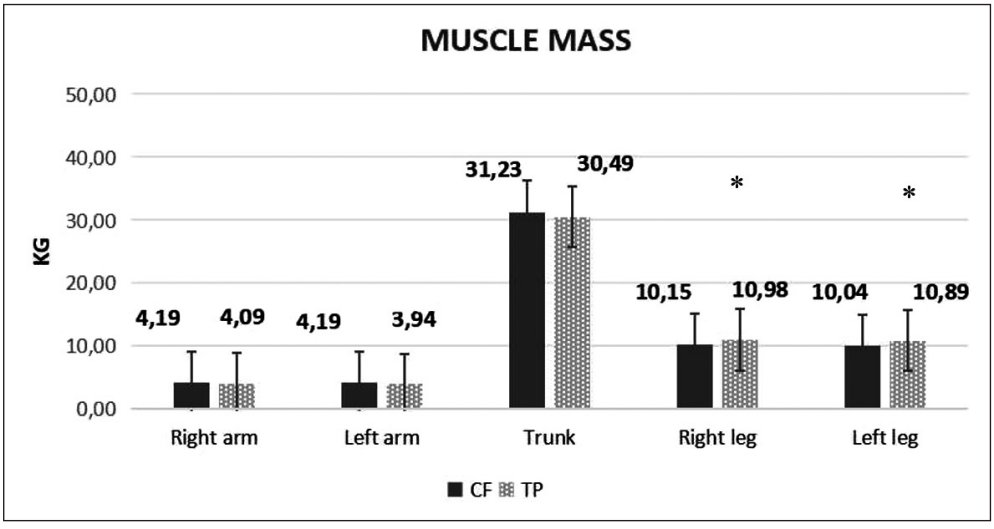

Fig. 1. Segmental distribution of absolute values of muscle mass in tennis players and Cross-Fit athletes.

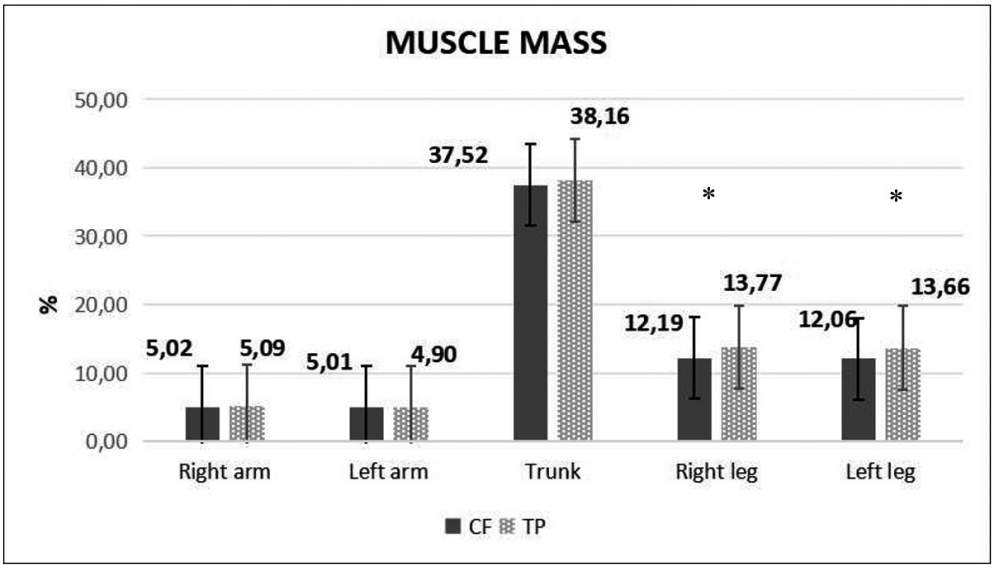

Fig. 2. Segmental distribution of relative values of muscle mass in tennis players and Cross-Fit athletes.

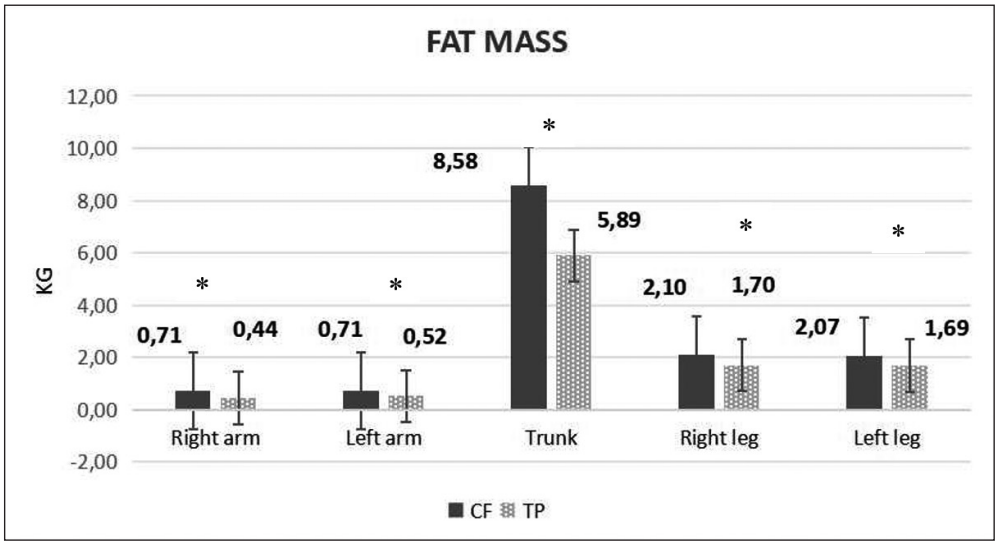

Fig. 3. Segmental distribution of absolute values of fat mass in tennis players and CrossFit athletes.

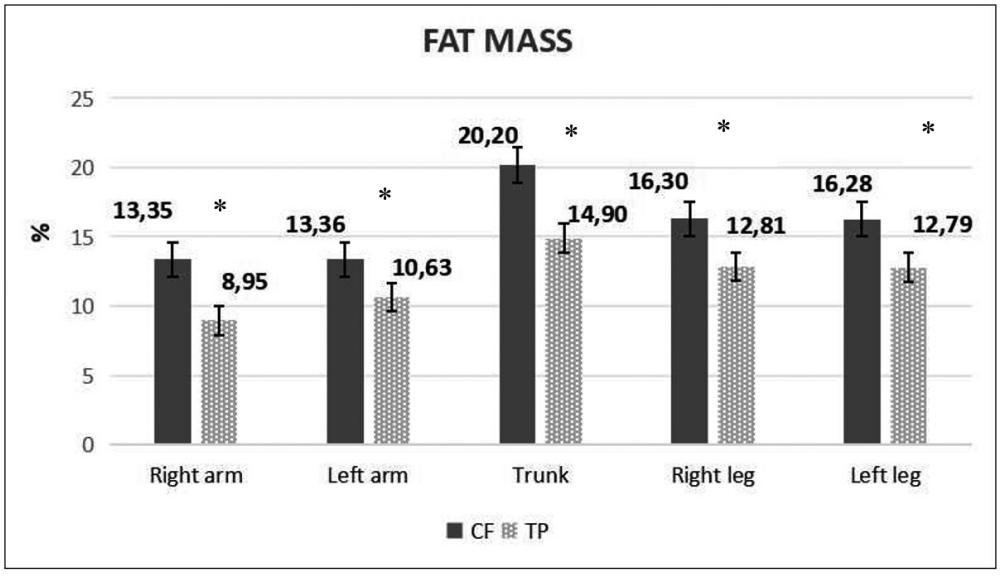

Fig. 4. Segmental distribution of relative values of fat mass in tennis players and CrossFit athletes.

Discussion

The current study presents comparative results for segmental and whole-body analysis in athletes who practice two different sports, with both aerobic and anaerobic performance.

Tennis players and CrossFit athletes exhibit distinct body composition characteristics due to the differing demands of their respective sports. The results from the current study indicate that TP have a higher percentage of muscle mass and lower body fat, while CrossFit athletes have a higher body fat percentage but potentially lower muscle mass in comparison to tennis players. Assessing the relation between whole-body and segmental body composition and anaerobic performance Ponce-Garcia et al. (2024) create a prediction model for optimal performance in CrossFit athletes. The authors found a moderate relationship between muscle and fat mass development in all body parts and anaerobic performance. Segmental and total lean mass distribution may be considered as good predictors of peak and mean power [15]. Tennis is an explosive sport training that has a very high requirement for the endurance of athletes. The fitness level and the muscle mass of the upper and lower limbs have a great impact on the TP performance on the court [10,23]. The morphological profile of tennis players is formed during adolescence, as shown by the study of Rica et al. (2019), which declared similar to our results for BC in TP athletes. The study distinguished typical morphological traits in adolescent TP as follow: normal BMI, low PBF and higher values of muscle mass, especially in the upper arms [17].

Segmental body composition analysis evaluates the distribution of muscle mass, fat mass, and other body tissues across different body segments (e.g., arms, legs, trunk). This analysis can help to optimize sports training, identify potential injury risks, improve performance and maintain overall athletic health [2,18]. Segmental analysis reveals that CF athletes and TP tend to have a greater proportion of muscle mass in their limbs and trunk compared to the general population, which can be advantageous for the diverse movements and demands of sports modality [4]. The distribution of muscle mass is not uniform. The legs, particularly the thighs, are crucial for power and agility in tennis. Analysis can reveal differences in muscle mass and fat distribution that may affect performance [17,19]. The trunk muscles are vital for generating power and stability. Analysis can help identify imbalances that could affect serve speed or overall core strength [2,22]. The diverse nature of CrossFit workouts often leads to increased muscle mass across different body segments. CrossFit athletes, especially those with higher performance levels, tend to have significantly higher muscle mass in their arms and legs and trunk compared to less active individuals [13]. Considering that CF workout significantly improves aerobic endurance, anaerobic endurance and explosive power, Wang and Yao (2023) assessed the effect of CF training on tennis players' performance. They declared significant improvement on backhand and forehand strokes and increasing of the overall performance level of tennis [25].

Conversely, higher fat mass in the same segments is negatively associated with performance, highlighting the importance of optimizing fat distribution [14]. CrossFit athletes generally maintain a low body fat percentage, which is beneficial for exercises and overall performance [4,13]. An investigation of BC in CF athletes showed an average PBF for men and women 11.60 % and 15.23 %, respectively [4]. The results we get for male CF athletes are significantly higher (18.18 %). Competitive male tennis players typically maintain a low body fat percentage, generally fewer than 12%. While the ideal body fat percentage can vary slightly, a range of 6-12% is generally considered optimal for male tennis players. According to the results of Martinez-Rodriguez et al. (2015) the mean PBF in adult male TP is 16.2 %, which is significantly different from our results (13.97 %) [12].

The body composition of tennis players and CrossFit athletes reflects the unique demands of their respective sports. While both groups prioritize high muscle mass, tennis players may place a greater emphasis on lean muscle for agility and speed, while CrossFit athletes focus on overall muscle development for strength and power.

Conclusion

The current study confirms the great prevalence of muscle mass accumulation in the lower limbs in TP group in comparison with CF athletes and equal values in the upper body parts between groups. The comparative analysis of body composition in the TP and the CF provides new insights into both assessed sports populations and could serve as a basis for the development of specific reference values in future investigations.

References

1. **Bertuccioli, A., M. Cardinali, P. Benelli.** Segmental Bioimpedance Analysis as a Predictor of Injury and Performance Status in Professional Basketball Players: A New Application Potential? – *Life (Basel)*, **12**(7), 2022, 1062.
2. **Bilić, Z., P. Martić, P. Barbaros, F. Sinković, D. Novak.** Neuromuscular Fitness Is Associated with Serve Speed in Young Female Tennis Players. – *Sports (Basel)*, **12**(4), 2024, 97.
3. **Campa, F., S. Toselli, M. Mazzilli, L. A. Gobbo, G. Coratella.** Assessment of Body Composition in Athletes : A Narrative Review of Available Methods with Special Reference to Quantitative and Qualitative Bioimpedance Analysis. – *Nutrients*, **13**, 2021, 1620.
4. **Cebrian-Ponce, A., S. Serafini, C. Petric, M. Carrasco-Margineta, P. Izzicupo, G. Mascherini.** Somatotype and bioelectrical impedance vector analysis of Italian CrossFit® practitioners. – *Heliyon*, **10**, 2024, e29139.
5. **Chiarlitti, N. A., P. Delisle-Houde, R. E. R. Reid, C. Kennedy, R. E. Andersen.** Importance of Body Composition in the National Hockey League Combine Physiological Assessments. – *J. Strength Cond Res.*, **32**, 2018, 3135-3142.
6. **Chathuranga, W., D. S. L. Perera.** Relationship Between Body Composition and Sports Performances of Wushu Sanda Players Abstract. – *Journal of Sports and Physical Education*, **9**(4), 2022, 36-43.
7. **Esco, M. R., M. V. Fedewa, Z. S. Cicone, O. A. Sinelnikov, D. Sekulic, C. J. Holmes.** Field-Based Performance Test are Related to Body Fat Percentage and Fat-Free Mass, But Not Body Mass Index, in Youth Soccer Player. – *Sport*s, 2018, *6*. https://doi.org/10.3390/sports6040105.
8. **Ishida, A., S. K.Travis, M. H. Stone.** Associations of Body Composition, Maximum Strength, Power Characteristics with Sprinting, Jumping, and Intermittent Endurance Performance in Male Intercollegiate Soccer Players. – *J. Funct. Morphol. Kinesiol*., **6**, 2021, 0–7. https://doi.org/10.3390/jfmk6010007.
9. **Komici, K., S. Verderosa, F. D'Amico, A. Parente, L. Persichini, G. Guerra.** The role of body composition on cardio-respiratory fitness in futsal competitive athletes. – *Eur. J. Transl. Myol*., **33**(3), 2023, 11479.
10. **Kovacs, M**. Applied physiology of tennis performance. – *Br. J. Sports Med*., **40**, 2006, 381-386.
11. **Lukaski, H., C. J. Raymond-Pope**. New Frontiers of Body Composition in Sport. – *International Journal of Sports Medicine*, **42**(7), 2021, 588-601.

12. Martinez-Rodriguez, A., E. R. Collado, N. Vicente-Salar. Body composition assessment of paddle and tennis adult male players. – *Nutr. Hosp*., **31**(3), 2015, 1294-1301.
13. Menargues-Ramírez, R., I. Sospedra, F. Holway, J. A. Hurtado-Sánchez, J. M. Martínez-Sanz. Evaluation of Body Composition in CrossFit® Athletes and the Relation with Their Results in Official Training. – *Int. J. Environ. Res. Public Health,* **19**, 2022, 11003.
14. Marinho Ferreira, B., L. Vidal Andreato, B. Follmer, E. Franchini. Comparison of body composition and physical fitness in elite and non-elite Brazilian jiu-jitsu athletes. – *Science & Sports*, **31**, 2016, 129-134.
15. Ponce-García, T., J. Carmelo García-Romero, L. Carrasco-Fernández, A. Castillo-Domínguez, J. Benítez-Porres. The Association of Whole and Segmental Body Composition and Anaerobic Performance in CrossFit® Athletes: Sex Differences. – *PeerJ*, 2025, doi: 10.7717/peerj.18930. eCollection 2025.
16. Raković, A., V. Savanovic, D. Stanković, R. Pavlović, A. Simeonov, E. Petković. Analysis of the elite athletes' somatotypes. – *Acta Kinesiologica*, **9**(1), 2015, 47-53.
17. Rica, R. L., J. M. de Q, Miranda, J. H. Gomes, W. A. Barbosa, C. M. Santana, M. V. Viana, F. L. Pontes Junior, G. A. João, A. F. Maia, D. S. Bocalini. Morphological characterization of adolescents tennis players. – *Manual Therapy, Posturology & Rehabilitation Journal*, 1–3. https://doi.org/10.17784/mtprehabjournal.2018.16.629.
18. Rynkiewicz, M., T. Rynkiewicz, P. Żurek, E. Ziemann, R. Szymanik. Asymmetry of muscle mass distribution in tennis players. – *TRENDS in Sport Sciences*, **1**(20), 2013, 47-53.
19. Staśkiewicz-Bartecka, W., E. Grochowska-Niedworok, G. Zydek, M. Grajek, A. Kiciak, A. Białek-Dratwa, E. Niewiadomska, O. Kowalski, M. Kardas. Anthropometric Profiling and Changes in Segmental Body Composition of Professional Football Players in Relation to Age over the Training Macrocycle. – *Sports*, **11**, 2023, 172.
20. Toselli, S. Body Composition and Physical Health in Sports Practice : An Editorial. – International Journal of Environmental Research and Public Health, **18**, 2021, 4534.
21. Triki, M., H. Rebai, T. Abroug, K. Masmoudi, N. Fellmann, N. Zouari, Z. Tabka. Comparative Study of Body Composition and Anaerobic Performance between Football and Judo Groups. – *Sci. Sports*, **27**, 2012, 293-299.
22. Vacek, J., M. Vagner, J. Malecek, P. Stastny. Tennis Serve Speed in Relation to Isokinetic Shoulder Strength, Height, and Segmental Body Mass in Junior Players. – *J. Funct. Morphol. Kinesiol*., **10**(1), 2025, 57. doi: 10.3390/jfmk10010057. PMID: 39982297; PMCID: PMC11843948.
23. Vergauwen, L., A. J. Spaepen, J. Lefevre, P. Hespel. Evaluation of stroke performance in tennis. – *Med. Sci. Sports Exerc*., **30**(8), 1998, 1281-1288.
24. World Medical Association, Declaration of Helsinki - Ethical Principles for Medical Research Involving Human Subjects. – *WMJ*, **54**(4), 2008, 122-125.
25. Wang, Q., N. Yao. Impacts of Crossfit Training on the Tennis Athlete`s Performance. – *Rev. Bras. Med. Esporte*, **29**, 2023, e2023_0012.
26. Zaras, N., A. N. Stasinaki, P. Spiliopoulou, M. Hadjicharalambous, G. Terzis. Lean Body Mass, Muscle Architecture, and Performance in Well-Trained Female Weightlifters. – *Sports*, **8** (5), 2020, 67.

Institute of Experimental Morphology, Pathology and Anthropology with Museum
Bulgarian Anatomical Society

Acta Morphologica et Anthropologica, 32 (3-4)
Sofia ● 2025

A rare case of extensor medii proprius: anatomical and clinical considerations

Stancho Stanchev, Alexandar Iliev, Lyubomir Gaydarski, Nikola Stamenov, Boycho Landzhov*

Department of Anatomy, Histology, and Embryology, Medical University of Sofia, Bulgaria.

*Corresponding author e-mail: stanchev_1989@abv.bg

Anatomical variations of the extensor indicis muscle (EIM) are of particular clinical relevance due to their potential to mimic pathological conditions and their use in tendon grafting. Among these, the extensor medii proprius muscle (EMP) represents a rare accessory muscle in the posterior compartment of the forearm.

Herein, we report a case of an aberrant EMP identified during routine anatomical dissection with origin from the distal portion of the EIM. The variant muscle was supplied by the posterior interosseous artery and nerve, with no additional anomalies detected.

The described EMP demonstrates an atypical origin from the EIM, differing from the commonly reported origin from the distal ulna. This variation highlights the morphological diversity of forearm extensors and supports theories regarding evolutionary and embryological influences on muscle development. Clinically, such variants are important for differential diagnosis of soft-tissue masses, sources of dorsal wrist pain, and surgical planning.

Key words: Variation, Extensor indicis muscle, Extensor medii proprius muscle

Introduction

The classic anatomical description of the forearm muscles suggests the presence of three well-defined compartments – anterior, lateral and posterior. The posterior forearm muscles are further divided into superficial and deep groups [4]. The extensor indicis muscle (EIM) belongs to the deep group. It has a synergic function with the extensor digitorum muscle (ED), providing independent extension of the second finger at the metacarpophalangeal and proximal interphalangial joints, thus contributing to the extension of the hand at the wrist as well [5]. It is innervated by the posterior interosseous nerve and blood supplied mainly by the branches of the posterior interosseous artery [4].

EIM has an important clinical significance as it is commonly used for tendon grafting and transplantations [14, 20]. Review of the literature indicates numerous variations of EIM, including unusual origin and insertion, absence of EIM, presence of additional tendons or supernumerary muscle slips [1, 7, 8, 9, 13, 18]. Moreover, these variations are of great interest to clinicians as they must be discussed in the context of the differential diagnosis of various pathological conditions. For instance, the abnormal anatomy of EIM may provoke dorsal wrist pain and may be incorrectly considered as soft tissue hand mass, synovial cyst, ganglion or tenosynovitis [6, 10, 16]. In addition, the presence of additional tendons passing through the fourth osseofibrous canal may be associated with clinical symptoms [12].

The present case report aimed to describe an aberrant extensor medii proprius muscle (EMP) with origin from EIM – a rare variation with focus on its possible origin.

Case report

During a routine anatomical dissection of the right upper limb of a 75-year-old Caucasian male cadaver, preserved with a 10% formalin-based solution, an abnormal, well-defined muscle bundle was identified in the posterior compartment of the forearm. The specimen originated from autopsy material provided to the Department of Anatomy, Histology and Embryology, Medical University of Sofia, Bulgaria. The dissection was conducted with the approval of the Medical Legal Office and the Local Ethics Committee.

Following the removal of superficial structures and the antebrachial fascia, an additional muscle belly was observed along the ulnar aspect of the tendon of the ED to the fourth finger. This accessory muscle originated from the distal portion of the EIM. It presented as a slightly flattened, fusiform bundle measuring 26 mm in length and 4 mm in width.

Its tendon arose lateral to the ED tendon of the fourth finger but quickly crossed beneath it. Distally, the accessory muscle continued as a thin, band-shaped tendon measuring 126 mm in length. This tendon coursed parallel to those of the EIM and ED, traversed the fourth extensor compartment, and ultimately inserted into the dorsal aspect of the third metacarpophalangeal joint (**Fig. 1**).

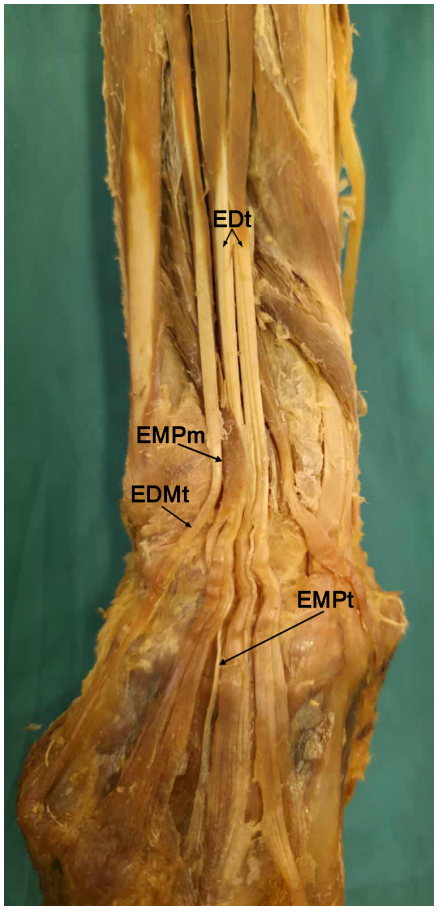

Fig. 1. Photograph of the right upper limb: EDt – extensor digitorum tendon; EDMt – extensor digiti minimi tendon; EMPm – extensor medii proprius muscle; EMPt – extensor medii proprius tendon.

The muscle bundle received vascular supply from branches of the posterior interosseous artery and innervation from the posterior interosseous nerve. No additional muscular variations, traumatic changes, or evidence of prior surgical interventions were noted in the posterior forearm region.

Discussion

The additional muscle belly described in the present case shows morphological similarity to the EMP, a rare variant muscle in the posterior forearm compartment. Indeed, our report suggests an unusual origin of EMP as well-defined muscle bundle from the distal portion of EIM, opposing the described origin of EMP from the distal third of the ulna in the literature. The scientific data indicate its incidence ranges between 0.8% and 10.4% in anatomical examinations [3, 17]. The presence of EMP differs among the population in the continents, but it is relatively low in the European population, thus suggesting a potential role of various factors, including race [18]. Komiyama et al. [11] have classified the variations of the EIM found in Japanese cadavers based on the presence of additional tendon slips and supernumerary muscles. The authors described and extensor indicis radialis as the most frequently observed variant without sex differences or prevalence between right and left upper limbs. According to our data, this is the second time we report the presence of EMP with such an atypical origin from EIP [14]. Yurasakpong et al. [19] have described a unique case of unilateral presence of extensor indicis radialis and EMP. EMP was associated with an unusual fibromuscular slip innervated by the posterior interosseous nerve. Further, the histological examination of the slip revealed it was composed of dense connective tissue and skeletal muscle fibres. The authors claimed this was the first time to describe the presence of a fibromuscular slip associated with the extensor tendon on the dorsal hand region.

The presence of EMP may be under the influence of phylogenetic and evolutionary mechanisms. EMP is described as part of the extensor compartment in primates belonging to the family Cercopithecidae. In contrast, its incidence in species from the family Hominidae is variable, as in the human population [2]. The embryonic development of the forearm muscles is associated with the migration of dorsolateral somite cells to the upper limb around the fourth week. Further, the extensor forearm muscles differentiate into three portions – the radial portion gives rise to the muscle of the mobile wad. Furthermore, the radial portion differentiates into a superficial portion, which forms the extensor digitorum communis, the extensor carpi ulnaris, and the extensor digiti minimi and a deep portion representing abductor pollicis longus and extensor pollicis brevis as well as extensor pollicis longus and EIM [15]. It seems the muscles originating from the superficial portion are dominant and show prominent stability in comparative anatomy studies, while those from the deep group are significantly variable [15].

The existence of variant muscles may not result in symptoms, but they have important clinical significance as they can be used as a donor for tendon grafting and transplantation. Moreover, the presence of accessory muscles may be associated with surgical complications or misdiagnoses of soft-tissue tumours [16, 20].

Conclusion

The present case report suggests an atypical origin of the EMP from the distal portion of the EIM. EMP is a relatively rarely observed muscle in the European population, and we discuss a possible link between its incidence and the potential role of phylogenetic, evolutionary and embryonic factors. Moreover, the described atypical EMP may be an interest to clinicians to avoid misdiagnoses and complications during surgical interventions in the posterior forearm region. Alternatively, the additional muscle can be used for tendon grafting and transplantation.

R e f e r e n c e

1 . Arathala, R., P. K. Sankaran, G. Ragunath, S. S. Harsha, T. S. Sugumar. The extensor indicis brevis – a rare variation and its significance. – J. *Clin. Diagn. Res*., **10**, 2016, AD03-AD04.

2. Ayer, A. A. The anatomy of semnopithecus entellus. – *Indian Publishing House*, 1948, 60-72.

3. Cauldwell, E. W., B. J. Anson, R. R. Wright. The extensor indicis proprius muscle: a study of 263 consequetive specimens. – *Q. Bull. Northwest. Univ. Med. School*, **17**, 1943, 267-279.

4. Chaudhry, M. A., A. M. Hafeez, M. A. Sinkler, A. Arian. Anatomy, shoulder and upper limb, forearm compartments. – In: *StatPearls*, Treasure Island (FL), StatPearls Publishing, 2025.

5. Doyle, J., M. J. Botte. Surgical anatomy of the hand and upper extremity. – Philadelphia, Lippincott Williams & Wilkins, 2003, 134-135, 141-142, 221.

6. Fernandez Vazquez, J. M., R. L. Linscheid. Anomalous extensor muscles simulating dorsal wrist ganglion. – *Clin. Orthop. Relat. Res*., **83**, 1972, 84-86.

7. Georgiev, G. P. Anatomical variations of muscles in the human body and their relevance for clinical practice. – *Int. J. Anat. Var.,* **11**, 2018, 48-49.

8. Georgiev, G. P. Significance of anatomical variations for clinical practice. – *Int. J. Anat. Var.*, **10**, 2017, 43-44.

9. Georgiev, G. P., R. S. Tubbs, A. Iliev, G. Kotov, B. Landzhov. Extensor indicis proprius muscle and its variants together with the extensor digitorum brevis manus muscle: a common classification. Clinical significance in hand and reconstructive surgery. – Surg. Radiol. Anat., **40**, 2018, 271-280.

10. Iliev, A., G. P. Georgiev, I. N. Dimitrova, B. Landzhov. Extensor indicis brevis muscle: anatomical and clinical considerations. – Acta Morphol. Anthropol., **22**, 2015, 75-78.

11. Komiyama, M., T. M. Nwe, N. Toyota, Y. Shimada. Variations of the extensor indicis muscle and tendon. – *J. Hand Surg. Br.*, **24**, 1999, 575-578.

12. Kumka, M. A variant extensor indicis muscle and the branching pattern of the deep radial nerve could explain hand functionality and clinical symptoms in the living patient. – *J. Can. Chiropr. Assoc.*, **59**, 2015, 64-71.

13. Ma, A., J. Kim, C. E. Miller, T. L. Mustapich, J. P. Abraham, S. A. Downie, P. L. Mishall. Pointing in a different direction: a case of bilateral absence of extensor indicis. – *Folia Morphol*. (Warsz)., **81**, 2022, 520-525.

14. Slavchev, S. A., G. P. Georgiev. Ultrasound diagnosis of a ganglionic cyst within an extensor digitorum brevis manus muscle. – *Chir. Main*, **34**, 2015, 269-271

15. Tan, S. T., P. J. Smith. Anomalous extensor muscles of the hand: a review. – *J. Hand Surg.*, **24**, 1999, 449-455.

16. **Vanhoenacker, F. M., M. Eyselbergs, E. Van Hul, P. Van Dyck, A. M. De Schepper.** Pseudotumoural soft tissue lesions of the hand and wrist: a pictorial review. – *Insights Imaging*, **2**, 2011, 319-333.
17. **Von Schroeder, H. P., M. J. Botte.** The extensor medii proprius and anomalous extensor tendons to the long finger. – *J. Hand Surg. Am*., **16**, 1991, 1141-1145.
18. **Yammine, K.** The prevalence of the extensor indicis tendon and its variants: a systematic review and meta-analysis. – *Surg. Radiol. Anat*., **37**, 2015, 247-254
19. **Yurasakpong, L., R. Diogo, A. Chaiyamoon, A. Suwannakhan.** Extensor indicis radialis and extensor medii proprius associated with an unknown fibromuscular slip: a case report. – *SN Compr. Clin. Med*., **2**, 2020, 2456-2459
20. **Zhou, J., C. Frey, N. Segovia, J. Yao.** Anatomic relationship of extensor indicis propius and extensor digitorum communis: implications for tendon transfer. – *World J. Orthop*., **13**, 2022, 978-985.

Institute of Experimental Morphology, Pathology and Anthropology with Museum
Bulgarian Anatomical Society

Acta Morphologica et Anthropologica, 32 (3-4)
Sofia ● 2025

Fatal gunshot trauma from a homemade weapon: case report

Deyana Velkova

Department of General and Clinic Pathology, Forensic Medicine and Deontology Medical University – Varna

* Corresponding author e-mail: deyana.velkova@mu-varna.bg

Injuries from homemade firearms are extremely rare in forensic practice and they present some difficulties due to the variety of injuries that can be observed on the victim's body. This paper presents a forensic case of suicide involving a 46-year-old male. Adjacent to the body was found an object resembling a firearm. During the external examination of the corpse, two deep slit-like wounds were observed at the corners of the mouth and communicated with the oral cavity. In the area of the soft palate, an irregularly shaped defect was noted. Tracing the defect revealed a wound tract extending into the cranial cavity with several damaged structures. The wound tract terminated within the occipital bone, where a metallic projectile was discovered. This forensic case underscores that homemade firearms can be as dangerous as factory-manufactured ones and the characteristics of the injuries they cause are of significant importance to all forensic practitioners.

Key words: homemade firearm, gunshot, suicide

Introduction

Injuries from homemade firearms are extremely rare in forensic practice. These cases present some difficulties for both ballistics specialists and forensic pathologists, due to the variety of injuries that can be observed on the victim's body. In most cases, injuries from homemade weapons significantly differ from those of typical, factory-made firearms [11, 12].

Injuries caused by firearms depend on a number of factors – the type of weapon (including factory-made, modified, homemade, etc.), the ammunition used and its characteristics, the distance of the shot, the materials through which the bullet passes and the location of the gunshot wound on the body itself, etc. In general, firearm injuries can be divided into three groups: blind injury, in which there is an entrance wound

and a wound tract, at the bottom of which the projectile settles; penetrating injury, in which there is an entrance wound, a wound tract and an exit wound; tangential injury, in which the projectile passes along the surface of the body without penetrating deep [1, 2, 9, 11, 12, 20].

Usually, the characteristics of the entrance wound, as well as the presence/absence of the associated products of the firearm discharge (and their effect on the tissues), are of essential importance for an approximate determination of the distance of the shot. In most cases of firearm injury caused by a manufactured weapon, the entrance gunshot wound is round or oval in shape, with a lack of tissue in the center, and often has an abrasion ring on the edges, which is the result of the skin being stretched by the projectile while simultaneously rubbing the edges of the wound. At close-range and contact shots, components such as soot, unburned gunpowder and metal particles, as well as other accompanying products, are usually found around or in the entrance wound. In contrast, at long-range shots, there is no deposition or effect of the associated products, and only the projectile damages the tissues [1, 2, 9].

The associated products of the shot (flame, explosive gases, soot, unburned gunpowder, metal particles and other residues) have an additional mechanical, thermal, and chemical effect on the tissues. For example, the gases released during the shot (for contact or close-range distance) can have a mechanical effect on the entry wound, leading to lacerations at its edges, especially when there is bone under the skin. In the case of a gunshot wound with a muzzle placed in the mouth, similar lacerations of the soft tissues of the oral cavity are commonly observed [11,12].

Another factor that plays a significant role in tissue damage is the phenomenon of the temporary (pulsative) cavity. When the projectile reaches the contact surface (skin) and penetrates into the depth, part of its kinetic energy is transferred to the surrounding tissues in the vicinity of the permanent cavity, thus obtaining a temporary cavity, characterized by a rapid change from positive to negative pressure. This, in turn, also leads to additional damage (destruction) to the tissues surrounding the projectile tract [1, 2, 20].

Homemade firearms can also cause injuries that have the elements of a firearm (an entrance wound with a defect with a lack of tissue and an abrasion ring, a permanent cavity (wound channel) and destructive changes from the temporary cavity, etc.), but they can often cause changes that resemble other types of trauma, such as injuries from hard, blunt objects. In this sense, a thorough forensic examination plays a leading role in the investigation of the incident [11, 12].

Case Description: This paper presents a forensic case of suicide involving a 46-year-old male discovered deceased in his residence. Adjacent to the body was found an object resembling a firearm. Closer examination revealed that the object consisted of a wooden board with an attached metal tube. The tube exhibited a wide opening with a diameter of approximately 1.5 cm at one end and a narrower opening measuring 2–3 mm in diameter at the opposite end. Additionally, empty matchboxes were located in the immediate vicinity of the corpse.

The body was found seated on a bed with the back resting against the wall, the head bent forward, and the lower limbs flexed at the hip and knee joints with the feet in contact with the floor. The upper limbs were positioned in a relaxed state alongside the torso, with a lighter observed in the right hand. The skin on the left hand exhibited extensive staining with soot. Blood staining was prominently noted on the anterior surface of the

clothing, originating from the facial region. Examination of the mouth and nose revealed significant deformation of the soft tissues and substantial blood staining**.**

The body of the deceased was transported to the Clinic of Forensic Medicine at the Saint Marina University Hospital – Varna for a forensic autopsy. Before the examination of the corpse was initiated, forensic specialists from the police department collected and documented all trace evidence from the clothing and body for ballistic testing and took standard photographs of all evidence. Autopsies at the Saint Marina University Hospital – Varna, including the present forensic case, are performed in accordance with the guidelines outlined in Recommendation No R(99)3 of the Council of Europe Committee of Ministers [13]. In cases of gunshot injuries, special attention is given to the following aspects: detailed description and localization of each wound according to the main anatomical points and their location in relation to the lowest point of the legs; morphological description of the injuries, noting the presence/absence of the characteristic elements of the gunshot wound (shape, presence of a defect with lack of tissue, abrasion ring, bullet wipe, muzzle mark, etc.); description of the presence/absence of associated products of the firearm discharge and assistance to the forensic experts in taking the relevant samples; layer-by-layer dissection of the tissues underlying the gunshot wounds along the wound tract to determine its direction and identification of traumatic changes in the affected tissues.

In the present case, during the external examination of the corpse, two deep slit-like wounds with irregular edges were observed at the corners of the mouth. These wounds extended to and communicated with the oral cavity. Additional, smaller wounds of similar appearance were identified on both the skin and mucosal surfaces of the lips. The oral cavity was filled with blood, and the mucous membranes exhibited extensive staining with soot. The tongue also displayed soot and exhibited multiple slit-like lacerations on its anterior portion, some of which penetrated its entire thickness. The edges of these lacerations were uneven, bruised and covered with soot. In the area of the soft palate, an irregularly shaped defect was noted, characterized by tissue loss with dimensions around 1.1×1.5 cm (after slight stretching of the tissue) and extensive hemorrhagic bruising in the surrounding tissue with a diameter around 3.5 cm. Some parts of the edges of the defect were irregularly abraded and markedly bruised, and were covered with soot.

During the internal examination of the corpse, multiple traumatic injuries were identified in the head region. Both the upper and lower jaws were fractured into several fragments with significant displacement of the bone pieces. Tracing the defect through the soft palate revealed a wound tract (permanent cavity) extending into the cranial cavity. The tract traversed several critical structures, including: the clivus of the occipital bone with an irregular defect measuring approximately 1.8×2.5 cm on the outer bone plate and around 1mm larger on the inner plate (only on a part of the defect) and a corresponding rupture of the adjacent dura mater (**Fig. 1)**; irregular damage to the brain structures – the pons and medulla oblongata, the fourth cerebral ventricle, and the cerebellar vermis with destruction of the brain substance and severe hemorrhages on the walls of the permanent cavity **(Fig. 2).** The tract terminated medially within the occipital bone, slightly above the protuberantia occipitalis interna. At this site, an irregularly shaped fracture of the inner bone plate with mild depression was observed, while the outer plate remained intact. This fracture was with dimensions around 3.5/4 cm. Within this area, a metallic projectile was discovered. The object was

cylindrical in shape, measuring approximately 3 cm in length and 1.5 cm in diameter **(Fig. 3).** No additional traumatic injuries were observed elsewhere on the body, and no pathological changes were identified in other organs. The cause of death was determined to be extensive brain damage resulting from a gunshot wound to the head. This injury was deemed incompatible with life due to the destruction of vital brain structures along the projectile's trajectory.

Fig. 1. The defect on the clivus of the occipital bone.

Fig. 2. The injury of the brain structures – pons, medulla oblongata, fourth cerebral ventricle, cerebellar vermis.

Fig. 3. The metallic projectile discovered in the area of the occipital bone.

Discussion

Under the Law On Weapons, Ammunition, Explosives and Pyrotechnic Articles in force in the Republic of Bulgaria, firearms are defined as weapons capable of discharging a bullet or projectile through the action of an explosive substance [6]. The literature describes numerous cases of injuries caused by weapons that mimic the effects of firearms [5, 7, 16, 19]. Air weapons (pneumatic weapons) occupy a special place in this context. Despite lacking the use of explosive substances, these weapons can produce injuries that closely resemble those inflicted by factory-manufactured firearms [10,14,18]. Homemade weapons can also be classified as firearms if they meet the legal criteria specified in the legislation. In the present case, the homemade weapon discharged a projectile – a piece of metal – through the ignition of an explosive substance, likely derived from matches.

Such improvised weapons often use metal tubes to serve as barrels, typically constructed as short-barreled firearms regardless of the type of ammunition intended for use. While factory ammunition may serve as projectiles, random objects such as nails or metal fragments are frequently utilized. The incendiary material can vary widely, including substances such as gunpowder or the flammable material from matches, as suggested in this case [8,11,12,15]. In factory-made weapons, the ignition of gunpowder is of primary importance in the mechanism of producing a shot. As a result, a significant amount of gases and heat is released, which creates a large pressure, through which kinetic energy is imparted to the projectile. Usually, the heads of matches contain a mixture of fuel, oxidizer and binding components. When rubbed or heated (additional ignition), a rapid exothermic reaction occurs with the release of a large amount of heat and gases. When this reaction occurs in a closed and small volume space, an explosive effect is created, similar to that of gunpowder [2, 11, 12, 17]. In the present case, the empty matchbox found next to the victim's body suggests that matches were probably used as the incendiary substance, and they were probably placed at one end of the tube, behind the projectile. The lighter found in the victim's hand suggests that they were ignited by it.

The functioning of a homemade firearm depends on two key factors: the materials used in its construction and the knowledge and skills of the individual fabricating it [21]. These weapons pose a significant risk not only to the intended target but also to the shooter. The materials used are often unstable and may fail to withstand the pressure generated during firing, leading to the potential explosion of the barrel and the release of shrapnel. This inherent instability necessitates extreme caution during ballistic testing of such weapons. Test firings must be conducted with robust safety measures in place to mitigate the risk of injury [3, 8, 21].

The combustion of the explosive substance during the discharge of a homemade weapon is typically incomplete, leading to the release of large quantities of unburned particles along with the projectile. This phenomenon is primarily attributed to two factors: the inherent properties of the explosive material and the frequent mismatch between the diameters of the barrel and the projectile. As a result, unburned particles tend to deposit at greater distances compared to those from factory-made firearms. This is often accompanied by pronounced gunpowder tattooing, observed on the skin of the shooter's hands and around the entrance wound [4, 8, 15]. In the present case, similar

findings were noted, including abundant soot on the left hand of the shooter and within the oral cavity, which also contained the entrance wound.

The kinetic energy of projectiles fired from homemade weapons is generally low, sometimes rendering the injuries ineffective. Consequently, such injuries are often blind, with the projectile remaining lodged within the body. Lethal injuries from homemade firearms are typically observed only at close-range, most often at point-blank range [4, 8]. The characteristic features of entrance gunshot wounds caused by homemade weapons – such as tissue loss, abrasion rings - may be absent or poorly defined, complicating forensic evaluation. Unlike the typically round entrance wounds caused by factory-made firearms, those from homemade firearms can vary significantly in shape. Even when a factory-manufactured projectile is used, lateral penetration can result in non-circular wound patterns. At point-blank range, the imprint of the muzzle may sometimes be found on the skin surrounding the entrance wound, enabling a comparative analysis with the suspected weapon [11, 12, 15]. In this case, the entrance wound was located in the soft palate and presented as an irregularly shaped defect with tissue loss, but the abrasion ring was not well presented. The slit-like wounds in the oral area, on the other hand, are a common finding when the muzzle of the firearm is placed in the mouth. They most likely resulted from rapid expansion of gases under high pressure in the oral cavity, one of the vicinity effects associated with the firearm discharge.

The wound channel created by the projectile's penetration into the body can also exhibit characteristics distinct from those typically observed in factory-manufactured firearms. These differences depend on the projectile itself and its kinetic energy. In most cases, the wound channel ends blindly within the tissues without forming an exit wound. Occasionally, the projectile may fragment upon entry, resulting in additional wound channels [11, 12, 15]. In the present case, the wound channel ended blindly in the occipital bone, where the projectile was extracted. The channel crossed soft tissues and bone structures, forming a permanent cavity with destruction of the structures along its course, which indicates that the projectile possessed significant kinetic energy. This is also confirmed by the morphological changes in the tissues surrounding the wound tract, which are the result of the effect of the temporary cavity (lacerations of the tissues of the oral cavity, fracturing of bone structures, etc.).

Although rare, injuries caused by homemade firearms can result in exit wounds, which may vary greatly in size and shape. In some instances, fragmentation of the projectile or the displacement of bone fragments along the wound channel can lead to multiple exit wounds. [15] In the case presented, the kinetic energy of the projectile was insufficient to produce an exit wound. However, an irregularly shaped fracture of the inner plate of the occipital bone was observed, highlighting the destructive potential of the projectile even in the absence of an exit wound.

Conclusion

This forensic case underscores that homemade firearms can be as dangerous as factory-manufactured ones. Understanding the mechanisms of these weapons and the injuries they cause is of significant importance to forensic medical practitioners and ballistics specialists.

References

1. **Dettmeyer, R., M. Verhoff, H. Schütz.** Forensic Medicine: *Fundamentals and Perspectives.* Berlin, Heidelberg: Springer Berlin Heidelberg, 2014, 155-169.
2. **Di Maio, V., K. Molina.** DiMaio's forensic pathology. *Boca Raton, FL: CRC Press*, 2022, 199-231.
3. **Ghadage, G. N., R. K. Jagtap.** Forensic ballistics analysis of an unusual/unrifled/homemade firearm in the absence of the action. – *Can. Soc. Forensic Sci. J*., **50** (4), 2017, 175-180.
4. **Gojanovic, M.** Fatal firearm injuries caused by handmade weapons. – *J. Clin. Forensic Med*., **2** (4), 1995, 213-216.
5. **Hagemeier, L., C. Schyma, B. Madea.** Extended suicide using an atypical stud gun. – *Forensic Sci. Int.*, **189** (1–3), 2009, 9-12.
6. Law on Weapons, Ammunition, Explosives and Pyrotechnic Articles. [In Bulgarian] – Ministry of Interior of the Republic of Bulgaria. 2010. Available at: https://lex.bg/laws/ldoc/2135696097
7. **Mackley. P., K. Püschel, E. Turk.** Suicide by shooting with a tiling hammer. – *Int. J. Legal Med.*, **124** (1), 2010, 75-77.
8. **Modi, J. K., C. Nigam, K. Kumar.** Improvised firearms versus regular firearms. – *Forensic Sci. Int.*, **26** (3), 1984, 199-205.
9. **Payne-James, J., R. Jones, S. Karch, J. Manlove.** Simpson's Forensic Medicine. *London: Hodder Education*, 2011, 111-120.
10. **Petrus, K., M. Angyal, D. Tóth, V. S. Poór, V. Heckmann, G. Simon.** Forensic assessment of a life-threatening penetrating abdominal air gun injury. – *Leg Med.,* **60**, 2023, 102182.
11. **Radanov, St.** *Forensic medicine and deontology*. – Sofia, Siela, 2006, 126-152. [In Bulgarian]
12. **Radanov, St., P. Lisaev.** *Encyclopedic reference book on forensic medicine*. – Sofia, Siela, 2004, 256-257. [In Bulgarian]
13. Recommendation No R(99)3 of the Committee of the Ministers to Member States on the Harmonisation of Medico-Legal Autopsy Rules. Council of Europe Committee of Ministers. 1999. Available at: recr(99)3.pdf
14. **Shah, H., R. Elshaer, T. Arabi, B. Sabbah, G. Alokby.** Endoscopic endonasal retrieval of air gun pellet retained in the frontal sinus: A case report. – *Int. J. Surg. Case Rep*., **96**, 2022, 107280. DOI: 10.1016/j.ijscr.2022.107280
15. **Sinha, J.** Forensic Investigation of Unusual Firearms: Ballistic and Medico-Legal Evidence – New York CRC Press, 2014, 132-133, 146-155.
16. **Skavysh, A., R. Wojcik, R. Murphy, M. Kazahaya, M. Pasquale, R. Barraco.** Facial injuries by potato gun: Spuds as scuds. – *Inj Extra*, **38** (3), 2007, 81-83.
17. **Stam, M.** The forensic analysis of wooden stick matches in a southern California arson case and subsequent examinations in two other arson cases. "The Great Scientific Exchange SCIX2013", Milwaukee, Wisconsin, USA, 29 September – 4 October 2013
18. **Tsranchev, I., P. Timonov, A. Alexandrov.** Penetrating Brain Trauma due to Air Gun Shot – a case report. – *Folia Med* (Plovdiv), **63** (6), 2021, 977-980.
19. **Vadysinghe, A., P. Dassanayake, M. Wickramasinghe.** Unusual Case of Suicide With a Modified Trap Gun. – *Am. J. Forensic Med. Pathol.*, **38** (2), 2017, 97-99.
20. **Whitwell, H., P. Harvey, A. Kolar, K. Thorne.** Mason's Forensic Medicine and the Law. London: Bloomsbury Professional, 2023, 131-144.
21. **Yalçın Sarıbey, A., A. G. Hannam.** Homemade Heavy Caliber Rifles – Two Unusual Firearms. – *J. Forensic Sci.*, **61** (3), 2016, 773-774.

Institute of Experimental Morphology, Pathology and Anthropology with Museum
Bulgarian Anatomical Society

Acta Morphologica et Anthropologica, 32 (3-4)
Sofia ● 2025

Perihilar Branching Patterns of Renal Arteries and Extrarenal Length of Arterial Branches: A Study Using Peripheral Angiography

Divia Paul. Aricatt[1], Subramanyam Kodangala[2]*

[1] Department of Anatomy, MVJ Medical College and Research Hospital, Hoskote, Bangalore, Karnataka, India
[2] Department of Cardiology, Srinivas Medical College and Research Center, Mukka-Suratkal, Mangalore,Karnataka, India

* Corresponding author e-mail: diviaaricatt@gmail.com

Renal arteries supply blood to the kidneys, and variations in their branching patterns and extra-renal lengths can influence surgical and interventional outcomes. This is critical for clinical practice.A cross-sectional study of 100 kidneys (50 right, 50 left) from patients undergoing peripheral angiography classified perihilar branching into four types: Type I (single artery, normal bifurcation), Type II (multiple arteries), Type III (early branching), and Type IV (complex branching). Extrarenal lengths were measured from the renal hilum to the first arterial branch, with significance set at $p<0.05$.Type I was most common (60% right, 62% left), followed by Type II (18–20%), Type III (14–15%), and Type IV (5–6%). Mean extrarenal lengths were 20.5 mm (right) and 22.1 mm (left), with no significant difference ($p=0.24$). Type I is the standard renal artery configuration, while variations (Types II–IV) underscore the need to account for anatomical differences to optimize surgical planning.

Key words: renal artery anatomy, perihilar branching patterns, extra renal length, peripheral angiography, renal vascular variations

Introduction

The renal arteries are vital blood vessels responsible for supplying oxygenated blood to the kidneys, playing a crucial role in maintaining renal function. Their anatomical configuration is important not only for normal kidney function but also for guiding surgical and interventional procedures. Variations in the renal artery structure, particularly in the perihilar region where the artery branches before entering the kidney, can have significant clinical implications. These variations may impact the

outcomes of renal surgeries, diagnostic procedures, and interventions, such as renal transplantation, nephrectomy, renal artery revascularization, and stenting. Given the advancements in renal surgery and interventional techniques, understanding these variations is increasingly vital for ensuring optimal clinical outcomes [1,8].

In addition to anatomical variations, knowledge of the extrarenal length of arterial branches – the distance from the renal hilum's bifurcation to the first arterial division – provides important insights for clinicians when planning surgical or interventional procedures [12]. The length and branching patterns of renal arteries can vary significantly among individuals, whether due to anatomical differences or congenital anomalies. These variations range from a simple bifurcation (Type I) to multiple or early branching (Types II and III), and even more complex configurations, such as trifurcations (Type IV). Research in recent years has emphasized how these variations influence renal health, particularly in conditions like renovascular hypertension and renal transplantation [10, 11]. Understanding these branching patterns is crucial for improving diagnostic accuracy and tailoring interventions for individuals with complex renal vascular anomalies.

The classification of renal arterial morphology, used in this study, is based on Shoja et al.'s (2008) classification system [15]. Renal artery branching patterns were categorized into two types: fork-type and ladder-type. In the fork-type configuration, there is a single point of division, which can either be duplicated (Type I, with an upper and lower branch) or triplicated (Type II, with upper, middle, and lower branches). In contrast, the ladder-type configuration (Type III) involves sequential branching points, resulting in multiple branches along the artery.

Peripheral angiography, especially digital subtraction angiography (DSA), is a non-invasive imaging technique that remains essential for visualizing the renal vascular anatomy. Recent advancements in DSA technology have enhanced the clarity and detail of renal artery visualization, particularly for perihilar branching patterns and the extrarenal lengths of arterial branches [4,18]. These advancements have facilitated a more accurate understanding of renal artery anatomy, which is critical for the success of renal surgeries and interventions. Despite significant advancements in imaging technology, renal angiography continues to be the gold standard for diagnosing renal artery diseases. When performed with appropriate techniques, it delivers detailed anatomical visualization of the renal arteries, including their segmental and subsegmental branches, providing critical information for the diagnosis and management of renal vascular disorders. The study was aimed to investigate the perihilar branching patterns of the renal arteries and the extrarenal length of their branches using peripheral angiography with objectives to categorize the perihilar branching patterns of the renal arteries in both the right and left kidneys, to measure and compare the extrarenal lengths of the arterial branches in the right and left kidneys and to investigate the relationship between the perihilar branching patterns and the extrarenal lengths of the renal arteries.

Materials and Methods

Study Design

This was a single-center observational cross-sectional study conducted over a six-month period at a tertiary care center specializing in vascular and renal interventions.

Ethical principles for human research were strictly followed, and ethical approval was obtained from the Institutional Ethics Committee of the hospital from which the data was collected. Participants were randomly selected from patients undergoing peripheral angiography for non-renal-related conditions. The study received approval from the Institutional Review Board (IRB) before patient enrollment, and written informed consent was obtained from each participant. The sample size was determined in consultation with a statistician using the G*Power 3.0.10 software. A total of 100 subjects were selected using a systematic sampling strategy, which included 50 right kidneys and 50 left kidneys.

The inclusion criteria consisted of participants aged 18 years or older of either sex, who were undergoing peripheral angiography for clinical indications unrelated to renal vascular abnormalities. The exclusion criteria included individuals with a history of congenital renal anomalies (e.g., horseshoe kidneys), renal tumors, or previous renal surgeries.

Angiographic Technique

Arterial access was obtained by inserting a 5F or 6F sheath into the femoral or brachial artery using the modified Seldinger technique [14]. In renal angiography, a 5F catheter was positioned in the abdominal aorta via the femoral or brachial artery. Contrast material was administered either manually or through an automatic injection pump, generating a series of diagnostic images. Typical parameters for contrast injection were 10–20 mL/K over 2 seconds. The imaging sequence was captured over 3–5 seconds, acquiring approximately 1–2 frames per second. If detailed visualization of renal arterial branches or venous phases was required, the imaging duration could be extended by an additional 3–5 seconds, facilitating the assessment of both intra-parenchymal structures and vascular flow dynamics [2,7].

Imaging was performed using a biplane angiography system equipped with high-resolution fluoroscopy and digital subtraction angiography (DSA), ensuring precise visualization of the renal vasculature. Multiple angiographic views were obtained to assess the complete branching pattern of both the right and left renal arteries, with particular focus on the perihilar region. Calibration of the systems was conducted using the same method as the catheter employed for the angiography. Calibration was performed by automated edge detection techniques, producing corresponding calibration factors (mm/pixel), and the vessel contours were identified using operator-independent edge detection algorithms. Angiographic views for calibration were selected to minimize foreshortening of artery segments and ensure accurate separation from adjacent structures.

Database Pooling

The primary anatomical parameters assessed in this study were:

a. Perihilar branching patterns

The configuration of the main renal artery and its branching near the renal hilum was classified according to a modified version of the renal artery classification system:

- Type I: Single renal artery with normal bifurcation.
- Type II: Multiple renal arteries (accessory or aberrant).
- Type III: Early branching (before reaching the hilum).
- Type IV: Complex branching patterns (e.g., trifurcation or other anomalous configurations).

Morphologically, the arterial branching patterns were classified into fork-type, where there is a common point of division, and ladder-type, characterized by sequential branching points (**Figs. 1 and 2**).The fork-type could either be duplicated (Type I, with upper and lower branches) or triplicated (Type II, with upper, middle, and lower branches). The first divisions of the main renal artery were defined as the primary branches, and the subsequent divisions were classified as secondary and tertiary branches. The branches of fork-type arteries were designated as the upper, middle (if present), or lower branches in two-dimensional images. The main renal artery was then classified based on its primary and secondary divisions and their respective patterns.

"Cardinal perihilar renal arterial morphology" referred to those configurations that accounted for 5% or more of the total observed types. The remaining types (< 5%) were categorized as "minor" (m). The subtypes under each of Types I, II, and III were arranged in descending order of prevalence. Types with infrequent prevalence were categorized as "infrequent" morphologies [16]. Three cardinal primary division patterns of the main renal artery were identified, which were further subdivided based on their secondary divisions. Considering both the primary and secondary branching patterns, eight "cardinal" perihilar renal arterial morphologies were recognized, as follows (**Figs. 1 and 2**),

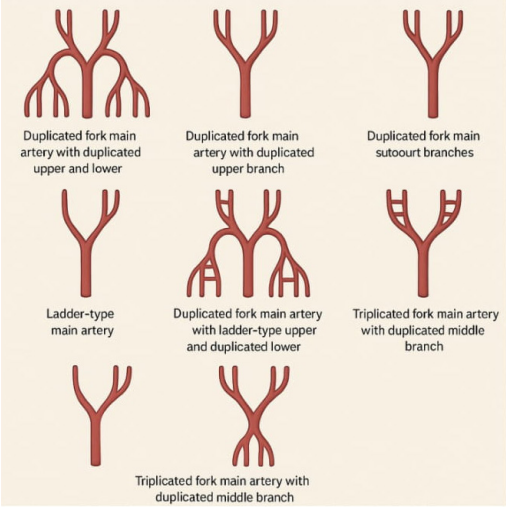

Fig. 1. Cardinal perihilar morphologies of the main renal artery. Illustration of cardinal perihilar morphologies of the main renal artery as observed in imaging and dissection studies. It highlights common anatomical variants including early bifurcation, accessory renal arteries, and extrahilar branching patterns. Each morphological type is labeled and depicted with schematic or radiographic representations to aid in visual differentiation.

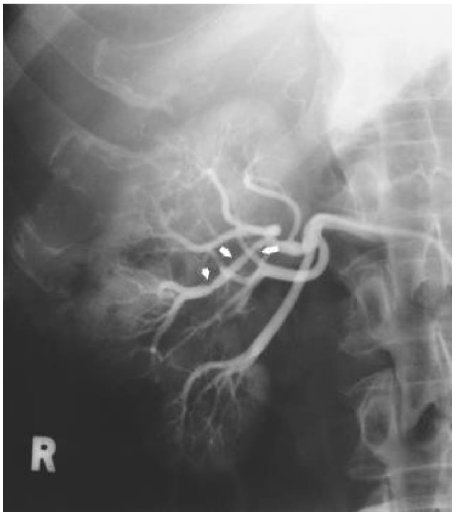

Fig. 2. Ladder pattern of renal artery branching morphology. Angiographic image demonstrates the "ladder pattern" of renal artery branching morphology. In this variant, multiple segmental branches arise in a stepwise, near-parallel arrangement from the main renal artery, resembling the rungs of a ladder. This pattern is typically observed in both prehilar and intrarenal segments and is important for planning endovascular procedures and renal surgeries due to its impact on vascular access and perfusion zones.

• Duplicated fork main artery with duplicated upper and lower branches.
• Duplicated fork main artery with duplicated upper branch.
• Duplicated fork main artery without secondary branches.
• Ladder-type main artery.
• Duplicated fork main artery with ladder-type upper and duplicated lower branches.
• Duplicated fork main artery with duplicated upper and ladder-type lower branches.
• Triplicated fork main artery with duplicated middle branch.
• Duplicated fork main artery with ladder-type lower branch.

b. Extrarenal length of arterial branches

The extrarenal length was measured from the bifurcation point at the renal hilum to the point where the vessels leave the kidney. Measurements were recorded using a calibrated scale on the angiograms, with values expressed in millimeters.

Data Analysis

Statistical analysis of the present study was performed using the GraphPad Prism v9. $P<0.05$ was considered statistically significant.

Results

A total of 100 kidneys were included in the study, consisting of 50 right kidneys and 50 left kidneys. The following findings were observed regarding perihilar branching patterns and extrarenal length measurements.

Perihilar branching patterns

• Type I (single renal artery with normal bifurcation) was the most prevalent branching pattern, observed in 60% of right kidneys and 62% of left kidneys.
• Type II (multiple main renal arteries) was found in 20% of right kidneys and 18% of left kidneys. Most of these cases involved accessory arteries arising from the aorta, typically supplying the lower poles of the kidneys.
• Type III (early branching) occurred in 15% of right kidneys and 14% of left kidneys, where the main renal artery divided shortly after entering the renal hilum.
• Type IV (complex or anomalous branching patterns) was less common, occurring in 5% of right kidneys and 6% of left kidneys. This included trifurcations and other unusual configurations, where multiple branches emerged before reaching the hilum.

Cardinal perihilar morphologies of the main renal artery

Three primary division patterns of the main renal artery were identified, each further subcategorized according to their secondary divisions. Eight “cardinal” perihilar renal arterial morphologies were found, accounting for 77% of all cases. The remaining 23% (23cases) were classified as ‘infrequent’ morphologies.

The cardinal morphologies included (**Figs. 1 and 2**).

• Duplicated fork main artery with duplicated upper and lower branches (n = 24, 23.5%).
• Duplicated fork main artery with duplicated upper branch (n = 16, 16.1%).

• Duplicated fork main artery without secondary branches (n = 9, 8.6%).
• Ladder-type main artery (n = 7, 7.4%).
• Duplicated fork main artery with ladder-type upper and duplicated lower branches (n = 7, 7.4%).
• Duplicated fork main artery with duplicated upper and ladder-type lower branches (n = 8, 8.4%).
• Triplicated fork main artery with duplicated middle branch (n = 7, 7.2%).
• Duplicated fork main artery with ladder-type lower branch (n = 6, 6.2%).

This distribution maintains the original percentages and proportions, now applied to a sample of 100 kidneys (50 right-sided and 50 left-sided).

Extra renal length of arterial branches

• The average extrarenal length for the right kidney was 20.5 mm (range: 10-30 mm).
• For the left kidney, the average extrarenal length was 22.1 mm (range: 12-32 mm).
• No significant difference was found between the extrarenal lengths of the right and left kidneys (p = 0.24), although left kidneys tended to have slightly longer branches.
• The extrarenal length was measured from the bifurcation at the hilum to the first branching point of the main renal artery. No significant correlation was observed between the extrarenal length and the branching pattern.

Additional Observations

• Sex differences: Type I branching patterns were slightly more common in male patients, while Type II and Type III patterns were more frequent in female patients.
• Age: The patient's age did not significantly affect the perihilar branching pattern, with no noticeable differences observed between age groups (p = 0.12).

Discussion

The findings of this study provide valuable insights into the perihilar branching patterns and extrarenal lengths of renal arteries, contributing to the growing body of literature on renal vascular anatomy. The most common branching pattern observed in our study was Type I, characterized by a single renal artery with normal bifurcation. This is consistent with earlier studies, which have found that the majority of individuals possess a single renal artery supplying each kidney [1,8]. The prevalence of Type I branches supports the notion that the single renal artery configuration is the standard anatomical pattern, representing around 60–70% of cases in general populations.

However, the presence of Type II branching, which involves multiple renal arteries, was notable in 18–20% of the kidneys studied. This is in agreement with findings from recent studies [10, 11], which have documented a significant occurrence of accessory renal arteries in up to 25% of individuals. Accessory renal arteries typically originate from the aorta or common iliac artery and supply either the upper or lower poles of the kidney. The identification of these variations is clinically significant, particularly for procedures such as nephrectomies, renal transplantations, and endovascular interventions [4,9]. In cases of renal revascularization or transplantation, the presence of accessory arteries can complicate surgical planning and may require more intricate procedures to ensure proper vascular supply to the kidney.

The findings of Type III (early branching) and Type IV (complex or anomalous branching) are particularly interesting, as they suggest that renal artery anatomy can be more complex than previously acknowledged. Type III (early branching) was noted in approximately 15% of cases, while Type IV, which includes configurations such as trifurcation, was found in 5 - 6% of the kidneys. These patterns can pose substantial challenges during surgical or interventional procedures, as they may interfere with the access and visualization of the renal vessels [8]. Trifurcations and other unusual branching configurations may increase the risk of complications during procedures like renal artery stenting or transplant, as the vascular access may be more challenging and require precise manipulation to avoid damaging the renal parenchyma.

In terms of the extrarenal length of arterial branches, our study found an average length of approximately 20.5 mm for the right kidney and 22.1 mm for the left kidney. These values align with those reported in the literature, where the typical length of extrarenal arterial branches has been described as ranging from 15 to 25 mm [6,10]. The slight difference between the right and left kidneys in this study was not statistically significant, though the left kidney exhibited slightly longer branches. Such variations in extra renal artery length are important for surgical planning, especially in renal surgeries or interventions like stent placement or renal revascularization, where precise measurements of artery length are crucial for successful outcomes [13, 18]. While the difference was not significant, understanding this variability is critical for improving surgical accuracy and preventing inadvertent injury to renal vessels.

Interestingly, our study found no significant correlation between branching patterns and patient age or sex, suggesting that renal artery anatomy is primarily determined by individual anatomical variation rather than demographic factors. This finding is in line with recent studies that have reported no consistent relationship between branching patterns and patient age or gender [3,8,17]. Thus, while some studies suggest slight predilections for certain patterns in different populations, our results reinforce the idea that renal artery branching is largely an anatomical trait that may not be influenced by factors such as age or sex.

The current study highlights the importance of understanding the anatomical variations in renal artery branching and extrarenal length for clinical applications. The data support findings from previous research that accessory and anomalous branching patterns are common and may require special consideration in renal surgery and intervention. Understanding these variations can help improve preoperative planning and enhance the success of surgical procedures involving the renal vasculature. Further studies with larger sample sizes and more diverse populations may provide additional insights into the impact of demographic factors on renal vascular anatomy and surgical outcomes.

Conclusion

In conclusion, this study provides valuable insights into the perihilar branching patterns and extrarenal lengths of renal arteries using peripheral angiography. The results underscore the variability in renal arterial anatomy, with Type I being the most common pattern, though accessory and anomalous arteries were also observed. The extrarenal length of arterial branches was similar for both the right and left kidneys,

with no significant correlation found between length and branching patterns. These findings are important for clinical practice, as they can inform surgical planning and interventions, improving outcomes for procedures like renal artery stenting, transplant surgeries, and nephrectomies.

Acknowledgements: We would like to acknowledge the technical staff and radiologists who assisted in performing the peripheral angiography and collecting data for this study. Special thanks to all the patients who consented to participate in this research.

References

1. Andrian, T., **L. Voroneanu**, **L., A. Covic**. Kidney transplantation and renal vascular issues. In: *Contemporary Approaches to Renal Vessel Disorders: Updates in Management Strategies* (Eds. A. Covic, A. Burlacu), Springer, Cham, 2024, 47-156.

2. Baum, S., **M. J. Pentecost**. *Abrams' angiography: Interventional radiology* (2nd ed.). Philadelphia, Lippincott Williams & Wilkins, 2006, 512 p.

3. Burgan, C. M., **D. Summerlin**, **M. E. Lockhart**. Renal transplantation: pretransplant workup, surgical techniques, and surgical anatomy. – *Radiol. Clin. North Am.*, **61**(5), 2023, 797-808.

4. Caroli, A., **A. Remuzzi**, **L. O. Lerman**. Basic principles and new advances in kidney imaging. – *Kidney Int.,* **100**(5), 2021, 1001-1011.

5. Gebremickael, A., **M. Afework**, **H. Wondmagegn**, **M. Bekele**. Renal vascular variations among kidney donors presented at the national kidney transplantation center, Addis Ababa, Ethiopia. – *Transl. Res. Anat.,* **25**, 2021, 100145.

6. Gulas, E., **G. Wysiadecki**, **J. Szymański**, **A. Majos**, **L. Stefańczyk**, **M. Topolet al.** Morphological and clinical aspects of the occurrence of accessory (multiple) renal arteries. – *Arch. Med. Sci.,* **14**(2), 2018, 442-453.

7. Jeffrey, J. P., **K. Scott**, **D. L. Bhatt**. Coronary arteriography and intra-coronary imaging. – In: *Braunwald's Heart Disease*: *A Textbook of Cardiovascular Medicine* (Eds. D. Mann et al., 10th edition), Philadelphia, Elsevier/Saunders, 2015, 392-428.

8. Kang, W. Y., **D. J. Sung**, **B. J. Park**, **M. J. Kim**, **N. Y. Han**, **S. B. Choet, et al.** Perihilar branching patterns of renal artery and extrarenal length of arterial branches and tumour-feeding arteries on multidetector CT angiography. – *Br. J. Radiol.,* **86**(1023), 2013, 20120387.

9. Kumaresan, M., **J. Saikarthik**, **A. Sangeetha**, **I. Saraswathi**, **K. S. Kumar**, **P. Roselin**. Peri-hilar branching pattern and variations of the renal artery among Indian kidney donors using pre-operative computed tomography angiography: an anatomical study and review. – *Folia Morphol.,* **81**(4), 2022, 971-982.

10. Maringhini, S., **L. Pape.** Kidney transplantation in congenital abnormalities of kidney and urinary tract (CAKUT). – *Biomedicines*, **13**(4), 2025, 932.

11. Nagata, D., **E. Hishida**. Elucidating the complex interplay between chronic kidney disease and hypertension. – *Hypertens. Res.,* **47**(12), 2024, 3409-3422.

12. Oceguera, I. N., **O. Thaher**, **D. Bausch**, **S. Pouwels**. Vascular and anatomical challenges in renal transplant surgery; what a urologist needs to know. – *Curr. Urol. Rep.*, **26**(1), 2025, 1-10.

13. Pan, L., **L. Shen**, **M. Fan**, **Z. Xing**, **J. Ding**, **Y. Duet, et al.** Assessment of transplant renal artery stenosis with non-contrast-enhanced magnetic resonance angiography: comparison with digital subtraction angiography. – *Acad. Radiol.,***31**(6), 2024, 2405-2411.

14. **Saikia, M.**, **R. D. Roy**, **S. Thakuria**. Anatomical variations in arrangement of renal hilar structures and its applied importance: a cadaveric cross-sectional study among North East population of India. – *Int. J. Anat. Radiol. Surg.,* **13**(5), 2024, AO05-AO09.
15. **Shoja, M. M.**, **R. S. Tubbs**, **A. Shakeri**, **M. Loukas**, **M. R. Ardalan**, **H. T. Khosroshahiet, et al.** Peri-hilar branching patterns and morphologies of the renal artery: a review and anatomical study. – *Surg. Radiol. Anat.,* **30**(5), 2008, 375-382.
16. **Siqueira, D. E.**, **A. T. Guillaumon**. Angiography for renal artery diseases. – In: *Angiography* (Ed. B. Pamukcu), London, Intech Open, 2019.
17. **Valenzuela Fuenzalida, J. J.**, **K. Vera-Tapia**, **C. Urzúa-Márquez**, **J. Yáñez-Castillo**, **M. Trujillo-Riveros**, **Z. Koscinaet, et al.** Anatomical variants of the renal veins and their relationship with morphofunctional alterations of the kidney: a systematic review and meta-analysis of prevalence. – *J. Clin. Med.,***13**(13), 2024, 3689.
18. **White, C. J.**, **S. R. Ramee**. Renal artery stent placement. – In: *Peripheral Vascular Stenting* (Eds. R. R. Heuser, G. Biamino, 2nd ed.), London, CRC Press, 2024, 117-125.

Institute of Experimental Morphology, Pathology and Anthropology with Museum
Bulgarian Anatomical Society

Acta Morphologica et Anthropologica, 32 (3-4)
Sofia ● 2025

Anthropological study of five skeletons from a pit sanctuary near the village of Malko Tranovo, Chirpan municipality (late 12th-11th centuries BCE)

*Atanas Katsarov**

Institute of Experimental Morphology, Pathology and Anthropology with Museum, Bulgarian Academy of Sciences, Sofia, Bulgaria

* Corresponding author e-mail: zanasko@gmail.com

The objective of this study is to conduct a comprehensive anthropological analysis of four human skeletons discovered in proximity to a pit sanctuary near the village of Malko Tranovo, dated to the Early Bronze Age (12th–11th centuries BCE).
Osteometric measurements were obtained following the methodologies established by Martin and Saller, Y. Yordanov, and Alekseev and Debetz.
A total of five skeletons were unearthed from four burial pits. Two individuals were interred in the first pit, probably a woman and a child, while the remaining three were found singly in separate pits. The first three burial features are situated in close proximity to one another, whereas the fourth is located approximately 50 meters to the east. All burials are primary in nature.
Stature estimations were derived from the lengths of the long bones of the limbs using the regression formulae proposed by Pearson, Trotter and Gleser, and Steele.

Key words: Anthropological data, Thracian, pit, sanctuary, Iron Age, Malko Tranovo, Kozluka

Introduction

The 2004 excavations in the Kozluka area along the Trakia highway uncovered a multi-period ritual complex centered on a pit sanctuary, primarily active between the 5th and early 4th centuries BC [2, 6]. The diverse burial practices, ceramic assemblages, and stratigraphic data reveal intricate ritual behaviors, elements of ancestor worship, and evidence of long-term site continuity from the Early Iron Age to the Roman period. These findings provide new insights into Thracian funerary traditions, socio-religious structures, and cultural interactions within the Upper Thracian Lowland during the 1st millennium BC.

Materials and Methods

The archeological studies were conducted in May–June and August–September 2004 by a team led by Prof. A. Bozhkova (NAIM) and lasted three months. The site is in the Kozluka area [2,3,4,6,7,8], on a northeastern slope above a semi-dry ravine between km 188+760 and 189+140 of the Trakia highway route. It is a pit sanctuary with over 270 studied facilities, of which 168 were studied in 2004 with different sizes - from shallow excavations to deep pits with a length of 7 m and a depth of 2.2 m. They date back to the Early Bronze Age, Early Iron Age, Classical, Roman and undetermined eras, with most belonging to the 5th - early 4th centuries BCE. Some are multi-part, without a strict arrangement, but with partial planning and grouping by periods. Their openings are disturbed by agricultural activity and appear as dark spots in the sterile layer. The shapes vary – round, elliptical, rectangular and irregular, with dimensions from 0.60×0.80 to 2.10×7.20 m.

The pits are hemispherical, conical, beehive-shaped, bell-shaped or vessel-shaped, often asymmetrical, with the cylindrical ones being characteristic of the Early Iron Age, and the vessel-shaped ones – of the Classical Age. The filling contains dark soil with stones, charcoal, ash, plaster, animal bones and ceramics. Some facilities stand out – pit № 106 is probably a ditch from the Early Iron Age, and № 128 contains the remains of a furnace. Among the finds are ceramics, clay figurines and idols from the Early Iron Age, and from the Classical Age – hand- and wheel-made vessels, local and imported Greek ceramics (black-fired and painted vessels, amphorae from Chios, Lesbos, Thassos, Mende, etc.), as well as cult objects, a stone figure of a horse, vertebrae, tokens, bronze ornaments and iron knives. Fragments of coarse kitchen and table ceramics have been found from the Roman era [2, 3].

Each of the graves was assessed according to several indicators: 1. Assessment of the burial; 2. Type of burial; 3. Position of the bones in the pit; 4. Species belonging of the bones; 4. Condition of the bones [5].

Osteometric measurements were obtained following the methodologies established by Martin and Saller, Y. Yordanov, and Alekseev and Debetz [1, 5, 10]. Stature estimations were derived from the lengths of the long bones of the limbs using the regression formulae proposed by Pearson, Trotter and Gleser, and Steele [11, 12, 15].

Results and Discussion

In the area near the village of Malko Tranovo, near the town of Chirpan, 4 grave pits were discovered. The first three are in close proximity to each other (in the eastern half of the easement) with the same orientation, and the fourth is about 50 meters away in an easterly direction [2]. The graves are rectangular pits dug into the mainland with rounded corners and dimensions: length between 2.40–3.00 m and width from 0.60 to 1.00 m.

In grave pit № 1, two human skeletons were discovered, in the remaining three grave pits - one each. A total of five human skeletons. In grave № 3, the northernmost of the group, a grave inventory was discovered: a complete vessel – a cup with one handle, dating from the Early Iron Age (**Fig. 1**)

Fig. 1. General view of the three graves before the excavation of the skeletal remains

Grave № 1 – Two skeletons were discovered in grave pit № 1. The first, № 1, is of an adult individual, and the second, № 2, is of a younger individual. Based on the specific arrangement of the discovered bones, it can be stated that the two individuals were laid with their heads and feet towards each other (a "valve" type position) (**Fig. 2**).

The burial is primary (the bones are in anatomical order). The burial is on the back, in a stretched position. The skeletons are one on top of the other - № 1 is with its head to the south, and the skeleton № 2 is with its head to the north. The burial is double, the bones are human, significantly damaged secondarily, without traces of burning.

The location of the Burial facility № 1 is in North – South direction. The dimensions are: Length – 240 cm, width 50 – 55 cm, depth 5-10 cm.

It is a rectangular burial pit, dug into the mainland terrain, without additional shaping. The pit is strongly elongated along the N/S axis with rounded corners. The preserved depth of the burial pit is 5 –10 cm, since the burial facility was affected by agricultural activities. The bottom is relatively flat, made of sterile mainland soil [2]. The pit is filled with black, strongly compacted clay soil, individual spots of brown compacted clay, lumps of mainland and charcoal. When clearing the skeleton, several small, uncharacteristic fragments of ceramics were found that fell into the burial pit.

Skeleton № 1 – Total length of skeleton № 1 is about 160 cm [1,5,10]. Situated in Supine position. The orientation is as follows: Longitudinal axis head-feet is south-north. Skull turned towards right shoulder (facing east).

Fig. 2. Skeleton № 1 & № 2 (Grave pit № 1)

Characteristics of the bones

Skull: Highly fragmented. Almost the entire left half of the skull is missing. Preserved parts of individual bones – upper jaw, left eye socket, right temporal bone, occipital bone.

Maximum Cranial Length (g-op distance) is 20 cm. The bones of the skull are of a smaller thickness than the average – about 3-4 mm.

Bones of the trunk: Bones of the chest, spine and ribs are not preserved. Partially preserved pelvic bones.

Bones of the limbs: Preserved: Upper limb: 1. Left humerus with a length of 26 cm. 2. Left ulna – 21 cm. Single carpal and metacarpal bones were found.

Lower limb: 1. Right femur – 34 cm. 2. Right tibia – 33 cm. The remaining bones are fragmented, relatively preserved. They do not allow for accurate measurement. Single bones of both feet were found.

This was a skeleton buried in a supine position, with parallel lower limbs. Head turned towards the right shoulder; upper limbs strongly flexed at the elbow joints (right more than left) with forearms crossed in front of the chest and hands towards the head. Due to the unnatural flexion at the elbow joints, it is assumed that the upper limbs were tied distally (around the wrists or the palms of the hands) to hold them in the described position. The hands were clenched into fists, which is evident from the typical spatial relationship between the preserved metacarpal bones and the phalanges of the fingers. The right hand is higher than the left and touched the left shoulder. The wings of the two hip bones are relatively preserved, visible about 3 cm above the ground. They are quite low and spread, as in a female pelvis.

When determining the height based on the preserved long bones, it was found:

Femur – 141.82 cm, Humerus – 149.78 cm, Tibia – 155.09 cm, Average value – 149 cm [1,5,10]. It should be noted that preserved lengths of the long bones were used, which suggests that the height is significantly greater.

Skeleton № 2 – In the same grave pit, another skeleton was discovered – skeletal remains of younger individual, lying over skeleton №1. Total length of the skeleton – about 60cm, supine position, with orientation head to north, feet to south, missing bones of the skull.

Characteristic of the bones:

Skull: A single fragment of flat skull bone was lying between the femoral bones of skeleton №1.

Bones of the postcranial skeleton: Bones of the postcranial skeleton are extremely poorly preserved in very poor condition. Most of the bones of the upper part of the skeleton are missing. Fragments of pelvic bones were found.

Limb bones: Preserved: Upper limb: 1. Humerus with a preserved length of 10 cm.

Lower limb: 1. Left femur – 40 cm. 2. Right tibia – 34 cm [1, 5, 10]. A fragment of a calcaneal bone was found.

This is a skeleton buried in a supine position, with a straight left lower limb and a slightly abducted right, bent about 15° at the knee.

The head is probably at the feet of skeleton № 1. There are no bones from the upper part of the skeleton that would indicate the position of the body. The discovered fragment of the humerus is at the right knee of skeleton № 1, which suggests that the fragment is from the right humerus, assuming that the individual was buried on his back. The specific arrangement of the parts of the bones from the left pelvic half, which were found on the femur of skeleton № 1, also suggests a supine position.

Unfortunately, the bone material is in very poor condition and the sex of the buried individual cannot be determined with certainty. A very approximate determination of height can only be made from the preserved femur from the Trotter-Gleser formula, namely approximately 158 cm [15].

The molars and canines from the deciduous dentition revealed deep hypoplastic defects on the occlusal surface which resembles a disease state caused by an infectious agent during the 2nd trimester of pregnancy [9]. It is assumed that the buried individual was between 8 and 12 years old, i.e. infans II.

Grave № 2 – It is located immediately to the east and parallel to grave № 1. The two graves are 0.40 m apart. The grave pit appears to be intermediate (between № 1 and № 3) in location and depth. A skeleton of 1 adult individual was discovered in grave pit № 2.

The burial is primary (the bones are in anatomical order). The burial is sideways in a crouched position resembling a Hocker, with the head to the south. The burial is single; the bone remains are human. The bones are relatively well preserved, without traces of burning and other manipulations and rituals.

Burial facility № 2 is located in the North-South direction. The dimensions are as follows: Length at the opening - 260 cm and at the bottom 240 cm, width at the head 104 cm, and at the feet 85 cm. The depth of the burial pit from the level of the terrain from which it is fixed is 30 cm (**Fig. 3**).

The burial pit has no additional design; it is dug into the mainland soil. Its corners are rounded, which is why it has an approximately elliptical shape, slightly expanding to the south. The pit is filled with dark brown to black soil, strongly compacted. Small charcoal, fragments of plaster and single uncharacteristic fragments of ceramics were found in the soil from the pit [2, 3].

Fig. 3. Skeleton № 3 (Grave pit № 2)

Skeleton № 3 – total length about 160 cm, right-side position, longitudinal axis – head-feet is south-north. Skull turned to the right shoulder face to the east

Characteristics of the bones

Skull: Relatively well-preserved cranial bones, slightly fragmented in place by the pressure of the soil. The height of the skull – 22 cm. The forehead is low, strongly sloping. Well-developed occipital relief. The existing teeth have abrasio III – IV degree. Last molars (wisdom teeth) are missing.

Bones of the postcranial skeleton: Bones from the chest and spine are preserved. Single ribs were found. Well-preserved pelvic bones.

Limb bones: Preserved: Upper limb: 1. Left humerus, 29.5 cm long. 2. Left ulna (fragment) – 23 cm. Single carpal and metacarpal bones were found.

Lower limb: 1. Left femur – 40 cm. 2. Right tibia – 36 cm.

The remaining bones are fragmented and less well preserved. Single bones from both feet were found, most of them from the left.

This is a skeleton of an individual buried in a lateral position to the right with the head turned towards the right shoulder. The position of the body is slightly bent at the expense of the cervical spine and the hip and knee joints, while the rest of the spinal column is upright. The lumbar and thoracic vertebrae are in a position of moderate right rotation. The position resembles the embryonic one. The upper limbs are strongly flexed at the elbow joints, with the forearms crossed in front of the chest and the hands towards the head. The left humerus is parallel to the body. Due to the unnatural flexion at the elbow joints, it is assumed that the upper limbs were tied distally (around the wrists or the

palms folded) to hold them in the described position. The hands were clenched into fists, which is evident from the typical spatial relationship between the preserved metacarpal bones and the phalanges of the fingers. The right hand is higher than the left, both below the chin. A deformation of one of the metacarpal bones of the right hand was found.

The lower limbs are parallel, probably one on top of the other (left on right), but when the earth settled they shifted. From the position of the bones of the lower limbs, it can be said that the hip joints are in a position of about 40° anteflexion; the knee joints – about 30° flexion, and the ankle joints - about 30° extension.

The bones of the left pelvic half are above the ground, while the right are dug in. The pelvic wings are like those of a male pelvis. The preserved bones have a strongly developed relief.

When determining the height based on the preserved long bones, it was found:

Femur – 159.98 cm, Tibia – 172.71 cm, Humerus – 165.36 cm. Average value – 166 cm.

The buried individual is probably a man of mature age – about 35 – 40 years old.

Grave № 3 – It is located immediately east and parallel to graves № 1 and № 2.

It is 30 – 40 cm from grave № 2. In grave pit № 3, a skeleton of 1 adult individual was discovered.

The burial is primary (the bones are in anatomical order). The burial is sideways in a crouched position resembling a Hocker, with the head to the south. The burial is single; the bone remains are human. The bones are relatively well preserved, without traces of burning and other manipulations and rituals.

Burial facility № 3 is located in the North-South direction.

The dimensions are as follows: Length at the opening – 307 cm and at the bottom 275 cm, width at the head 78 cm, and at the feet 62 cm. The depth of the grave pit at the head is 30 cm, and at the feet – 40 cm. It is an ordinary grave pit dug into the mainland terrain. The pit has a strongly elongated and slightly trapezoidal shape. The corners of the pit are slightly rounded. The two long walls of the pit curve in an arc to the E. The bottom is uneven with a slope to the S of mainland soil. The grave pit is filled with an inhomogeneous layer of dark brown to black in color, strongly compacted soil, lumps of mainland. In the soil around the skeleton, individual charcoals, lumps of burnt clay, plaster and few uncharacteristic fragments of ceramics are observed. Behind the back of the skull, a ceramic cup with one handle, flutes and loops, made by hand, was discovered [4,14].

Fig. 4. Skeleton № 4 (Grave pit № 3)

Skeleton № 4 – total length about 150cm, supine to right-side position, longitudinal axis – head feet is south-north. Skull turned to the right shoulder face to the east.

Characteristics of the bones

Skull: Fragmented skull bones. Relatively preserved in place. Greater than average thickness – about 6-7 mm. Skull height – 20 cm.

The preserved teeth are long, large – with a large root and high crowns. Abrasion – II to III degree.

Bones of the postcranial skeleton: Bones from the chest and spine are preserved. Single ribs were found. Well-preserved pelvic bones.

Limb bones: Preserved : Upper limb: 1. Left humerus with a length of 28 cm. 2. Left ulna (fragment) – 26 cm. Single carpal and precarpal bones were found.

Lower limb: 1. Left femur – 41 cm. 2. Right femur – 39 cm 3. Right tibia – 40 cm. The remaining bones are fragmented and less well preserved. Single bones from both feet were found. The forefoot bones on the left are severely deformed, both talar bones are preserved. The bones are relatively gracile, with good relief.

This is a skeleton of an individual buried in a dorsal-lateral position to the right with the head turned towards the right shoulder. Fragments of ribs were found. The lumbar vertebrae and part of the thoracic vertebrae are missing. The upper limbs are strongly flexed at the elbow joints, with the forearms crossed in front of the chest and the hands towards the head. The left humerus is in an anteverted position of about 90°. Flexion in the left elbow at the time of burial was complete, although the bones of the forearm are not quite parallel to the humerus. This is not a discrepancy in position, since in living individuals the factor that limits flexion in the elbow is the soft tissues on the front side of the arm. The bones of the left hand are located under the left ramus of the lower jaw and. Due to the unnatural flexion in the elbow joints, it is assumed that the upper limbs were tied distally (around the wrists or the folded palms) to hold them in the described position. The hands were clenched into fists, which is evident from the typical spatial relationship between the preserved metacarpal bones and the phalanges of the fingers. The right hand is lower than the left, and is located under the chin.

The right lower limb is in a position of abduction in the hip joint of about 10° and flexion in the knee joint of about 15°. The left lower limb is in a neutral position in the hip joint and full extension in the knee. Antetorsion of the left femur is almost absent. The distal ends of the femur and tibia, which participate in the knee joint, are changed as if from static deformation. The bones of the foot are also deformed. This suggests a contracture in the left knee joint that occurred during life (the individual could not perform movements in the left knee). His gait was pathological (probably duck-like). The latter is also indicated by the high position of the left hip bone compared to the right. The left foot was on the right.

Both pelvic halves are identified, with the wings of the hip bones and part of the ischial bones above the ground. Both acetabulums are found. Overall, the pelvis has the characteristics of a male.

When determining the height from the preserved long bones, it was found:

Femur – 157.5 cm, Tibia – 182.79 cm, Humerus – 160.74 cm. Average value – 167 cm. The buried individual is probably a man of mature age – about 40 years old.

Grave № 4 – It is located about 50m east of the three described graves. Bone remains of 1 individual were discovered. The bones are poorly preserved and poorly

exposed. The burial is probably primary, sideways to the right, head – northwest. Bone remains are human and its condition is poor with predominant amount of bone fragments and detritus (**Fig. 5**).

Fig. 5. Skeleton № 5 (Grave pit № 4)

Skeleton № 5 – total length is impossible to measure, longitudinal axis – head-feet is south-north. Skull turned to the right shoulder and supine, face to the east

Burial facility № 5 is located in the Northwest-Southeast direction.

The dimensions are as follows: Length 250 cm, width at the head 60 cm, and at the feet 40 cm. The preserved depth of the grave pit is a maximum of 5-7 cm, as the grave was damaged by agricultural activities. The grave pit is simple, dug into the mainland terrain, without additional design. The pit has an elongated rectangular shape. The corners of the pit are slightly rounded.

Characteristics of the bones

Skull: Mechanically turned in an unnatural position, with the skull base up. Heavily fragmented. Parts of the lower jaw, temporal bone, both eye sockets and occipital bone are preserved. The height of the skull is 20 cm. The preserved teeth have initial abrasion – I – II degree.

Bones of the postcranial skeleton: Single bones from the chest and spine were found. A second cervical vertebra (axis) was found under the left side of the skull, and a first cervical vertebra, heavily fragmented, was embedded in the skull base itself.

Limb bones: Preserved : Upper limb: 1. Right humerus with a length of 29.5 cm. 2. Right ulna (fragment), 3. Right radius (fragment).

Fragment of right scapula, diaphysis of left humerus and proximal end of left ulna. Single carpal and precarpal bones and phalanges were found.

Lower limb: 1. Left fibula – 32 cm. 2. Right tibia – 34 cm 3. Right fibula – fragmented. The remaining bones are fragmented and less well preserved. Single bones from both feet were found.

The discovered skeleton belongs to a young male individual – about 20-25 years old. He was buried in a dorsal – lateral position. He had a slightly inclined and high forehead. The three long bones of the right upper limb are in one line, which indicates full flexion in the elbow joint. Both hands are gathered on the right next to the skull, with palms outstretched (due to the specific spatial arrangement of the phalanges at the

base of the skull). At the level of the chest, numerous bone fragments (bone detritus) mixed with soil are observed, as well as parts of vertebrae and ribs. The pelvic halves and the vertebrae of the final cervical, thoracic and lumbar regions are missing. In the place where the pelvis should be, numerous longitudinal cortical plates were found, similar to the corticalis of the femur. In their lower part (below the knees) the two lower limbs were laid parallel to each other, laterally.

This is indicated by the location of the two fibulae and the fragments of the left tibia. At the most distal, mixed with a small pile of soil, several foot and forefoot bones were found, which I cannot identify.

When determining the height from the preserved fragment of the proximal tibia using the regression equation of G. Steele, it was found that the height of the individual during life was about 180 cm.

Conclusion

The 2004 archaeological investigations in the Kozluka area along the Trakia highway revealed a complex, multi-period ritual site functioning primarily as a pit sanctuary, with most features dated to the 5th–early 4th centuries BC [7,8]. Four grave pits near the village of Malko Tranovo provided valuable anthropological data, including five individuals representing different ages and burial types. The graves displayed diverse orientations and body positions, from extended supine to flexed (Hocker-like) forms, with several cases indicating bound limbs suggestive of ritualized funerary practices [13]. The associated ceramic assemblage, particularly the hand-made cup from Grave № 3, supports the attribution of the burials to the Early Iron Age.

The studies confirmed the known data on the rites in the pit sanctuaries, but also revealed new cult elements – large multi-component structures, pit-pits, graves and pits with fragments of earlier ceramics. In over 56 pits from the classical era, ceramic pieces from the Early Iron Age were found, probably as an expression of ancestor worship – a practice also known from the sanctuary at Koprivlen [3].

Despite partial post-depositional disturbance from agricultural activities of one of the skeletons, the bone remains of others preserved sufficient integrity for reliable interpretation. The evidence reflects complex funerary behavior and possible social differentiation within the Thracian cultural sphere.

Following the completion of the excavations, it was ascertained that the site constituted an extensive and significant pit sanctuary of high hierarchical status within the Thracian settlement network of the Upper Thracian Lowland during the 1st millennium BC. Stratigraphic and material evidence indicate prolonged and continuous utilization of the site, spanning from the Early Iron Age – possibly extending back to the Early Bronze Age – through to the Roman period. The assemblage of Early Iron Age ceramics provides a crucial empirical basis for further investigation into the cultural dynamics and developmental trajectories of the region. The presence of imported Greek pottery and amphorae from the 5th century BC offers valuable insights into socio-economic interactions and aspects of daily life within the early Odrysian polity. Conversely, the absence of material culture from the Hellenistic period implies a reconfiguration of the settlement pattern after the mid-4th century BC. The stratigraphic contexts associated with the Roman era further introduce interpretative challenges and stimulate scholarly

inquiry regarding their spatial and functional relationship with earlier structural phases. Overall, the Kozluka findings significantly enhance understanding of Early Iron Age burial customs and ritual traditions in southeastern Bulgaria [13].

References

1. **Alekseev, V.** Osteometry, methods of anthropological research. Moscow, Science, 1966. [In Russian]
2. **Bozhkova, A., K. Nikov**. Archaeological investigation of the site "Thracian Pit Sanctuary" in the land of the village of Malko Tranovo, Chirpan municipality (Site No. 10, LOT 1, "Trakia" Motorway), in 2004. – *Collection of reports from the XLIV National Archaeological Conference "Archaeological Discoveries and Excavations in 2004"*, Sofia 2005, pp. 94-97. [In Bulgarian]
3. **Bozhkova, A., P. Delev.** Archaeological monuments from the Middle Places. Monuments from prehistory and Thracian antiquity. – In: *Koprivlen vol. I, comp. A. Bozhkova, P. Delev*, Sofia, 2002, 39-49. [In Bulgaria]
4. **Bozhkova, A., K. Nikov.** Archaeological investigation of a complex of pits in the territory of the village of Malko Tranovo, Chirpan municipality – Southwestern sector. Preliminary notes. – In: *Georgieva, R., Stoyanov, T., Momchilov, D. (eds.) Southeastern Bulgaria in the 2nd–1st millennium BC. Varna, Zograf*, 2010, 213-220. [in Bulgarian]
5. **Yordanov, Y.** Handbook of Anthropology for Physicians and Dentists, Sofia, 1997. [in Bulgarian]
6. **Tonkova, M.** Results of the Research of the Eastern Sector of a Thracian Pit Sanctuary from the 5th to the Beginning of the 3rd Century BC. In the Kozluka District, Malko Tranovo Village, Municipality. Chirpan (site 11, LOT 1 according to the EIA of the Trakia Motorway). – In: *Southeast Bulgaria in the 2nd-1st millennium BC*, Varna, 2010, pp. 198-212, 208. [in Bulgarian]
7. **Tonkova, M., Z. Dimitrov.** Archaeological investigation of a Thracian pit sanctuary and a late Roman household in the Kozluka area, Malko Tranovo village, Chirpan municipality (site № 11 according to the Trakia Motorway, LOT 1). *Archaeological discoveries and excavations in 2004*. Sofia, 2005, 97-100. [in Bulgarian]
8. **Tonkova, M., I. Lozanov.** Rescue archaeological excavations of a Thracian pit sanctuary and a late Roman estate in the Kozluka area, Malko Tranovo village, Chirpan municipality (site № 11 along the route of Trakia Motorway, LOT 1). *Archaeological Discoveries and Excavations in 2003*. Sofia, 2004, 58-60. [in Bulgarian]
9. **Hillson S., C. Gigson, S. Bond.** Dental defects of congenital syphilis. – *American Journal of Biological Anthropology*, **107**(1), 1998, 25-40.
10. **Martin, R., K. Saller.** *Lehrbuch der Anthropologie* 2. Stuttgart: Gustav Fischer Verlag, 1959.
11. **Pearson, K.** Mathematical contributions to the theory of evolution.V. *On the reconstruction of the stature of prehistoric races*, 1899, pp. 169-175.
12. **Pearson, K.** Biometrika, 1901.5; *Index v.1-5; Suppl.* (1906-1907).
13. **Rouseva, V.** Anthropological peculiarities of the human bone remains from two diachronic pit complexes from the Iron Age (near Svilengrad and the village of Malko Tranovo, Chirpan community. – *Bulgarian e-Journal of Archaeology Supplements*, **10**, 2023, 177-186.
14. **Torbatov, S., K. Bachvarov, K. Nikov, A. Belivanova, P. Dimitrov.** Archaeological Discoveries and Excavations in 2004. – *XLIV National Conference on Archaeology*, Sofia **1**, 2005, pp. 94-97. [in Bulgarian]
15. **Trotter, M., G. C. Gleser.** Estimation of stature from long bones of American Whites and Negroes. – *Am. J. Phys. Anthropol*., **10**(4), 1952, 463-514.

Institute of Experimental Morphology, Pathology and Anthropology with Museum
Bulgarian Anatomical Society

Acta Morphologica et Anthropologica, 32 (3-4)
Sofia ● 2025

Review Articles

Isotopic Perspectives on Past Human Lifestyles: Methods, Applications, and Interpretations in Bioarchaeology

Tolga KÖROĞLU

Eberhard Karls Universitat Tübingen, Tübingen, Germany

*Corresponding author e-mail: tkoroglu1989@gmail.com

Abstract

Bioarchaeology integrates osteological and biochemical analyses to reconstruct various aspects of past human lifestyles, including diet, mobility, and social organization. Stable isotope analysis represents a key methodological approach, providing direct geochemical evidence for interpreting dietary habits and geographic origins. This paper reviews the principal methods and interpretative frameworks of isotopic research in bioarchaeology. Carbon ($\delta^{13}C$) and nitrogen ($\delta^{15}N$) isotopes are employed to distinguish dietary sources such as C_3 and C_4 plants, marine versus terrestrial foods, and trophic levels. Strontium ($^{87}Sr/^{86}Sr$) and oxygen ($\delta^{18}O$) isotopes serve as indicators of mobility and provenance, while sulfur ($\delta^{34}S$) and selected trace elements complement dietary and environmental assessments. The study highlights the main biological substrates bone collagen, dentin, and enamel and discusses essential analytical procedures, including IRMS and MC-ICP-MS. Case studies from Türkiye and other regions demonstrate how isotopic evidence contributes to a comprehensive understanding of economic systems and population dynamics in past societies.

Key words: Stable Isotope Analysis, Paleodiet, Paleomobility, Social Structure, Bioarchaeology.

Introduction

Bioarchaeology is an interdisciplinary field that investigates biological and cultural processes in the archaeological record through the analysis of human skeletal remains. By combining biological, cultural, and environmental perspectives, it reconstructs aspects of past human life such as diet, mobility, and social organization [37, 64]. Through these

approaches, bioarchaeology provides tangible evidence for understanding environmental adaptations, economic systems, and social hierarchies in ancient societies. Human skeletons thus serve not only as biological entities but also as biographical archives that reflect individual life histories and collective social structures.

Within this framework, stable isotope analysis has become a central methodological tool, offering direct geochemical evidence about diet, geographic origin, and environmental conditions. Isotopes of carbon ($\delta^{13}C$), nitrogen ($\delta^{15}N$), oxygen ($\delta^{18}O$), and strontium ($^{87}Sr/^{86}Sr$) extracted from human tissues enable the reconstruction of dietary patterns, mobility, and ecological contexts [58, 61]. Compared to indirect paleoenvironmental proxies such as sediments or tree rings, isotopic data provide information that can be directly linked to human activities [13].

Carbon and nitrogen isotope analyses of bone collagen and dental dentin allow the identification of dietary sources and trophic levels. $\delta^{13}C$ values differentiate between C_3 and C_4 plants and between marine and terrestrial food resources, while $\delta^{15}N$ values reflect protein intake and trophic position [1, 62]. These isotopic indicators reveal not only nutritional strategies but also broader aspects of economy and environmental adaptation among populations.

The analysis of strontium and oxygen isotopes provides complementary information on geographic origin and mobility. Strontium isotope ratios ($^{87}Sr/^{86}Sr$) mirror local geological signatures, while oxygen isotope values ($\delta^{18}O$) reflect climatic conditions and drinking-water sources [5]. Combined, they allow the identification of individuals who migrated between regions or experienced changes in living environments during their lifetime. Such data are crucial for understanding demographic movements, trade networks, and patterns of interaction within and between ancient communities.

Isotopic investigations also contribute to interpreting social structure and inequality. Variations in diet or mobility may correspond to differences in social status, gender, or occupation. For instance, isotope studies have demonstrated that elite individuals often consumed diets higher in trophic level proteins, while non-local individuals might exhibit distinct isotopic signatures linked to migration and integration processes [35]. When integrated with spatial and burial data, isotope evidence enhances interpretations of community organization and social stratification.

The development of isotope analysis in archaeology has its roots in mid-20th-century geochemical research. Early studies demonstrated that isotopic compositions in biological and geological materials reflected environmental conditions [75]. By the late 1970s and 1980s, pioneering work by Van der Merwe, Vogel, and Ambrose established the use of carbon and nitrogen isotopes in reconstructing human diets [77, 2]. Subsequently, isotopic methods expanded to explore geographic mobility through strontium and oxygen systems [16, 5]. In recent decades, isotope research has moved beyond subsistence and provenance studies to encompass social and cultural interpretations, such as migration, marriage exchange, and inequality [48].

Technological advancements have further broadened the analytical potential of isotope research. High-resolution instruments like Isotope Ratio Mass Spectrometry (IRMS) and Multi-Collector Inductively Coupled Plasma Mass Spectrometry (MC-ICP-MS) enable precise multi-isotope measurements. Incremental sampling methods, meanwhile, permit temporal reconstructions of individual life histories [58]. These innovations have consolidated isotope analysis as an indispensable component of archaeological science.

The present study synthesizes these methodological and interpretative developments, focusing on how isotope analyses inform key bioarchaeological themes diet, mobility, settlement patterns, and social organization. By integrating case studies from Türkiye and other regions, the paper aims to demonstrate how isotopic data can refine archaeological interpretations and illuminate the complex interplay between biological signals and cultural practices. Ultimately, isotope analysis has evolved from a purely methodological technique into an interdisciplinary research paradigm central to the holistic reconstruction of past human lives.

1. Isotopes Used in Human Skeletal Remains

In bioarchaeological research, the analysis of various isotopic systems preserved in human skeletal tissues has been shown to provide valuable insights into past diets, mobility, and environmental interactions. Each element proffers distinct yet complementary information. For instance, carbon and nitrogen isotopes primarily reflect dietary protein sources and trophic levels; oxygen and strontium record geographic and climatic signatures that inform on migration and provenance; while sulfur and lead isotopes contribute additional data on local ecology and exposure to anthropogenic or geological influences. The subsequent sections delineate the principles and interpretive potential of these major isotopic systems in the context of human skeletal remains. **Table 1** provides an overview of the main isotopic systems used in bioarchaeology, illustrating their analytical scope, interpretative value, and major limitations.

1.1. Carbon Isotopes

Carbon isotopes ($\delta^{13}C$) are among the most frequently employed indicators in the reconstruction of past societies' diets. This isotope displays marked variations based on the photosynthetic pathways of plants. C3 plants (e.g. wheat, barley, rice, many fruits and vegetables) are characterised by low δ13C values (approximately –35‰ to –20‰), while C4 plants (e.g. corn, millet, sorghum) have higher values (approximately –14‰ to –9‰). It is evident that these isotopic differences are directly reflected in human and animal tissues; as such, the analysis of the carbon isotope ($\delta^{13}C$) is a powerful tool with which to gain a greater understanding of agricultural strategies and dietary patterns [70, 79]. Furthermore, the analysis of carbon isotopes is of critical importance in the differentiation of marine and terrestrial sources. In terrestrial ecosystems, diets based on C3 plants in particular show lower δ13C values, while marine ecosystems are distinguished by richer carbon isotope values (~ –12‰). Consequently, the analysis of the stable isotope δ13C in human faeces provides a reliable indication of the relative proportion of marine sources in an individual's diet [9, 66]. From an archaeological perspective, the analysis of δ13C data provides insights into not only the dietary preferences of individuals but also the processes of agricultural diffusion, the dietary differences between coastal and inland communities, and the effects of social stratification on diet. For instance, the early adoption of corn cultivation in the Americas has been clearly documented through the use of δ13C analyses [79]. The analysis of δ13C data can provide a biochemical indicator for archaeological research, contributing to a comprehensive understanding of economic subsistence patterns and environmental adaptations.

1.2. Nitrogen Isotopes

Nitrogen isotopes ($\delta^{15}N$) are a fundamental indicator in dietary analysis, particularly for determining trophic levels and protein sources. As protein consumption is directly reflected in bone collagen, the $\delta^{15}N$ values of these bones are of critical importance in distinguishing between animal and plant-based proteins in an individual's diet. As demonstrated in the seminal study by Minagawa and Wada [46], there is an approximate 3–5‰ increase in the values of the delta-15N isotope at each trophic level in the food chain. This results in individuals consuming the meat of herbivorous animals or seafood having higher delta-15N values. Terrestrial ecosystems characteristically exhibit lower δ15N values, in contrast to the elevated levels observed in marine ecosystems, a phenomenon attributable to the extended duration of the food chain [66]. Consequently, the analysis of nitrogen isotopes ($\delta^{15}N$) is imperative in elucidating the extent to which coastal communities are reliant on seafood, as well as the significance of agricultural production and animal husbandry in the diet of terrestrial communities. Furthermore, the use of $\delta^{15}N$ values has been employed to evaluate the impact of cultural factors, including social stratification and gender roles, on dietary habits. For instance, elevated $\delta^{15}N$ levels among elites in certain societies suggest that their diets were rich in animal protein, particularly meat [26]. However, it should be noted that the $\delta^{15}N$ values are sensitive not only to diet but also to environmental factors. Variables such as fertiliser use in soil, climatic conditions, or water stress have been shown to affect the nitrogen isotope composition of plants [6]. These environmental factors can also affect human tissues indirectly. Analysis of nitrogen isotopes ($\delta^{15}N$) is a key method for understanding dietary intricacies, environmental adaptation and agricultural strategy in the past.

1.3. Oxygen Isotopes

Oxygen isotopes ($\delta^{18}O$) have been shown to provide significant insights into environmental conditions, climate variability, and the geographical origins of individuals in bioarchaeological research. In particular, oxygen isotope ratios in phosphate groups found in apatite reflect the isotopic composition of the water consumed by individuals throughout their lives [43, 45]. It is evident that the ingestion of water directly corresponds to the delta-18O values of precipitation. Consequently, deductions can be made concerning the climatic characteristics and geographical disparities in the environment in which the subjects inhabited. For instance, the study found that precipitation exhibited relatively elevated δ18O values at low latitudes and in warmer regions, while the opposite was observed at high latitudes, high altitudes, and in cold climates [11, 23]. In this context, the analysis of oxygen isotopes ($\delta^{18}O$) is a significant tool for determining not only the climatic environments of individuals but also for the study of migration and mobility. As posited by White et al. [81] and Bentley [5], discrepancies in the $\delta^{18}O$ values measured in different teeth or bone tissues of the same individual may suggest that they inhabited disparate geographical regions during their lifetimes. Furthermore, oxygen isotopes are known to reflect not only environmental information, but also the type of water sources; for example, it is well documented that river and lake waters typically carry $\delta^{18}O$ values derived from precipitation, while it is equally well documented that $\delta^{18}O$ values increase in areas close to seawater or in areas exposed to evaporation effects [65]. In bioarchaeology, δ18O analysis complements collagen nitrogen and carbon isotope analysis, helping us understand past climate and human mobility.

1.4. Strontium Isotopes

Strontium isotopes ($^{87}Sr/^{86}Sr$) are a geochemical tool frequently employed in archaeological studies of human and animal remains, particularly in mobility and geographic origin determination studies. The primary rationale for this phenomenon is that the distribution of strontium on Earth is directly related to the age and structure of the underlying geological strata. As Faure and Mensing [20] demonstrated, the $^{87}Sr/^{86}Sr$ ratio varies depending on the age of the rock, with different rock types and geological regions offering distinguishable isotopic signatures. This isotopic difference is transferred from soils to plants and then to human and animal tissues through the food chain. Consequently, the $^{87}Sr/^{86}Sr$ ratios measured in an individual's bones and teeth reflect the geological identity of the geography where they were fed and drank water throughout their life [5]. From a bioarchaeological perspective, it is imperative to recognise that different tissues are indicative of varying periods throughout an individual's lifespan. Tooth enamel, which is formed during childhood, provides permanent information about an individual's geographical origin during their early life. Conversely, bones, which are subject to a continuous process of remodelling, offer insights into mobility during the final 10–15 years of life [59]. This feature facilitates the determination of whether an individual has relocated during different stages of their life by comparing strontium values in teeth and bones. This facilitates a detailed examination of social phenomena, including migration, inter-community mobility of individuals through marriage, the utilisation of trade routes, and even the mobility strategies employed by elite classes. In the domain of archaeological research, strontium isotopes are frequently utilised in conjunction with oxygen isotopes to ensure the attainment of more reliable results. This is due to the fact that strontium analysis alone can be limited in some regions due to the presence of overlapping geological signals. However, when combined with the analysis of δ18O, the geographical origin of an individual can be determined with a greater degree of reliability, taking into account both climatic and geological variability [18]. Furthermore, the use of regional isotope maps, termed "isoscapes," enables the precise determination of the geographical origins of individuals and the timing of their migratory movements to different regions during their lifetimes. The significance of strontium isotopes in archaeology extends beyond the realm of individual mobility, encompassing the broader context of large-scale historical processes. To illustrate this point, consider the mobility of farmers throughout the Neolithic period in Europe, which has been thoroughly documented through 87Sr/86Sr analysis. This method has enabled the reconstruction of interactions with local hunter-gatherer communities and migration routes [5]. Furthermore, the migration of individuals from disparate regions of the Roman Empire to metropolitan areas has been elucidated through enamel strontium analyses [48]. Strontium isotopes have been identified as a scientific tool with the capacity to facilitate comprehension of both the life histories of individuals on a micro level and the processes of social and cultural change on a macro level.

1.5. Sulfur Isotopes

Sulfur isotopes ($\delta^{34}S$) are utilised as a complementary tool in bioarchaeological research to facilitate comprehension of diet and mobility. These elements provide a robust indicator, especially when distinguishing between marine and terrestrial protein sources. The isotopic composition of sulfates in marine environments exhibits higher

$\delta^{34}S$ values in comparison to terrestrial ecosystems; this allows individuals who consume marine products to be distinguished [63]. Furthermore, sulfur isotopes have been demonstrated to reflect regional environmental differences. For instance, individuals residing in coastal regions characteristically exhibit elevated $\delta^{34}S$ values, while those inhabiting inland areas frequently display diminished values. Consequently, sulfur isotopes offer insights into not only dietary patterns but also the geographical origins and potential migratory patterns of individuals [50]. Sulfur analysis in archaeological human remains is typically done on bone collagen. Combined with carbon and nitrogen isotope analyses, it can help show what people ate. $\delta^{34}S$ analysis is special because it can show how much marine protein was eaten. Sulfur isotopes are important for bioarchaeological studies because they can show dietary habits and how people adapted to their environment.

1.6. Lead Isotopes

Lead isotopes (Pb isotopes) represent a potent instrument in the domain of bioarchaeology, employed not primarily for the acquisition of direct dietary information but rather for the elucidation of individuals' geographic origins, environmental exposures, and relationships to human activities such as mining or metalworking. Lead isotope composition is specific to its geological source; Pb isotope ratios in rocks and ores from different regions are distinguishable [47]. This feature enables the measurement of Pb isotope ratios in human and animal remains, thereby facilitating the identification of the environmental sources to which individuals were exposed during their lifetimes and, consequently, their geographical origins. For instance, elevated levels of lead (Pb) and region-specific isotopic signatures have been identified in the bones and teeth of individuals inhabiting areas with intensive mining operations in ancient times [24]. In this context, the use of Pb isotopes in conjunction with strontium and oxygen isotopes in mobility studies has been shown to contribute to the determination of whether individuals migrated or resided in different regions [48]. Furthermore, lead isotopes play a critical role in understanding environmental pollution and toxic exposure in past societies. Lead used in water pipes during the Roman period left detectable isotopic traces in individuals' skeletons, thus providing insight into the discussion of environmental poisoning in ancient societies [60]. In summary, Pb isotope analyses are regarded as a multifaceted research instrument in bioarchaeology, encompassing geographical mobility and human-environment interactions.

1.7. Other Isotopes

In recent bioarchaeological research, the use of hydrogen isotopes (δD or $\delta 2H$) has increased. As Ehleringer et al. [14] demonstrate, hydrogen isotopes are essentially linked to drinking water sources and are therefore considered a powerful complementary factor in determining geographical origin. This phenomenon can be attributed to the fact that the δD value of precipitation is subject to variation in accordance with climatic factors, including latitude, altitude, and distance from the coast. The analysis of hydrogen isotope values in biological tissues, such as tooth enamel and hair, has been demonstrated to yield insights into the climate region in which an individual resided. When utilised in conjunction with $\delta 18O$, particularly within the context of migration and mobility studies, they facilitate the discernment of climatic and environmental variations.

Another development is the isotope analysis of elements such as calcium ($\delta^{44/42}$Ca) and barium (Ba/Ca ratios). Calcium isotopes have been demonstrated to be directly linked to individuals' mineral metabolism [74], and are utilised, particularly in weaning studies, to track childhood nutrition. Barium, too, has been observed to demonstrate distinct isotopic changes during the transition from breast milk to a normal diet. Studying Ca and Ba isotopes offers new insights into the health, growth and life cycles of historical communities.

Furthermore, the use of zinc isotopes (δ^{66}Zn) has become a significant tool in the reconstruction of dietary habits in recent years. Zinc isotope ratios have been shown to be sensitive to trophic levels and can be used to distinguish between carnivorous, herbivorous, and omnivorous diets [33]. This provides a valuable additional data source, especially when carbon and nitrogen isotopes are limited (e.g., when comparing communities consuming similar resources within the same ecosystem).

It has been established through further research that iron (Fe) and copper (Cu) isotopes are associated with metabolism, nutrition, and health status. For instance, the monitoring of health issues such as anaemia or iron deficiency is facilitated by iron isotopes, while the analysis of differences in the food chain is enabled by copper isotopes [31]. These isotope systems are still in the process of becoming widespread in bioarchaeology; however, due to their direct linkage to human metabolism and health biochemistry, it is anticipated that their utilisation will be more prevalent in the future.

Table 1 Comparative overview of major isotope measurement techniques used in bioarchaeology

2. Sample Types

2.1. Dental Enamel

Dental enamel is a frequently utilised sample type in the domain of archaeological isotope analysis. The primary rationale for this phenomenon pertains to the high mineralisation level and absence of organic matter characteristic of enamel, which renders it highly resistant to decay. This characteristic renders enamel one of the most resistant biological tissues to both diagenetic (environmental change-related) deterioration during burial and post-depositional chemical processes [41]. Consequently, tooth enamel is regarded as a reliable source for the analysis of oxygen (δ^{18}O) and strontium (^{87}Sr/^{86}Sr) isotopes. Tooth enamel begins to mineralise during early childhood and does not undergo biological reshaping after this process is complete. This property is attributed to the capacity of tooth enamel to serve as a "fixed record" of the individual's childhood nutrition and environmental conditions, as previously described by Hillson [28]. For instance, while analyses of oxygen isotopes (δ^{18}O) reflect the isotopic composition of drinking water and provide information about the climatic and geographical characteristics of the region where the individual resided [43], strontium isotopes carry traces of the geological strata in the region where the individual resided [5].

Furthermore, analyses of carbonate (δ^{13}C) in enamel provide indirect insights into dietary patterns. The carbonate fraction has been demonstrated to be a reliable indicator of C3 and C4 plant consumption patterns, as it reflects the carbon isotope composition of the nutrients metabolically processed by the individual [39]. However, it should be noted that, in contrast to collagen, carbonate does not directly reflect the

Table 1 Comparative overview of major isotope measurement techniques used in bioarchaeology

Technique	Sample type	Target isotopes / elements	Analytical method	Information provided	Main limitations
Carbon ($\delta^{13}C$)	Bone collagen, dentin, enamel carbonate	$^{13}C/^{12}C$	IRMS	Differentiates C_3 and C_4 plant consumption; distinguishes marine vs terrestrial diets	Requires well-preserved collagen; subject to diagenetic alteration
Nitrogen ($\delta^{15}N$)	Bone collagen, dentin	$^{15}N/^{14}N$	IRMS	Indicates trophic level and main protein source	Influenced by physiological stress and environmental variability
Oxygen ($\delta^{18}O$)	Tooth enamel carbonate and phosphate	$^{18}O/^{16}O$	IRMS	Reflects local drinking water composition and paleoclimate; used in mobility studies	Affected by temperature shifts and water isotope variability
Strontium ($^{87}Sr/^{86}Sr$)	Tooth enamel, bone	$^{87}Sr/^{86}Sr$	MC-ICP-MS	Identifies geographic origin and migration patterns based on local geology	Requires detailed baseline data; post-depositional contamination possible
Sulfur ($\delta^{34}S$)	Bone collagen, hair, keratin	$^{34}S/^{32}S$	IRMS	Differentiates marine and terrestrial protein sources; supports mobility and diet reconstruction	Sensitive to diagenetic and environmental sulfur variation
Lead (Pb isotopes)	Bone, enamel	^{206}Pb, ^{207}Pb, ^{208}Pb	MC-ICP-MS	Traces exposure to metal sources; reflects industrial or geological background	Contamination risk; complex interpretive framework
Trace elements (e.g., Zn, Ca, Ba)	Bone, enamel	Elemental ratios	ICP-MS	Supplements isotope data in dietary and environmental reconstruction	Strongly affected by diagenesis; indirect dietary indicator

protein source, but rather indicates the overall nutritional signal. Consequently, enamel carbonate data are typically evaluated in conjunction with collagen data to perform a more comprehensive dietary reconstruction [2].

2.2. Dentin

Dental dentin is a critical biological record source for examining an individual's life history through isotope analysis. In contrast to enamel, which is predominantly composed of organic components, dentin contains both organic (particularly collagen) and inorganic elements. In this respect, dentin facilitates the analysis of both carbon ($\delta^{13}C$) and nitrogen ($\delta^{15}N$) isotopes, thereby revealing the dietary and nutritional patterns of individuals during the periods of childhood and adolescence with high resolution [69, 4]. Dentin samples are widely utilised in the assessment of individuals' dietary habits during early life stages, particularly due to the collagen fraction's capacity to provide reliable information regarding protein-based nutrition. The most significant attribute of dental dentin is its incremental (layered) growth. The accumulation of these tissues during dentinogenesis enables the separate storage of biochemical records reflecting distinct age periods within an individual. Consequently, the analysis of dentin using isotope techniques, such as micromilling or serial sampling, facilitates the tracking of dietary shifts and nutritional transitions across various life stages, from childhood to adolescence [3]. To illustrate this point, the weaning period, alterations in protein sources, or nutritional variations associated with social crises can be traced in meticulous detail through dentin isotope profiles.

Furthermore, dentin has been shown to be a reliable indicator of environmental stresses and nutritional deficiencies experienced during childhood. As posited by Fuller et al. [22], sudden increases or decreases in nitrogen isotope values have been shown to be indicative of metabolic stress or disease processes. Consequently, dentin functions not only as a biochemical archive of diet but also of health and stress factors. Dentin has been shown to be more fragile than enamel in post-burial processes and is more sensitive to diagenetic changes [34]. Samples must be carefully preserved and diagenetic tests conducted as part of dentin analysis. Dentin is a valuable sample type for isotope analysis as it provides unique information about an individual's early life.

2.3. Bone Collagen

Bone collagen is the most commonly used organic fraction in archaeological isotope analyses and is a critical source of information, particularly for carbon ($\delta^{13}C$) and nitrogen ($\delta^{15}N$) isotope analyses. It has been determined that collagen constitutes approximately 90% of the organic composition of bone and provides direct information about protein-based nutrition [1]. Consequently, through the analysis of bone collagen, the long-term dietary habits of individuals can be evaluated in detail, as well as the diversity of their food sources. The defining biological characteristic of bone tissue is its continuous remodelling. It is important to note that this process occurs at different rates in different bone types. For instance, the cortical part of long bones exhibits a slow metabolism, while bones such as ribs are subject to more rapid renewal. As a result, the isotope values obtained from collagen usually show the average dietary information for the final 10–20 years of a person's life [27]. This makes collagen a powerful tool for investigating the dietary habits of adults.

Carbon isotopes ($\delta^{13}C$) have been shown to reveal C_3/C_4 plant differentiation and the consumption ratios of marine/terrestrial food sources [12, 66]. Nitrogen isotopes

($\delta^{15}N$) have been demonstrated to reflect trophic level in the food chain and, in particular, animal protein consumption. Consequently, bone collagen is pivotal in comprehending the agricultural strategies employed by communities and their subsistence patterns, encompassing hunting-gathering, pastoralism, and mixed economies. Furthermore, increases in $\delta^{15}N$ values have been shown to indicate weaning processes in children or metabolic changes associated with environmental stress conditions [21]. However, diagenetic processes represent a significant limitation in the analysis of collagen. It is hypothesised that organic molecules may undergo degradation as a consequence of the burial conditions to which they are subjected, with the result that the isotopic signal may be compromised. As a result, quality control standards such as the C: N ratio are often used to judge the preservation state of collagen. In well-preserved samples, this ratio is expected to fall within the range of 2.9 to 3.6 [1, 77]. This criterion enhances the reliability of the obtained isotope data and prevents misinterpretation.

2.4. Appatite Carbonate Samples

Apatite carbonate, the inorganic component of bones and teeth, provides a valuable alternative to collagen for dietary reconstruction, in addition to the information collagen offers in isotope analyses. The carbonate ions embedded within hydroxyapatite crystals reflect the comprehensive traces of the foods consumed throughout an individual's lifetime. While collagen, the organic fraction, essentially represents protein sources, the carbonate portion of apatite reveals a broader dietary spectrum encompassing all macronutrient groups, including carbohydrates and lipids [39, 2]. Consequently, the δ13C values obtained from apatite are pivotal in determining agricultural consumption and different energy sources. A notable benefit of apatite carbonate is its dual presence in both bones and teeth. Bone apatites have been shown to represent the diet of adults in the last decades of their lives on account of the continuous biological transformation (remodelling) they undergo [71]. Conversely, the crystal structure of apatite in tooth enamel undergoes mineralisation during development and remains biologically unchanged thereafter. This feature provides a reliable record of the foods consumed during childhood through enamel apatite [83].

Isotope data obtained from apatite carbonate are generally based on $\delta^{13}C$ analyses. These values provide a collagen-independent control for determining C3/C4 plant consumption ratios and are particularly helpful in understanding the energy contribution of different food groups [41]. For instance, while collagen is indicative of a collagen-protein-rich diet, the δ13C signal from apatite may offer a more precise reflection of the consumption of plant sources such as grains and starch. Consequently, a combined evaluation of these fractions facilitates a more comprehensive interpretation of the diet. Furthermore, it has been demonstrated that apatite is subject to limitations in terms of its resistance to diagenetic changes. In comparison with collagen, it has been shown that the inorganic structure of apatite is more susceptible to such changes, and this is dependent upon the burial conditions [36, 51]. In particular, the processes of dissolution or recrystallization in groundwater have the potential to distort the original isotopic signal of apatite. Therefore, quality control methodologies that verify crystal structure, such as Fourier transform infrared spectroscopy (FTIR), are widely used to ensure the reliability of data obtained from apatite [71].

2.5. Post-cremation Isotope Analysis

Despite the fact that cremation was a widespread component of funeral practices within various communities during both the ancient and medieval periods, it nevertheless imposes considerable constraints on the feasibility of conducting isotope analysis. It has been established that elevated temperatures, ranging from 600 to 900 degrees Celsius, result in the complete combustion and destruction of the organic fraction, including components such as bone collagen. Thus, conventional diet analyses based on carbon and nitrogen isotopes are largely unfeasible [78]. However, it should be noted that not all biochemical information is necessarily lost; the inorganic fraction, namely the carbonate and phosphate components of apatite, is often partially preserved. Appropriate processing methodologies can be used to extract paleoenvironmental and biogeographic insights from both carbon and oxygen isotopes within these structures [83].

Furthermore, the degree of cremation is a pivotal factor in the success of the analysis. It has been demonstrated that bones exposed to medium temperatures (approximately 300–500 °C) may undergo partial changes in isotopic fractions without compromising their structural integrity. In contrast, bones that have undergone high-temperature burning may exhibit microscopic recrystallization, a process that has the potential to distort the original isotopic signal [38]. As a result, investigators must first evaluate the trustworthiness of the information by carrying out mineralogical inspections, such as Fourier Transform Infrared Spectroscopy (FTIR) or X-ray diffraction (XRD), on burned remains [15].

In the domain of post-cremation studies, the isotopes strontium ($^{87}Sr/^{86}Sr$) and oxygen ($\delta^{18}O$) hold particular significance. This phenomenon can be attributed to the fact that these elements are embedded within the inorganic fraction, thereby retaining their traces even after the process of combustion. For instance, strontium analysis continues to serve as a reliable method for elucidating the geographic mobility of individuals; nevertheless, the implementation of comparative controls is imperative in light of the diagenetic effects engendered by cremation [25]. Furthermore, oxygen isotopes have been shown to be a reliable indicator of climatic and geographical conditions. However, it should be noted that the process of bone combustion can result in deviations from the expected values of the delta-18O ratio, primarily due to the loss of water from the bone during this process.

3. Methodological Approaches in Isotope Analysis

The reliability of isotope analyses in bioarchaeological research is contingent on the rigour of the methodological approaches applied. In this context, numerous stages play a critical role, from sampling strategies to laboratory preparation processes, measurement techniques to contamination control. Given that each biological tissue (bone collagen, dental dentin, dental enamel, carbonate fraction of apatite) possesses different biochemical properties, it is essential to select the most appropriate material and method for the research question being addressed [1, 39].

One of the most significant steps in the process of obtaining isotope samples from bioarchaeological material is the evaluation of the preservation status of said samples. In the context of archaeological environments, bones and teeth are subject to diagenetic processes, which have the capacity to degrade organic components and result in deviations from the original biological signals in terms of isotopic values [73].

Before sampling, the collagen's integrity is verified through microscopic examinations, Fourier-transform infrared spectroscopy (FTIR) analyses, and amino acid profile measurements. Similarly, surface cleaning procedures are imperative prior to laser ablation analyses on tooth enamel to remove environmental contaminants [47].

The standard method for carbon and nitrogen isotope analysis involves the extraction of collagen from human and animal bones. The protocols developed by Longin [42] and subsequently modified have enabled the isolation of the organic fraction (collagen) from bone. The process typically involves demineralisation of bone powder, removal of humic acids with an alkaline solution, and subsequent gelatinisation [7]. A carbonate content of less than 1% and a nitrogen expectation of 3–5% are considered to be indicative of well-preserved collagen, which is essential for the preservation of tissue integrity [1].

In the context of inorganic fraction analyses, the carbonate portion of apatite is targeted. Apatite carbonate, while an additional source of carbon isotopes, is more susceptible to diagenetic alteration [68]. In final, results obtained without testing the preservation of the crystal structure using XRD (X-ray Diffraction) or FTIR analysis are not considered reliable.

Dental dentin and enamel are unique in that they provide "time series" for different periods of life. Incremental sampling, utilising micro-milling or laser ablation techniques, facilitates high-resolution tracking of dietary and mobility changes during childhood and adolescence [4]. This methodology facilitates meticulous scrutiny of discrete phases within an individual's life history, including, but not limited to, weaning periods, migratory patterns, and periods of infirmity.

The most common method employed in the analysis of isotopes is Isotope Ratio Mass Spectrometry (IRMS). The measurement of gases (CO_2, N_2, SO_2), obtained from organic fractions, is conducted using an IRMS device. Subsequently, the calculation of $\delta^{13}C$, $\delta^{15}N$, and $\delta^{34}S$ values is undertaken [12]. Thermal Ionization Mass Spectrometry (TIMS) and, more commonly, Multi-Collector Inductively Coupled Plasma Mass Spectrometry (MC-ICP-MS) are utilised for the measurement of strontium, lead, and rare elements [5]. The precision of these methods is such that they can determine $^{87}Sr/^{86}Sr$ ratios with very low error margins (± 0.00001).

The most significant methodological challenge encountered in the analysis of archaeological samples pertains to the issue of contamination and diagenetic changes, which are primarily influenced by environmental factors. Carbonates from soil water, humic acids bound to collagen, or elements integrated into the phosphate structure have been shown to distort the original isotopic signal [72]. Therefore, it is recommended that samples undergo chemical pretreatment, be compared with reference modern samples, and that different tissues from the same individual be analysed for cross-checking purposes.

All isotope analyses are reported in accordance with international standards. The δ13C values are then normalised to Vienna Pee Dee Belemnite (VPDB), the δ15N values to Air-N2, the δ18O values to Vienna Standard Mean Ocean Water (VSMOW), the δ34S values to Canyon Diablo Troilite (CDT), and the strontium isotopes to the NIST SRM 987 standard [10]. This standardisation ensures the comparability of analyses performed in different laboratories and forms the basis of methodological reliability.

Isotope Measurement Techniques: The instruments employed in bioarchaeological isotope analysis are contingent on the specific isotope to be measured. Light element isotopes (e.g. carbon, nitrogen, oxygen, sulphur and hydrogen) are typically measured using Isotope Ratio Mass Spectrometry (IRMS), while heavy element isotopes (e.g. strontium, lead, neodymium, calcium and zinc) are measured using Thermal Ionization Mass Spectrometry (TIMS) or the more modern and accurate method, Multi-Collector Inductively Coupled Plasma Mass Spectrometry (MC-ICP-MS) [5, 10].

IRMS (Isotope Ratio Mass Spectrometry): Gas products (CO_2, N_2, SO_2, H2) obtained from organic fractions (collagen, keratin) are ionized, and their isotopic ratios (e.g. 13C/12C, 15N/14N) are measured. The device has been engineered to detect differences at the ppm level, with a documented accuracy of ±0.1‰. Thus, it is the most frequently employed device in paleodiet studies [12].

TIMS (Thermal Ionization Mass Spectrometry): This technique, whilst not the most contemporary, is one that has been demonstrated to be both dependable and effective in measuring the isotopic ratios of heavy elements. The sample is ionised on a heated filament and separated in a mass spectrometer. It has played a pioneering role in strontium isotope analysis, but due to the lengthy sample preparation and low throughput, it has largely been replaced by MC-ICP-MS today [20].

MC-ICP-MS (Multi-Collector Inductively Coupled Plasma Mass Spectrometry): The plasma environment is used to ionize the sample, with different isotope masses being measured simultaneously in multiple collectors. This method provides high precision (±0.00001) for elements such as Sr, Pb, Ca, and Zn and has become indispensable, especially in mobility studies [48]. Moreover, the necessity for reduced sample quantities represents a substantial benefit for archaeological material.

Sample Preparation and Preliminary Preparations: In the domain of isotope analysis, laboratory preparations are of paramount importance for the reliability of the results obtained, in equal measure to the sensitivity of the instruments utilised. In the preparation of collagen samples, a two-step procedure is employed. Initially, demineralization is carried out using hydrochloric acid, followed by the removal of humic acids through the use of sodium hydroxide. In the final stage, gelatinization is performed at temperatures ranging from 58 to 70°C. The preservation of collagen is determined by the %C, %N, and C/N ratio (3.2–3.6) [1, 7]. In the process of preparing apatite carbonate, organic and secondary carbonates are meticulously removed from the sample using a combination of NaOCl and acetic acid. The carbonate-phosphate ratio and crystallinity index are evaluated using Fourier-transform infrared spectroscopy (FTIR). High crystallinity is generally indicative of diagenetic alteration [67]. In the case of strontium/Pb, tooth enamel is micro-milled into powder. The substance is then dissolved in an acid solution, after which Sr or Pb ions are separated using selective chromatographic resins. This step is critical, especially in Sr isotope analysis, to prevent environmental contamination [5].

In recent years, the advent of sophisticated techniques in the analysis of isotopes has resulted in a paradigm shift within the domain of bioarchaeological research,

thereby introducing novel dimensions to the field. Laser Ablation (LA-MC-ICP-MS) has been instrumental in facilitating micro-scale incremental analysis of tooth enamel or bone. This methodology enables the identification of fluctuations in migration, disease, or dietary patterns over time [47]. In dual isotope approaches, the combination of δ13C–δ15N provides more reliable results regarding diet, while the combination of δ18O–87Sr offers insights into mobility. The combination of δ34S–δ13C provides insights into the marine versus terrestrial sources of nutrition [62]. New biomarker isotopes, including zinc (Zn) and calcium (Ca) isotopes, have recently emerged as a means to determine predator-herbivore separation or plant/animal protein consumption ratios [32]. This approach enables the execution of more detailed dietary interpretations that extend beyond the scope of classical C–N analyses.

Bioarchaeological Applications

Isotope analysis is a powerful research method that enables the understanding of biological, cultural and social processes through the analysis of archaeological human skeletons. In this context, the primary research areas include dietary reconstruction, determining mobility and migration movements, and analysing lifestyles related to social structure.

It is imperative to recognise that diet constitutes a pivotal parameter for comprehending the economic organisation, environmental adaptations, and social distinctions of bygone societies. Analyses based on carbon ($\delta^{13}C$) and nitrogen ($\delta^{15}N$) isotopes have been used to reveal the photosynthetic pathways (C_3/C_4) of the plants consumed by individuals, and thus determine their trophic levels in the food chain. For instance, the analysis of the isotope composition of European Neolithic societies indicates the predominant consumption of C3 plants such as wheat, barley, and legumes [2, 76], while the analysis of the isotope composition of agricultural societies in Central and South America shows that C4 plants such as corn were the primary food source [76]. Conversely, analyses of nitrogen isotopes have facilitated the differentiation of diets derived from marine sources and those originating from terrestrial sources. This provides substantial evidence that these distinctions mirrored social and economic transformations, particularly during the transition from the Mesolithic to the Neolithic era [63].

Strontium ($^{87}Sr/^{86}Sr$) and oxygen ($\delta^{18}O$) isotope analyses are utilised to elucidate individuals' exposure to disparate geographical environments throughout their lifetimes and potential migratory movements. It is evident that data obtained from tooth enamel offers a unique identifier of an individual's geographical origin during childhood. Sr and O isotope analyses conducted on individuals buried near Stonehenge in England have shown that these people came from outside the British Isles in the early stages of their lives, reflecting labour mobility in monumental architecture [19]. Analyses of cemeteries from the Roman and Byzantine periods have revealed the biological traces of inter-imperial migration and urbanisation, thereby contributing to a more concrete documentation of social diversity [47].

Isotope analysis has been demonstrated to reflect not only environmental adaptations but also differences in social structure. When compared with parameters such as dietary differences, gender, age, social status, or ethnic identity, traces of hierarchical structures in past societies can be seen. For instance, isotope analysis of individuals with high social status in Maya societies revealed a greater consumption of corn and seafood compared to individuals with lower status [80]. In medieval European

urban societies, significant dietary disparities were observed between monastic individuals and the lay population, a phenomenon attributed to religious directives and social constraints [49].

The examples presented illustrate the effectiveness of isotope analysis as a tool for understanding a variety of phenomena, such as biological processes, social organisation, economic systems, and cultural preferences. As a result, when assessed in an archaeological context with material culture, isotope information allows for a thorough comprehension of the habits of ancient human societies.

The Neolithic Revolution is widely regarded as one of the most significant economic and social transformations in the history of humankind. The transition from hunter-gatherer strategies to agriculture during this period can be directly traced through isotope analysis. Carbon ($\delta^{13}C$) and nitrogen ($\delta^{15}N$) isotope analyses conducted in Europe demonstrate that hunter-gatherer societies maintained a diet comprising marine and hunter-gatherer food sources with elevated $\delta^{15}N$ values [61]. In Neolithic agricultural societies, an analysis of δ13C values indicates a transition to a diet comprising C3 plants, accompanied by a significant decrease in δ15N values. This change is indicative not only of the transformation of the economic system, but also of the diversification of food sources and the contribution of animal husbandry to social organisation.

The vast geography and multicultural structure of the Roman Empire renders it a significant case study for research into mobility. Strontium ($^{87}Sr/^{86}Sr$) and oxygen ($\delta^{18}O$) isotope analyses conducted on cemeteries from the Roman period have enabled the biochemical identification of individuals who migrated to the empire's major cities [17]. For instance, analyses conducted at the Casal Bertone cemetery in Rome revealed that some individuals came from outside Italy, providing strong evidence of the city's cosmopolitan structure [47]. The findings of this study illuminate not only the phenomenon of population movements but also the social dynamics associated with labour, military campaigns, and trade within the empire.

Isotope analysis of medieval European remains has provided biochemical evidence indicative of social differences. A comparative analysis of monastic and lay cemeteries in England revealed distinct differences in the isotope values of carbon and nitrogen. As Müldner and Richards [49] observed, low $\delta^{15}N$ values were detected in monastic communities due to limited meat consumption, while higher protein consumption was observed among the lay population. This discrepancy is indicative of the influence of religious doctrine on day-to-day life and the manner in which dietary practices have contributed to the formation of social structures.

Carbon and nitrogen isotope analyses conducted in Maya societies in Mesoamerica reveal how social stratification was reflected through diet. The δ13C values of the elite classes indicate a high consumption of maize (a C4 plant) and a greater inclusion of marine products in their diet [80]. Conversely, the general populace adhered to a dietary regime comprising primarily C3 plants and land animals. This discrepancy suggests that economic power was not the sole factor influencing the dietary choices of the elite; religious rituals and ideological systems also played a significant role.

Türkiye boasts a rich archaeological heritage, spanning from the prehistoric era to the Byzantine period. Isotope analysis is a pivotal tool in understanding dietary habits, mobility patterns, and social structures during this historical era. Carbon ($\delta^{13}C$) and nitrogen ($\delta^{15}N$) isotope analyses conducted on Neolithic settlements, particularly

at centres such as Çatalhöyük and Aşıklı Höyük, demonstrate that the diets of these societies were predominantly based on C3 plants (e.g. wheat, barley, legumes) and that animal protein consumption was limited [56, 2]. The data presented herein provide direct evidence of the economic and social dimensions of the transition to Neolithic agriculture.

Table 2. Isotope analysis studies conducted on Anatolian archaeological societies

Archaeological Period	Site / Region	Main Isotopes Analysed	Key Findings (Diet, Mobility, Weaning)	References
Neolithic	Çatalhöyük (Central Anatolia)	$\delta^{13}C$, $\delta^{15}N$	C_3-based terrestrial diets; moderate animal protein; infant $\delta^{15}N$ elevation indicating breastfeeding; weaning generally completed around 2.5-3 years.	Richards et al. 2003; Pearson et al. 2015
Neolithic	Aşıklı Höyük & Çayönü	$\delta^{13}C$, $\delta^{15}N$	Breastfeeding detectable through $\delta^{15}N$ enrichment; weaning estimated at ~1–2 years for Aşıklı and ~2–3.5 years for Çayönü.	Pearson et al. 2015
Neolithic–Chalcolithic	Tepecik-Çiftlik	$\delta^{13}C$, $\delta^{15}N$	Very early weaning (0.2–1.3 years); C_3-based plant diets; limited high-trophic protein.	Özdemir et al. 2024
Late Neolithic–Chalcolithic	Aktopraklık (NW Anatolia)	$\delta^{13}C$, $\delta^{15}N$	Late weaning (>3–4 years in some contexts); evidence for subsistence diversification.	Budd et al. 2013
Late Chalcolithic – Early Bronze Age	İkiztepe (Black Sea region)	$\delta^{13}C$, $\delta^{15}N$, $\delta^{34}S$	Weaning beginning at 1–1.5 years and ending ~2.25 years; mainly C_3 terrestrial diet; limited marine protein despite coastal location.	Özdemir et al. 2019; Irvine & Erdal 2020
Early–Middle Bronze Age	Kültepe (Central Anatolia)	$\delta^{13}C$, $\delta^{15}N$	Weaning begins at ~1–1.5 years, ends ~3 years; exclusively C_3 terrestrial foods; isotopic data match textual evidence on childcare and wet-nursing.	Özdemir et al. 2025
Middle–Late Bronze Age	Alalakh (Hatay)	$^{87}Sr/^{86}Sr$, $\delta^{18}O$	Clear local vs non-local differentiation; substantial human mobility consistent with trade networks of the Levant–Anatolia corridor.	Ingman et al. 2021

Roman	Ephesus (Gladiator Cemetery)	$\delta^{13}C$, $\delta^{15}N$, $\delta^{34}S$	Distinct diet groups; mostly C_3 terrestrial diet; sulfur values show limited marine input; social stratification detectable isotopically.	Lösch et al. 2014
Roman–Byzantine	Hierapolis (SW Anatolia)	$^{87}Sr/^{86}Sr$, $\delta^{18}O$	Mostly local individuals; a subset of immigrants, especially in Byzantine layers—consistent with pilgrimage and regional mobility.	Wong et al. 2018
Byzantine	Kovuklukaya (Sinop)	$\delta^{13}C$, $\delta^{15}N$ (+ AA-specific data)	C_3 diets with modest C_4 contribution (millet); $\delta^{15}N$ shows limited marine input despite Black Sea proximity.	Özdemir et al. 2025

Research on stable isotopes in Anatolia and the Near East has documented a long-term stability of C_3-dominated terrestrial diets, versatile mobility, and culturally based weaning in the region over thousands of years. Neolithic settlements including Çatalhöyük, Aşıklı Höyük, and Çayönü provide clear $\delta^{15}N$-based evidence of breastfeeding, and on average weaning occurred between 2 and 3.5 years of age [52, 56, 62]. In contrast, the site of Tepecik-Çiftlik noted remarkably early weaning (0.2–1.3 years) which likely reflects ecological or cultural circumstances [52]. Late Chalcolithic and Early Bronze Ages settlements, such as Aktopraklık and İkiztepe, display an overall pattern of heterogeneous weaning, from early weaning (~1.5 years) to later weaning (>4 years) [8, 53]. Within the general pattern of changing weaning, Kültepe provides one of the best datasets for isotopic evidence of weaning practices, where $\delta^{13}C$ and $\delta^{15}N$ values demonstrate a regular process of weaning beginning c. 1–1.5 years, ending around 3 years of age, and correlating closely with textual evidence pertaining to wet nurses, child care, and household labor [54]. The mobility indicators in the Bronze and Iron Ages (Alalakh to Van and the later Roman-Byzantine Hierapolis) indicate that Anatolia was a pathway for constant migration. Dietary reconstructions of infants from Ephesus and Sinop further represent potential social and geographical variation in protein source of Terrestrial diets with C_3 [29, 30, 44, 55, 82]. Overall, these datasets support that as infant feeding strategies, diet compositions, and mobility were happening concurrently and in relation to an evolving economic structure and urbanization, as well as interregional interactions, Kültepe remains important for assessing childhood, diet, and cultural practice in early complex societies of Anatolia.

Conclusion

Isotope analysis of archaeological human skeletons provides comprehensive information about the lifestyles of past communities. Carbon and nitrogen isotopes have been shown to reveal the basic character of the diet, while strontium and oxygen

isotopes have been demonstrated to provide direct evidence about individuals' lifelong mobility and migration movements. Isotopes such as sulfur and lead provide additional information, particularly about protein sources and environmental interactions, illuminating the ecological context of diets and lifestyles.

The isotopic studies conducted across Anatolia on Neolithic farming villages, complex Bronze Age trade centers, and later Byzantine urban contexts reveal that diet and mobility were assimilated into the economic and social strategies of each time period. Variation in $\delta^{13}C$, $\delta^{15}N$ and strontium–oxygen signatures illustrates how access to food resources, exposure to different ecological zones, and participation in regional networks were influenced by the social status of the individual, household labor, and broader political arrangements. High and low-status groups frequently consumed different types of protein, or resources drawn from different locations, and individuals with non-local isotopic signatures indicate long-distance movement, interregional exchange, and cultural integration. The patterns identified in this study therefore extend beyond the biochemical signatures of individuals; rather, they reflect how communities organized labor, created and maintained social hierarchies, formed external connections, and practiced adaptability to changing environments. In this regard, isotopic evidence is a powerful lens in which to view the more holistic economic, cultural, and demographic processes of ancient Anatolian societies.

Methodologically, the combined use of different tissues (bone collagen, dental dentin, dental enamel, carbonate in apatite) allows for detailed tracking of an individual's lifetime diet and migration movements. However, limitations such as post-mortem changes, tooth wear, and environmental effects must be considered. The reliability of the results is increased by the interpretation of isotope analyses in conjunction with archaeological context and other paleoecological data.

References

1. **Ambrose, S. H.** Preparation and characterization of bone and tooth collagen for isotopic analysis. – *J. Archaeol. Sci.*, **17(4)**, 1990, 431-451.
2. **Ambrose, S. H., L. Norr.** Experimental evidence for the relationship of the carbon isotope ratios of whole diet and dietary protein to those of bone collagen and carbonate. – In: *Prehistoric Human Bone: Archaeology at the Molecular Level* (Eds. J. B. Lambert, G. Grupe), Berlin; New York, Springer-Verlag, 1993, 1-37.
3. **Beaumont, J., J. Montgomery.** The great Irish famine: Identifying starvation in the tissues of victims using stable isotope analysis of bone and incremental dentine collagen. – *PLoS One*, **11(8)**, 2016, e0160065.
4. **Beaumont, J., A. Gledhill, J. Lee-Thorp, J. Montgomery.** Childhood diet: A closer examination of the evidence from dental tissues using stable isotope analysis of incremental human dentine. – *Archaeometry*, **55(2)**, 2013, 277-295.
5. **Bentley, R. A.** Strontium isotopes from the earth to the archaeological skeleton: A review. – *J. Archaeol. Method Theory*, **13(3)**, 2006, 135-187.
6. **Bogaard, A., T. H. E. Heaton, P. Poulton, I. Merbach.** The impact of manuring on nitrogen isotope ratios in cereals: Archaeological implications for reconstruction of diet and crop management practices. – *J. Archaeol. Sci.*, **34(3)**, 2007, 335-343.
7. **Brown, T. A., D. E. Nelson, J. S. Vogel, J. R. Southon.** Improved collagen extraction by modified Longin method. – *Radiocarbon*, **30(2)**, 1988, 171-177.

8. Budd, C., Lillie, M., Alpaslan-Roodenberg, S., Karul, N., Pinhasi, R. Stable isotope analysis of Neolithic and Chalcolithic populations from Aktopraklık, northern Anatolia. – *J. Archaeol. Sci.,* **40(2),** 2013, 860-867.
9. Chisholm, B. S., D. E. Nelson, H. P. Schwarcz. Stable-carbon isotope ratios as a measure of marine versus terrestrial protein in ancient diets. – *Science*, **216(4550)**, 1982, 1131-1132.
10. Coplen, T. B. Guidelines and recommended terms for expression of stable-isotope-ratio and gas-ratio measurement results. – *Rapid Commun. Mass Spectrom.*, **25(17)**, 2011, 2538-2560.
11. Dansgaard, W. Stable isotopes in precipitation. – *Tellus*, **16(4)**, 1964, 436–468.
12. DeNiro, M. J., S. Epstein. Influence of diet on the distribution of nitrogen isotopes in animals. – *Geochim. Cosmochim. Acta*, **45(3)**, 1981, 341–351.
13. Depaermentier, M. L. C., M. Kempf, M. Vander Linden, et al. Das paläoökologische Potenzial bioarchäologischer Isotopendaten. – *Commun. Earth Environ.*, **6**, 2025, 501. [in German]
14. Ehleringer, J. R., T. E. Cerling, M. D. Dearing. Stable isotopes and the environment. – In: *Stable Isotopes in Ecology and Environmental Science* (Eds. R. Michener, K. Lajtha), Oxford; Malden, MA; Carlton, Blackwell Publishing, 2008, 1-26.
15. Ellingham, S. T. D., T. J. U. Thompson, M. Islam, G. Taylor. Estimating temperature exposure of burnt bone – A methodological review. – *Sci. Justice*, **55(3)**, 2015, 181-188.
16. Ericson, J. E. Strontium isotope characterization in the study of prehistoric human ecology. – *J. Hum. Evol.*, **14(5)**, 1985, 503-514.
17. Emery, M. V., J. Montgomery, J. A. Evans. Mapping the origins of Imperial Roman workers (1st–4th centuries CE): Strontium and oxygen isotope evidence from the Vagnari cemetery, southern Italy. – *Am. J. Phys. Anthropol.*, **167(1)**, 2018, 11-22.
18. Evans, J. A., J. Montgomery, G. Wildman, N. Boulton. Isotopes in archaeology: The role of lead isotope analysis. – *Antiquity*, **86(332)**, 2012, 853-868.
19. Evans, J. A., N. Stoodley, C. A. Chenery. A strontium and oxygen isotope assessment of a possible fourth-century immigrant population in a Hampshire cemetery, southern England. – *J. Archaeol. Sci.*, **33(2)**, 2006, 265-272.
20. Faure, G., T. M. Mensing. *Isotopes: Principles and Applications.* – Hoboken, NJ, Wiley, 2005.
21. Fogel, M. L., N. Tuross, D. W. Owsley. Nitrogen isotope tracers of human lactation in modern and archaeological populations. – *Annual Report of the Director, Geophysical Laboratory, Carnegie Institution of Washington*, 1989, 111-117.
22. Fuller, B. T., J. L. Fuller, D. A. Harris, R. E. M. Hedges. Detection of breastfeeding and weaning in modern human infants with carbon and nitrogen stable isotope ratios. – *Am. J. Phys. Anthropol.*, **129(2)**, 2006, 279-293.
23. Gat, J. R. *Isotope Hydrology: A Study of the Water Cycle.* – London, Imperial College Press, 2010.
24. Gulson, B. L., D. S. Wilson. History of lead exposure in humans. – *Sci. Total Environ.*, **145(1-2)**, 1994, 1-7.
25. Harvig, L., N. Lynnerup, A. Fischer. Strontium isotope signals in cremated human remains: A pilot study. – *Archaeometry*, **56(3)**, 2014, 464-476.
26. Hedges, R. E. M., L. M. Reynard. Nitrogen isotopes and the trophic level of humans in archaeology. – *J. Archaeol. Sci.*, **34(8)**, 2007, 1240-1251.
27. Hedges, R. E. M., J. G. Clement, C. D. L. Thomas, T. C. O'Connell. Collagen turnover in the adult femoral mid-shaft: Modeled from anthropogenic radiocarbon tracer measurements. – *Am. J. Phys. Anthropol.*, **133(2)**, 2007, 808-816.
28. Hillson, S. *Dental Anthropology.* – Cambridge, Cambridge University Press, 1996.
29. Ingman, T., P. R. Duffy, L. Welton. Mobility and migration at Middle and Late Bronze Age Alalakh (Tell Atchana, Turkey): Strontium and oxygen isotope evidence. – *PLOS ONE*, **16(1),** 2021, e0241883.

30. Irvine, B., Erdal, Y. S. Analysis of dietary habits in a prehistoric coastal population from İkiztepe, North Turkey, using stable isotopes of Carbon, Nitrogen, and sulphur. – *J. Archaeol. Sci.: Reports*, **32**, 2020, 102067.
31. Jaouen, K., V. Balter. Menopause effect on bone δ66Zn: A new biomarker of bone loss? – *Metallomics*, **6(9)**, 2014, 1701-1709.
32. Jaouen, K., M.-L. Pons. Zinc isotopes as a dietary indicator: Historical perspectives and current state of knowledge. – *Am. J. Biol. Anthropol.*, **178 (S73)**, 2022, 118-133.
33. Jaouen, K., V. Balter, E. Herrscher. Zinc isotope evidence for dietary habits of Neandertals. – *Proc. Natl. Acad. Sci. U. S. A.*, **110(44)**, 2013, 17644-17649.
34. Katzenberg, M. A. Stable isotope analysis: A tool for studying past diet, demography, and life history. – In: *Biological Anthropology of the Human Skeleton* (Eds. M. A. Katzenberg, S. R. Saunders), Hoboken, NJ, Wiley, 2008.
35. Knipper, C., M. Fragata, N. Nicklisch, A. Siebert, A. Szécsényi-Nagy, V. Hubensack, C. Metzner-Nebelsick, et al. Central European mobility before and during the Bell Beaker phenomenon: Insights from strontium isotope data. – *PLoS One*, **12(12)**, 2017, e0188302.
36. Knudson, K. J., C. M. Stojanowski. New directions in bioarchaeology: Recent contributions to the study of human social identities. – *J. Archaeol. Res.*, **16(4)**, 2008, 397-432.
37. Larsen, C. S. *Bioarchaeology: Interpreting Behavior from the Human Skeleton.* – 2nd ed., Cambridge, Cambridge University Press, 2015.
38. LeGeros, R. Z. Calcium phosphates in oral biology and medicine. – *Monogr. Oral Sci.*, **15**, 1991, 1–201. Basel; New York, Karger.
39. Lee-Thorp, J. A. On isotopes and old bones. – In: *Stable Isotopes as Indicators of Ecological Change* (Eds. T. E. Dawson, R. T. W. Siegwolf), London; Burlington, MA, Academic Press, 2008, 113-132.
40. Lee-Thorp, J. A., M. Sponheimer. Three case studies used to reassess the reliability of fossil bone and enamel isotope signals for paleodietary studies. – *J. Anthropol. Archaeol.*, **22(3)**, 2003, 208-216.
41. Lee-Thorp, J. A., J. C. Sealy, N. J. van der Merwe. Stable carbon isotope ratio differences between bone collagen and bone apatite, and their relationship to diet. – *J. Archaeol. Sci.*, **16(6)**, 1989, 585-599.
42. Longin, R. New method of collagen extraction for radiocarbon dating. – *Nature*, **230(5291)**, 1971, 241-242.
43. Longinelli, A. Oxygen isotopes in mammal bone phosphate: A new tool for paleohydrological and paleoclimatological research? – *Geochim. Cosmochim. Acta*, **48(2)**, 1984, 385–390.
44. Lösch, S., Moghaddam, N., Grossschmidt, K., Risser, D. U., & Kanz, F. Stable isotope and trace element studies on the diet of a Roman gladiator group from Ephesus (Turkey). *PLOS ONE*, **9(10)**, 2014, e110489.
45. Luz, B., Y. Kolodny. Oxygen isotope variations in phosphate of biogenic apatites, IV. Mammal teeth and bones. – *Earth Planet. Sci. Lett.*, **75(1)**, 1985, 29–36.
46. Minagawa, M., E. Wada. Stepwise enrichment of 15N along food chains: Further evidence and the relation between δ15N and animal age. – *Geochim. Cosmochim. Acta*, **48(5)**, 1984, 1135-1140.
47. Montgomery, J. *Lead and strontium isotope compositions of human dental tissues as an indicator of ancient exposure and population dynamics* (Doctoral dissertation). – Bradford, University of Bradford, 2002.
48. Montgomery, J., J. A. Evans, T. Neighbour. Sr isotope evidence for population movement within the Hebridean Norse community of NW Scotland. – *J. Geol. Soc.*, **167(1)**, 2003, 11-22.
49. Müldner, G., M. P. Richards. Stable isotope evidence for 1500 years of human diet at the city of York, UK. – *Am. J. Phys. Anthropol.*, **133(1)**, 2007, 682-697.

50. Nehlich, O. The application of sulphur isotope analyses in archaeological research: A review. – *Earth-Sci. Rev.*, **142**, 2015, 1–17.
51. Nelson, K., H. W. Krueger, C. H. Sullivan. Carbon isotope fractionation between diet and bone in fossil hominids. – *Nature*, **322(6074)**, 1986, 822–823.
52. Özdemir, K., B. Irvine, T. Doğan, A. M. Büyükkarakaya, Y. G. Çakan, F. Kulak, E. Bıçakçı. A biogeochemical approach to examining sub-adult diet and the weaning process at Neolithic Tepecik-Çiftlik, Türkiye. – *J. Archaeol. Sci.: Reports*, **60,** 2024, 104848.
53. Özdemir, K., Y. S. Erdal, Y. Itahashi, B. Irvine. A multi-isotope approach to diet and weaning at İkiztepe. – *J. Archaeol. Sci.*, **108,** 2009, 104974.
54. Özdemir, K., B. Irvine, H. Üstündağ, C. Michel, T. Doğan, F., Kulak, F. Kulakoğlu. A stable isotopic and textual examination of the weaning process at Bronze Age Kültepe, Türkiye. – *J. Archaeol. Sci.: Reports,* 68, 2025, 105458.
55. Özdemir, K., Y. Itahashi, M. Yoneda, Y. S. Erdal. Diet and subsistence in Byzantine Sinop: A compound-specific isotope approach. – *Front. Environ. Arch.*, **4**, 2025, 1525886.
56. Pearson, J. A., R. E. M. Hedges, T. I. Molleson, M. Özbek. Exploring the relationship between weaning and infant mortality: An isotope case study from Anatolia. – *Am. J. Phys. Anthropol.*, **157(2)**, 2015, 234-247.
57. Pederzani, S., K. Britton. Oxygen isotopes in bioarchaeology: Principles and applications, challenges and opportunities. – *Earth-Sci. Rev.*, **188**, 2019, 77-107.
58. Price, T. D., J. H. Burton, R. A. Bentley. The characterization of biologically available strontium isotope ratios for the study of prehistoric migration. – *Archaeometry*, **44(1)**, 2002, 117-135.
59. Retief, F. P., L. Cilliers. Lead poisoning in ancient Rome. – *Acta Theol.*, **26(2)**, 2006, 147-164.
60. Richards, M. P., R. E. M. Hedges. Stable isotope evidence for similarities in the types of marine foods used by late Mesolithic humans at sites along the Atlantic coast of Europe. – *J. Archaeol. Sci.*, **26(2)**, 1999, 717-722.
61. Richards, M. P., B. T. Fuller, R. E. M. Hedges. Sulphur isotopic variation in ancient bone collagen from Europe: Implications for human palaeodiet, residence mobility, and radiocarbon dating. – *Earth Planet. Sci. Lett.*, **191(3-4)**, 2001, 185–190.
62. Richards, M. P., R. J. Schulting, R. E. M. Hedges. Sharp shift in diet at onset of Neolithic. – *Nature*, **425(6956)**, 2003, 366.
63. Roberts, C. *Human Remains in Archaeology: A Handbook.* – York, Council for British Archaeology, 2013.
64. Rozanski, K., L. Araguás-Araguás, R. Gonfiantini. Isotopic patterns in modern global precipitation. – In: *Climate Change in Continental Isotopic Records* (Eds. P. K. Swart, K. C. Lohmann, J. McKenzie, S. Savin), Washington, DC, American Geophysical Union, 1993, 1-36.
65. Schoeninger, M. J., M. J. DeNiro. Nitrogen and carbon isotopic composition of bone collagen from marine and terrestrial animals. – *Geochim. Cosmochim. Acta*, **48(4)**, 1984, 625-639.
66. Schoeninger, M. J., K. Moore. Bone stable isotope studies in archaeology. – *J. World Prehist.*, **6(2)**, 1992, 247-296.
67. Schoop, U. D., S. Riehl, A. Brysbaert. The archaeology of Anatolia: Recent discoveries. – *J. Archaeol. Res.*, **27(1)**, 2019, 1-54.
68. Sealy, J., N. J. van der Merwe, J. A. Lee-Thorp, J. L. Lanham. Nitrogen isotope ecology in southern Africa: Implications for environmental and dietary tracing. – *Geochim. Cosmochim. Acta*, **49(7)**, 1995, 1525-1531.
69. Smith, B. N., S. Epstein. Two categories of 13C/12C ratios for higher plants. – *Plant Physiol.*, **47(3)**, 1971, 380-384.

70. Sponheimer, M., J. A. Lee-Thorp. The oxygen isotope composition of mammalian enamel carbonate from South Africa: A clue to seasonality in palaeoenvironments? – *J. Archaeol. Sci.*, **28(9)**, 2001, 973-982.
71. Trueman, C. N., K. Privat, J. Field. Why do crystallinity values fail to predict the extent of diagenetic alteration of bone mineral? – *Palaeogeogr. Palaeoclimatol. Palaeoecol.*, **266(3-4)**, 2008, 160-167.
72. Tuross, N. The biochemistry of ancient DNA in bone. – *Experientia*, **50(6)**, 1994, 530-535.
73. Tütken, T., T. W. Vennemann, H.-U. Pfretzschner. Fossil bones and teeth as proxies for seasonality reconstruction in terrestrial ecosystems. – *Palaeogeogr. Palaeoclimatol. Palaeoecol.*, **373**, 2013, 1-16.
74. Urey, H. C., H. A. Lowenstam, S. Epstein, C. R. McKinney. Measurement of paleotemperatures and temperatures of the Upper Cretaceous of England, Denmark, and the southeastern United States. – *Geol. Soc. Am. Bull.*, **62(4)**, 1951, 399-416.
75. Van der Merwe, N. J., J. C. Vogel. 13C content of human collagen as a measure of prehistoric diet in woodland North America. – *Nature*, **276(5690)**, 1978, 815-816.
76. Van Klinken, G. J. Bone collagen quality indicators for palaeodietary and radiocarbon measurements. – *J. Archaeol. Sci.*, **26(6)**, 1999, 687-695.
77. Van Strydonck, M., M. Boudin, M. Hoefkens. 14C dating of cremated bones: The issue of sample contamination. – *Radiocarbon*, **47**, 2005, 27-40.
78. Vogel, J. C., N. J. van der Merwe. Isotopic evidence for early maize cultivation in New York State. – *Am. Antiq.*, **42(2)**, 1977, 238-242.
79. White, C. D., F. J. Longstaffe, K. R. Law. Reconstructing community life at Chichen Itza: Diet, mobility, and origins. – *J. Anthropol. Archaeol.*, **20(3)**, 2001, 341-360.
80. White, C. D., M. W. Spence, F. J. Longstaffe, K. R. Law. Testing the nature of Teotihuacan imperialism at Kaminaljuyu using stable isotope analysis. – *J. Anthropol. Res.*, **56(4)**, 2000, 535-558.
81. Wright, L. E., H. P. Schwarcz. Stable carbon and oxygen isotopes in human tooth enamel: Identifying breastfeeding and weaning in prehistory. – *Am. J. Phys. Anthropol.*, **106(1)**, 1998, 1-18.
82. Wong, M., Valentine, B., Afonso, C., Crowder, C., & Beckett, S. Strontium isotope analysis of human remains from ancient Hierapolis (Turkey): A study of mobility in a Greco-Roman city. – *J. Archaeol. Sci.: Reports,* **17**, 2018, 151-161.
83. Zazzo, A., J.-F. Saliège, A. Person, H. Boucher. Radiocarbon dating of calcined bones: Insights from combustion experiments under natural conditions. – *Radiocarbon*, **51(2)**, 2009, 647-654.

Institute of Experimental Morphology, Pathology and Anthropology with Museum
Bulgarian Anatomical Society

Acta Morphologica et Anthropologica, 32 (3-4)
Sofia ● 2025

Medico-Anthropological Characteristics of Flatfoot and Its Clinical Significance

*Atanas Katsarov**

Institute of Experimental Morphology, Pathology and Anthropology with Museum, Bulgarian Academy of Sciences, Sofia, Bulgaria

*Corresponding author e-mail: zanasko@gmail.com

Flatfoot (pes planus) is the reduction or collapse of the foot's medial longitudinal arch, with both clinical and anthropological significance. It may be flexible or rigid, congenital or acquired, and its prevalence varies by age, sex, body mass, footwear, and occupation. Anthropological studies reveal wide population differences, from under 5% in some European adults to over 20% in Asian and African groups. Clinically, flatfoot ranges from asymptomatic to causing pain, altered gait, and musculoskeletal problems. Diagnosis combines footprint indices, radiographs, and modern 3D scanning. From a medico-anthropological view, flatfoot reflects both evolutionary adaptation and a condition needing early recognition and management. Standardized diagnostic criteria and integration of anthropological insight are essential for accurate assessment and care.

Key words: foot, flatfoot, pes planus, anthropology, medial longitudinal arch, footprint analysis

Introduction

The human foot is an evolutionary innovation central to bipedal locomotion. Its complex skeletal and ligamentous architecture allows efficient propulsion, weight distribution, and shock absorption. A key element of this structure is the medial longitudinal arch, whose presence and height are often considered hallmarks of foot morphology.

Flatfoot, or pes planus, is defined as the reduction or collapse of the medial longitudinal arch of the foot, leading to excessive plantar surface contact with the ground [10]. It is among the most frequently observed morphological variants in human populations. While often benign, in some cases it contributes to pain, functional limitation, and predisposition to musculoskeletal disorders. From an anthropological perspective, flatfoot is an important marker of developmental and evolutionary variation [1, 21]. The human foot arch evolved as an adaptation to bipedal locomotion, and its collapse has both biomechanical and cultural implications. This paper provides a medicoanthropological review of flatfoot, focusing on diagnostic methods,

prevalence, and clinical significance. Recent studies highlight updated prevalence rates and functional impacts, such as reduced balance, agility, and core strength in young females [8], as well as prevalence data from Chinese adolescents [18].

Anthropometric approaches for study footprint

This review was conducted between January and July 2023 using PubMed, Scopus, and Web of Science. Search terms included 'flatfoot', 'pes planus', 'foot arch', 'footprint analysis', 'anthropometry', and 'epidemiology'. Reference lists were manually screened. Both English- and Bulgarian-language studies were considered. Studies included had to report prevalence, diagnostic criteria, or clinical outcomes. Exclusion criteria were case reports with fewer than 10 participants, surgical series without anthropometric data, and reports without clear definitions of flatfoot.

Data extracted included population characteristics, diagnostic methods used, prevalence, and clinical consequences. Anthropometric approaches primarily included footprint indices such as the, Staheli Arch Index (SAI), Chippaux – Smirak Index (CSI), and Clarke's Angle (CA) which remain widely used for their simplicity. Radiographic evaluation focused on the Calcaneal Pitch Angle, Meary's Angle, and the Talocalcaneal Angle, which are considered gold standards in clinical orthopedics. Modern methods such as 3D foot scanning, dynamic plantar pressure analysis, and gait analysis were also reviewed, providing detailed biomechanical insights but with limited availability for large-scale studies. Their methodological robustness has been reaffirmed in recent reviews [3], with studies showing correlations between CSI and clinical assessment [17].

The Staheli Arch Index (SAI) is obtained by dividing the minimum width of the midfoot by the maximum width of the heel in a footprint. Values greater than 1.0 are indicative of flatfoot. This index is especially useful in pediatric studies due to its simplicity, but it may overestimate prevalence in young children where the plantar fat pad obscures the arch (**Fig. 1**).

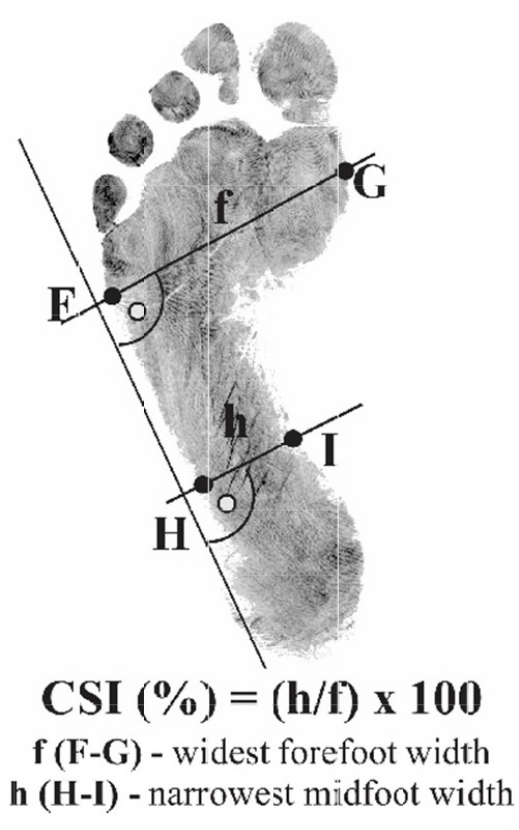

Fig. 1. Staheli Arch Index (SAI). The ratio of the minimum width of the midfoot to the maximum width of the heel; values >1.0 indicate flatfoot

Fig. 2. Chippaux–Smirak Index (CSI). Calculated as the ratio of the narrowest midfoot width (**h**) to the widest forefoot width (**f**) ×100; values >45% indicate flatfoot

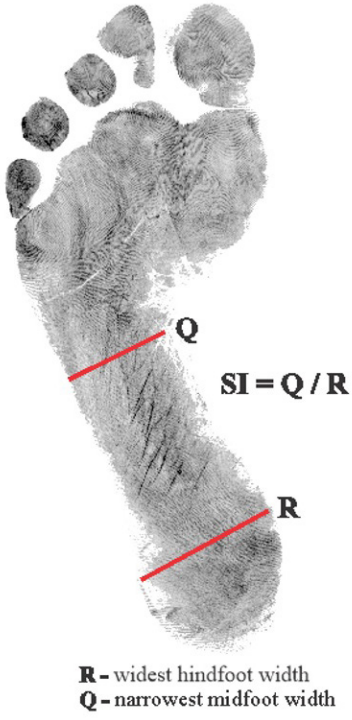

The Chippaux–Smirak Index (CSI) is calculated by dividing the narrowest width of the midfoot by the widest part of the forefoot, multiplied by 100. A value above 45% is diagnostic of flatfoot, while values below 25% suggest a high arch. This index is considered highly sensitive and reliable for epidemiological surveys **(Fig. 2**).

Clarke's Angle (CA) is formed by the intersection of a tangent drawn along the medial border of the footprint and a line connecting the most medial point of the forefoot to the heel. Angles less than 31° indicate flatfoot, while values greater than 45° indicate a high arch. This method is easy to apply in clinical practice but can be influenced by body weight and the position of the foot during measurement (**Fig. 3**).

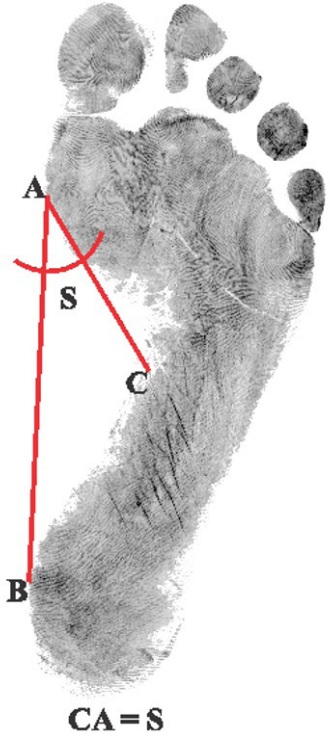

Fig. 3. Clarke's Angle

The review analyzed children and adolescents separately due to natural arch development, adults for persistence of flatfoot, and occupational groups such as military recruits and athletes where prevalence may be influenced by load-bearing demands. Barefoot versus shod populations were also compared, highlighting the role of culture and environment. Findings were synthesized from a medico anthropological perspective, integrating biological, cultural, and clinical insights.

Clinical Significance of flatfoot

Flatfoot prevalence was highest in early childhood, affecting 40–50% of children aged 2-5 years, largely due to the plantar fat pad and immature arches [14,23]. By 6–10 years, prevalence dropped

to 15-25%, and by adolescence stabilized at 10-15% [4, 7] **(Fig. 4).** In adulthood, prevalence was 2-6% in European cohorts and 13-20% in Asian populations [21, 13]. African barefoot populations showed prevalence below 5%, while urbanized, shod groups had higher rates, reaching up to 15% [15] (**Table 1**). Indigenous communities demonstrated naturally low arches without associated pathology, underscoring the importance of cultural context [19]. In addition, Shen et al. [18] reported a prevalence of approximately 5.5% among Chinese adolescents, with slightly higher rates in girls than boys. Birhanu et al. [18] observed a notable prevalence in Ethiopian children, highlighting regional differences. Giuca et al. [9] demonstrated correlations between severity of flatfoot and risk factors such as BMI and physical inactivity in children and adolescents.

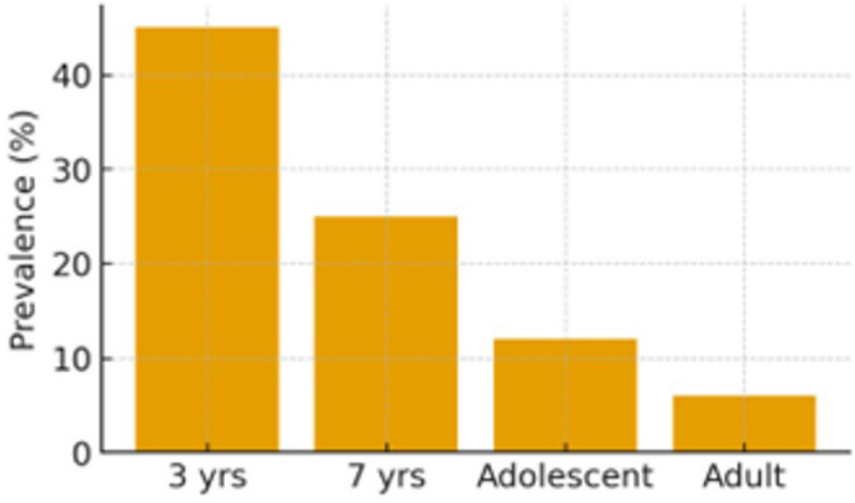

Fig. 4. Prevalence of Flatfoot Across Age Groups

Sex differences were inconsistently reported: some studies suggested higher prevalence in females, potentially linked to ligamentous laxity, but these often diminished after adjusting for BMI [13]. Overweight and obese individuals consistently demonstrated higher prevalence, reflecting mechanical overload of the medial arch [5,23]. Lifestyle also played a role: barefoot groups showed stronger arches, while urban, shod populations exhibited greater collapse [15] (**Table 1).** Occupational influences were significant. Military recruits showed prevalence of 10-20% due to load carriage and training demands [10]. Athletes displayed divergent patterns: runners and dancers had lower prevalence, likely due to strengthening of intrinsic muscles, while gymnasts and weightlifters had higher rates (12-20%) due to repetitive stress and ligamentous strain [16, 6]. Symptomatic flatfoot was associated with pain, altered gait, and higher risk of plantar fasciitis, tibialis posterior dysfunction, knee malalignment, and low back pain [4, 14, 23]. Recent evidence further emphasizes functional outcomes: Ghorbani et al. [8] reported that young females with flatfoot showed reduced balance, agility, and core strength. Yu et al. [24] found impaired jump height performance in athletes with flatfoot, while Jia et al. [11] demonstrated that exercise therapy could improve arch function in adults.

Table 1. Prevalence of flatfoot across populations and age groups.

Population	Prevalence (%)	Method	Notes
Children (2-5 yrs)	40–50	Footprint indices	Physiological flatfoot
Children (6-10 yrs)	15–25	Footprint indices	Arch development
Adolescents	10–15	Footprint + radiography	Mature arch
European adults	2–6	Radiographic	Lowest prevalence
Asian adults	13–20	Mixed	Higher prevalence
African barefoot	<5	Footprint	Protective effect
African urban	Up to 15	Mixed	Urban lifestyle risk
Military recruits	10–20	Radiographic + clinical	Load effects
Athletes (runners/ dancers)	2–8	Mixed	Protective sports
Athletes (gymnasts/ weightlifters)	12–20	Mixed	Stress-related risk

The findings confirm that flatfoot is largely developmental in children, with spontaneous resolution in many cases [7, 22]. Persistent flatfoot into adulthood, however, may indicate structural abnormality or predispose to clinical symptoms (**Fig. 4**). Evolutionary perspectives highlight the human arch as a recent adaptation for efficient bipedal locomotion [1, 21]. Barefoot populations demonstrate stronger arches and lower prevalence, while shod, urban groups exhibit higher rates [19, 15]. These findings emphasize the cultural and environmental role in foot morphology.

BMI and lifestyle strongly influence prevalence, with overweight individuals consistently more likely to present with flatfoot [5, 22]. Occupational load-bearing, such as in military service, is another strong predictor [10]. Athletic training demonstrates dual effects, with some sports protective and others predisposing. Symptomatic flatfoot is clinically relevant, associated with pain, altered gait, and comorbidities such as plantar fasciitis, posterior tibial tendon dysfunction, and back pain [4, 14, 22].

Methodological diversity complicates prevalence estimates. Footprint indices, radiographic parameters, and modern 3D measures often yield different thresholds, limiting cross-population comparison [20, 4] **(Table 2).** Standardization and creation of normative population-specific databases would improve both clinical and anthropological assessments. Preventive approaches should emphasize early detection, strengthening of intrinsic muscles, and culturally sensitive interventions. Footprint indices such as the SAI, CSI, and Clarke's Angle remain invaluable in large-scale anthropological surveys due to their low cost and ease of application. The CSI generally provides higher diagnostic accuracy, the SAI is most widely used in pediatric populations, and Clarke's Angle, while simple, can be subject to variability based on

foot posture and observer interpretation. For comprehensive evaluation, these indices are best applied in combination with radiographic or modern digital techniques. Recent studies confirmed their continued relevance and diagnostic value in both children and adults [12, 18, 11, 23, 8, 9].

From an anthropological perspective, flatfoot is not only a pathology but also a morphological variant reflecting the interplay of biology and culture.

From a public health standpoint, screening programs in school-aged children may allow early identification of persistent flatfoot, particularly in populations with high BMI or limited physical activity. Occupational health also requires attention: prevalence rates among military recruits remain elevated [10, 6], reinforcing the need for preventive conditioning and supportive footwear.

Clinically, however, recognition of risk factors and appropriate treatment are essential to prevent long-term disability.

Table 2. Diagnostic approaches for flatfoot

Method	Parameter	Threshold	Notes
Staheli Arch Index	Midfoot/heel width	>1.0	Anthropometric
Chippaux–Smirak Index	Midfoot/forefoot ratio	>45%	Anthropometric
Clarke's Angle	Medial footprint angle	<31°	Anthropometric
Calcaneal Pitch	Radiographic angle	<15°	Skeletal measure
Meary's Angle	Talus–metatarsal axis	>4° deviation	Structural collapse
Talocalcaneal Angle	Hindfoot alignment	Increased	Valgus correlation
3D Scanning	Arch height index	Low volume	High precision

Conclusion

Flatfoot represents both a normal morphological variant and a condition of clinical significance. In childhood, it is largely physiological and self-correcting, but persistent or adult flatfoot can result in pain, gait alteration, and secondary musculoskeletal problems. Its prevalence varies by age, sex, body weight, occupation, and culture, underscoring the combined influence of biology and environment. While barefoot populations tend to have stronger arches, urban lifestyles and overweight contribute to higher prevalence. Symptomatic flatfoot requires tailored management, ranging from conservative treatment to surgery. Methodological inconsistencies in diagnosis remain a challenge, highlighting the need for standardized criteria. Future research should focus on longitudinal studies, cross-cultural comparisons, and integration of digital imaging to refine understanding and improve prevention and treatment. By adopting a medico anthropological approach, clinicians and researchers can better appreciate the dual role of flatfoot as a reflection of human variation and as a clinical entity

requiring intervention. Recent studies underscore that beyond structural prevalence, functional consequences such as impaired balance, agility, and jump performance are clinically significant [23, 8]. Furthermore, regional surveys [18, 2, 9] highlight the variation of prevalence and risk factors across populations, while interventional research confirms that exercise therapy may improve arch stability and function [11]. These findings reinforce the importance of integrating preventive exercise programs, population-specific screening, and culturally adapted interventions into both clinical and anthropological practice.

References

1. **Aiello, L. C., C. Dean**. An Introduction to Human Evolutionary Anatomy. London: *Academic Press, Cambridge, MA*, 1990, pp. 507-538, ISBN 0120455900
2. **Birhanu, A., K. Nagarchi, F. Getahun, M. A. Gebremichael, H. Wondmagegn.** Magnitude of flat foot and its associated factors among school-aged children in Southern Ethiopia: an institution-based cross-sectional study. – *BMC Musculoskelet Disord*., **24**, 2023, 966. https://doi.org/10.1186/s12891-023-07082-6
3. **Carrasco, A. C., M. F. Silva, L. C. Guenka, C. T. Silva, F. A. Moura, et al.** Non-radiographic validity and reliability measures for assessing foot types: A systematic review. – *Foot Ankle Surg*., **27**(8), 2021, 839-850.
4. **Cavanagh, P. R., M. M. Rodgers.** The arch index: a useful measure from footprints. – *J. Biomech*., **20**(5), 1987, 547-551.
5. **Chang, J. H., H.W. Sheng, C. L. Kuo, C. S. Hsian, Y. W. Hong, et al.** Prevalence of flexible flatfoot in Taiwanese school-aged children in relation to obesity, gender, and age. – *Eur. J. Pediatr. Orthop.,* **169**(4), 447-452.
6. **Deland, J. T.** Adult -acquired flatfoot deformity. – J. Am. Acad. Orthop. Surg., **16**(7), 2008, 399-406.
7. **Evans, A. M.** The flat-footed child – To treat or not to treat: what is the clinician to do? – *J. Am. Podiatr. Med. Assoc*., **98**(5), 2008, 386–393.
8. **Ghorbani, M., R. Yaali, H. Sadeghi, G. A. Koumantakis.** The impact of flatfeet on the correlation between functional movement scores, balance, agility, and core muscle strength in young females: a cross-sectional study. – *Sci. Rep*., **15**, 2025, 5077. https://doi.org/10.1038/s41598-025-89364-8
9. **Giuca, G., D. A. Marletta, B. Zampogna, I. Sanzarello, M. Nanni, D. Leonetti.** Correlation between severity of flatfoot and risk factors in children and adolescents: A Systematic Review. – *Osteology*, **5**(2), 2025, 11.
10. **Harris, R. I., T. Beath.** *Army Foot Survey*. Ottawa: National Research Council of Canada. 1947.
11. **Jia, Y., X. Sai, E. Zhang.** Comparing efficacy of exercise therapy on adult flexible flatfoot individuals through a network meta-analysis of randomized controlled trials. – *Sci Rep*., **14**, 2024 21186. https://doi.org/10.1038/s41598-024-72149-w
12. **Kardm, S. M., Z. A. Alanazi, T. Abdullah, S. Aldugman, R. S. Reddy, A. P. Gautam**. Prevalence and functional impact of flexible flatfoot in school-aged children: a cross-sectional clinical and postural assessment. – *J. Orthop. Surg. Res*., **20**, 2025, 783. https://doi.org/10.1186/s13018-025-06207-y
13. **Smith, M. A.** Flat feet in children. – *BMJ,* 301(6758), 1990, 942-943.
14. **Pfeiffer, M. R. Kotz, T. Ledl, G. Hauser, M. Sluga.** Prevalence of flat foot in preschool-aged children. – Pediatrics, 118(2), 2006, 634-639.

15. Rao, U. B., B. Joseph. The influence of footwear on the prevalence of flat foot: a survey of 2300 children. – *J. Bone Joint Surg. Br*., 74(4), 1992, 525-527.
16. Sánchez-Rodríguez, R., A. M. Nova, E. E. Martínez, J. D. P. Zamorano. Can the Foot Posture Index or their individual criteria predict dynamic plantar pressures? – *Gait Posture*, **36**(3), 2012, 591-595. doi: 10.1016/j.gaitpost.2012.05.024.
17. Sapogovskiy, A., A.V. Ovechkina, I. A. Abramov, O. E. Agranovich, A. I. Shubina, T. G. Budkevich. Footprint analysis in flatfoot assessment. – *Pediatr. Traumatol. Orthop. Reconstr. Surg*., **11**(1), 2023, 67-74.
https://doi.org/10.17816/PTORS121335
18. Shen, J., J. Liu, F. Liang, X. Liu, M. Zhang. Prevalence of flatfoot and analysis of plantar pressure in Chinese adolescents. – *J. Orthop. Surg. Res*., **19**, 2024, 864. https://doi.org/10.1186/s13018-024-05365-9
19. Sim-Fook, L., A. R. Hodgson. A comparison of foot forms among the non-shoe and shoe-wearing Chinese population. – *J. Bone Joint Surg. Am*., 40-A(5), 1958, 1058-1062.
20. Staheli, L.T. Evaluation of planovalgus foot deformities with special reference to the natural history. – *J. Am. Podiatr. Med. Assoc*., **77**(1), 1987, 2-6,
doi: 10.7547/87507315-77-1-2.
21. Susman, R.L. Evolution of the human foot: evidence from Plio-Pleistocene hominids. – *Foot Ankle,* **3**(6), 1983, 365–376.
22. Uden, H., R. Scharfbillig, R. Causby. The typically developing paediatric foot: how flat should it be? A systematic review. – *J. Foot Ankle Res*., **10**, 2017, 37,
doi: 10.1186/s13047-017-0218-1
23. Yu H, W. Wu, W. Tai, J. Li, R. Zhang, et al. The arch myth: investigating the impact of flat foot on vertical jump height: a systematic review and meta-analysis. – *BMC Sports Science, Medicine and Rehabilitation*, **16**, 2024, 236,
https://doi.org/10.1186/s13102-024-01018-w

Institute of Experimental Morphology, Pathology and Anthropology with Museum
Bulgarian Anatomical Society

Acta Morphologica et Anthropologica, 32 (3-4)
Sofia ● 2025

The territory of abkhazia as a part of the eastern black sea route of hominide migration and settlement

David A. Kandelaki

Pitsunda Historical and Archeological Museum, Pitsunda, Abkhazia

*Corresponding author e-mail: david_kandelaki@mail.ru

This article provides a general overview of the settlement of the territory of Abkhazia by ancient hominids. Special attention is paid to the chronology and routes of settlement by anatomically modern humans and their relationship with preceding populations. As a historical review, the article provides an extensive bibliography on the topic.

Key words: Anthropogenesis, Hominization, Sapientation, Paleolithic, Abkhazia

Introduction

Anthropogenesis is traditionally considered in two main aspects: hominization, which concerns the evolution of ancient primates into the *Homo* genus, and sapientation, which addresses the origin of anatomically modern humans, or *Homo sapiens* [58, 59].

The territory of Abkhazia, as an integral part of the Caucasian Black Sea region, has long served as a crossroads for cultural and historical contacts between neighboring regions, including Transcaucasia, the North Caucasus, Asia Minor, Western Asia, Crimea, and Eastern Europe. These connections emerged during the earliest stages of human societal development, as evidenced by the most ancient material culture sites in the former USSR. Sites in Abkhazia date back to the Acheulean era and include the first cave sites of the Mousterian era [39, 43]. Consequently, Abkhazia was a corridor for the movement of ancient hominids even before the final evolutionary formation of biologically modern humans. The region thus formed part of a Black Sea migration route for Paleolithic populations, with the Caspian route recently also being considered in light of new research (**Fig. 1**).

Although Stone Age archaeological sites are widely represented in Abkhazia, the region is notably lacking in paleoanthropological material from the Paleolithic era. Most hominid finds have been discovered outside its borders and are singular and fragmentary, making it difficult to form a complete picture of the morphological features of the local populations.

Map of Paleolithic human fossil finds in the Caucasus

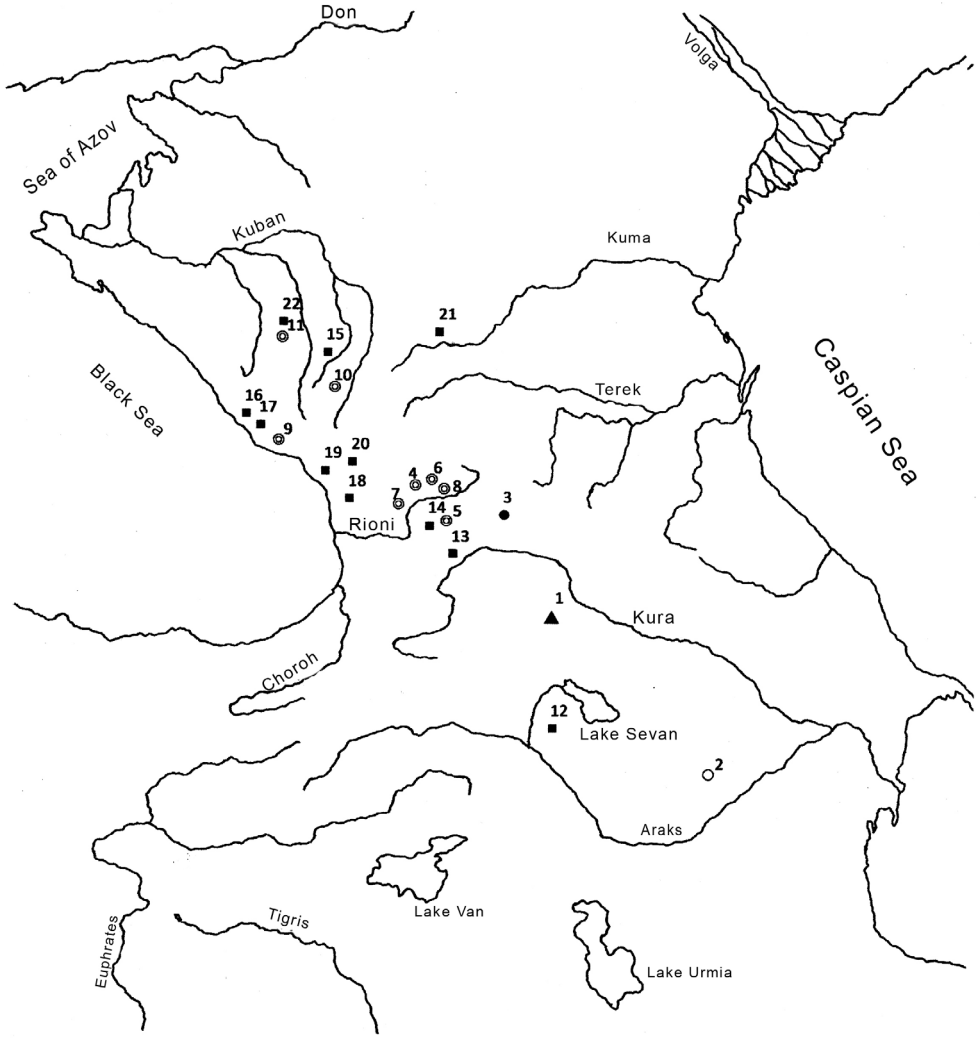

Legend

▲ Dmanisi hominid
● **Homo erectus**
○ **Homo haidelbergensis**
◎ **Homo neanderthalensis**
■ **Homo sapiens**

1. Dmanisi
2. Azykh
3. Kudaro
4. Sakaziya
5. Dzhruchula
6. Bronze
7. Ortvala
8. Tsutskhvati
9. Machagua
10. Mezmayskaya
11. Barakayevskaya
12. Razdan
13. Devis-Khvreli
14. Bodi
15. Kasozhskaya
16. Akhshtyrskaya
17. Navalishenskaya
18. Okum I
19. Kuab-Chara
20. Kholodny Grotto
21. Podkumok
22. Satanay

Author and compiler: D.A. Kandelaki

Fig. 1

The oldest and most significant find near Abkhazia comes from the Dmanisi site in Eastern Georgia. Dated to 1.75 million years ago and associated with Villafranchian fossil fauna, this is the oldest paleoanthropological find in Eurasia. The "Dmanisi man" shares morphological features with erectoid forms like *Homo ergaster*, as well as with *Homo habilis* and *Homo rudolfensis* [8, 9, 28, 69]. These distinct characteristics led anthropologists to assign a new taxonomic status, *Homo georgicus*, which is now widely recognized in the scientific community[1].

Remains from this period also include the so-called "Azokh anthrop" from Azokh Cave in Azerbaijan, represented by fragments of a lower jaw likely dating to the Pleistocene. These remains are attributed to either Archanthropines (*Homo erectus*) or pre-Neanderthals/Heidelberg man (*Homo heidelbergensis*) [15, 32, 66, 67].

Further evidence comes from Kudaro I Cave, where a human tooth was found in an Acheulean layer (Mindel-Riss). This tooth may belong to Archanthropines of the *Homo erectus* type or the Neanderthal taxon, though it is more closely related to erectoid forms. A permanent incisor and premolar were also found at the site; the incisor has a modern structure, while the premolar is characteristic of ancient forms [27, 8, 69].

In Sakazhia Cave, fragments of an upper jaw with four teeth were discovered in Mousterian level 3d, associated with Levallois-Mousterian tools. Additional teeth and skull fragments were found elsewhere in the same cave [52, 53, 54, 56, 57]. These remains exhibit features that suggest a Neanderthal similar to Palestinian forms, with some even approaching sapient characteristics, possibly indicating a hybrid population [13, 52, 14].

A Neanderthal first upper permanent molar was discovered in Mousterian layer II of Djruchula Cave, which is morphologically close to the finds from Sakazhia [64, 12, 41, 69]. Other Neanderthal dental remains have been found in Bronze Cave (Bronzovaya Peschera), Ortvala Cave [55], and Tstsukhvati Cave [50, 52].

Materials from the Upper Paleolithic and Mesolithic periods are also present. A skull from Western Georgia, dated to the Meso-Neolithic period, carries a proto-Australoid combination of features typically characteristic of the Upper Paleolithic era [16]. The lower jaw of a young sapient woman was found in the Aurignacian layer of Devis-Khvreli Cave [48, 1]. In 2012, a tooth belonging to *Homo sapiens* was discovered in Bondi Cave, Georgia, in a layer dated to 24-21 thousand years ago, providing crucial evidence for the timing of the first sapiens' appearance in the region [73].

Human remains have also been discovered within the Caucasian Black Sea region. Of particular interest are finds of anatomically modern human remains, albeit with archaic features, from Mousterian layers 3a and 3 of Akhshtyr Cave [10, 26, 11, 67]. However, these are represented only by minor fragments, including individual teeth and postcranial skeleton pieces. There is also a reported discovery of an anatomically modern human skull in Navalishenskaya Cave in the Khosta River gorge, which displays Euro-African traits [30].

---

[1] The geographical naming convention is widespread in paleoanthropology, with examples including Neanderthal (Neander Valley, Germany), the Azokh anthrop (Azokh Cave, Azerbaijan), Peking Man (China), and Java Man (Indonesia).

In Abkhazia specifically, finds of individual teeth in the Mousterian layers of Machagua Cave may belong to either the Neanderthal taxon or modern humans, though a lack of detailed morphological data prevents a definitive taxonomic assignment [70]. Human remains were also found in the Upper Paleolithic layers of Okum I Cave [4]. Two lower jaws of *Homo sapiens* with archaic, pre-sapient features were recovered from the presumably Late Paleolithic or Early Mesolithic layers of Kuab-Chara Cave, likely belonging to late archaic sapiens or early anatomically modern humans [7].

The most intriguing finds from Abkhazia are the human remains from the Cold Grotto (Grot Khuapinipshakhua), represented by an accumulation of eight skulls, including two from adolescents. The skulls allegedly bear cut marks that may indicate dismemberment. Published sources suggest the skulls exhibit proto-Australoid or non-differentiated Euro-African characteristics, though a detailed paleoanthropological study of these materials is still lacking.

This accumulation of skulls suggests the practice of a specific religious rite. They resemble skull remains found in the Imeretian caves Devis-Khvreli and Sakazhia, as well as more distant sites like Ofnet, indicating shared ritual practices across a wide geographical area. This archaeological evidence curiously echoes the historical and ethnographic literature documenting a cult of the skull among the Abkhazians [61, 62, 63, 65, 31].

Data from the North Caucasus are also highly significant. For instance, the remains of a Neanderthal with sapient features were discovered in Mezmaiskaya Cave, displaying traits that align it with the Skhul type [68, 69]. Genetic studies by German researchers, who sequenced the genome of the Mezmaiskaya individual, further established its closer affinity to Western European forms [20, 54][2]. A child's lower jaw found in Barakayevskaya Cave exhibits features of a transitional type between Paleoanthropes and Neoanthropes [40]. However, several morphological characteristics suggest the Barakay individual is closer to Western European Neanderthals than to Western Asian types like those from Shanidar and Skhul [40, 67]. In the Satanay Grotto (Gubsky Shelter No. 7), a *Homo sapiens* female skull was discovered, bearing similarities to sapient skulls from Central and, to a lesser extent, Western Europe, particularly specimens from Kostenki XIV, Kostenki II, Oberkassel, and Dolní Věstonice III [19, 60]. Additional human remains, including a skull fragment, have been found near Podkumok, close to Pyatigorsk [21].

Our current knowledge is constrained by the limited and fragmentary nature of these fossil finds, which significantly complicates a comprehensive understanding of hominid settlement in Abkhazia. Several critical problems remain unresolved, including:

- The chronology of the initial penetration of ancient hominids into the region.
- Their specific evolutionary lineages.
- The correlation of particular hominid types with specific archaeological industries.

---

[2] In recent years, the so-called archaeogenetic revolution has been underway, and there is a wealth of data on Neanderthal archeogenetics, including for the Caucasus Neanderthals. However, a review and synthesis of this literature could be the topic of a separate study [22].

• The ultimate fate of these ancient populations in Abkhazia.

A problem of equal importance is determining the timing and migration routes of *Homo sapiens* into the region.

The Caucasus has consistently served as a gateway to Eurasia for migrating hominids [68]. Current evidence suggests the first humans appeared here in the late Pliocene and early Pleistocene, most likely arriving via Eastern Anatolia and the Western Asian highlands from Africa. Around 2 to 1.5 million years ago, hominids of the species *Homo ergaster* emerged in Africa and began dispersing northward, reaching the Caucasus. Unfortunately, despite advances in Paleolithic archaeology in Abkhazia, sites from this early period remain undiscovered. Such early sites are rare but have been identified in Georgia, the Taman Peninsula, and Dagestan, attributed to *Homo georgicus* and *Homo ergaster*.

Some scholars argue that the absence of a continuous Oldowan and pre-Oldowan tradition in the Caucasus indicates that the bearers of these earliest industries did not undergo further evolutionary development in the region. Their presence may represent brief episodes of migration, following animal herds and seeking high-quality raw materials for tools. Conversely, other researchers posit that their appearance was part of the first global migration of hominids, with the Caucasian representatives being among the first humans on the Eurasian continent.

Abkhazia's role in this initial phase is unclear, as no finds chronologically associated with the Oldowan period (1.7-1.6 million years ago) have been found there. However, the nearby Bogatyri / Sinaya Balka site on the Taman Peninsula, with materials dating to 1.2-1.6 million years ago, and the slightly later site of Amiranic-Gora (c. 800,000 years ago), suggest that the earliest sites near Abkhazia fall within the 1.7-0.8 million years ago range. These sites represent the earliest, rare episodes of hominid presence in the Caucasus. The populations that left these traces likely did not establish a permanent presence and may have migrated southward, a theory supported by paleoclimatological data indicating a trend toward aridity and cooling around 1.75 million years ago. A subsequent thermal optimum may have facilitated a new wave of hominids, followed by a sharp cooling coinciding with the Günz glaciation (oxygen-isotope stage 22), which may have led to the departure or local extinction of *Homo georgicus* and *Homo ergaster* populations.

The next major settlement phase in the Caucasus and Abkhazia occurred during the Early Acheulean era[3]. The chronological gap between the Acheulean and the preceding industries is likely due to unfavorable climatic conditions. Critically, the Acheulean industries of the Caucasus show no direct technological continuity with the local Oldowan, indicating they were not the result of in-situ evolution but were introduced by a new wave of hominids from the south, likely late *Homo erectus*. The closest analogues to these Caucasian industries are found in the Levant.

The general chronological range for the Caucasian Acheulean is 600-300 thousand years ago, spanning from oxygen-isotope stage 15 to stage 9. Absolute dates from sites

---

[3] Since the archaeological attribution of Paleolithic sites will be addressed in subsequent sections, the present analysis deliberately bypasses this aspect of the problem to focus exclusively on the paleoanthropological and migratory evidence.

near Abkhazia, such as Triangular Cave (583 ± 25 kya) and Kudaro III Cave (560 ± 112 kya), fall within this range. The appearance of Acheulean toolmakers coincides with warm interglacial stages, which created favorable conditions for northward migration from southern regions.

In Abkhazia, the Yashtukha site provides key evidence for this process, reflecting multiple settlement episodes during the Günz-Mindel and Mindel-Riss interglacials. The earliest settlers were likely *Homo erectus* during the Günz-Mindel interglacial, with later stages dated to 358-330 kya (Mindel-Riss). During these warm periods, hominids penetrated the Caucasus and Black Sea region, likely migrating along open foothill zones to avoid the swampy Colchis Lowland. The primary route probably ran from the Armenian Highlands through Eastern and Western Transcaucasia, then westward towards the Abkhazian Black Sea region and into the Trans-Kuban area [42]. This is supported by later sites in the Northern Black Sea region, which imply significant population infiltration from the south [5, 62]. Geological factors, such as lower elevation profiles of the Caucasus ridges (1-1.5 km lower than today) and asynchronous glaciation patterns compared to Europe, further facilitated these movements and led to periods of cultural isolation.

A later Acheulean stage in the Caucasus may be associated with *Homo heidelbergensis*, as suggested by the remains from Azokh Cave. This group likely penetrated the region around 300-350 kya (late Mindel-Riss interglacial), and the late Acheulean at Yashtukha may be attributed to them. Acheulean industries appear to have persisted until the end of the Riss glaciation, when the first Mousterian tools mark the beginning of the Middle Paleolithic.

Recent research indicates that the Middle Paleolithic (Mousterian) in the Caucasus did not evolve from local Acheulean traditions but was introduced from outside. The technological affinities of Caucasian Middle Paleolithic materials lie with sites in Western Asia (the Levant and Zagros). This suggests that bearers of these Mousterian technologies moved from the Zagros through the Western Asian highlands and from the Levant through Eastern Anatolia into the Western Caucasus, including Abkhazia.

The lack of genetic continuity between Acheulean and Mousterian industries supports the theory that these new technologies were brought by a new wave of hominids: *Homo neanderthalensis*. Fossil evidence confirms Neanderthals were the bearers of nearly all Mousterian sites in the Caucasus.

The timing of their appearance is linked to the earliest Mousterian sites. The oldest dated Mousterian layer in the Caucasus is at Myshtulagty-Lagat (North Ossetia), around 250 kya, with the latest layers dating to approximately 70 kya. Transcaucasian sites have slightly later dates; for example, Kudaro I Cave dates to 90-60 kya. In Abkhazia, a date from Apiancha Cave of around 38 kya reflects a much later Mousterian stage.

Two distinct stages of Neanderthal penetration into the Caucasus are identified, supported by technological disparities between early and late Mousterian industries. The first stage, around 250 kya (Riss-Würm interglacial), is derived from early Middle Paleolithic cultures of the Levant. The second stage occurred during a significant climatic deterioration in the “Mousterian Würm” (oxygen-isotope stage 4, 75-71 and 60-57 kya), which may have reduced or extirpated the “first wave” Neanderthals. In this second phase, settlement included populations from the south of the Russian Plain and Crimea, with North Caucasian sites showing Central and Western European affinities, while Transcaucasian sites gravitated towards Zagros cultures [39, 43].

The cultural differences observed in the Mousterian could result from different technological traditions, diverse genetic origins of populations, or even early ethnic formations [39]. Climatic fluctuations likely caused population movements between highland and lowland areas, leading to concentration, increased cultural contact, and the formation of distinct archaeological cultures like the Kudar, Tskhinvali, and Gub groups. The so-called Khosta culture and the somewhat isolated position of the Abkhazian Mousterian further highlight this regional diversity [34].

The subsequent Upper Paleolithic era in the Caucasus, while diverse, shares commonalities with cultures of the Near East, forming a distinct West Asian cultural region separate from North Africa, Central Asia, and the South Russian steppes. Within the Caucasus, the Imeretian and Gub cultures can be identified. Cultural differences became more pronounced by the end of the Upper Paleolithic, suggesting independent development after an initial common origin. A cultural divide between the North Caucasus and Transcaucasia is also evident, likely due to the glacial barriers presented by the Caucasian ridge. In contrast, sites on the Black Sea coast show evidence of constant movement and cultural connections.

The Imereti sites are closest to the Baradostian and Zarzian cultures of the Zagros and differ from those in the Levant [3], suggesting a possible ethnic unity within this interaction zone.

The origins of early *Homo sapiens* in the region should be sought in the Near East, as evidenced by the material culture similarities between Imereti, Zagros, and Luristan [3]. This indicates that *Homo sapiens* in the Caucasus are not of local autochthonous origin [8].

The timing of their arrival is discernible from the Upper Paleolithic archaeological record. It is well-established that Mousterian cultures are predominantly associated with Neanderthals, while Upper Paleolithic industries are genetically unrelated to the Mousterian. Any apparent connections likely reflect cultural contact between Neanderthals and sapiens, not local evolution.

The Caucasus was part of the vast Neanderthal range, which bordered the habitat of *Homo sapiens* in the southern regions of Western Asia. The Upper Paleolithic appeared in the Caucasus relatively late. The first traces of Upper Paleolithic industries, and thus the first representatives of *Homo sapiens*, appear during a period of relative warming at the onset of the powerful Würm II glaciation (oxygen-isotope stage 3), dated to 36-38 thousand years ago. This period marks the replacement of Neanderthals by anatomically modern humans in the Caucasus.[4]

Today, the processes of coexistence between different hominid lineages in the Caucasus remain elusive. It is even more challenging to determine whether the region, including Abkhazia, constituted a formative center for anatomically modern humans. A more plausible scenario is that the Caucasus lay on the periphery of a primary sapientation zone, receiving slow but successive waves of migrants at various evolutionary stages.

---

[4] Given the scope of this article, we will bypass a detailed discussion of theories concerning the origin of anatomically modern humans, such as the monocentric (Out-of-Africa) and polycentric (Multiregional) hypotheses.

This interpretation is supported by the morphological evidence. Paleoanthropes from Georgian sites such as Sakazhia, Djruchula, and Tstsukhvati exhibit features that place them on a trajectory toward sapientation, sharing affinities with Western Asian finds of the Skhul type. This aligns with the scholarly consensus that the early Caucasian Mousterian originated from the Levant, the very region that produced the Skhul groups.

These migrations inevitably led to multiple cultural and genetic contacts between hominids of different evolutionary levels. For instance, the first paleoanthropes entering the Caucasus likely encountered residual groups of Acheulean culture bearers, possibly *Homo heidelbergensis*. Subsequently, during a second wave of paleoanthrope settlement, local groups may have mixed with migrants from the Zagros. Furthermore, when conditions allowed, populations from Crimea could have penetrated Transcaucasia via the Black Sea coast, introducing another demographic layer. This complex chronology means that earlier migrants, such as Skhul-type groups from the Levant, could have been more progressive than later arrivals, indicating that the process of sapientation, though perhaps attenuated, was already underway in the region.

Against this backdrop, it is conceivable that even during the Mousterian, there were early, episodic incursions of fully sapient groups. If so, the first modern humans arriving in the Caucasus may have encountered not "classical" Neanderthals but populations of paleoanthropes with intermediate morphological traits. This supports the hypothesis of the Caucasus as a zone of hybridization, fostering erectoid-Neanderthaloid and Neanderthaloid-sapient groups.

Consequently, the appearance of modern humans in Abkhazia and adjacent regions likely occurred through multiple mechanisms. On one hand, there may have been a degree of *in-situ* sapientation within local populations. On the other, there was undoubtedly migration of already fully formed anatomically modern humans.

The archaeological record confirms that migration pulses from the Near East northward into the Caucasus persisted throughout the Upper Paleolithic and continued into the Mesolithic. The significant presence of early *Homo sapiens* remains, morphologically represented by undifferentiated proto-Australoid and Euro-African types, suggests their penetration into the region long before the definitive onset of the Upper Paleolithic era. This evidence paints a picture of the Caucasus not as an isolated cul-de-sac, but as a dynamic periphery - a complex corridor of migration, interaction, and potential hybridization over millennia.

References

1. **Alekseev, V. P.** *Origin of the peoples of the Caucasus: Craniological study*. Nauka, 1974. [in Russian]
2. **Alekseev, V. P.** Mesolithic skull from El-Wad Cave. – *Voprosy Antropologii*, **85**, 1983, 71-82. [in Russian]
3. **Bader, N. O.** Late Paleolithic of the Caucasus. – In: *Archaeology of the USSR: Paleolithic of the USSR*. Nauka, 1984. [in Russian]
4. **Berdzenishvili, I. Z., N. I. Burchak-Abramovich, G. P. Khubutia.** Fossil vertebrates of the Upper Paleolithic site of Okumi in Southern Abkhazia. – *Caves of Georgia*, **12**, 1978, 125-140. [in Russian]

5. Bibikov, S. N. Some issues of the settlement of Eastern Europe during the Paleolithic. – *Sovetskaya Arkheologiya*, **4**, 1959, 3-25. [in Russian]
6. Bibikov, S. N. Excavations in the Fatma-Koba canopy and some aspects of the study of the Mesolithic in Crimea. – In: *At the origins of ancient cultures (Mesolithic era)* (MIA USSR), **26**, 1966, pp. 88-102. [in Russian]
7. Clark, J. D. *Prehistoric Africa*. Progress, 1978. [in Russian]
8. Debets, G. F. Territory of the USSR and the problem of the human homeland. – *Kratkie Soobshcheniya Instituta Etnografii*, **17**, 1952, 45-58. [in Russian]
9. Debets, G. F. Skull from the Epipaleolithic burial ground near the village of Voloshskoye. – *Sovetskaya Etnografiya*, **3**, 1955, 105-118. [in Russian]
10. Debets, G. F., T. A. Trofimova, N. N. Cheboksarov. *The problem of the peopling of Europe according to anthropological data.* Nauka, 1951. [in Russian]
11. Formozov, A. A. Review of studies of Mesolithic sites in the Caucasus. – *Sovetskaya Arkheologiya*, **4**, 1963, 112-125. [in Russian]
12. Gabunia, L. K., A. K. Vekua. On the remains of paleoanthropes in Georgia. – *Kratkie Soobshcheniya Instituta Arkheologii*, **181**, 1985, 55-60. [in Russian]
13. Gabunia, L. K., M. G. Nioradze, A. K. Vekua. About the Mousterian man from Sakazhie (Western Georgia). – *Voprosy Antropologii*, **5**, 1978, 59-68. [in Russian]
14. Gabunia, L. K., D. M. Tushabramishvili, A. K. Vekua. The first find of Mousterian man remains in the Caucasus. – *Voprosy Antropologii*, **8**, 1961, 15-24. [in Russian]
15. Gadzhiev, D. V., M. M. Huseynov. The first find of Acheulean man (Azerbaijan, Azykh cave). – In: *Anniversary collection of scientific notes of the Azerbaijan State Medical Institute,* **31**, 1970, pp. 45-52. [in Russian]
16. Gerasimov, M. M. *Reconstruction of the face from the skull (modern and fossil man)*. Nauka, 1955. [in Russian]
17. Gerasimova, M. M., D. V. Pezhemsky. *Mesolithic man from Peschanitsa: Comprehensive anthropological analysis*. Nauka, 2005. [in Russian]
18. Gokhman, I. I. *Population of Ukraine in the Mesolithic and Neolithic (anthropological essay)*. Nauka, 1966. [in Russian]
19. Gokhman, I. I. Fossil neoanthropes. – In: *Fossil hominids and the origin of man*, TIE, **92**, 1966, pp. 88-105. [in Russian]
20. Golovanova, L. V. Age of the Neanderthal burial in the Mezmayskaya cave in the North Caucasus. – In: *Ecology and demography in the past and present*, Nauka, 2004, pp. 45-60. [in Russian]
21. Gremyatsky, M. A. Structural features of the fragments of the Podkum skull and its antiquity. – *Antropologicheskiy Zhurnal*, **3**, 1934, 45-58. [in Russian]
22. Hajdinjak M., Q. Fu, A. Hubner, M. Petr, F. Mafessoni, et al. Reconstructing the genetic history of late Neanderthals. – Nature, **555**, 2018, 652-656.
23. Inal-ipa, Sh. D. *Pages of the historical ethnography of the Abkhazians*. Alashara, 1971. [in Russian]
24. Inal-ipa, Sh. D. *Issues in the ethnocultural history of the Abkhazians*. Alashara, 1976. [in Russian]
25. Kasimova, R. M. *The first find of the most ancient cave man on the territory of the USSR*. Elm, 1986. [in Russian]
26. Konduktorova, T. S. Paleoanthropological materials from the Mesolithic burial ground Vasilyevka 1. – *Sovetskaya Antropologiya*, **2**, 1957, 89-102. [in Russian]
27. Korobkov, I. I. Paleolithic of the Eastern Mediterranean. – In: *Paleolithic of the Near and Middle East* (Paleolithic of the World series). Nauka, 1978, pp. 112-145. [in Russian]
28. Kharitonov, V. M. Acheulean hominids on the territory of the USSR. – In: *Features of morphofunctional characteristics in norm, development, and extreme conditions*, MOIP, 1989, pp. 78-95. [in Russian]

29. Kharitonov, V. M. The Caucasus in the Paleolithic: A review of finds and ideas. – In: *Human ecology in the past and present*. Nauka, 2004, pp. 134-150. [in Russian]
30. Kharitonov, V. M., & Batsevich, V. A. (1977). Finds of fossil hominids in Eastern Europe and adjacent regions of Asia. – *Vestnik Antropologii*, **3**, 1977, 25-40. [in Russian]
31. Kharitonov, V. M., G. P. Romanova. Anthropological analysis of the skeletal bones of a fossil hominid from the Mousterian layer of Mezmayskaya Cave (North Caucasus). – *Voprosy Antropologii*, **90**, 2000, 112-128. [in Russian]
32. Khvartskiya, M. Kh., N. E. Polyakova, A. K. Ocherednoy. *Machagua – a Middle Stone Age site in Abkhazia*. – Evropeyskiy Dom, 2005. [in Russian]
33. Lyubin, V. P. The Paleolithic of Turkey and the problem of early human settlement. – *Sovetskaya Arkheologiya*, **27**, 1957, 45-58. [in Russian]
34. Lyubin, V. P. Paleolithic cave sites and remains of Paleolithic man in Turkey. – *Voprosy Antropologii*, **9**, 1962, 25-35. [in Russian]
35. Lyubin, V. P. *Natural environment and man in the Pleistocene*. Nauka, 1974. [in Russian]
36. Lyubin, V. P. Early Paleolithic of the Caucasus. – In: *Paleolithic of the USSR* (Archaeology of the USSR), Nauka, 1984, pp. 45-89. [in Russian]
37. Lyubin, V. P. Paleolithic of the Caucasus. – In: *Paleolithic of the World*, Nauka, 1989, pp. 78-115. [in Russian]
38. Lyubin, V. P. *Acheulean epoch in the Caucasus*. – Peterburgskoe Vostokovedenie, 1998. [in Russian]
39. Lyubin, V. P., P. U. Autlev, A. A. Zubov, G. P. Romanova, V. M. Kharitonov. Discovery of skeletal remains of Paleoanthropus at the Barakayevskaya site (Western Caucasus). – *Voprosy Antropologii*, **77**, 1986, 35-45. [in Russian]
40. Lyubin, V. P., E. V. Belyaeva. *Early prehistory of the Caucasus*. Aleteyya, 2006. [in Russian]
41. Lyubin, V. P., E. V. Belyaeva. Early prehistory of the Caucasus. – In: *Ethnocultural interaction in Eurasia*, Nauka, Book 1, 2006, pp. 45-67. [in Russian]
42. Masson, V. M. On the Mesolithic in Western Asia. – In: *At the origins of ancient cultures (the Mesolithic era)*, MIA USSR, **126**, 1966, pp. 112-125. [in Russian]
43. Muratov, V. M. Quaternary history of the Black Sea basin in comparison with the history of the Mediterranean Sea. – *Byulleten Moskovskogo Obshchestva Ispytateley Prirody. Otdel Geologicheskiy*, **35**(5), 1960, 45-58. [in Russian]
44. Muratov, V. M. *Paleogeographic conditions of Paleolithic sites in the Northern Caucasus*. Nauka, 1969. [in Russian]
45. Nioradze, G. K. Paleolithic of Georgia. – In: *Proceedings of the II International Conference of the Association for the Study of the Quaternary Period in Europe*, **5**, 1934, pp. 112-120. AN SSSR. [in Russian]
46. Nioradze, G. K. *Paleolithic man from Devis-Khvreli cave*. Metsniereba, 1973. [in Russian]
47. Nioradze, M. G. Archaeological work in Sakazhiya Cave. – *Soobshcheniya Akademii Nauk Gruzinskoy SSR*, **84**(1), 1976, 205-208. [in Russian]
48. Nioradze, M. G. Archaeological works of the Tskhaltsiteli expedition. – In: *Polevye Arkheologicheskie Issledovaniya v 1975 godu*, Metsniereba, 1978, pp. 45-48. [in Russian]
49. Nioradze, M. G. Excavations in the Sakazhiya Cave. – In: *Polevye Arkheologicheskie Issledovaniya v 1976 godu*, Metsniereba, 1979, pp. 50-52. [in Russian]
50. Nioradze, M. G. Results of the Tskaltsiteli archaeological expedition. – In: *Polevye Arkheologicheskie Issledovaniya v 1978 godu*, Metsniereba, 1982, pp. 55-57. [in Russian]
51. Nioradze, M. G. Results of the Tskaltsiteli expedition. – In: *Polevye Arkheologicheskie Issledovaniya v 1979* godu, Metsniereba, 1982, pp. 58-60. [in Russian]
52. Nioradze, M. G. Archaeological research in the Tskaltsiteli River Gorge. – In: *Polevye Arkheologicheskie Issledovaniya v 1980 godu,* Metsniereba, 1982, pp. 61-63. [in Russian]

53. Nioradze, M. G., A. K. Vekua, L. K. Gabunia, N. S. Mamatsashvili. (1978). Sakazhiya Cave. – In: *Arkheologicheskie Pamiatniki Prirodnykh Raionov Prichernomorskoi Kolkhidy*, Metsniereba, 1978, pp. 88-95. [in Russian]
54. Ovchinnikov, I., A. Götherström, G. Romanova, V. Kharitonov, K. Liden, et al. Molecular analysis of Neanderthal DNA from the northern Caucasus. – Nature, **404**, 2000, 490-493.
55. Roginsky, Ya. Ya. *Problems of anthropogenesis*. Vysshaya Shkola, 1977. [in Russian]
56. Roginsky, Ya. Ya., M. G. Levin. *Anthropology*. Prosveshchenie, 1963. [in Russian]
57. Romanova, G. P., V. M. Kharitonov. Morphological features of the human skull from the Paleolithic site in the Satanay canopy. – *Voprosy Antropologii*, **73**, 1984, 45-55. [in Russian]
58. Shnirelman, V. A. Natufian cultures. – *Sovetskaya Arkheologiya*, **1**, 1973, 105-118. [in Russian]
59. Soloviev, L. N. The importance of the archaeological method for the study of karst in the northern part of the Black Sea coast of the Caucasus. – In: *Karst issues in the south of the European part of the USSR*, Naukova Dumka, 1956, pp. 78-85. [in Russian]
60. Soloviev, L. N. On the results of archaeological research in the Khupynipshahva grotto. - *Trudy Abkhazskogo Instituta Yazyka, Literatury i Istorii*, **32**, 1961, 145-150. [in Russian]
61. Soloviev, L. N., V. S. Orelkin. Find of human bones in the Khupynipshakhva grotto (Cold grotto) in Abkhazia. – *Voprosy Antropologii*, **6**, 1961, 25-30. [in Russian]
62. Tushabramishvili, D. M. Results of excavations of the Jruchulchi cave in 1960-1961. – In: *Caves of Georgia*, Metsniereba, **2**, 1963, pp. 112-125. [in Russian]
63. Tushabramishvili, N., D. Pleurdeau, M.-H. Moncel, T. Agapishvili, A. Vekua, A., et al. Human remains from a new Upper Pleistocene sequence in Bondi Cave (Western Georgia). – *Journal of Human Evolution*, **62**(1), 2012, 179-185.
64. Vasiliev, S. V. Anthropology of the Paleolithic population of the Caucasus. – In: *Ancient Caucasus: Retrospective of cultures*. Nauka, 2004, pp. 45-67. [in Russian]
65. Vasiliev, S. V. Paleolithic of the Caucasus: Retrospective of anthropological finds. – *Vestnik Antropologii*, **11**, 2004, 78-95. [in Russian]
66. Vekilova, E. A., A. A. Zubov. (1972). Anthropological remains from the Mousterian layers of Akhshtyr Cave. – *Kratkie Soobshcheniya Instituta Arkheologii*, **131**, 1972, 45-50. [in Russian]
67. Vekilova, E. A., V. P. Grichuk, Z. P. Gubonina, N. M. Ermolova, A. A. Zubov, V. M. Muratov, E. O. Fridenberg. Akhshtyrskaya Cave. – In: *Arkheologicheskie Pamiatniki Prirodnykh Raionov Prichernomorskoi Kolkhidy*. Nauka, 1978, pp. 45-67. [in Russian]
68. Voronov, Yu. N. *Archaeological map of Abkhazia*. Alashara, 1969. [in Russian]
69. Yakimov, V. P. Population of the European part of the USSR in the Late Paleolithic and Mesolithic. – *Voprosy Antropologii*, **7**, 1961, 15-30. [in Russian]
70. Zubov, A. A. Anthropological remains from the Akhshtyrskaya cave. – In: *Arkheologicheskie Pamiatniki Prirodnykh Raionov Prichernomorskoi Kolkhidy*. Nauka, 1978, pp. 68-70. [in Russian]
71. Zubov, A. A. On the tooth of an archanthropus from the Kudaro I cave. – In: *Kudar caves* (KPPSUO), Nauka, 1980, pp. 112-115. [in Russian]
72. Zubov, A. A. *Paleoanthropological genealogy of humanity*. Nauka, 2004. [in Russian]
73. Zubov, A. A. Differentiation of Ancient Humanity in the Upper Paleolithic-Mesolithic of Europe. – *Races and Peoples*, **30**, 2004, 45-67.

Author Guidelines

Acta Morphologica et Anthropologica is an open access peer review journal published by Bulgarian Academy of Sciences, Prof. Marin Drinov Publishing House.
Corporate contributors are Bulgarian Academy of Sciences, Institute of Experimental Morphology, Pathology and Anthropology with Museum and Bulgarian Anatomical Society.

Acta Morphologica et Anthropologica is published in English, 4 issues per year.

The journal accepts manuscripts in the following **fields**: experimental morphology, cell biology and pathology, anatomy and anthropology.

Publication types: original articles, short communications, case reports, reviews, Editorial, letters to the Editors.

Acta Morphologica et Anthropologica is the continuation of Acta cytobiologica et morphologica

The **aim** of the Journal is to disseminate current interdisciplinary biomedical research and to provide a forum for sharing new scientific knowledge and methodology. The general editorial policy is to optimize the process of issuing and distribution of *Acta Morphologica et Anthropologica* in line with modern standards for scientific periodicals focusing on content, form, and function.

Scope – experimental morphology, cell biology and pathology (neurobiology, immunobiology, tumor biology, environmental biology, reproductive biology, etc.), new methods, anatomy and pathological anatomy, anthropology and paleoanthropology, medical anthropology and physical development.

Acta Morphologica et Anthropologica is published twice a year as one volume with 4 issues. For the first two issues (1-2) the deadline for manuscript submission is March 15th and for the next two issues (3-4), the deadline is September 15th. Electronic version for issues 1-2 is uploaded on the website till June 30th and for issues 3-4 – till December 30th.

Contact details and submission

Manuscript submission is electronical only. The manuscripts should be sent to the Managing Editor's e-mail address ama.journal@iempam.bas.bg, ygluhcheva@hotmail.com with copy to iempam@bas.bg

All correspondence, including notification for Editor's decision, requests for revision, is sent by e-mail.

Article structure

Manuscripts should be in English with total length not exceeding 10 standard pages, line-spacing 1.5, justified with 2.5 cm margins. The authors are advised to use Microsoft Word 97-2003, Times New Roman, 12 pt throughout the text. Pages should be numbered at the bottom right corner of the page.

The article should be arranged under the following headings: Introduction, Material and Methods, Results, Discussion, Conclusion, Acknowledgements and References.

Title page – includes:

- **Title** – concise and informative;
- **Author(s)' names and affiliations** – indicate the given name(s) and family name(s) of all authors. Present the authors' affiliation addresses below the names. Indicate all affiliations with a lower-case superscript after the author's name and in front of the appropriate address. Provide the full postal address information for each affiliation, including the country name.
- **Corresponding author** – clearly indicate who will handle the correspondence for refereeing, publication and post-publication. An e-mail should be provided.
- **Abstract** – state briefly the aim of the work, the principal results and major conclusions and should not exceed 150 words. References and uncommon, or non-standard abbreviations should be avoided.
- **Key words** – provide up to 5 key words. Avoid general, plural and multiple concepts. The key words will be used for indexing purposes.

Introduction – state the objectives of the work and provide an adequate background, avoiding a detailed literature survey or summary of the results.

Material and Methods – provide sufficient detail to allow the work to be reproduced. Methods already published should be indicated as a reference: only relevant modifications should be described.

Results – results should be clear and concise.

Discussion – should explore the significance of the results in the work, not repeat them. A combined *Results and Discussion* section is often appropriate. Avoid extensive citation and discussion of published literature.

Conclusions – the main conclusions of the study should be presented in a short section.

Acknowledgements – list here those individuals who provided help during the research and the funding sources.

Units – please use the International System of Units (SI).

Math formulae – please submit math equations as editable text, not as images.

Electronic artwork – number the tables and illustrations according to their sequence in the text. Provide captions for them on a separate page at the end of the manuscript. The proper place of each figure in the text should be indicated in the left margin of the corresponding page. **All illustrations (photos, graphs and diagrams)** should be referred to as "figures" and given in abbreviation "Fig.", and numbered in Arabic numerals in order of its mentioning in the manuscript. They should be provided in grayscale as JPEG or TIFF format, minimum 300 dpi. The illustrations should be submitted as separate files.

References – they should be listed in alphabetical order, indicated in the text by giving the corresponding numbers in parentheses. The "References" should be typed on a separate sheet. The names of authors should be arranged alphabetically according to family names. In the reference list titles of works, published in languages other than English, should be translated, original language must be indicated at the end of reference (e.g., [in Bulgarian]). Articles

should include the name(s) of author(s), followed by the full title of the article or book cited, the standard abbreviation of the journal (according to British Union Catalogue), the volume number, the year of publication and the pages cited, for books - the city of publication and publisher. In case of more than one author, the initials of the second, third, etc. authors precede their family names. Ideally, the names of all authors should be provided, but the usage of "et al" after the fifth author in long author lists will also be accepted.

For articles: **Davidoff, M. S., R. Middendorff, G. Enikolopov, D. Riethmacher, A. F. Holstein, D. Muller**. Progenitor cells of the testosterone-producing Leydig cells revealed. – *J. Cell Biol.,* **167**, 2004, 935-944.

Book article or chapter: **Rodriguez, C. M., J. L. Kirby, B. T. Hinton. The development of the epididymis.** - In: *The Epididymis - from molecules to clinical practice* (Eds. B. Robaire, B. T. Hinton), New York, Kluwer Academic Plenum Publisher, 2002, 251-269.

Electronic books: **Gray, H.** *Anatomy of the human body* (Ed. W.H.Lewis), 20th edition, NY, 2000. Available at http://www.Bartleby.com.

PhD thesis: **Padberg, G**. Facioscapulohumeral diseases. *PhD thesis*, Leiden University, 1982, 130 p.

Website: National survey schoolchildren report. National Centre of Public Health and Analyses, 2014. Available at http://ncphp.government.bg/files

Page charges

Manuscript publication is free of charges.

Ethics in publishing

Before sending the manuscript the authors must make sure that it meets the Ethical guidelines for journal publication of Acta Morphologica et Anthropologica.

Human and animal rights

If the work involves the use of human subjects, the authors should ensure that work has been carried out in accordance with *The Code of Ethics of the World Medical Association* (Declaration of Helsinski). The authors should include a statement in the manuscript that informed consent was obtained for experimentation with human subjects. The privacy rights of human subjects must always be observed.

All animal experiments should comply with the *ARRIVE guidelines* and should be carried out in accordance with the U.K. Animals (Scientific procedures) Act, 1986 and the associated guidelines *EU Directive 2010/63/EU* for animal experiments, or the National Institutes of Health guide for the care and use of Laboratory animals (NIH Publications No. 8023, revised 1978) and the authors should clearly indicate in the manuscript that such guidelines have been followed.

Submission Details

Acta Morphologica et Anthropologica is published twice a year as one volume with 4 issues. For the first two issues (1-2) the deadline for manuscript submission is March 15th and for the next two issues (3-4), the deadline is September 15th. Electronic version for issues 1-2 is uploaded on the website till June 30th and for issues 3-4 – till December 30th.

Manuscript submission is electronical only.

The manuscripts should be sent to the Managing Editor email address ama.journal@iempam.bas.bg, ygluhcheva@hotmail.com with copy to iempam@bas.bg

All correspondence, including notification for Editor's decision, requests for revision, is sent by e-mail.

Submission declaration

Submission of the manuscript implies that the work described has not been published previously, is not considered under publication elsewhere, that its publication is approved by all authors, and that if accepted, it will not be published elsewhere in the same form, in English or in any other language, including electronically, without the informed consent of the copyright-holder.

Contributors

The statement that all authors approve the final article should be included in the disclosure.

Copyright

http://www.iempam.bas.bg/journals/acta/Author%20Copyright%20Agreement_last.pdf

Upon acceptance of an article, the authors will be asked to complete a "**Copyright Transfer Agreement**".

http://www.iempam.bas.bg/journals/acta/Copyright_Transfer_Agreement_Form_AMA.doc

Peer review

Once a manuscript is submitted, the Managing Editor (or the Editor-in-Chief) briefly checks the manuscript for conformance with the journal's Focus, Scope, Policies and style requirements and decide whether it is potentially suitable for publication and can be processed for review, or rejected immediately, or returned to the author for improvement and re-submission.

Manuscripts are peer-reviewed by the Editors, Editorial Board members, and/or external experts before final decisions regarding publication are made. The entire editorial workflow is performed in the following steps:

1. The submitted manuscript is checked in the editorial office whether it is suitable to go through the normal peer review process.

2. If deemed suitable, the manuscript is sent to 2 reviewers for peer-review. The choice of reviewers depends on the subject of the manuscript, the areas of expertise of the reviewers, and their availability.

3. Each reviewer will have 2 weeks to provide evaluation of the manuscript. The Editor may recommend publication, request minor, moderate or major revision, or provide a written critique of why the manuscript should not be published (rejected).

4. In case only one reviewer suggests rejection of the manuscript, the latter is subjected to additional evaluation by a third reviewer.

5. The manuscript will be published in a revised form provided that the authors successfully answer the critics received. The Editor-in-Chief is the final authority on all editorial decisions.

Open Access

This journal provides immediate open access to its content on the principle that making research freely available to the public supports a greater global exchange of knowledge.

After acceptance

Proof correction

The corresponding author will receive proofs by e-mail in PDF format and will be requested to return it with any corrections within two weeks.

ISSN 1311-8773 (print)
ISSN 2535-0811 (online)